

# Monday Morning, October 18, 2010

## Actinides and Rare Earths Topical Conference

Room: Isleta - Session AC+SS-MoM

### Surface Science of Actinides

**Moderator:** J.G. Tobin, Lawrence Livermore National Laboratory

9:00am **AC+SS-MoM3 High Resolution Auger Electron Spectroscopy of Plutonium Metal and Oxide Surfaces**, *D.P. Moore, A.L. Broach, D.L. Pugmire*, Los Alamos National Laboratory, *H.G. Garcia Flores*, University of Nebraska-Lincoln, *P. Roussel*, Atomic Weapons Establishment

There has been considerable new study of the oxidation of plutonium in recent years. Much of this study has focused on the properties of the thin film oxide layers that form on the plutonium metal surface under exposure to oxygen. For these studies, x-ray photoelectron spectroscopy (XPS) has typically been the technique of choice as it is ideally suited for the study of oxidation states by analyzing XP peak shape and position changes. This allows for the identification of relative changes in the Pu 4f manifold in going from Pu metal, to the Pu sesquioxide ( $\text{Pu}_2\text{O}_3$ ), to the Pu dioxide ( $\text{PuO}_2$ ). But there are advantages of other surface science techniques, specifically Auger electron spectroscopy (AES), over XPS for certain types of studies. Prime among them is that AES has a much higher spatial resolution than XPS allowing for analysis of specific areas and features on a surface down to a few tens of nanometers. And although AES typically suffers from less sensitivity and specificity to chemical state differences in its peak shape and position, modern Auger systems with field emission sources and hemispherical electron analyzers have alleviated much of this shortcoming.

For plutonium, Auger peaks for the metal and dioxide have been used for investigation whereas the Auger peaks for the sesquioxide have not received the same study. Peak positions from derivative spectra have been used for distinguishing between metal and oxide with quantification of the oxides from peak-to-peak heights and estimates of relative sensitivity factors. In order to more fully utilize AES for the study of the oxidation of plutonium surfaces, the relative changes in the Auger peaks in going from Pu metal to all its oxides must be quantified. We have used high resolution AES to identify the Auger peak structure of Pu metal,  $\text{PuO}_2$ , and  $\text{Pu}_2\text{O}_3$ . We have studied the OPP and OVV Auger transitions in the 80 – 110 eV range as well as the NOV transitions at approximately 315 eV via oxygen dosing on Pu metal surfaces. Oxygen doses from less than a Langmuir up to over 500 Langmuirs have been investigated. Relative changes in both the integrated and derivative Auger peak structures for Pu metal,  $\text{PuO}_2$ , and  $\text{Pu}_2\text{O}_3$  have been identified and will be presented. Using this new information we will be able to take advantage of the higher spatial resolution of AES to further study plutonium oxide properties such as layer structure, oxidation kinetics, and auto reduction on polycrystalline plutonium samples.

9:20am **AC+SS-MoM4 The Behavior of Gallium During the Initial Stages of Plutonium/Gallium Alloy Oxidation**, *D.L. Pugmire*, Los Alamos National Laboratory, *H.G. Garcia Flores*, University of Nebraska-Lincoln, *D.P. Moore, A.L. Broach*, Los Alamos National Laboratory, *P. Roussel*, Atomic Weapons Establishment

An area of significant importance to the oxidation of any alloy is the role that the constituent metals play. It has been previously shown that the oxidation rate for the  $\delta$ -phase stabilized, plutonium/gallium alloy can be significantly affected by the gallium content as well as composition of the oxidizing atmosphere ( $\text{O}_2$ ,  $\text{O}_2/\text{H}_2\text{O}$ ,  $\text{H}_2\text{O}$ ). Reasons for the observed rate changes upon alloying with gallium are not understood. A previous study of a variety of  $\delta$ -plutonium alloys shows that the significant structure difference between unalloyed  $\alpha$ -plutonium and alloyed  $\delta$ -plutonium cannot be the sole cause of different oxidation rates. This implies that the alloying metal must play some role in the slower oxidation rates observed for gallium-stabilized  $\delta$ -plutonium. In order to elucidate the oxidation mechanism of this commonly employed alloy, it is important to understand the role gallium plays during oxidation. The relatively low concentrations of alloying metals used, typically several atomic percent, can make the activities of gallium during oxidation of  $\delta$ -plutonium difficult to follow. This complication is compounded by the fact that the initial stages of oxidation are inherently a surface phenomenon, thereby significantly limiting the relative amount of affected material. Significant questions remain as to what is a realistic description for the Pu/Ga-oxide, thin-film system during the initial stages of oxidation.

An ultra-high vacuum (UHV) system equipped with surface sensitive techniques, such as x-ray photoelectron spectroscopy (XPS) and Auger

electron spectroscopy (AES), provides a controlled environment ideally suited to study the behavior of gallium during the initial stages of Pu/Ga oxidation. In addition to information about the oxidation states of the plutonium species in the near surface region provided by XPS, both XPS and AES are very useful for studying the relative atomic concentration of elements present at the sample surface (such as oxygen and gallium). While these surface sensitive techniques suffer from relatively high limits of detection, we have been able to qualitatively, and in some cases quantitatively, study the behavior of gallium during the oxidation of the  $\delta$ -plutonium alloy. The gallium content relative to plutonium is observed to decrease within the oxide film during oxidation, with the displaced gallium apparently moving to the oxide/metal interface to form a thin gallium rich region. The results of these studies and their implications on the mechanism of gallium-stabilized,  $\delta$ -plutonium oxidation will be discussed.

9:40am **AC+SS-MoM5 Angle-Resolved Photoemission and the 5f Electronic Structure of Pu Materials**, *J. Joyce, T. Durakiewicz, K.S. Graham, E.D. Bauer, J.N. Mitchell, D.P. Moore, J.A. Kennison, T.M. McCleskey, A.K. Burrell, E. Bauer, Q. Jia*, Los Alamos National Laboratory

#### INVITED

The electronic structure of Pu compounds ranging from Mott insulators to strongly correlated metals is investigated using angle-resolved photoemission (ARPES). The electronic properties of the Pu compounds  $\text{PuCoGa}_5$ ,  $\text{PuSb}_2$ , and  $\text{PuO}_2$  are compared with angle-integrated and temperature-dependent photoemission results for Pu metal. The balance in strongly correlated materials between the central and periodic potentials is directly probed through ARPES. For the strongly correlated metals, details of the sharp quasiparticle peak at the Fermi energy are presented, including crystal momentum dispersion, giving insight into the self-energy and ground state properties of these Pu materials. In  $\text{PuSb}_2$ , the ARPES data at a photon energy of 21.2 eV, indicates a quasiparticle peak that disperses through the Fermi energy. At 40.8 eV photon energy,  $\text{PuSb}_2$  shows f-electron intensity periodic with the lattice. Photoemission results for the Fermi level spectral intensity as well as the more localized 5f states well-removed from the Fermi energy are used to quantify adaptive character for these materials. Both  $\text{PuSb}_2$  and  $\text{PuCoGa}_5$  ARPES data show a dispersive peak which crosses the Fermi energy at a photon energy of 21.2 eV where the conduction states have a larger cross section than the 5f states. The results for 40.8 eV photon energy, with enhanced 5f strength, indicate a peak dispersing through the Fermi energy for  $\text{PuCoGa}_5$  but the  $\text{PuSb}_2$  data indicate an intensity modulated peak near the Fermi energy. The first ARPES results for the Mott insulator  $\text{PuO}_2$  show substantial dispersion consistent with hybrid functional calculations which predict significant covalency for  $\text{PuO}_2$  compared with the earlier ionic actinide dioxides such as  $\text{UO}_2$ . The ARPES, photon energy dependence, and the temperature dependent data for Pu materials will be discussed in terms of 5f adaptive character and the implications for Pu ground state properties.

Work supported by the U.S. Department of Energy, Basic Energy Sciences, the Los Alamos National Laboratory LDRD program, and Campaign II.

10:40am **AC+SS-MoM8 Novel Band Renormalization Mechanism in f-electron Systems**, *T. Durakiewicz, J. Joyce*, Los Alamos National Laboratory, *P.S. Riseborough*, Temple University, *P.M. Oppeneer*, Uppsala University, Sweden, *J.-C. Griveau*, ITU, Germany, *E.D. Bauer*, Los Alamos National Laboratory, *E. Guziewicz*, Polish Academy of Sciences, Poland

Several mechanisms may lead to band renormalization in strongly correlated systems. Inter-band scattering was recently shown to produce significant renormalization effects in high temperature superconductors. Here we show, for the first time, that inter-band processes may lead to strong band renormalization in the vicinity of Fermi level in a 5f-electron system,  $\text{USb}_2$ . The Fermi surface of this compound consists of several uniaxial cylindrical sheets. We show that the bare band LDA calculation over-counts the number of sheets, because it lacks the renormalization part. But our high resolution angle resolved photoemission (ARPES) experiments demonstrate that one of the calculated cylinders shrinks below the Fermi level, forming a closed cigar-shaped Fermi surface rather than an open cylindrical one. In normal emission experiments, we measure the dispersion of the bands of interest in the Gamma-Z direction. The measured results disagree with the LDA result, but the bare LDA bands can be renormalized by using a low order self-energy expansion in three-band inter-band scattering model, and very good fit is obtained. We conclude that inter-band scattering in  $\text{USb}_2$  influences the fermiology of this system in terms of changing the shape and number of Fermi sheets.

11:00am **AC+SS-MoM9 The Initial Oxidation of Polycrystalline Thorium**, *M. Bagge-Hansen, R.A. Outlaw, D.M. Manos*, College of William & Mary

The initial oxidation of clean, polycrystalline  $\alpha$ -Th from background CO/CO<sub>2</sub> and saturation of the Th surface by O<sub>2</sub> has been examined in ultrahigh vacuum ( $p < 2 \times 10^{-11}$  Torr, H<sub>2</sub>) by angle resolved Auger electron spectroscopy (ARAES) and time of flight secondary ion mass spectrometry (ToF-SIMS). Following dissociative adsorption of background CO/CO<sub>2</sub>, the accompanying oxygen surface population increased at a rate roughly one third that of the carbon, suggesting significant oxygen incorporation into the bulk. The admission of O<sub>2</sub> following heating and sputter cleaning of the Th, showed similar behavior in that some oxygen atoms continued to diffuse into the bulk until formation of stoichiometric ThO<sub>2</sub> was observed at  $\sim 37$  L. The thickness of the oxide complex was determined by both ARAES and ToF-SIMS and found to be  $\sim 5$  nm. The thermal stability of the ThO<sub>2</sub> over the temperature range of 25 – 1000°C was also studied. Rapid decomposition of the oxide by CO desorption and subsequent oxygen dissolution into the bulk was observed to occur within a temperature range of  $\sim 550$ -750°C.

11:20am **AC+SS-MoM10 The Non-Equilibrium Nature of Uranium Oxide Surfaces**, *R.K. Schulze, D.P. Johnson, M.A. Hill*, Los Alamos National Laboratory

We examine the surface reactions of bulk single crystal uranium oxide (UO<sub>2</sub>) and thin films of uranium oxide on metal using Kelvin probe (surface work function and chemical potential) measurements and x-ray and ultraviolet photoelectron spectroscopy. The processes of surface and sub-surface reactions with small gas phase molecules are examined through in-situ work function measurements (dynamic) while the surface chemistry and configuration are probed with photoemission and LEED measurements (equilibrium). The hyperstoichiometric uranium oxide (UO<sub>2+x</sub>) is shown to be composed of, in the surface region, labile interstitial oxygen that can be moved relatively easily in and out of the fluorite structure lattice through control of the headspace oxygen activity. The transport of oxygen in this near surface region of the oxide is examined through changes in the surface work function with exposure to various partial pressures of oxygen. The amount of excess oxygen in the oxide lattice of the surface is shown to affect the reactivity of this surface with small gas phase molecules directly. A measurement and description of the band structure of the uranium oxide surface for different levels of oxygen content (UO<sub>3</sub>, UO<sub>2+x</sub>, UO<sub>2</sub>, UO<sub>2-x</sub>) is presented.

11:40am **AC+SS-MoM11 Characterization of the Surface Changes During the Activation of Erbium/Erbium Oxide for Hydrogen Storage**, *M.T. Brumbach, K.R. Zavadil, C.S. Snow, J.A. Ohlhausen*, Sandia National Laboratories

## Graphene Focus Topic

**Room: Brazos - Session GR+SS+TF+EM-MoM**

### Epitaxial Graphene on SiC

**Moderator:** P.E. Sheehan, Naval Research Laboratory

8:20am **GR+SS+TF+EM-MoM1 Controlling Carriers in Graphene**, *G.G. Jernigan, P.E. Thompson, C.S. Hellberg, J.L. Tedesco, V.D. Wheeler, L.O. Nyakiti, P.M. Campbell, D.K. Gaskill*, Naval Research Laboratory

No technique for graphene synthesis yields controllably doped material. Measurements of carrier density and carrier type produce results that are dependent on extrinsic factors. For example, exfoliated graphene and metal-catalyzed graphene on SiO<sub>2</sub> often obtain carriers through unwanted charges in the oxide[1] or by gas adsorption[2] making graphene p-type. Similarly, epitaxial graphene on SiC should be n-type due to work function differences with the underlying SiC substrate[3]. Our recent measurements of graphene grown on Si-face SiC show that device processing steps can cause it to switch between carrier types. Additionally, we have found graphene grown on C-face SiC to be highly doped by Si impurities, which can produce either electrons or holes.

We have begun a series of investigations to impart properties after growth on epitaxial graphene formed on Si- and C-face SiC[4-5]. Substitutional incorporation of impurity atoms can lead to doping in a graphene sheet, if their concentration does not drastically affect the pi-network. This can be achieved by selective oxidation to remove C atoms from the graphene lattice and by molecular beam deposition (MBE) of dopants with controllable ultra-low fluxes to fill the C vacancies. It is important to note that Group III and V dopants can maintain the 2D geometry of the graphene sheet without producing an unsaturated bond (as they do when incorporated into the bulk of Si.) Thus, the extra p-orbital electrons from the Group V

elements can be added to the graphene pi-network, or Group III elements can provide extra holes, without adversely affecting carrier mobility. Using MBE, we have substitutionally doped graphene with B and P. Ultraviolet photoelectron spectroscopy (UPS) is used to observe shifts in the Fermi level resulting from doping, and we have seen up to a 110 meV shift with 1% B in the lattice of graphene. Discussion of scanning tunneling microscopy (STM) observations of dopant placement and electrical properties will be presented. Density functional theory has been used to compute the density of states for the doped system in support of the STM and electrical measurements.

[1] S. S. Datta, D. R. Strachan, E. J. Mele, and A.T.C. Johnson, *Nano Lett.* 9 (2009) 7.

[2] Y. Dan, Y. Lu, N.J. Kybert, Z. Luo and A.T.C. Johnson, *Nano Lett.*, 9 (2009) 1472.

[3] T. Filleter, K. V. Emtsev, Th. Seyller, and R. Bennewitz, *Appl. Phys. Lett.* 93 (2008) 133117.

[4] G.G. Jernigan, et al., *Nano Lett.* 9, 2605 (2009).

[5] J.L. Tedesco, B.L. VanMil, R.L. Myers-Ward, J.M. McCrate, S.A. Kitt, P.M. Campbell, G.G. Jernigan, J.C. Culbertson, C.R. Eddy, Jr., and D.K. Gaskill, *Appl. Phys. Lett.*, 95, 122102 (2009).

8:40am **GR+SS+TF+EM-MoM2 The Role of Carbon Surface Diffusion on the Growth of Epitaxial Graphene on SiC**, *T. Ohta, N.C. Bartel, S. Nie, K. Thürmer, G.L. Kellogg*, Sandia National Laboratories

Growth of high quality graphene films on SiC is regarded as one of the more viable pathways toward graphene-based electronics. Graphene films are readily formed on SiC by preferential sublimation of Si at elevated temperature. Little is known, however, about the atomistic processes of interrelated Si sublimation and graphene growth. We have observed the formation of graphene on SiC by Si sublimation using low energy electron microscopy, scanning tunneling microscopy, and atomic force microscopy. This work reveals unanticipated growth mechanisms, which depend strongly on the initial surface morphology. Carbon diffusion governs the spatial relationship between Si sublimation and graphene growth. Isolated bilayer SiC steps generate narrow ribbons of graphene by a distinctive cooperative process, whereas triple bilayer SiC steps allow large graphene sheets to grow by step flow. We demonstrate how graphene quality can be improved by controlling the initial surface morphology to avoid the instabilities inherent in diffusion-limited growth. This work is supported by the LDRD program at Sandia Labs and the US DOE Office of Basic Energy Sciences, Division of Materials Science and Engineering (DE-AC04-94AL85000), and was performed in part at CINT (DE-AC04-94AL85000). Sandia is a multiprogram laboratory operated by Sandia Corporation, a Lockheed Martin Co., for the U.S. DOE NNSA (DE-AC04-94AL85000).

9:00am **GR+SS+TF+EM-MoM3 Epitaxial Graphene on SiC(0001)**, *T. Seyller*, Universität Erlangen, Germany **INVITED**

The properties of graphene, its fabrication, and its application, and its active fields of research. The large carrier mobility and prospects for room-temperature ballistic transport raise hopes for application of graphene in electronic devices. Applications, however, demand growth methods suitable for producing graphene layers on a wafer scale. While this goal is impossible to reach with mechanical exfoliation, epitaxial graphene (EG) grown on the basal plane surfaces of silicon carbide (SiC) offers a much better prospective. In this talk I shall review studies of the structural, electronic, and transport properties of EG grown on SiC by solid-state decomposition at elevated temperatures. The first part describes a study of the electronic structure and structural properties of EG which can conveniently be determined using surface science techniques. In the second part I demonstrate how the growth of EG is improved by going from the traditional growth environment, namely ultrahigh vacuum, to an Argon atmosphere. The latter method leads to vastly improved EG films with properties similar to those of exfoliated graphene. Finally I shall discuss how the interface between SiC and graphene can be controlled by intercalation of foreign atoms.

9:40am **GR+SS+TF+EM-MoM5 Structural Defects in Epitaxial Graphene Layers Synthesized on 4H-SiC(000-1) Substrate - Transmission Electron Microscopy (TEM) Studies**, *J. Borysiuk, University of Warsaw, Poland, S.K. Krukowski*, Polish Academy of Sciences, Poland

Main structural defects in graphene layers, synthesized on the carbon-terminated face, i.e. SiC(000 $\bar{1}$ ) face of 4H-SiC substrate, are discussed. The discussed structures include in-plane edge dislocations, grain boundaries, puckers, etc. These defects are investigated using High Resolution Transmission Electron Microscopy (HRTEM), revealing their atomic arrangement. The mechanism of creation of such defects, in relation to the misalignment to the underlying crystallographic structure of the SiC

substrate is elucidated. The relation between the SiC surface structure, including the presence of the single atomic steps, the sequences of atomic steps, and also the macrosteps, and the emergence of edge dislocations or boundaries between the regions having different crystallographic orientation in the graphene layers, is shown. In addition, the structures containing different stacking sequences of carbon atoms in the graphene layers are presented. The presented C-layers stacking includes AA, AB, ABC sequences, and also the stacking close to turbostratic stacking.

10:00am **GR+SS+TF+EM-MoM6 Controlling the Growth Rate of Graphene on Silicon Carbide**, *D.B. Torrance, D.L. Miller, M. Phillips, H. Tinkey, E. Green, P.N. First*, Georgia Institute of Technology

Controlled thermal decomposition of silicon carbide is so far the most effective method for growing high-quality graphene epitaxially and at the wafer scale. In this work we simultaneously study the graphenization of SiC(0001) and SiC(000-1) as a function of temperature and buffer-gas pressure in a custom-built ultrahigh vacuum (UHV) induction furnace. The buffer gas is modeled as a homogeneous diffusion medium using kinetic theory. In-situ characterization by both Auger electron spectroscopy and low-energy electron diffraction (LEED) was used to determine the pressure- and temperature-dependent growth rate of graphene layers. Sample quality was further assessed ex-situ using a variety of techniques such as Raman spectroscopy and scanning tunneling microscopy.

10:40am **GR+SS+TF+EM-MoM8 Evidence of Screw Dislocations in Epitaxial Graphene Islands**, *J.K. Hite, J.C. Culbertson*, Naval Research Laboratory, *J.L. Tedesco*, National Institute of Standards and Technology, *M.E. Twigg, A.L. Friedman, P.M. Campbell, R.L. Myers-Ward, C.R. Eddy, Jr., D.K. Gaskill*, Naval Research Laboratory

Epitaxial graphene (EG) has lately garnered enormous interest, due to its high free-carrier mobility and compatibility with semiconductor processing. In fact, the first EG RF field effect transistor has been demonstrated.<sup>1</sup> However, the growth mechanism of this material is not well understood. Current RF device work has been on the Si polar face of (0001) semi-insulating SiC substrates as EG on this face mainly consists of 1 monolayer of graphene. In contrast, the C-face consists of a dozen or more graphene layers and has a rougher morphology. Yet, there is significant interest in obtaining few layer, smooth EG on the C-face of SiC due to its better electrical properties as compared to the Si-face. Recently, it was shown that C-face EG grown in Ar ambient slows the growth rate, and under certain conditions results in islanding of the graphene on the C-face.<sup>2</sup> These islands open the possibility of investigating the initial stages of graphene growth.

Electron channeling contrast imaging (ECCI) has previously been used to investigate threading dislocations in semiconductors such as GaN and SiC.<sup>3,4</sup> In this work, ECCI is used for the first time to investigate graphene island morphology as a function of island size and growth conditions. Using this characterization tool, single threading screw dislocations (TSDs) have been found in the center of small EG islands (>20 $\mu$ m diameter). ECCI images confirm that these small graphene islands are forming in hexagonal recesses below the surface of the SiC substrate. For larger islands, the evidence of TSDs disappears suggesting that as the islands grow or coalesce to larger diameters either the TSD becomes buried or no longer contributes to growth. Once the islands become this large, the graphene begins to grow above the SiC surface, unlike the smaller islands. After removal of the EG by various methods, TSDs are still observed in the centers of the pits formed by the small island graphene growth. After some removal efforts, many pits retained small triangles of graphene around the TSD. These results are consistent with Raman and AFM maps of the islands that demonstrate that the centers of the islands are much deeper and the graphene thicker than the surrounding graphene. The evidence of TSDs in the centers of these C-face EG islands strongly suggests that these dislocations serve as nucleation sites for EG growth, where the TSD may provide an escape pathway for sublimated silicon atoms during the growth process.

<sup>1</sup>J.S. Moon *et al.*, IEEE Electron Dev Lett **31**, 260, 2010

<sup>2</sup>J.L. Tedesco *et al.*, Appl Phys Lett, in press

<sup>3</sup>Y.N. Picard *et al.*, Scripta Materiala **61**, 773, 2009

<sup>4</sup>Y.N. Picard *et al.*, Appl Phys Lett **90**, 23401, 2007

11:00am **GR+SS+TF+EM-MoM9 Direct Measurement of the Energy Gaps Involved in the Lifting of the Valley and Spin Degeneracies in Epitaxial Graphene**, *Y.J. Song, A.F. Otte*, CNST/NIST; Maryland NanoCenter UMD, *D.B. Torrance, Y. Hu, P.N. First, W.A. de Heer*, Georgia Institute of Technology, *J.A. Stroscio*, CNST/NIST

Landau levels on epitaxially grown graphene were recently mapped both spatially and energetically using scanning tunneling spectroscopy in magnetic fields at 4 K [1]. In this talk we present new measurements, made at  $\approx 10$  mK, of all four electron states resulting from the lifting of the

fourfold spin- and valley-degeneracy of the  $N = 1$  Landau level in applied magnetic fields. We show that the energy splitting from the broken valley degeneracy is ten times larger than electron spin splitting in our samples. When the Fermi level lies inside the four-fold Landau manifold, significant electron correlation effects result in an enhanced valley splitting at even filling factors, and an enhanced electron spin splitting at odd filling factors. Most surprisingly, we observe new many body states with top-layer Landau level filling factors  $7/2$ ,  $9/2$ , and  $11/2$ .

[1] David L. Miller, Kevin D. Kubista, Gregory M. Rutter, Ming Ruan, Walt A. de Heer, Phillip N. First, and Joseph A. Stroscio, Science **324**, 924-927 (2009).

11:20am **GR+SS+TF+EM-MoM10 Morphology of Epitaxial Graphene on SiC: Nano-Objects, Nano-Cracks, and Ribbons**, *S. Chiang*, Univ. of California at Davis, *N. Camara*, IMB-CNM-CSIC, Spain, *S. Vizzini, D. Martinotti*, CEA-Saclay, France, *H. Oughaddou*, Univ. de Cergy-Pontoise & CEA Saclay, France, *H. Enriquez*, Univ. de Paris-Sud/Orsay & CEA-Saclay, France, *Ph. Godignon*, IMB-CNM-CSIC, Spain, *J. Camassel*, GES, UMR-CNRS, France, *P. Soukiassian*, Univ. de Paris-Sud/Orsay & CEA-Saclay, France

We use scanning tunneling microscopy/spectroscopy (STM/STS) and low energy electron microscopy (LEEM) to investigate epitaxial graphene grown under vacuum on a 4H-SiC(000-1)-C-face substrate and self-organized parallel graphene ribbons grown in a furnace on a 6H-SiC(000-1) C-face sample covered by a graphite cap. On the vacuum grown graphene, we observed two types of nanostructures including nano-objects and nano-cracks. The results reveal that these nano-objects are located at the graphene/SiC interface leading to electronic interface states. Their height profiles suggest that these objects are made of packed carbon nanotubes confined vertically and forming mesas at the SiC surface. We also find nano-cracks covered by the graphene layer that, surprisingly, is not broken going deep into the crack, with no resulting electronic interface state. Therefore, unlike the above nano-objects, these cracks should not affect the carrier mobility. LEEM has been used to observe the formation of graphene ribbons grown on SiC in a furnace. The morphology and distribution of the ribbons has been examined, and their typical size is about 1  $\mu$ m wide and 10  $\mu$ m long.

Work supported by Agence National pour la Recherche (ANR) under GraphSiC program

## Surface Science

### Room: Picuris - Session SS1-MoM

## Reactivity and Selectivity on Catalytic Surfaces

Moderator: C.T. Campbell, University of Washington

8:20am **SS1-MoM1 Structure and Reactivity of Alkyl Ethers Adsorbed on Hydroxylated CeO<sub>x</sub>(111) Model Catalysts**, *F.C. Calaza*, Oak Ridge National Laboratory, *T.-L. Chen*, Brookhaven National Laboratory, *D.R. Mullins, S.H. Overbury*, Oak Ridge National Laboratory

The study of adsorption and reactivity of oxygenated molecules on model oxide catalysts is of great interest to gain a better understanding of the mechanism of industrial reactions. Cerium oxide is commonly used in three-way auto exhaust and WGS catalysts. Our experimental design is intended to find the conditions where UHV experiments could mimic the real catalytic processes and from these results explain the reaction pathway from the atomistic level.

From the surface science point of view, previous studies of alcohols, ketones and aldehydes adsorbed on the surface of cerium oxide model catalysts have shown a variety of pathways for decomposition and reactivity. In the present work we have examined these pathways for two ethers, diethyl ether (DEE) and dimethyl ether (DME). Both ethers adsorb on fully oxidized CeO<sub>2</sub>(111) and highly reduced CeO<sub>x</sub>(111) under UHV conditions but only at low temperature ( $\sim 150$  K) and they do not decompose. If the catalyst surface is pre-covered by hydroxyls, by adsorbing water at room temperature on the reduced CeO<sub>x</sub>(111) surface, then the adsorption geometry of the ether on this hydroxylated surface

changes, indicating interaction with OH groups. Regarding their reactivity towards decomposition, the two ethers behave differently when exposed to hydroxylated CeOx(111) at 300-400 K. In the case of DEE, this molecule promptly reacts by breaking the C-O bond presenting a very interesting chemistry. By means of Reflection Absorption Infrared Spectroscopy (RAIRS) and soft X-Ray Photoelectron Spectroscopy (sXPS), we could detect ethoxide and possibly carboxylate species as adsorbed intermediates for the reaction. However, when the hydroxylated CeOx(111) is exposed to DME at same conditions, the ether shows no reactivity, indicating the importance of H on a carbon atom  $\beta$  to oxygen. Possible explanations for the role of hydroxyls in helping break the C-O bond of ether molecules will be given.

Research sponsored by the Division of Chemical Sciences, Geosciences, and Biosciences, Office of Basic Energy Sciences, US Department of Energy, under contract DE-AC05-00OR22725 with Oak Ridge National Laboratory, managed and operated by UT-Battelle, LLC. Use of the National Synchrotron Light Source, Brookhaven National Laboratory, was supported by the US Department of Energy, Office of Science, Office of Basic Energy Sciences, under Contract No. DE-AC02-98CH10886.

8:40am **SSI-MoM2 Adsorption and Activation of n-alkanes on a PdO(101) Thin Film**, J.F. Weaver, C. Hakanoglu, J.A. Hinojosa, Jr., A. Antony, J.M. Hawkins, A. Asthagiri, University of Florida

The formation of palladium oxide (PdO) is thought to be responsible for the exceptional activity of supported Pd catalysts toward the complete oxidation of alkanes under oxygen-rich conditions. In this talk, I will discuss our recent investigations of the adsorption and activation of n-alkanes on a PdO(101) thin film that is prepared by oxidizing Pd(111) in ultrahigh vacuum (UHV) using an oxygen atom beam. We find that alkanes adsorb relatively strongly on the PdO(101) surface by forming  $\sigma$ -complexes along the rows of coordinatively unsaturated Pd atoms. The formation of  $\sigma$ -complexes causes the alkane binding energies on PdO(101) to exceed those of alkanes physisorbed on Pd(111). We also find that the alkane  $\sigma$ -complexes on PdO(101) act as precursors for initial C-H bond cleavage; propane and n-butane undergo facile C-H bond cleavage below about 215 K in UHV. Finally, I will discuss density functional theory calculations which show that dative bonding between the alkane and *cus*-Pd atoms weakens the coordinated C-H bonds, thereby lowering energy barriers for C-H bond scission by as much as 100 kJ/mol. These findings provide insights for understanding the role of molecularly chemisorbed precursors in the initial activation of alkanes on PdO(101) and possibly other transition-metal oxide surfaces.

9:00am **SSI-MoM3 Stereo and Enantioselectivity in Surface Reactions**, F. Zaera, University of California, Riverside **INVITED**

Achieving high selectivity is arguably the main upcoming challenge in heterogeneous catalysis for the 21st century. In complex reaction with competing parallel pathways, small changes in the relative values of the different activation energies are sufficient to switch the selectivity of those processes from one product to another. We in our laboratory have been carrying out mechanistic studies on the conversion of hydrocarbons on model metal surfaces to try to identify the key factors that control such selectivity. In this talk we will present a couple of examples of increasing subtlety from that work. In the first, we will discuss a reaction involving a C=C double bond isomerization, in particular *cis-trans* isomerization reactions. The second example will be focused on issues of bestowing enantioselectivity on solid surfaces by using cinchona alkaloid modifiers. In both cases it will be shown how the mechanistic information obtained from surface-science studies can be extended to design more selective real catalysts.

9:40am **SSI-MoM5 Enantioselective Explosions on Chiral Surfaces**, A.J. Gellman, Y. Huang, F. Xu, V.V. Pushkarev, Carnegie Mellon University

The high Miller index surfaces of single crystal metals have chiral structures and interact enantiospecifically with chiral adsorbates. The enantiospecificity of surface reaction kinetics is dictated by the enantiospecificity of surface reaction energetics but can also be influenced by reaction order. Recently, it has been shown that tartaric acid decomposes with explosive reaction kinetics on Cu(110) surfaces. Tartaric acid is chiral and on naturally chiral Cu surfaces such as Cu(643), Cu(653), Cu(17,5,1), and Cu(531) the non-linear nature of the reaction kinetics leads to extremely high enantiospecificity. The explosive reaction kinetics originate with the need for empty surface sites for the decomposition process. At high coverages of tartaric acid the limited availability of empty sites constrains the decomposition process. Once nucleated, however, the reaction proceeds autocatalytically and occurs over a very narrow temperature range during heating. The decomposition kinetics of *R,R*- and *S,S*-tartaric acid depend on the handedness of the Cu substrate and the decomposition features observed

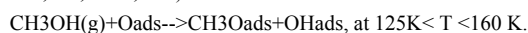
during temperature programmed reaction spectroscopy are completely resolved. Peak enantiospecificities in the decomposition reaction rates can reach a factor of fifty.

10:00am **SSI-MoM6 C-H Bond Activation of Light Alkanes on Pt(111): Dissociative Sticking Coefficients, Evans-Polanyi Relation, and Gas-Surface Energy Transfer**, G. Cushing, J. Navin, S. Donald, I. Harrison, University of Virginia

Effusive molecular beam experiments were used to measure alkane dissociative sticking coefficients,  $S(T_g, T_s)$ , for which the impinging gas temperature,  $T_g$ , and surface temperature,  $T_s$ , could be independently varied. The 500-1000 K temperature range primarily examined should be relevant to heterogeneously catalyzed industrial processes such as the steam reforming of alkanes. Methane, ethane, and propane all showed increasing dissociative sticking as either  $T_g$  or  $T_s$  was increased – indicative of activated dissociation reactions. Effusive beam experiments with gas impinging along the surface normal and  $T_g=T_s=T$  determined  $S_n(T)$ , a close approximation and formal upper bound to the thermal dissociative sticking coefficient,  $S(T)$ , appropriate to reaction with a thermal ambient gas. Activation energies determined from  $S_n(T)$  for methane, ethane, and propane are  $E_a = 58 \text{ kJ mol}^{-1}$ ,  $43 \text{ kJ mol}^{-1}$ , and  $34 \text{ kJ mol}^{-1}$ , respectively. An Evans-Polanyi plot of  $E_a$  for alkane dissociative chemisorption versus the alkane thermal desorption energy,  $E_d$ , is linear with a slope of -0.94. Assuming that the alkane  $E_d$  serves as a good approximation to the Van der Waals stabilization of the chemisorbed alkyl radical product of dissociative chemisorption, the slope of the Evans-Polanyi plot indicates a late transition state for alkane dissociative chemisorption on Pt(111). A microcanonical unimolecular rate theory model of dissociative chemisorption was used to model the effusive molecular beam experiments. Explicit accounting of the gas-surface energy transfer for the non-equilibrium experiments became increasingly important as the alkane size was increased. A simple exponential down model of the molecule/phonon collision step size distribution with a mean energy down parameter of  $\alpha = 350 \text{ cm}^{-1}$  for ethane, and  $\alpha = 1400 \text{ cm}^{-1}$  for propane, sufficed to provide a good description of the  $S_n(T_g, T_s)$  data.

10:40am **SSI-MoM8 Heat of Formation of Adsorbed Methoxy on Pt(111) by Adsorption Microcalorimetry**, E. Karp, M. Crowe, C.T. Campbell, University of Washington

The heat of adsorption of methanol on clean and oxygen pre-covered Pt(111) surfaces was measured in the temperature range of 100 to 160 K using Single Crystal Adsorption Calorimetry (SCAC). Our ultrahigh vacuum calorimeter, which also includes capabilities for AES, LEED and ISS, routinely achieves pulse-to-pulse standard deviations in heat measurements of 0.5 kJ/mol using methanol pulses containing only 0.02 ML. Averaging 8 runs reduces this to below 0.2 kJ/mol. These measurements provide the heat of formation of methoxy, an important intermediate in several catalytic reactions, including methanol reforming for highly pure H<sub>2</sub>. Above 125K, methanol is known to react with pre adsorbed oxygen adatoms to form methoxy and co-adsorbed OH (Akhter et. al., Surf. Sci., 167, 1986, 101):



Recently our group experimentally determined the heat of formation of OHads on Pt(111) to be -226.8 kJ/mol, using this value we have determined the heat of formation of adsorbed methoxy and compared this value to theoretical DFT work. Heats of adsorption of methanol were also measured on clean Pt(111) at 100K, as well as on the amorphous methanol multilayer, and compared to prior TPD measurements.

11:00am **SSI-MoM9 Interaction of Ethylene and Nitrogen Atoms on the Pt(111) Surface**, J. Yin, R. Meyer, M. Trenary, University of Illinois at Chicago

The selective catalytic reduction (SCR) of NO<sub>x</sub> by hydrocarbons on noble metals is critically important to the implementation of leaner burning more fuel efficient processes. Understanding the reaction mechanisms and pathways is essential for designing an effective catalytic system. As one small part of this effort, we focus on the interaction of nitrogen atoms and simple alkenes such as ethylene on the Pt(111) surface under UHV conditions in an effort to understand the potential intermediates in NO<sub>x</sub> reduction. The adsorption of ethylene on a nitrogen pre-covered Pt(111) surface has been investigated using reflection absorption infrared spectroscopy (RAIRS) and thermal desorption spectroscopy (TDS) as well as density functional theory calculations. Three interesting observations have been made. First, we observed the presence of  $\pi$ -bonded ethylene below 220 K, indicating a switch in the preferred binding site for ethylene on N-Pt(111) as compared to the clean surface. Second, above 500 K, CN coupling occurs as indicated by the desorption of HCN and the identification of CNH<sub>2</sub> with RAIRS. Third, the formation of ammonia is

observed through  $\text{NH}_3$  desorption as well as by observation of the  $d_e(\text{NH}_3)$  mode of  $\text{NH}_3$  at  $\sim 1170 \text{ cm}^{-1}$  with RAIRS. The appearance of ammonia is believed to be the result of a reaction between N atoms (or NH) with coadsorbed ethylidyne.

11:20am **SS1-MoM10 Probing the Reaction Intermediates for the Water-gas Shift Over Inverse  $\text{CeO}_x/\text{Au}(1\ 1\ 1)$  Catalysts, D.J. Stacchiola, S.D. Senanayake, J. Hrbek, J.A. Rodriguez, Brookhaven National Laboratory**

The water-gas shift (WGS) is an important reaction for the production of molecular  $\text{H}_2$  from CO and  $\text{H}_2\text{O}$ . An inverse  $\text{CeO}_x/\text{Au}(1\ 1\ 1)$  catalyst exhibits a very good WGS activity, better than that of copper surfaces or Cu nanoparticles dispersed on a ZnO substrate which model current WGS industrial catalysts. In this work we report on intermediates likely to arise during the  $\text{CO} + \text{H}_2\text{O}$  reaction over  $\text{CeO}_x/\text{Au}(1\ 1\ 1)$  using soft X-ray photoemission (sXPS) and near-edge X-ray absorption fine structure (NEXAFS). Several potential intermediates including formates (HCOO), carbonates ( $\text{CO}_3$ ) and carboxylates (HOCO) are considered. Adsorption of HCOOH and  $\text{CO}_2$  is used to create both HCOO and  $\text{CO}_3$  on the  $\text{CeO}_x/\text{Au}(1\ 1\ 1)$  surface, respectively. HCOO appears to have greater stability with desorption temperatures up to 600 K while  $\text{CO}_3$  only survives on the surface up to 300 K. On the  $\text{CeO}_x/\text{Au}(1\ 1\ 1)$  catalysts, the presence of  $\text{Ce}^{3+}$  leads to the dissociation of  $\text{H}_2\text{O}$  to give OH groups. We demonstrate experimentally that the OH species are stable on the surface up to 600 K and interact with CO to yield weakly bound intermediates. When there is an abundance of  $\text{Ce}^{4+}$ , the OH concentration is diminished and the likely intermediates are carbonates. As the surface defects are increased and the  $\text{Ce}^{3+}/\text{Ce}^{4+}$  ratio grows, the OH concentration also grows and both carbonate and formate species are observed on the surface after dosing CO to  $\text{H}_2\text{O}/\text{CeO}_x/\text{Au}(1\ 1\ 1)$ . The addition of ceria nanoparticles to Au(1 1 1) is essential to generate an active WGS catalyst and to increase the production and stability of key reaction intermediates (OH, HCOO and  $\text{CO}_3$ ).

11:40am **SS1-MoM11 Reactivity of CO towards Nanocrystals and Continuous Films of  $\alpha\text{-Fe}_2\text{O}_3$  on Au(111) at Ambient Pressure: Implications for the Water-Gas Shift Reaction, X. Deng, J. Lee, C. Wang, C. Matranga, National Energy Technology Laboratory (NETL), F. Aksoy, Z. Liu, Lawrence Berkeley National Laboratory**

The reactivity of CO towards nanocrystals and continuous films of  $\alpha\text{-Fe}_2\text{O}_3$  grown on Au(111) was investigated using in-situ X-ray photoelectron spectroscopy (XPS) at near ambient pressure (hundreds of mTorr). On Au(111) decorated with  $\alpha\text{-Fe}_2\text{O}_3$  nanocrystals (6-7nm), adsorbed CO was detected by XPS at room temperature when exposed to 200 mTorr of CO. At the same time, surface hydroxyl groups (adsorbed OH) were also observed as a result of  $\text{H}_2\text{O}$  dissociation. Upon heating the surface to 373 K, adsorbed formate (HCOO-) was detected on the surface and believed to originate from the reaction of CO with the OH groups. The adsorbed formate desorbed or decomposed above 473 K. Continuous  $\alpha\text{-Fe}_2\text{O}_3$  thin films on Au(111) were inert towards CO under the same conditions studied for nanocrystalline  $\alpha\text{-Fe}_2\text{O}_3$ . Specifically, adsorbed CO was *not* observed on this surface when it was exposed to 200 mTorr of CO at room temperature. This reactivity difference can be explained by the presence of  $\alpha\text{-Fe}_2\text{O}_3$  crystal edges and the interfaces between  $\alpha\text{-Fe}_2\text{O}_3$  and Au. These edges and interfaces are present for the nanocrystalline  $\alpha\text{-Fe}_2\text{O}_3/\text{Au}(111)$  system, but are not present in significant amounts for the continuous films of  $\alpha\text{-Fe}_2\text{O}_3$ . Implications of these experimental results for the water-gas shift reaction will be also discussed.

## Surface Science

Room: Santa Ana - Session SS2+EM-MoM

## Semiconductor Surfaces and Interfaces

Moderator: J. Millunchick, University of Michigan, Ann Arbor

8:20am **SS2+EM-MoM1 Spontaneous Microfaceting and Pyramid Growth during Si(100) Etching, M.F. Faggin, A. Gupta, M.A. Hines, Cornell University**

The spontaneous, etching-induced transformation of an initially flat Si(100) surface to a completely nanofaceted morphology consisting of overlapping pyramidal hillocks has been observed using a combination of morphological and spectroscopic probes and modeled using a fully-atomistic kinetic Monte Carlo (KMC) simulator of Si(100) etching. A novel silicon etchant has been developed that catalyzes the complete chemical transformation of a Si(100) surface into H-terminated Si{111} and Si{110} nanofacets. This finding was confirmed by infrared absorption spectroscopy, atomic force microscopy (AFM), and scanning electron microscopy (SEM). The

formation of pyramidal hillocks is highly reproducible and occurs on a time scale of several hours, enabling detailed studies of initial hillock formation and subsequent growth. The formation of microfaceted pyramidal hillocks during etching of Si(100) has previously been attributed to local masking on the surface by deposited impurities, etch products or gas bubbles. These mechanisms assume that an adsorbed impurity or gas bubble decorates the apex of every pyramid. Our atomistic simulations uncovered a second mechanism, one that is *intrinsic* to the etchant and that generates dynamically self-propagating pyramidal structures. Attempts to distinguish between these two mechanisms through rational modifications of the etchant chemistry will be described. For example, the kinetics of pyramid growth were followed spectroscopically, enabling quantitative assessment of the effects of chemical additives. These observations are more than an intellectual curiosity, as the silicon solar cell industry is actively searching for inexpensive, environmentally-friendly means of pyramidally texturing Si(100) surfaces to reduce reflection losses. Conversely, in microfabricated devices, suppression of pyramid formation is critical to high-yield manufacturing processes. An understanding of the hillock formation process may lead to the rational design of better etchants.

8:40am **SS2+EM-MoM2 Selective Ablation of Xe on Silicon Surfaces: MD Simulation and Experimental Laser Patterning, O. Stein, M. Asscher, The Hebrew University in Jerusalem, Israel**

Laser induced ablation of multilayer Xe on Si has been studied employing molecular dynamics (MD) simulations. 5nsec long laser pulse at  $\lambda=337\text{nm}$  was applied to a Xe slab at thicknesses of 16 32 and 40ML (774, 15488, 19360 atoms, respectively) adsorbed on top of a 8 layers 5408 atoms Si slab. Evaporative and explosive ablation thresholds were identified at absorbed laser power of 12 and 16MW/cm<sup>2</sup> which corresponds to surface temperature rise of 500 and 658K, respectively. Selective ablation was studied, where only a fraction of the lateral dimension of the computation cell was actually ablated. Extremely strong lateral dissipation among the Xe layers, has led the ablation threshold to shift to higher laser power as the fraction of heated area shrinks. Heated fraction (HF) less than 10% results in practically no ablation at laser power below substrate damage threshold. The MD studies were assessed and verified by experimental laser ablation measurements. A 10nsec Nd:YAG laser pulse operating at  $\lambda=532\text{nm}$  was employed. It was found that for 80 and 160ML Xe layer thickness, full ablation was reached at laser power of 6.9 and 8.4MW/cm<sup>2</sup> which corresponds to surface temperature rise of 180 and 220K respectively. Line-edge profile resulting from fractional laser induce desorption- coverage grating formation followed by metallic lift-off experiments were compared to the MD simulations of selective ablation, revealing a remarkable similarity.

Key words: Molecular Dynamics Simulations, Laser Ablation, adsorbed Xe on Si, Coverage Grating.

9:00am **SS2+EM-MoM3 Tuning Properties of Thin Films by Aminofunctionalization, A.V. Teplyakov, University of Delaware**

Surfaces and interfaces play an important role in development of modern microelectronics, optoelectronics, biosensing and other fields. This work will describe the approaches to tune the properties of interfaces, surfaces, and subsurface layers of participating materials by aminofunctionalization. The amino-groups of a general formula  $\text{NH}_x$  have been used in our group to control surface reactions on semiconductor surfaces, to promote deposition schemes on surfaces of thin solid diffusion barrier films, and to provide a reliable surface sites for biofunctionalization of self-assembled monolayers. In all of these cases, the reactivity of the amino-group can be designed to fit the required application. We will use selected temperature regimes, alkyl, aryl, and other substituents to alter the reactivity of amino-terminated surfaces and to reversibly tune the properties of surface and subsurface layers in thin solid films. Infrared spectroscopy was used to determine the chemical nature of the surface termination, X-ray photoelectron spectroscopy was applied to discover the stability of the surfaces and interfaces produced and to assist in assessing the chemical state of nitrogen-containing functional groups, microscopic techniques, including atomic force microscopy and transmission electron microscopy were employed to uncover the topographic properties and structure of the films based on titanium carbonitride that serve as a diffusion barrier and of the self-assembled amino-terminated layers utilized as platforms for biosensing devices. The preparation, structure, reactivity, and stability of these aminofunctionalized surfaces and interfaces will be discussed.

9:20am **SS2+EM-MoM4 Helium Atom Diffraction Measurements of the Surface Structure and Vibrational Dynamics of CH<sub>3</sub>-Si(111) and CD<sub>3</sub>-Si(111) Surfaces**, *J.S. Becker, R.D. Brown*, University of Chicago, *E. Johansson, N.S. Lewis*, California Institute of Technology, *S.J. Sibener*, University of Chicago

The surface structure and vibrational dynamics of CH<sub>3</sub>-Si(111) and CD<sub>3</sub>-Si(111) surfaces were measured using helium atom diffraction. The elastic diffraction patterns exhibited a lattice constant of 3.82 Å, in accordance with the spacing of the silicon underlayer. The high quality of the observed diffraction patterns indicates a high degree of long-range ordering for this novel interface. The vibrational dynamics were investigated by measurement of the Debye-Waller decay of the elastic diffraction peaks as the surface temperature was increased. The angular dependence of the specular ( $\theta_i = \theta_f$ ) decay revealed perpendicular mean-square displacements and He-surface well depths of  $1.0 \cdot 10^{-5} \text{ Å}^2 \text{ K}^{-1}$  and 7.5 meV for the CH<sub>3</sub>-Si(111) surface and  $1.2 \cdot 10^{-5} \text{ Å}^2 \text{ K}^{-1}$  and 6.0 meV for the CD<sub>3</sub>-Si(111) surface. Effective surface Debye temperatures of 983 K for CH<sub>3</sub> and 824 K for CD<sub>3</sub> were calculated. These unusually large Debye temperatures suggest that collisional energy accommodation at the surface occurs primarily through Si-C local mode. The parallel mean-square displacements were  $4.3 \cdot 10^{-4} \text{ Å}^2 \text{ K}^{-1}$  and  $4.5 \cdot 10^{-4} \text{ Å}^2 \text{ K}^{-1}$  for CH<sub>3</sub>- and CD<sub>3</sub>-Si(111) surfaces, respectively. The increase in thermal motion is consistent with interaction between the helium atoms and Si-CH<sub>3</sub> bending modes. These experiments yield new information on the dynamical properties of these robust and technologically interesting semiconductor interfaces.

9:40am **SS2+EM-MoM5 Comprehensive Descriptions of Surface Atomic Structure**, *J.C. Thomas, J. Mirecki Millunchick*, The University of Michigan, Ann Arbor, *N.A. Modine*, Sandia National Laboratories, *A. Van der Ven*, The University of Michigan, Ann Arbor **INVITED**

Comprehensive descriptions of surface atomic structure have been developed over the years for a wide range of metals and covalent crystals, but this understanding has typically been obtained only after extensive trial and error. Unfortunately, experimental and theoretical characterization of surfaces is complicated significantly in systems that can exhibit metastable surface reconstructions or in alloy systems, where atomic size mismatch and lattice mismatch strains play an important role and can give rise to phase coexistence. Clearly, a systematic and rigorous approach to determining surface structure is needed in order to explore surface phenomena in alloy systems or away from equilibrium. We have developed an approach that uses prior knowledge about the surface atomic structure of a pure system, along with first principles energy calculations and statistical mechanical methods, to systematically and efficiently explore new ground-state and near-stable surface reconstructions, finite temperature behavior, and alloying effects. We describe the automated generation of III-V (001) surface reconstruction candidates in the group V-rich regime and discuss how our approach is used to study the complex surface structure of the In<sub>x</sub>Ga<sub>1-x</sub>As (001) alloy, which exhibits nanoscale coexistence domains and where an unexplained ( $nx3$ ) reconstruction is observed over a wide range of conditions.

10:40am **SS2+EM-MoM8 The Structure of Metal-Rich (001) Surfaces of InAs and InSb**, *J.J. Kolodziej*, Jagiellonian University, Poland

Based on electron diffraction experimental observations the reconstructions of the indium-rich indium antimonide and indium arsenide (001) surfaces are assigned as  $c(8 \times 2)$  or closely related  $c(8 \times 2)/(4 \times 2)$ . At room temperature scanning tunneling and atomic force microscopy studies also evidence highly symmetric  $c(8 \times 2)$  or  $(4 \times 2)$  reconstructions. However, microscopic studies done at cryogenic temperatures indicate lowering of the surface structures symmetry from  $c2mm/p2mm$  to  $p2$ , structural domains, disorder and fluctuations. In the present paper we will show that the surfaces are well described by a so called zeta-family models with certain atomic rows occupied slightly above 50%. Atomic vacancies are confined to these rows and rapidly fluctuate at room temperature. Averaging effects cause that experiments done at elevated temperatures using slow methods evidence symmetric structures. In contrast, at low temperatures, the vacancies stabilize to form regular double-period structures along the rows, but this spontaneously leads to the complete surface structure having only  $p2$  symmetry group, structural domains and partial disorder on the surface. We have also identified a variety of local structures appearing at the domain walls. This complex surface structure is inherent to the thermodynamic equilibrium of the system as indicated by failed attempts to increase surface indium content by adsorption of In atoms from a gas phase. Density functional theory calculations confirm that the new surface structure is a minimum energy configuration at fixed stoichiometry. Simulated scanning tunneling microscopy images confirm proposed model of the structure.

11:00am **SS2+EM-MoM9 Monolayer Passivation of Ge(100) Surface via Nitridation and Oxidation**, *J.S. Lee, S. Bishop, T. Kaufman-Osborn, A.C. Kummel*, University of California at San Diego

11:20am **SS2+EM-MoM10 Formation of Titanium Sub-Oxide from TiO<sub>2</sub> ALD Films on Si and Ge Substrates after Vacuum Anneal**, *R.M. Methaapanon, P. Ardalán, S.F. Bent*, Stanford University

The formation of an oxide interlayer between a Si or Ge substrate and a metal oxide dielectric film has a direct influence on the physical and electrical properties of the field effect transistors made from these components. An oxide interlayer may form either during the deposition process or during a subsequent high temperature step. It is usually desirable to control or eliminate the formation of this oxide interlayer; one approach used is to create an oxide-free surface by chemically etching away the native oxide layer and adding a surface modifier such as hydrogen or halogens to inhibit further oxide formation.

In this work, we study the interlayer oxide formation on hydrogen-terminated silicon and halide-terminated germanium following TiO<sub>2</sub> atomic layer deposition (ALD). The surface analysis of TiO<sub>2</sub> films on silicon substrates is conducted immediately after the ALD process without exposure to ambient conditions by an integrated X-ray photoelectron spectroscopy (XPS)/ALD system. The results on hydrogen-terminated silicon show that no silicon oxide forms between the two materials during ALD at 100 °C. However, a silicon oxide interlayer is detected after annealing in ultrahigh vacuum. A concomitant depletion of oxygen in the TiO<sub>2</sub> films occurs, leading to generation of a Ti sub-oxide. The effect is shown to be correlated with both the annealing temperature and the thickness of the TiO<sub>2</sub> film. Control experiments carried out on TiO<sub>2</sub> film deposited by ALD on SiO<sub>2</sub>-coated silicon show significantly less depletion of oxygen in the TiO<sub>2</sub> films. Our results indicate that TiO<sub>2</sub> is the source of O for Si oxidation, and that migration of oxygen to this interface is a driving force for oxygen depletion in the TiO<sub>2</sub> film. The TiO<sub>2</sub> films on Br- and Cl-terminated germanium substrates are deposited by ALD at temperatures in the range of 100-300 °C and analyzed using *ex-situ* synchrotron radiation photoemission spectroscopy (SR-PES). Formation of titanium germanate (TiGeO<sub>x</sub>) was observed after annealing to 400 °C. Upon annealing to 700 °C, titanium sub-oxide formation is also observed for this system. However, this reduction was more pronounced in thinner TiO<sub>2</sub> films. The stability of these oxide structures upon annealing, and the prospect for eliminating the oxide interlayer in the TiO<sub>2</sub>/Si and TiO<sub>2</sub>/Ge systems will be discussed.

11:40am **SS2+EM-MoM11 Interfacial Effects of Near-surface Dopant Diffusion and Electrical Activation in Silicon**, *P. Gorai, Y. Kondratenko, E.G. Seebauer*, University of Illinois at Urbana-Champaign

Defect behavior in silicon can be controlled by manipulating the chemical state of nearby surfaces and solid-solid interfaces, with important implications for transistor fabrication by ion implantation and annealing. Silicon interstitials formed during the ion implantation step are responsible for unwanted transient enhanced diffusion (TED) of dopants, and affect the degree of dopant activation as well. Earlier work in our laboratory has shown that certain chemical treatments of surfaces and interfaces changes its ability to act as sinks for interstitials. The fundamental kinetic quantity describing "sink" behavior can be described by an annihilation probability ( $S$ ). Yet surfaces and interfaces also support electrically charged defects, which create local strong electric fields that influence the local motion of interstitials that are charged. The degree of charge buildup can be quantified by an electric potential ( $V_i$ ). The combined effects of  $S$  and  $V_i$  not only influence the annihilation of interstitials, but lead under some conditions to the pile up of electrically active dopant near the surface or interface. However, up to now, the precise nature of the interplay, including the most relevant time scales during annealing, has never been quantified. Through continuum modeling on the nanometer length scale, the present work provides such quantification. Differential equations describing the diffusion and reaction of silicon and boron interstitials are solved to yield the time evolution of boron profiles that are compared in important cases to experiment.

## Surface Science

Room: Picuris - Session SS1-MoA

### Nanocluster Reactivity

Moderator: G.B. Fisher, University of Michigan

2:00pm **SS1-MoA1**, *J. Jupille*, Inst. des Nanosciences de Paris, France, *M.-C. Saint-Lager*, *A. Bailly*, Inst. Néel, France, *G. Cabailh*, Inst. des Nanosciences de Paris, France, *S. Garaudée*, Inst. Néel, France, *R. Lazzari*, Inst. des Nanosciences de Paris, France, *P. Dolle*, Inst. Néel, France, *O. Robach*, CEA, France, *I. Laoufi*, Inst. Néel, France, *H. Cruguel*, Inst. des Nanosciences de Paris, France

The catalytic activity of supported gold nanoparticles [1] has generated great excitement over the two last decades. In contrast with the inertness of the bulk gold, the catalytic activity of gold nanoparticles increases dramatically as their size decreases. Most studies have focused on the catalytic oxidation of CO in particular because gold catalyzes that reaction at temperature as low as 200 K with an even better activity than platinum [2]. The origin of the property is still debated. Following the earlier suggestion that reactive sites are at the edge of the Au/oxide interface [2], it was alternatively proposed from density functional approaches, in the frame of a pure gold pathway, that the activity of gold nanoparticles mostly comes from low coordinated atoms [3]. In a very different manner, the activity of gold nanoparticles was attributed to a quantum size effect with a maximum in activity for two-atom-thick clusters [4].

To date, a direct characterization of the morphology of gold nanoclusters during catalytic reactions is lacking. The present work reports on observations by Grazing Incidence Small Angle X-Ray Scattering (GISAXS) of Au/TiO<sub>2</sub>(110) supported particles during the catalytic oxidation of CO, by using a dedicated set up. The analysis chamber, operated from ultra-high vacuum to normal pressure, is acting as a reactor [5]. The reactivity is determined by mass spectrometry. In the present case (20 mbar O<sub>2</sub> + 0.1 mbar CO on Au/TiO<sub>2</sub>(110) at 200 K), it rapidly increases for particles < 5 nm. GISAXS demonstrates that reacting gold particles are always three-dimensional with an aspect ratio H/D ≈ 0.6 (H and D are the height and diameter of the particles, respectively) which, for the smallest particles under study (D = 2 nm) still corresponds to 4 atomic layers of gold. The reaction mechanism is discussed via the relationship between the reactivity and the particle geometry.

[1] M. Haruta et al., *Chem. Lett.* 2 (1987) 405.

[2] G. R. Bamwenda et al., *Catal. Lett.* 44 (1997) 8.

[3] I. N. Remediakis et al., *Angew. Chem. Int. Ed.* 44 (2005) 1824.

[4] M. Valden et al., *Science* 281 (1998) 1647.

[5] M.-C. Saint-Lager et al., *Rev. Sci. Instrum.* 78 (2007) 083902.

2:20pm **SS1-MoA2** **Formation and Thermal Stability of Platinum Oxides on Size-Selected Platinum Nanoparticles: Support Effects**, *L.K. Ono*, *J.R. Croy*, *H. Heinrich*, *B. Roldan Cuenya*, University of Central Florida

Metal-loaded diblock-copolymer micelles have been used to synthesize size-selected self-assembled Pt nanoparticles (NPs). Ex-situ atomic force microscopy (AFM) and transmission electron microscopy (TEM) as well as in-situ X-ray photoelectron spectroscopy (XPS) measurements were performed to investigate the formation and thermal stability of PtO<sub>x</sub> species on Pt NPs supported on SiO<sub>2</sub>, ZrO<sub>2</sub>, and TiO<sub>2</sub> thin films. For a given particle size distribution, the role played by the NP support on the stability of Pt oxides was studied. Our findings are: (i) the formation of PtO<sub>x</sub> species upon atomic oxygen exposure and a two-step thermal decomposition process (PtO<sub>2</sub> → PtO → Pt) from 300 K to 600 K upon annealing in vacuum; (ii) the enhanced stability of PtO<sub>x</sub> species on ZrO<sub>2</sub> as compared to SiO<sub>2</sub> and TiO<sub>2</sub> upon annealing in O<sub>2</sub>, and in vacuum, possibly due to its stabilization at the NP/support interface; (iii) the onset of strong NP/support interactions above 600 K and the formation of Pt-Ti and/or Pt-Ti-O alloys for the Pt-NP/TiO<sub>2</sub> system associated with the creation of O-vacancies on TiO<sub>2</sub> upon annealing in vacuum, leading to the encapsulation of Pt by TiO<sub>x</sub> above 700 K.

The size-dependent stability of PtO<sub>x</sub> species in Pt NPs supported on SiO<sub>2</sub> as compared to bulk Pt(111) will be demonstrated based on temperature programmed desorption measurements.

2:40pm **SS1-MoA3** **Catalytic Reactivity of Mass Selected Nanoparticles**, *I. Chorkendorff*, Technical University of Denmark  
**INVITED**

It has recently been shown that for both the technologically important steam reforming process [1] and the methanation reaction [2] the rates are strongly dependent on the particles' size. This is ascribed to the nature of the nanoparticles and in particular the presence of step and kink sites on the nanoparticles. The abundance of such sites is expected to be very dependent on the size and the synthesis procedure. In this work we have investigated the nature of mass selected Ruthenium nanoparticles and specifically their reactivity with respect to gasses relevant for the above mentioned processes. Ruthenium is known to be a very good catalyst for both processes, and in some situations it may be superior to the commonly used Nickel catalyst despite its much higher price. Nanoparticles of sizes relevant for the above mentioned processes (2-10 nm) are manufactured by a sputter magnetron and subsequently mass selected by a quadropole mass spectrometer. The nanoparticles are soft landed on various substrates (HOPG or SiO<sub>2</sub>) and the influence and the advantages of the substrates will be discussed. The nanoparticles have been characterized in situ by SEM, AES, ISS, TPD and STM while ex-situ TEM has been used. The surface area and the stability of the nanoparticles were initially determined by temperature programmed desorption, and their ability to dissociate CO was evaluated using isotopically labeled gasses. The nature of the CO bonding and dissociation will be correlated with similar investigations on purpose stepped single crystals of Ruthenium (Ru(0 1 54)) demonstrating how the activity can be evaluated as a function of size. The reactivity of such mass selected nanoparticles has also been measured in a newly developed micro reactor on a chip with a volume of only 235 nl. This small volume combined with the fact that all the reactants and products can be led directly into a quadropole mass spectrometer for analysis allows for a close correlation of size and overall reactivity at high pressure and temperature conditions.

References:

[1] G. Jones, J. G. Jakobsen, S. S. Shim, J. Kleis, M. P. Andersson, J. Rossmel, F. Abild-Pedersen, T. Bligaard, S. Helveg, B. Hinnemann, J. R. Rostrup-Nielsen, I. Chorkendorff, J. Sehested, and J. K. Nørskov, "First Principles Calculations and Experimental Insight into Methane Steam Reforming over Transition Metal Catalysts", *J. Catal.* 259 (2008) 147-160.

[2] M. P. Andersson, F. Abild-Pedersen, I. Remediakis, J. Engbaek, O. Lytken, S. Hørch, J. H. Nielsen, J. Sehested, J. R. Rostrup-Nielsen, J. K. Nørskov, and I. Chorkendorff, "H<sub>2</sub> Induced CO dissociation on nickel surfaces", *J. Catal.* 255 (2008) 6-19.

3:40pm **SS1-MoA6** **Optical Nanocalorimetric Measurements of Pd Catalytic Light-Off Temperature and Catalytic Activity of Pd Nanoparticles-Size Dependent Effects**, *C. Langhammer*, *M.K. Larsson*, *B.H. Kasemo*, *I.L. Zorić*, Chalmers University of Technology, Sweden

4:00pm **SS1-MoA7** **Photochemistry on Metal Nanoparticles: Comparison of Nanosecond and Femtosecond Laser Induced NO Photodesorption from NO Dimer Layers on Supported Ag Nanoparticles**, *K.H. Kim*, *D. Mulugeta*, Fritz-Haber-Inst. der Max-Planck-Gesellschaft, Germany, *K. Watanabe*, Tokyo Univ. of Science, Japan, *D. Menzel*, Fritz-Haber-Inst. der Max-Planck-Gesellschaft and TU München, Germany, *H.-J. Freund*, Fritz-Haber-Inst. der Max-Planck-Gesellschaft, Germany

Metal nanoparticles (MNP) have special electronic and optical properties due to their dimensions being smaller than many length parameters of electrons and photons with solids; this leads to drastic changes of surface photochemistry [1]. For oxide-supported Ag nanoparticles (AgNPs), we have reported before on strong influences of the initial excitation (2.3 – 4.7 eV, in particular of Mie plasmons at 3.5 eV), and of the mean particle size (2 to 12 nm), on the photodesorption cross sections (PCSS) of NO from NO dimer layers [2,3], using nanosecond laser pulses. However, the mechanism of desorption remains the same as on Ag(111) [2-4], as indicated by detailed measurements of final state energy distributions (translational, rotational, and vibrational) of the desorbing molecules [5], except for the smallest particles at the highest excitation energy [2] where much higher final state energies are found. These results are compatible with desorption via a transient ion, negative (TNI) in most cases [4], and positive (TPI) in the latter case [2]. In the entire range of nanosecond laser excitation, strictly linear behavior is found.

We have now done similar measurements using femtosecond laser excitation (3.1 eV photons only), increasing the excitation density by more than 10<sup>4</sup> for the same photon fluences. No change is seen on Ag(111), while for AgNPs femtosecond plasmon excitation drastically increases the PCSS



as well as changes the dynamics, as indicated by different final state energies of the desorbed NO. We interpret this behavior as due to the confinement of excitation in the NPs which then leads to multiple pump-up of hot electrons during the laser pulse.

After a general survey of the basics of photochemistry on nanoparticles as compared to surfaces of bulk crystals, and of the indicated previous results, the recent measurements will be described and discussed, aiming at conclusions about their relevance for the understanding of excitations and photochemistry on nanoparticles.

[1] K. Watanabe, D. Menzel, N. Nilius, and H.-J. Freund, *Chem. Rev.* **106**, 4301 (2006)

[2] D. Mulugeta, K. H. Kim, K. Watanabe, D. Menzel, and H.-J. Freund, *Phys. Rev. Lett.* **101**, 14613 (2008).

[3] K. H. Kim, K. Watanabe, D. Menzel, and H.-J. Freund, *J. Am. Chem. Soc.*, **131**, 1660 (2009).

[4] F.M. Zimmermann and W. Ho, *Surf. Sci. Rep.* **22**, 127 (1995), and references therein.

[5] D. Mulugeta, Ph.D. Thesis, TU Berlin 2010; and D. Mulugeta, K. Watanabe, D. Menzel, and H.-J. Freund, to be published.

**4:20pm SS1-MoA8 H/D Exchange on Pd Nanoparticles: Effects of *cis*-2-butene Co-adsorption, and Implications for Isomerization and Hydrogenation of Alkenes over Pd, A. Savara, W. Ludwig, Fritz-Haber-Institut der Max-Planck-Gesellschaft, Germany, R.J. Madix, Harvard University, S. Schauer, H.-J. Freund, Fritz-Haber-Institut der Max-Planck-Gesellschaft, Germany**

On Pd(111), HD production from H<sub>2</sub> and D<sub>2</sub> is believed to occur by a Langmuir-Hinshelwood mechanism: H + D → HD. However, there has been discussion about the possibility that subsurface hydrogen plays a role in the associative desorption of hydrogen, and consequently the H/D exchange reaction.

The ability of Pd nanoparticles to accommodate weakly bound subsurface hydrogen differs from that of Pd(111) single crystals. As such, we have studied H/D exchange over well-defined Pd nanoparticles and Pd(111) for comparison, in the temperature range between 200 K and 350 K.

Over the Pd nanoparticles, the HD production occurs at a slightly higher rate than over Pd(111), but with a similar temperature dependence. From both the pressure and temperature dependence of the steady state reaction rate, it is not possible to tell if there is an influence from subsurface hydrogen on the HD production, over either the single crystals or the nanoparticles.

Unexpectedly, co-adsorbed *cis*-2-butene nearly deactivates the H/D exchange reaction, while the catalyzed isomerization of and hydrogenation of *cis*-2-butene occur with persistent activity under these reaction conditions – indicating that hydrogen/deuterium is still available on the catalyst despite deactivation of the H/D exchange reaction.

We interpret these results to be indicative of a “portal” model for dissociative hydrogen adsorption in the presence of butene. In a “portal” model, adsorption occurs at dispersed sites on the surface, and from there the adsorbates diffuse to the rest of the surface prior to reaction. Under this interpretation, hydrocarbons block most of the surface sites for hydrogen, thus inhibiting both dissociative adsorption of hydrogen molecules and recombination of adsorbed hydrogen atoms. Consequently, hydrogen molecules dissociate on the minority of open spaces remaining, and the formed hydrogen atoms diffuse between the organic adsorbates. These hydrogen atoms then react with organic adsorbates, while only a small percentage of hydrogen atoms find an open space at the same time as a second hydrogen/deuterium atom to desorb with: thereby preventing HD formation under these conditions, while persistent isomerization and hydrogenation occurs. These findings may have important kinetic and mechanistic implications for alkene hydrogenation and isomerization over Pd catalysts, and potentially other transition metal catalysts.

**4:40pm SS1-MoA9 Cu/CuOx Nanoclusters on ZnO(1010): Electronic, Catalytic, Morphological Structure, Z. Zhang, M. Patterson, M. Ren, Y. Losovyj, J. Flake, R.L. Kurtz, P.T. Sprunger, Louisiana State University**  
ARUPS, STM, and EELS has been used to study the electronic, atomic and chemical structure of Cu and CuO nanoclusters on non-polar ZnO(1010) surface. Within the backdrop of developing high performance CO<sub>2</sub> reduction catalyst (methanol production), our studies show that higher yield rate are found for Cu(I) surface species. ARPUS results from nanocluster CuOx/ZnO reveals that the oxidation process is highly dependent on the cluster size (smaller size). Moreover, CO adsorption (BE and vibrational) are distinctly different between Cu and CuOx nanoclusters supported on ZnO. Reaction studies confirm that methanol production is 4 times higher on partially oxidized Cu nanoclusters. Photoemission shows a small amount of Cu(II) even upon repeated oxidation/annealing processes, indicating a

preferential stability of Cu(I) in the supported nanoclusters, due to interfacial effects with the substrate. This talk will include results from EELS/TPD and STM/AFM studies to better elucidate the chemical adsorption and intermediates as a function of CuOx size and structure.

**5:00pm SS1-MoA10 Femtosecond-laser Photoemission of Deposited MoxSy Clusters on Al2O3/NiAl(110), J. Zhou, State University of New York at Stony Brook, N. Camillone III, Brookhaven National Laboratory, M.G. White, State University of New York at Stony Brook**

The electronic structures of supported size-selected Mo<sub>x</sub>S<sub>y</sub> clusters on an ultrathin aluminum oxide film on NiAl(110) are studied by two-photon photoemission spectroscopy. The Mo<sub>x</sub>S<sub>y</sub> clusters are produced by magnetron sputtering in gas phase and selected by a quadrupole mass filter. The mass-selected clusters are deposited on the ultrathin aluminum oxide film which has wide band gap to minimize the electronic interaction between clusters and NiAl(110) substrate. The formation of the aluminum oxide film on NiAl(110) results in a 0.3 eV decrease in work function and disappearance of the surface state of NiAl(110). With 0.1 ML Mo<sub>4</sub>S<sub>6</sub> deposited on the surface, the photoemission spectrum is similar with that of bare alumina oxide film because of the absence of interaction between isolated clusters on the film. When the cluster coverage increases to 0.2 ML, some features origin from the cluster are observed and reveal that the clusters are semiconductor with a band gap of about 0.6 eV. A variety of other molybdenum sulfide clusters, Mo<sub>x</sub>S<sub>y</sub> (x/y: 2/6, 3/7, 5/7, 6/8, 7/10), are also investigated and they exhibit different electronic properties with specific molybdenum to sulfide ratio.

**5:20pm SS1-MoA11 Formation of Homogeneous Rh Clusters on Al2O3 from [Rh<sup>III</sup>(OAc)<sub>2</sub>]<sub>2</sub> Precursor Elucidated by STM and XAFS Analyses, Z.W. Chen, Osaka University, Japan, W.-J. Chun, International Christian University, Japan, K. Fukui, Osaka University, Japan**

## Surface Science

**Room: Santa Ana - Session SS2-MoA**

## Stress and Bonding Energetics in Nucleation and Growth

**Moderator: G.L. Kellogg, Sandia National Laboratories**

**2:00pm SS2-MoA1 Epitaxy of Disilane on Si(100)-H using Scanning Tunneling Microscope-induced Hydrogen Depassivation Patterns, J.B. Ballard, J.R. Von Ehr, J.N. Randall, J. Alexander, R. Saini, Zyvex Labs, M. Huang, H.-S. Choi, K.J. Cho, J.-F. Veyan, Y.J. Chabal, University of Texas at Dallas, J.W. Lyding, University of Illinois at Urbana-Champaign**  
**INVITED**

Atomically precise manufacturing on silicon requires a precise understanding both of patterning techniques as well as the chemistry of molecular deposition. Using a UHV Scanning Tunneling Microscope (STM), we show progress towards a constant temperature process for creating epitaxial structures on Si(100) by alternating STM induced hydrogen depassivation and disilane dosing of the atomically flat surfaces. Emphasizing the detailed mechanisms of patterned deposition, large area patterns are studied as well as patterns consisting of small numbers of dangling bonds revealing a minimum size constraint for patterning. Work is being done towards elevated temperature deposition of disilane with the goal of enhancing epitaxial versus amorphous growth. In addition to growth on atomically flat regions three-dimensional structures are studied. Large area IR spectroscopy as well as theoretical modeling of small area deposition support the STM results. A successful understanding of the physics of patterned epitaxy will lead the way toward high precision manufacturing of previously unobtainable structures and devices.

**2:40pm SS2-MoA3 Stress Balance in Nanopatterned N/Cu(001) Surfaces, T.S. Rahman, S. Hong, University of Central Florida, E.Z. Ciflikli, B.J. Hinch, Rutgers University**

Helium atom scattering (HAS) and density functional theory (DFT) within pseudopotential methods have been used to investigate stress balance in nano-patterned N/Cu(001) surfaces. HAS shows that the stress-relief-driven lateral expansion of the averaged lattice parameter within finite-sized N containing patches reduces, with increasing N coverage (and decreasing stripe widths), from 3.5% to 1.8% and then, beyond a critical exposure, the patches' lateral expansion increases again slightly to 2.4%. This implies that, in this higher coverage range, the compressive stress is partially relieved with another mechanism; namely Cu vacancy trenches are nucleated. The trenches serve to enable further surface stress reduction and expansion in the N lattice parameters. In full agreement with above and



previous experimental observations, DFT calculations show that an optimized N-induced  $c(2 \times 2)$  structure has a net surface stress level  $\sim 4$  N/m and such stress is effectively relieved when stripes of clean Cu(001) form along the  $\langle 100 \rangle$  direction or when trench-like steps of Cu atoms form along the  $\langle 110 \rangle$  direction. On the other hand, the calculations demonstrate that (contrary to the suggestions of Driver *et al.*[1]) rumpling displacements within the outermost Cu layer do not act to relieve the compressive surface stress levels while clock-like displacements could relieve stress levels, although such displacements are energetically unstable.

[1] S. M. Driver, J-T Hoefl, M. Polcik, M. Kittel, R. Terborg, R. L. Toomes, J-H. Kang, and D. P. Woodruff, *J. Phys. Cond. Mat.* 13, L601 (2001).

Work supported in part by NSF Grant CHE-0741423

### 3:00pm SS2-MoA4 The Effect of Lattice Strain on Adatom Diffusion Barriers on Terraces and Step Edges, T.S. Rahman, H. Yildirim, University of Central Florida

While it is well known that lattice strain has an effect on adatom diffusion barriers, its material specificity has not yet been explored. In a comparative study based on density functional theory, we find that self diffusion barriers for Pd(100) terraces and step edges are not affected by tensile strain (up to 5%) as much as their counterparts on Ag(100) and Cu(100). This difference is particularly significant for the step edge barriers (Ehrlich-Schwobel) which for the cases of the Ag and Cu surfaces may be reduced to zero (or become negative) under strain but remain positive for the Pd surface. In other words, growth modes on Pd surfaces are less susceptible to changes in strain, as compared to Ag and Cu surfaces. We trace these differences to local geometric response and characteristics in the electronic structure. In particular we argue that strain is less effective in changing diffusion barriers on transition metal surfaces than on the coinage metal surfaces.

### 3:40pm SS2-MoA6 Long-range Self-ordered Ge Nanostressors on Silicon Nanomembranes, M. Huang, F. Chen, University of Wisconsin-Madison, Y. Zhang, University of Utah, D.M. Paskiewicz, F.S. Flack, D.E. Savage, University of Wisconsin-Madison, F. Liu, University of Utah, M.G. Lagally, University of Wisconsin-Madison

Silicon nanomembranes (SiNMs) are defect-free, single-crystal Si sheets with thickness ranging from 2 to 500 nm. This thinness makes them flexible, transferable, bondable and, most importantly, mechanically ultracompliant. This compliance makes nanomembranes fundamentally different from bulk materials [1,2]. Growth of three-dimensional Ge islands (Ge "huts", or quantum dots) on freestanding Si membranes exploits this unique mechanical behavior to induce self-organization of the dots, resulting in a periodic strain in Si nanomembranes or nanoribbons [1,2].

To understand better the effects of strain and substrate compliance on lattice-mismatched heteroepitaxy, we grow Ge islands on stretched (i.e., tensilely strained), freestanding, (001)-oriented SiNMs. We drape a SiNM over a substrate patterned with high ridges. The bending of the SiNM over the edges of the ridges creates regions of local strain that enhance and direct Ge island nucleation. The ridge height and separation are varied to manipulate the draped-membrane strain. Ge 3D islands are grown on the draped SiNM via chemical vapor deposition or molecular beam epitaxy. We demonstrate two-dimensional self-ordering of a single layer of Ge dots, with uniform dot size and spacing. The islands, however, differ from the classic [105]-faceted structures. We find that, while our new Ge dots still have square or rectangular bases, they have steeper facets than those of conventional Ge "huts". We perform finite-element analysis to map the local strain in the draped membrane and to investigate the influence of membrane thickness and substrate ridge height on the dot ordering.

This work is supported by DOE, NSF, and AFOSR.

#### References:

[1] M. Huang et. al., *ACS Nano* 3, 721 (2009)

[2] H-J. Kim-Lee et. al., *Phys. Rev. Lett.*, 102, 226103 (2009)

### 4:00pm SS2-MoA7 Atomic Layer Epitaxy of Ge on Si(100)-(2x1), J.-F. Veyan, M.P. Nadesalingam, M. Huang, H. Dong, University of Texas at Dallas, J.N. Randall, Zyvex Labs, W.P. Kirk, J. Cho, R.M. Wallace, Y.J. Chabal, University of Texas at Dallas

Atomic Layer Epitaxy (ALE) is a critical step for constructing 3-D structures at the atomic scale, necessary for Atomically Precise Manufacturing (APM) of new devices such as quantum dots. We present here a comprehensive study of Ge ALE on Si(100) $\times$ (2x1) surface using digermane (Ge<sub>2</sub>H<sub>6</sub>) as a precursor. Si(100) samples are clean at passivated by SiO<sub>2</sub> by standard wet chemical procedures. The oxide is then removed in

ultra high vacuum ( $1.5 \times 10^{-10}$  Torr) by resistive annealing (1173 K). The clean and Ge<sub>2</sub>H<sub>6</sub> exposed Si(100)-(2x1) surfaces are characterized using Infrared absorption spectroscopy (IRAS) and X-ray Photoelectron Spectroscopy (XPS). IRAS measurements are performed in transmission at the Brewster angle, and XPS measurements at a takeoff angle of 45 degrees. The Ge<sub>2</sub>H<sub>6</sub> is introduced through either capillaries for the IR measurements or a directed doser for the XPS studies. In both cases, the fluxes on the samples are calculated to be  $\sim 10^{-6}$  Torr.sec.

At room temperatures, a saturation coverage was achieved on a clean Si(100) surface after  $\sim 10$  L, corresponding to an estimated sticking coefficient of  $\sim 0.5$ . IR absorption bands in the  $\sim 1950$ - $2000$   $\text{cm}^{-1}$  range indicate that mono- (GeH), di- (GeH<sub>2</sub>) and tri- (GeH<sub>3</sub>) -hydrides species are chemisorbed on the surface, consistent with the shifts of the Ge 2p<sub>3/2</sub> core level observed by XPS. In addition, a feature observed at  $2098$   $\text{cm}^{-1}$ , associated with silicon monohydride (Si-H), indicates that Ge<sub>2</sub>H<sub>6</sub> dissociates via beta-hydride elimination, involving the intermediate states Si-H and Si-GeH<sub>2</sub>-GeH<sub>3</sub>. Measurements of Ge-H and Si-H stretch intensities at saturation coverage as a function of substrate temperature from 173 K up to 700 K suggest that the mechanism involved in the chemisorption of Ge<sub>2</sub>H<sub>6</sub> on Si(100) proceeds via dissociation of Ge<sub>2</sub>H<sub>5</sub> into GeH<sub>3</sub>, GeH<sub>2</sub>, and GeH. At a temperature of 600 K, all the vibrational modes associated with Ge hydrides species vanish, which is consistent with the thermal desorption temperature of H on pure Ge(100) surface. However, the intensity of the Si-H vibrational mode increases with the temperature, reaching a maximum intensity around 600 K, and then decreases and vanishes at 713 K, which is 100 K lower than the normal desorption temperature of H on pure Si(100). A quantitative understanding of both the chemisorption pathway and desorption mechanisms is achieved using Density Functional Theory (DFT) calculations.

This work is supported by the Defense Advanced Research Project Agency (DARPA), Space, Naval Warfare Center, San Diego (# N66001-08-C-2040), and the Emerging Technology Fund of the State of Texas to the A.P.M. Consortium.

### 4:20pm SS2-MoA8 The Influence of Metal - Substrate Bonding Energetics on Metal Atom Adsorption, Cluster Nucleation and Film Growth, C.T. Campbell, University of Washington INVITED

Oxide-supported late transition metal nanoparticles form the basis for many important industrial catalysts. The activity, selectivity and sintering rates of these catalysts can depend strongly on the particle size, the oxide support, and the extent of reduction of the oxide. The microkinetics of sintering are essentially the same as for nucleation and growth. All of these kinetic properties are closely related to the variation of metal atom energy (chemical potential) with nanoparticle size. We will review our calorimetric measurements of the energies of metal atoms in nanoparticles supported on different oxide surfaces, and relate those to nucleation/growth kinetics. We will discuss these results in the light of DFT calculations by our collaborators, H. Jonsson, G. Henkelman and L. Xu. The stability of Ag nanoparticles increases with particle size on both MgO(100) and reduced CeO<sub>2</sub>(111), until the number of atoms per particle exceeds  $\sim 5000$ . At any given size, Ag nanoparticles have much higher stability on reduced CeO<sub>2</sub>(111) than on MgO(100). This difference is due to the much larger adhesion energy of Ag nanoparticles to reduced CeO<sub>2</sub>(111) compared to MgO(100). Increasing the extent of reduction of the CeO<sub>2</sub> surface increases Ag particle stability. The energetics and growth of Li and Ca on MgO(100) are dominated by defect sites, and differences in migration barriers there. The migration rates of Pd clusters on MgO(100) vary in unusual ways with size below 5 atoms, and this impacts nucleation.

The above results for oxide surfaces will be contrasted with similar studies of metal film growth on polymer surfaces, where diffusion of metal atoms below the surface and highly exothermic reactions with subsurface heteroatoms can dominate the early stages of growth.

Work supported by NSD and DOE-OBES.

### 5:00pm SS2-MoA10 Growth of Ag on Ge(110) and Ge(111) Studied by LEEM, C. Muller\*, S. Chiang, University of California, Davis

We studied Ag island growth on reconstructed Ge(110) and Ge(111) surfaces with low energy electron microscopy (LEEM). At 480 C, one-dimensional (1D) island growth was observed on Ge(110). Island nucleation proceeds from defects in the Ge substrate, with island thickness corresponding to the size of the substrate defect where the island nucleation occurred. As Ag is deposited, islands lengthen but do not thicken. At 9 ML, Ag coverage islands were up to 10  $\mu\text{m}$  long, and thicknesses varied from 100 nm to 250 nm. One-dimensional islands were also produced by Ag deposition at room temperature followed by sample heating. Round Ag islands resolvable in LEEM were observed and coalesced into many long

\* Morton S. Traum Award Finalist

1D islands as temperature was increased. Islands formed by deposition at room temperature followed by heating to a particular temperature were shorter and thicker than islands grown by deposition on a substrate held at that same temperature. Ag growth on Ge(111) is Stranski-Krastanov. Multilayer Ag island formation begins after the Ag ( $\sqrt{3}\times\sqrt{3}$ )R30° phase completes at one monolayer. Ag islands exhibit hexagonal faceting. For both the Ge(111) and Ge(110) surfaces, Ag islands induce changes in the Ge substrate that leave a “footprint” observable in LEEM after all Ag has been desorbed from the surface.

\*Funding from NSF CHE-0719504; NSF PHY-0649297 (REU)

5:20pm **SS2-MoA11 Growth of Au Islands and Thin Films on NiAl(110): STM Experiments and DFT - Based Analysis**, *C. Yuen, T. Duguet*, Iowa State University & Ames Laboratory U.S. D.O.E., *Y. Han*, Institute of Physical Research and Technology, *J. Evans*, Iowa State University, *P.A. Thiel*, Iowa State University & Ames Laboratory U.S. D.O.E.

Both Au(110) and Ag(110) have a  $0.29\times 0.41$  nm<sup>2</sup> rectangular surface unit cell matching almost perfectly that for NiAl(110). This provides the opportunity to grow epitaxial thin films free of lateral mismatch strain. One might expect in both cases layer-by-layer growth of two-dimensional fcc(110) islands given the low surface energy of Au and Ag. However, observed behavior is distinctly different for the two metals. Our STM experiments of Au deposition on NiAl(110) between 200-350 K reveal initial formation of islands with a height of 0.23-0.25 nm. Island densities and size distributions are determined. At 300 K, islands are irregular and regions with 3x1 periodicity are sometimes evident. For the coverage of about 60%, there is significant population by islands of second "layer" or level with heights of ~0.24 nm. Extensive DFT analysis were performed to determine low-energy structures of supported Au films for various coverages. Isolated Au atoms on NiAl(110) prefer sites between two Ni separated by 0.29 nm. However, rather than a simple (110) overlayer with Au at these sites, lower energy structures exist also populating 3-fold sites (e.g., NiAl<sub>2</sub>) and displaying combinations of square and hexagonal motifs of adatoms. We believe that observed islands have such structures and present a model for their formation. Behavior is contrasted with Ag/NiAl(110) where bilayer Ag(110) islands form due to quantum size effects (QSE) [1]. However, Ag/NiAl(110) is known to exhibit a bilayer-by-bilayer growth mode due to QSE [1], and the bulk Au(110) surface exhibits 2x1 and 3x1 reconstructions.

[1] Y. Han et al. PRL 100, 116105 (2008); PRB 81, 115462 (2010).

# Tuesday Morning, October 19, 2010

## In Situ Microscopy and Spectroscopy Topical Conference

Room: Acoma - Session IS+SS-TuM

## In Situ Spectroscopy – Interfacial Chemistry/Catalysis

Moderator: D.R. Baer, Pacific Northwest National Laboratory

8:00am **IS+SS-TuM1 Oxidation and Reduction of Pd(100) and Supported Pd Nanoparticle Model Catalysts**, *R. Westerstrom, S. Blomberg, N. Martin, J. Gustafson, E. Lundgren, J.N. Andersen, M.E. Messing, K. Deppert*, Lund University, Sweden, *H. Bluhm*, Lawrence Berkeley National Laboratory, *O. Balmes, R. van Rijn*, ESRF Grenoble, France

Using *in situ* high pressure X-ray photoelectron spectroscopy, we study the oxidation and reduction by O<sub>2</sub> and CO in the mbar pressure regime of Pd(100) and Pd nanoparticles of 15 or 35 nm diameter supported on a SiO<sub>x</sub> substrate. We find the oxidation behavior of these model catalysts to be qualitatively similar, with an ultra-thin surface oxide forming prior to the onset of bulk PdO formation. However, the Pd nano particles are observed to bulk oxidize at sample temperatures 40 degrees lower than Pd(100). For the PdO surface, we identify a core level shift of the Pd 3d and O 1s levels of -0.3 and -1.3 eV, respectively, relative to the corresponding levels in bulk PdO. In a CO atmosphere, the Pd 3d shift changes by +0.55 eV due to CO adsorption, and CO adsorbed on the oxide can be identified in the C1s. Also the reduction by CO is similar between the single crystal and the nanoparticle samples, but after the complete removal of the oxide, the nanoparticles incorporate carbon to form a Pd carbide. This is not observed for the single crystal sample.

8:20am **IS+SS-TuM2 In-situ XPS Studies of CO<sub>2</sub> Captured by Aqueous Monoethanolamine (MEA) Solutions**, *T. Lewis, A. Chaudhuri*, University of California, Irvine, *M. Faubel*, Max-Planck Institut fur Dynamik und Selbstorganisation, Germany, *B. Winter*, Helmholtz-Zentrum Berlin fur Materialien und Energie, Germany, *J.C. Hemminger*, University of California, Irvine

XPS on a micro liquid jet has been used to study solutions of monoethanolamine (MEA), which is commonly used in gas stream scrubbing for carbon dioxide capture. It is likely that interactions between CO<sub>2</sub> and the aqueous MEA solution at the gas/liquid interface are important to this process, yet there is little information available concerning the spatial distribution of species at the interface of such solutions. In the present work, aqueous solutions of MEA with a range of pH values as well as solutions of MEA reacted with CO<sub>2</sub> have been measured using tunable synchrotron radiation from the BESSY facility in Berlin, where the photoelectron kinetic energy can be varied to obtain depth dependent composition information. N1s photoemission spectra allow for the identification of protonated versus unprotonated MEA by the different binding energies of the two species, and likewise, C1s spectra allow for the determination of CO<sub>2</sub>-reacted versus unreacted MEA. Depth profiling reveals that deprotonated MEA is more surface active than both protonated MEA and the CO<sub>2</sub>-reacted species. The mechanism of the reaction of CO<sub>2</sub> with aqueous solutions of monoethanolamine will be discussed in light of our results.

8:40am **IS+SS-TuM3 Photoelectron Spectroscopy Under Humid Conditions**, *H. Bluhm*, Lawrence Berkeley National Laboratory **INVITED**

The interaction of water with surfaces plays a major role in many processes in the environment, atmosphere and technology. Weathering of rocks, adhesion between surfaces, and ionic conductance along surfaces are among many phenomena that are governed by the adsorption of molecularly thin water layers under ambient humidities. The properties of these thin water films, in particular their thickness, structure and hydrogen-bonding to the substrate as well as within the water film are up to now not very well understood. Ambient pressure photoelectron spectroscopy (APXPS) is a promising technique for the investigation of the properties of thin water films. We will discuss the basics of APXPS as well as the particular challenges that are posed by investigations in water vapor at Torr pressures, as well as show examples of the application of APXPS to the study of water films on metals and oxides.

9:20am **IS+SS-TuM5 Chemistry of Aminoacids at the Water – Metal Interfaces under UHV and AP Conditions**, *A. Shavorskiy*, Lawrence Berkeley National Laboratory, *T. Eralp*, The University of Reading, UK, *F. Aksoy, Z. Liu, H. Bluhm*, Lawrence Berkeley National Laboratory, *A. Cornish, D. Watson*, The University of Reading, UK, *K. Schulte, J.N. Andersen*, Lund University, Sweden, *G. Held*, The University of Reading, UK

Many important catalytic reactions take place at the interface between a solid catalyst and a solution, in particular aqueous solutions play a crucial role in all biological systems. The presence of the solvent at the solution-catalyst interface can dramatically change the chemical surface properties and, therefore, the entire catalytic process. Although surface science has been very successful in studying gas-surface reactions, most UHV-based surface science techniques cannot be applied to the co-adsorption of solvent and reactant molecules of important reaction systems because the solvent desorption temperature in UHV is too low to allow co-adsorption at realistic reaction temperatures. In order to keep significant amounts of water adsorbed near room temperature pressures of up to 1 mbar are needed for most metals. Recently, ambient pressure X-ray photoelectron spectroscopy (APPEs), has become available for studying these systems at close-to-real conditions [Bluh09].

For the experiments reported here we chose to study the influence of water on the adsorption of glycine and alanine on Pt[111] and Pt[110] in UHV and on Cu[110] at near-ambient pressure. The comparison between results obtained in UHV and at AP allows us to reveal importance of the reaction conditions (in particular reaction pressure and temperature) on the chemical composition and stability of the molecular adlayers on metals. It also bridges the pressure gap in studies of such kind of bio-related systems. Our results show an absence of any noticeable changes in the chemical composition of the aminoacids on Pt[111] and Pt[110] when co-adsorbed with water in UHV. On the other hand we observed clear decrease of the amino acid desorption temperature and a change of the desorption pathway (compared to UHV [Barl05]) on Cu[110] when the H<sub>2</sub>O pressure is increased above 10<sup>-5</sup> mbar. Two possible mechanisms of lowering the stability of the amino acids in the presence of water are discussed: (a) oxidation of the amino acid by OH or O or (b) hydrogenation of the anionic amino acid followed by desorption of the less stable intact form [Jone06].

[Bluh09] H. Bluhm, J. El. Spec. Rel. Phen., doi:10.1016/j.elspec.2009.08.006, 2009.

[Jone06] G. Jones et al Surf. Sci. 600 (2006) 1924.

[Barl05] S. M. Barlow et al Surf. Sci 590 (2005) 243.

[Ande07] K. Andersson et al. J. Phys. Chem. C 111 (2007) 14493.

9:40am **IS+SS-TuM6 In-situ Ambient Pressure XPS Observations of Reversible Charge Storage in Ni Electrodes**, *A.H. McDaniel, F. El Gabaly*, Sandia National Laboratories, *M. Grass, Z. Liu*, Lawrence Berkeley National Laboratory, *K.F. McCarty*, Sandia National Laboratories, *H. Bluhm*, Lawrence Berkeley National Laboratory

10:40am **IS+SS-TuM9 Hard X-ray Photoelectron Spectroscopy: an Effective Probe for Electronic Structure in Materials Science**, *W. Druhe*, Deutsches Elektronen-Synchrotron DESY, Germany **INVITED**

The use of hard X-ray excitation in the range from about 2 to 15 keV for photoelectron spectroscopy (HAXPES) is a rapidly emerging technique at synchrotron sources worldwide since it significantly widens the range of applications, in particular in the study of complex materials and buried nano-structures or interfaces. Due to the increased electron inelastic mean free paths, it becomes possible to probe chemical composition and electronic structure in the bulk of materials with considerable sensitivity, down to typically 10-20 nm at 10 keV kinetic energy. This not only is essential in the study of complex correlated materials which often exhibit a modified surface electronic structure but also is very relevant for technologically interesting multi-layered materials with buried interfaces. As an additional benefit, "as-grown" materials can be measured without need for prior surface treatment.

A drawback is the rapidly decreasing photoelectric cross section in the hard X-ray range, especially for shallow core levels and valence states, and - until recently - the limited availability of suitable high-voltage electron spectrometers. The latter are available meanwhile and the high X-ray flux at undulator beamlines has been shown to effectively compensate the cross section decrease. In addition, the X-ray tunability over a large energy range not only allows to significantly vary the electron probing depths and the photoelectric cross sections, but also enables the study of resonance phenomena at deep inner-shell thresholds. Further, the excitation of X-ray

standing wave fields within single crystals or multi-layered structures can be effectively used to correlate geometric and electronic structure information.

In the past five years, HAXPES activities at synchrotron laboratories worldwide have increased dramatically and the trend continues as new instruments are currently being built and planned. A brief overview is given on the current activities worldwide, both on instrumental developments and results obtained. At DESY, HAXPES experiments routinely use a dedicated spectrometer at an X-ray wiggler with moderate energy resolution (~0.5 eV), well suited for many core level studies. Very recently, high-resolution studies also became possible at DESY with the availability of PETRA III, a new storage ring source providing the highest X-ray brilliance.

11:20am **IS+SS-TuM11 Novel Applications in Surface Science – *In situ* Sample Analysis in Extreme Environments, A. Thissen**, SPECS Surface Nano Analysis GmbH, Germany

Modern devices are often only functional in environments far away from ultrahigh vacuum, still being the standard operation conditions for all Surface Science techniques. In parallel the importance of surfaces for the correct device operation is continuously increasing due to miniaturization down to the nanoscale. To contribute to advanced materials analysis in future means using Photoelectron spectroscopy, Scanning Probe Microscopies and related techniques in the generic or near generic device environments. This means high, elevated or near ambient pressures of defined working gas mixtures, liquid media, potentials or magnetic fields applied. Also extremely low or high temperatures might be necessary. In past all standard Surface Science Techniques did not work under these *extreme* environments. This work summarizes and presents existing solutions nowadays and future development routes to new instruments and materials analysis methods being functional under these working conditions. Opportunities and limits will be discussed. From the perspective of a supplier of scientific instruments. Finally applications, examples and results from existing *In situ* methods like high pressure treatments cells, complete High Pressure or Near Ambient Pressure Photoelectron Spectroscopy Systems (NAP-PES or HP-SPM), liquid and electrochemical cells, Liquid sample “manipulators“, and concepts and status of equipment working in highest or lowest temperatures, high magnetic fields and static or dynamic potentials will be demonstrated.

## Surface Science

Room: Picuris - Session SS1-TuM

## Catalysis on Metal and Alloy Surfaces

Moderator: A.J. Gellman, Carnegie Mellon University

8:00am **SS1-TuM1 Sulfur-Induced Reconstruction of the Ag(100) Surface, S.M. Russell, M. Shen**, Iowa State University, C.J. Jenks, D.-J. Liu, Ames Laboratory, US-DOE, P.A. Thiel, Iowa State University & Ames Laboratory, US-DOE

Sulfur adsorption on Ag(100) is the object of this investigation because sulfur affects reshaping and decay of Ag nanostructures on this, and other, surfaces. We have studied sulfur on Ag(100) using STM. Consistent with prior LEED work [1-2], we find two structures that coexist at room temperature: a p(2x2) chemisorbed phase, and a ( $\sqrt{17} \times \sqrt{17}$ )R14° reconstruction, the latter being the phase with higher sulfur coverage. As sulfur coverage increases, sulfur atoms replace Ag in the surface plane to form the  $\sqrt{17}$ , resulting in ejection of Ag and development of  $\sqrt{17}$  islands on the terraces. DFT supports a model in which 5 Ag atoms are ejected per unit cell. In STM, the dominant local motif of the  $\sqrt{17}$  reconstruction consists of rectangular groups of (primarily) four sulfur atoms, very similar to sulfur on Cu(100) in the  $\sqrt{17}$  phase [3]. At room temperature, the  $\sqrt{17}$  islands are dynamic, and can develop extensions of disordered material that link and island, transiently, to another  $\sqrt{17}$  island or domain.

### References

- [1] G. Rovida and F. Pratesi, *Surf. Sci.* **104**(2-3), 609 (1981).
- [2] M. P. Sotro and J. C. Boulliard, *Surf. Sci.* **162**(1-3), 285 (1985).
- [3] M. L. Colaianni and I. Chorkendorff, *Phys. Rev. B* **50**(12), 8798 (1994).

8:20am **SS1-TuM2 In-situ Spectroscopic Investigation of Adsorption and Reaction of Pyridine Molecules on Modified Pt Surfaces, R. Denecke, C. Wöckel, K. Fischer, S. Wickert**, Universität Leipzig, Germany, R. Streber, Universität Erlangen, Germany

Using high-resolution and time-dependent x-ray photoelectron spectroscopy (XPS) adsorption and reaction processes can be followed *in-situ*. From the data, adsorbed species as well as reaction intermediates and products can be

determined and quantitatively analyzed. Time-dependent data allow for the determination of kinetic parameters.

We are applying this method to pyridine molecules adsorbed on flat and stepped Pt surfaces. Using a regularly stepped Pt(355) surface with (111) oriented terraces which are five atomic rows wide and (111) oriented monatomic steps, C 1s and N 1s core level data are recorded during adsorption at various temperatures. As additional parameter, the free Pt terrace width is varied by deposition of Ag atoms on the surface. At 300 K, they form rows along the step edges, thus effectively reducing the terrace width. Following the core level data while increasing the temperature with a fixed heating rate, temperature-programmed XPS data allow to follow the thermal reaction of the adsorbed species. The experiments have been performed at the synchrotron radiation facility BESSY II in Berlin.

Literature reports a temperature- and coverage-dependent reorientation of the pyridine molecules on Pt(111) [1]. While at 300 K an upright molecule is proposed, the situation changes for low temperatures from flat-lying at low to upright at higher coverages. In line with these reports, we observe distinct changes in the core level binding energies and intensities. While at 200 K only one strong N 1s feature is observed for all coverages, there is a change from two features to one for 300 K. Here, the remaining feature is observed at a higher binding energy. Temperature-dependent data show the change from the low to the high energy feature. This is accompanied by respective changes in the C 1s data, thus suggesting again temperature- and coverage-dependent changes.

The presence of steps and especially their decoration by Ag changes the situation quite drastically. This manifests itself in changed binding energies and reaction schemes. From a comprehensive analysis a scheme for adsorption and thermal reaction of pyridine on Platinum surfaces is derived.

[1] S. Haq, D.A. King, *J. Phys. Chem.* **100** (1996) 16957.

8:40am **SS1-TuM3 Mechanisms of Catalytic Processes on Au: Imaging, Spectroscopy and Reactivity, C. Friend, Xu, Liu, Baker, Haubrich, R.J. Madix**, Harvard University **INVITED**

The need for energy-efficient catalytic processes and the long fascination with Au as a material has spurred intense activity in the investigation of gold-based catalysis. There is on-going discussion of the origin of the activity of gold for oxidation reactions, including changes in the oxidation state and electronic properties of Au nanoparticles. We have demonstrated that atomic oxygen bound to Au is highly active for a range of oxidative transformations on metallic Au. Well-prepared gold crystal surfaces are inactive for O<sub>2</sub> dissociation, so that ozone was used as an oxidant in order to probe the bonding and reactivity of O on Au. Oxidation of Au(111) leads to the release of Au nanoparticles on which O is adsorbed. A combination of scanning tunneling microscopy (STM), high resolution electron energy loss spectroscopy experiments complemented by density functional theory calculations show that the local bonding and degree of longer range order of the O-Au islands depends on the temperature of oxidation and the overall O coverage. Reactivity studies show that low coverages of O bound in sites of local three-fold coordination are most active for selective reactions. Investigations of the molecular-scale mechanism for oxidative coupling reactions promoted by atomic oxygen on Au will be presented. Oxidative coupling of oxygenates—alcohols and aldehydes—will be the focus of the talk. The coupling reactions yield organic esters, which are important products industrially because of their widespread use as precursors for fragrances, flavorings, and fabrics. We construct a general mechanism for this class of reactions that provides insight into the optimum conditions of selectivity for even complex mixtures of alcohols. These fundamental studies will also be related to parallel studies using nanoporous Au as a catalyst at atmospheric pressure to illustrate the value of fundamental studies of catalytic processes. In this case, the reactions of Au under ultrahigh vacuum conditions provide an understanding of reactions at higher pressure because of the low intrinsic reactivity of Au itself, the weak bonding of water to Au, and the low steady state concentration of reactants on the surface even at high pressure because of the low rate of O<sub>2</sub> dissociation on Au. This is an unprecedented success in bridging the pressure gap between fundamental studies and working catalytic conditions.

9:20am **SS1-TuM5 An Atomic-scale View of Metal Alloy Surface Chemistry, E.C.H. Sykes**, Tufts University

Palladium and its alloys play a central role in a wide variety of industrially important applications such as hydrogen reactions, separations, storage devices, and fuel cell components. The exact mechanisms by which many of these processes operate have yet to be discovered. Low-temperature scanning tunneling microscopy (STM) has been used to investigate the atomic-scale structure of Pd/Au and Pd/Cu bimetallics created by depositing Pd on both Au(111) and Cu(111) at a variety of surface temperatures. We demonstrate that *individual isolated* Pd atoms in an inert Cu matrix are active for the dissociation of hydrogen and subsequent spillover onto Cu sites. The same mechanism does not operate for Pd in Au(111) surfaces,

however, because the spillover is thermodynamically unfavorable. These results demonstrate the powerful influence an inert substrate has on the catalytic activity of individual Pd atoms supported in its surface. In addition, differential conductance spectroscopy has enabled the electronic structure of these active sites to be measured and quantitatively compared to that of the host metal.

**9:40am SS1-TuM6 Prediction of Surface Ensembles in Au-based Bimetallic Alloys using Combined DFT and Monte Carlo Simulations, J.A. Stephens, H.C. Ham, G.S. Hwang, University of Texas at Austin**

Bimetallic materials have shown great promise for the development of superior catalysts. The recent surge of new interest in catalysis by gold has led researchers to investigate the effects of adding gold to other metals. While mechanisms underlying the alloying effect are still not understood in detail, recent evidence suggests that the enhanced reactivity of bimetallic catalysts can be attributed to a combination of metal-metal interactions (ligand effect) and unique mixed-metal surface sites (ensemble effect). The ability to accurately predict the arrangements of constituent atoms in a surface alloy is indispensable to unraveling the roles played by the ensemble and ligand effects in the performance of bimetallic model catalysts. We have developed a scheme to predict the equilibrium arrangement of atoms in surface alloys at finite temperatures. It is based on the Ising model and is capable of reproducing DFT-predicted total energies to within no more than a few meV per surface atom. We have used it successfully to predict monomer and dimer concentrations in Au-Pd and Au-Pt fcc (111) surface alloys. The scheme will be presented in detail, as well as what we have learned about the effects of temperature and composition on ensemble formation in both fcc (111) and (100) surface alloys, including the size and shape distributions of larger ensembles. We will also discuss how the atomic arrangements affect the reactivity of gold-based alloy surfaces, particularly towards oxidation of hydrogen and carbon monoxide.

**10:40am SS1-TuM9 Structure and Segregation at Clean and Oxidized Pd<sub>3</sub>Fe(111) Alloy Surfaces, X. Yang, B. Koel, Lehigh University**

**11:00am SS1-TuM10 Role of Ensembles in Determining the Catalytic Activity of Au-Pd and Au-Pt Surface Alloys towards CO Oxidation and Oxygen Reduction Reaction: A First Principles Study, H.C. Ham, J.A. Stephens, G.S. Hwang, University of Texas at Austin**

Gold-based bimetallic alloys have been found to significantly increase catalytic efficiency, compared to their monometallic counterparts in various reactions including low temperature oxidation of CO, direct synthesis of H<sub>2</sub>O<sub>2</sub> from H<sub>2</sub> and O<sub>2</sub>, and production of vinyl acetate monomers. Recent experimental and theoretical studies have suggested that the reactivity of bimetallic catalysts can be governed by creation of unique mixed-metal surface sites (ensemble effect) and/or electronic structure change by metal-metal interactions (ligand effect), while mechanisms underlying the alloying effect still remain unclear. In this talk, we will present the recent results of our first principles calculations on the mechanisms of CO oxidation and oxygen reduction reaction (ORR) on AuPd and AuPt alloy surfaces. Using periodic density functional theory calculations, we find that the rate of CO oxidation can be a strong function of Pd/Pt ensembles, while the ensemble effect is likely to be more important in the AuPd case. In addition, we find that ORR tends to be promoted on PdAu alloys, compared to the pure Pd case. This work provides valuable hints on the importance of the interplay of the ensemble and ligand effects in determining the catalytic activity of Au-based bimetallic catalysts particularly toward CO oxidation and ORR.

**11:20am SS1-TuM11 Adsorption Studies on Unsupported PdZn Alloy Powders, B. Halevi, University of New Mexico, B. Kiefer, New Mexico State University, K. Artyushka, P. Atanassov, A. Datye, University of New Mexico**

Estimating the true catalytically active surface area for complex 3-D surfaces such as powders is both important for evaluating the true catalytic performance of the material and difficult. Since most industrially relevant catalysts are metallic particles supported on Carbon or Oxides evaluating their chemically relevant surface area is even more difficult. In an effort to better quantify the active surface area of supported catalysts we synthesized an unsupported phase pure and compositionally homogeneous PdZn powder and evaluated by DFT and experiments the thermo- and electro-chemical adsorption of H<sub>2</sub>, O<sub>2</sub>, and CO on the powder. These benchmark values can be used to evaluate the available surface area of supported catalysts as well.

**11:40am SS1-TuM12 Reactivity of Epitaxial Vanadium Oxide Layers, M. Li, E.I. Altman, Yale University**

Monolayers of vanadia supported on other oxides can be uniquely active and selective for a number of reactions including the selective catalytic reduction of NO and the partial oxidation of methanol to formaldehyde. A

number of explanations have been offered in the literature to explain the unique properties of vanadia monolayers and the influence of the support, but these have been hampered by the inability to control both the chemical interaction of the vanadia with the substrate and the structure of the vanadia layer. We have addressed this issue by using oxygen plasma-assisted molecular beam epitaxy (OPA-MBE) to grow ordered vanadia monolayers and multilayers on rutile (110), anatase (001) and (101), WO<sub>3</sub>(100) and LaCoO<sub>3</sub> (100). By control of the atomic oxygen flux, monolayers and multilayers with the same surface structure can be obtained. For the monolayers, oxygen adsorption oxidizes all of the vanadium to 5+ while for the multilayers the bulk stoichiometry is VO<sub>2</sub> but oxygen adsorption oxidizes the surface to V<sub>2</sub>O<sub>5</sub>. Comparing the reactivity of monolayers and multilayers of vanadia on rutile (110) and anatase (001) reveals the importance of direct chemical interactions with the support versus the importance of maintaining non-bulk V<sub>2</sub>O<sub>5</sub> structures. For both the rutile and anatase support, we find that as long as the films are epitaxial that the direct chemical interaction with the support is not required to observe oxidative dehydrogenation of 1-propanol to propionaldehyde in thermal desorption; vanadia on both supports desorbed 1-propionaldehyde in a peak at ~400 K independent of the thickness of the vanadia layer. Differences between anatase and rutile as well as monolayers and multilayers were observed however. In particular, the fraction of adsorbed alcohol that reacted on the vanadia monolayer was much higher than any other vanadia surface, a finding attributed to the propensity of the rutile (110) surface to form defects that are highly active for alcohol deprotonation, the first step in the reaction. Thus the titania supports can influence the reactivity by both stabilizing reactive, non-bulk structures, and by facilitating the first step in reactions of alcohols. The reactivity data will be compared with results for vanadia on LaCoO<sub>3</sub>(100) which has the same surface unit cell as anatase (001), and thus in the monolayer regime the influence of chemical interactions on the reactivity of the vanadia are characterized with the structure held constant.

## Surface Science

### Room: Santa Ana - Session SS2-TuM

#### Aromatic Molecular Films

**Moderator:** C. Wöll, Karlsruhe Institute of Technology, Germany

**8:00am SS2-TuM1 Relating Aromatic Molecule Structure to Film Structure/Property Relationships, J.E. Anthony, University of Kentucky**

**INVITED**

The ease with which small-molecule organic semiconductors can be functionalized allows a single chromophore framework to be tuned for use in a myriad of electronic applications. Careful selection of substituents allows tuning of both solubility and crystal packing, allowing optimum structures for both film morphology and charge transport to be dialed in by careful structure-property studies. Additional substituents on the chromophore can be added to improve stability, shift phase transitions, or change the dominant carrier type for the material. Using 4, 5 and 6 fused-ringed acenes and heteroacenes as the chromophore, our straightforward functionalization approach has created organic materials for use in high-performance organic transistors and organic solar cells. The crystal-packing arrangements for these two types of devices are dramatically different. This talk will examine how materials with two-dimensional pi-stacking arrangements yield high-performance transistors, and how subtle tuning of the substituents can further improve performance and alter solubility. In the optimum case, hole mobility as high as 5 cm<sup>2</sup> / Vs was observed from a dip-cast film. Structure-property relationships in organic transistors are also explored in high-quality single crystals, showing how changes in crystalline order changes the intrinsic carrier properties of a homologous series of materials. In the case of bulk heterojunction organic solar cells, substitution of the acene chromophore with small electron-withdrawing groups yielded effective acceptors in blends with polythiophene donors. In this case, materials with strong pi-stacking interactions yielded the poorest-performing solar cells. In contrast, materials with weak, 1-dimensional pi-stacking interactions yielded the best performance, with power conversion efficiencies greater than 1.5% in these fullerene-free blends.

8:40am **SS2-TuM3 Optimal Electron Doping of a C<sub>60</sub> Monolayer on Cu(111) via Interface Reconstruction**, *W.W. Pai*, National Taiwan Univ., *H.T. Jeng*, Academia Sinica, Taiwan, *C.-M. Cheng*, National Synchrotron Radiation Research Center, Taiwan, *C.-H. Lin*, National Taiwan Univ., *X.D. Xiao*, *A.D. Zhao*, *X.Q. Zhang*, Hong Kong Univ. of Sci. and Tech., *G. Xu*, *X.Q. Shi*, *M.A. Van Hove*, City Univ. of Hong Kong, *C.-S. Hsue*, National Tsing Hua Univ., Taiwan, *K.-D. Tsuei*, National Synchrotron Radiation Research Center, Taiwan

We demonstrate the charge state of C<sub>60</sub> on a Cu(111) surface can be made optimal, i.e., forming C<sub>60</sub><sup>3-</sup> as required for superconductivity in bulk alkali-doped C<sub>60</sub>, purely through interface reconstruction rather than with foreign dopants [1]. We link the origin of the C<sub>60</sub><sup>3-</sup> charge state to a reconstructed interface with ordered (4 × 4) 7-atom vacancy holes in the surface. In contrast, C<sub>60</sub> adsorbed on unreconstructed Cu(111) receives a much smaller amount of electrons. Specifically, we used multiple techniques of scanning tunneling microscopy and spectroscopy (STM/STS), angle-resolved and angle-integrated photoemission spectroscopy (AR-,AI-PES), ab initio calculations, and low-energy electron diffraction I-V analysis (LEED I-V) to convincingly establish the C<sub>60</sub><sup>3-</sup> charge state and the reconstructed interface model. With STM, in-situ monitoring of C<sub>60</sub> growth at ~400 K revealed that each C<sub>60</sub> removes 7 atoms. STS showed the LUMO band sits nearly at the Fermi energy when the interface is reconstructed, or ~0.8 eV above the Fermi energy at unreconstructed interface. AI-PES indicated the initial charge state of C<sub>60</sub> over reconstructed interface is already close to C<sub>60</sub><sup>3-</sup> because very few extra K atoms are needed to reach maximal LUMO spectra intensity. AR-PES showed two hole-like bands crossing k<sub>bar</sub> that account for most of the charge transfer, and a shallow electron-like band near Γ<sub>bar</sub>. An extensive LEED I-V analysis using a total fitting range of ~3500 eV and 33 independent beams resolved the preferred structure model as the unfaulted fcc 7-atom monolayer vacancy model. We obtained a very good Pendry factor of ~0.27. Finally, although the C<sub>60</sub> has an optimal doping level for bulk superconductivity, we did not observe surface superconductivity down to ~5 K. Our result adds a new dimension in understanding functional molecular thin films; it illustrates a definitive interface structure-doping effect that affects the electronic properties of molecule-electrode contact.

[1] Woei Wu Pai et al., *Phys. Rev. Lett.* **104**, 036103 (2010)

9:00am **SS2-TuM4 Pattern Formation of Arenes and their Derivates on Cu(111)**, *D.Z. Sun*, *D.H. Kim*, *Z.H. Cheng*, *Y.M. Zhu*, *W.H. Lu*, *M. Luo*, University of California at Riverside, *S. Hong*, *T.S. Rahman*, University of Central Florida, *L. Bartels*, University of California at Riverside

Intermolecular force plays an important role in self-assembly and surface pattern formation. Unsubstituted arenes, such as anthracene, attach to a metallic substrate predominantly through van der Waals interaction leading to substrate binding that is less sensitive to the precise adsorption configuration and allows a range of ordered surface patterns. In contrast, substitution of the arenes can lead to strong intermolecular forces within the film and amplified substituent-substrate interactions that strictly define the adsorption configuration and film pattern. In this contribution we present the pattern formation of anthracene on Cu(111) and show how addition of thiol and carbonyl groups can vary the resultant surface pattern. For each case we investigate the chemical and physical interaction underlying the pattern formation using a combination of variable temperature scanning tunneling microscopy (STM) imaging and density functional theory (DFT) simulation.

9:20am **SS2-TuM5 Step Edge Barriers and Island Nucleation in Organic Thin Film Growth**, *C.K. Teichert*, *A. Hlawacek*, *S.B. Lorbek*, *P.C. Puschig*, *D. Nabok*, *C.E. Ambrosch-Draxl*, University of Leoben, Austria, *P.F. Frank*, *T.G. Potocar*, *A.H. Winkler*, Graz University of Technology, Austria

Crystalline films of conjugated organic semiconductors offer attractive potential for optoelectronic and electronic applications on flexible substrates. Due to the complexity and anisotropy of the molecular building blocks, novel growth mechanisms can occur as is demonstrated for the growth of the rod-like oligophenylene molecule parasexiphenyl (6P) on mica surfaces. On clean mica(001), the self-organization of crystallites into one-dimensional chains is observed on a wetting layer where the 6P molecules lie flat with their long molecular axis parallel to the surface [1].

Here, we demonstrate by atomic force microscopy that on an ion bombarded mica surface, the formation of terraced mounds composed by almost upright standing molecules is observed. In inorganic growth systems such a mound morphology is frequently due to a kinetic effect, the so-called Ehrlich-Schwoebel barrier for step-edge crossing [2]. Quantitative analysis of the mound morphology together with transition state theory calculations revealed the existence of molecule bending during step edge crossing and level dependent step edge barriers [3]. A lower barrier due to a larger molecular tilt angle (with respect to the surface normal) in the first layer

results in the completion of one monolayer before mound formation starts. This is convincingly demonstrated by transverse shear microscopy measurements.

By temperature and rate dependent growth experiments we also determined the size of the critical nucleus to be significantly larger than one. These findings are again complemented by force-field calculations revealing the size of an energetically stable island of upright standing molecules.

Our analysis shows that procedures developed and verified for inorganic systems [2] can be successfully applied to organic thin film growth. However, we have also demonstrated that the complexity and anisotropy of the molecular building blocks lead to additional effects [3] that are not observed in atomic inorganic growth systems.

[1] C. Teichert, G. Hlawacek, A. Andreev, H. Sitter, P. Frank, A. Winkler, N.S. Sariciftci, *Appl. Phys. A* **82** (2006) 665.

[2] T. Michely and J. Krug: *Islands, Mounds and Atoms* (Springer, Berlin 2004).

[3] G. Hlawacek, P. Puschig, P. Frank, A. Winkler, C. Ambrosch-Draxl, C. Teichert, *Science* **321** (2008) 108.

This work has been funded by Austrian Science Fund (FWF) within NFN "Organic Thin Films" Projects S9707 + S9714 as well as P19197.

9:40am **SS2-TuM6 Filamentous C<sub>60</sub> Structures at C<sub>60</sub>-ZnPc Interfaces**, *L. Tskipuri*, *W. Jin*, *Q. Liu*, *J. Weeks*, University of Maryland, *D.B. Dougherty*, North Carolina State University, *S.W. Robey*, NIST, *J.E. Reutt-Robey*, University of Maryland

Since the introduction of the bulk heterostructure concept, efficiencies of organic photovoltaic devices have improved markedly. This has spurred intense interest in controlling chemical morphologies to achieve more efficient charge separation. Unfortunately, there is surprisingly little guidance on how to achieve vertical nanophase separation in small-molecule materials. Basic studies of interface formation and nanophase separation in molecular materials are needed to understand how local chemical forces direct chemical morphology.

We present STM investigations of interface-formation and nanophase separation in binary films of zinc phthalocyanine (ZnPc) and C<sub>60</sub> on Ag(111) and Au(111) supports. Physical vapor deposition provides exquisite control of the growth kinetics, allowing access to both metastable and thermodynamic phases. We demonstrate the controlled formation of ZnPC:C60(1-D) and 2-D interfaces with distinctive molecular orientations and packing densities. Of particular interest is the formation of filamentous C<sub>60</sub> structures at the ZnPC surface. C<sub>60</sub> chains of single-molecular width wander the ZnPC substrate without registration to the underlying ZnPC template, islanding into a disordered chain phase. (Similar structures are also observed on Pn and 6-T surfaces.) These structures are reminiscent of dipole fluids (albeit of single molecular widths!) We present detailed measurements and analysis of C<sub>60</sub> wandering chain formation on ZnPC/Ag(111) and ZnPC/Au(111) substrates. We then explore the physical origin of these structures through simulations with a model potential that incorporates short-range C<sub>60</sub>-C<sub>60</sub> attraction and a long-range dipolar repulsion. From simulations of realized structures, we estimate the effective dipole needed for chain formation. We account for unexpected magnitude through the combined influences of the charge-transfer (interface) moment and the induced moment in these highly polarizable materials.

\*\*This work has been supported by the UMD MRSEC (DMR 0520471) and NSF Surface and Analytical Chemistry (CHE0750203)

10:40am **SS2-TuM9 Manipulating Island Density and Shape in Organic Thin Film Growth: the Nucleation of Perfluoropentacene on Self-Assembled Monolayers**, *T.V. Desai*, *A.R. Woll*, *J.R. Engstrom*, Cornell University

We have examined the nucleation and growth of perfluoropentacene (PFP) on SiO<sub>2</sub> and on a variety of surfaces possessing different terminating self-assembled-monolayers (SAMs) using *in situ* synchrotron x-ray scattering and *ex situ* atomic force microscopy (AFM). The SAMs ranged from very low surface energy hydrophobic surfaces (perfluorooctyltrichlorosilane, FOTS), to higher surface energy hydrophilic surfaces (3-methacryloxypropyltrichlorosilane, MAOPTS). From real time x-ray scattering we find that the growth of PFP, while crystalline, becomes very 3D after completion of the first 1-2 monolayers, independent of the substrate surface termination. Concerning growth in the submonolayer regime, we find that nucleation is homogeneous, and that the absolute density of islands depends strongly on the surface termination, while the relative change of the island density with increasing growth rate is essentially independent of the underlying SAM. From the latter we find that a critical island size of ~ 3 molecules can describe all the data. On the other hand, the dependence of the island density on termination implicates a significant change in the diffusivity of PFP with the identity of the SAM, with values differing by over 2 orders of magnitude. The shape of the

islands also depends on the surface termination, but somewhat unexpectedly—the islands are most compact and faceted on surfaces where the diffusivity of isolated PFP molecules is the smallest. The shapes of the islands on these surfaces can be interpreted by arguments based on equilibrium, where polygonal islands expose low energy facets. These results demonstrate the sensitivity of the initial stages of nucleation to the nature and identity of the underlying substrate.

11:00am **SS2-TuM10 Surface Structure Directed Chemistry: A Scanning Tunneling Microscopy Study of Chemically Reactive Self-Assembled Monolayers**, *D.H. Dahanayaka*, The University of Oklahoma, *R.D. Abrahams*, University of Maryland, *A. Singh*, *L.P. Jackson*, *L.A. Bumm*, *R.L. Halterman*, The University of Oklahoma

Self-assembled monolayers (SAMs) are flexible substrates for surface chemistry. A wide variety of SAM-surface functionalities can be prepared using alkanethiols with different terminal functional groups. Typically this requires a different alkanethiol for each. Another strategy uses a single alkanethiol to create a reactive surface which can be chemically modified post self-assembly. We are exploring azido-functional monolayers, which are reactive under mild conditions. The best known reaction is the copper catalyzed catalytic 1,3-dipolar cycloaddition with terminal alkynes. This approach has already been demonstrated for general surface chemical modification. We demonstrate molecularly-resolved STM imaging of these SAMs before and after the reaction. The surface structure affects the local reactivity and can be used to direct the reaction at the nanometer scale.

This work has been supported by NSF CAREER grant No. CHE- 0239803, NSF MRSEC No. DMR-0080054, and NSF No. DMR-0805233.

11:20am **SS2-TuM11 Molecular Organization and Odd-Even Effects in in Perfluoroterphenyl-Based Monomolecular Films**, *F. Chesneau*, Universität Heidelberg, Germany, *B. Schüpbach*, Universität Frankfurt, Germany, *K. Szelałowska-Kunstman*, Jagiellonian University, Poland, *N. Ballav*, Universität Heidelberg, Germany, *P. Cyganik*, Jagiellonian University, Poland, *A. Terfort*, Universität Frankfurt, Germany, *M. Zharnikov*, Universität Heidelberg, Germany

Self-assembled monolayers (SAMs) formed by perfluoroterphenyl-substituted alkanethiols (PFTP-ATs) with variable length of the aliphatic linker (either 2 or 3 methylene units) were prepared on (111) Au and Ag and characterized by a combination of several complementary spectroscopic and microscopic techniques. A specific feature of these systems is the helical conformation of the PFTP moieties, which, along with the high electronegativity of fluorine, distinguishes them from the analogous non-fluorinated systems and makes them attractive for different applications. The SAMs were found to be well-defined, highly ordered, and densely packed, which suggests a perfect correlation between the orientations and, in particular, twists of the PFTP helices in the adjacent molecules. Significantly, the SAM exhibited pronounced odd-even effects, i.e. a dependence of the molecular orientation and packing density on the length of the aliphatic linker in the target molecules, with parity of  $n$  being the decisive parameter and the direction of the effects on Au opposite to that on Ag. The presence of the odd-even effects in the FTPn system brings new aspects into the discussion about the origin and mechanism of these phenomena. Specifically, the helical conformation of the FTP moieties in the dense phase excludes a variation of the intramolecular torsion and molecular twist as the mechanism behind the odd-even effects.

11:40am **SS2-TuM12 From Selective Adsorption to Substrate Reconstruction: A Scanning Tunneling Microscopy Study of 4'-nitro-1,1'-biphenyl-4-thiol Self-Assembled Monolayers on Au(111)**, *H. Muzik*, *L. Kankate*, *A. Turchanin*, *A. Götzhäuser*, University of Bielefeld, Germany

Self-assembled monolayers (SAMs) of 4'-nitro-1,1'-biphenyl-4-thiol (NBPT) on gold surfaces are extensively used for applications in chemical nanolithography and fabrication of chemically functionalized ultrathin (down to 1 nm) nanomembranes. However, the structure of NBPT SAMs has not yet been investigated in detail. Here we present the first scanning tunneling microscopy (STM) study of NBPT SAMs on the Au(111) surface. NBPT SAMs were prepared both in solvent and by vapor deposition in vacuum. We show by complementary STM and X-ray photoelectron spectroscopy (XPS) measurements that NBPT SAMs exhibits a complex polymorphic phase behavior which strongly correlates with the surface density of NBPT molecules. We have found that at low NBPT coverage, the molecules selectively adsorb outside the bridging regions of the herringbone reconstructed Au(111) surface, whereas at high coverage intermolecular interactions lead to a reorganization of the Au(111) substrate. These findings can be very relevant for the tuning of nanomaterials and devices fabricated by chemical nanolithography from NBPT SAMs and give new insights in the molecular self-assembly of aromatic thiols on gold surfaces.

[1] A. Turchanin, A. Tinazli, M. El-Desawy, H. Großmann, M. Schnietz, H. H. Solak, R. Tampé, and A. Götzhäuser, Molecular self-assembly, chemical

lithography, and biochemical tweezers: A path for the fabrication of functional nanometer-scale protein arrays: *Adv. Mater.* 20, 471-477 (2008).

[2] L. Kankate, A. Turchanin, and A. Götzhäuser: On the Release of Hydrogen from the S-H groups in the Formation of Self-Assembled Monolayers of Thiols. *Langmuir* 25, 10435-10438 (2009).

[3] M. Schnietz, A. Turchanin, C. T. Nottbohm, A. Beyer, H. H. Solak, P. Hinze, T. Weimann, A. Götzhäuser, Chemically functionalized carbon nanosieves with 1 nm thickness. *Small* 5, 2651-2655 (2009).



# Tuesday Afternoon, October 19, 2010

## In Situ Microscopy and Spectroscopy Topical Conference

Room: Acoma - Session IS+SS-TuA

## In Situ Microscopy/Spectroscopy – Interfacial Chemistry/Catalysis

Moderator: S. Kodambaka, University of California Los Angeles

2:00pm **IS+SS-TuA1 *In-situ* LEEM Study of Ceria Growth on Cu(111)**, J.T. Sadowski, S.D. Senanayake, F. Yang, Y.M. Choi, Brookhaven National Laboratory, J.I. Flege, J. Falta, B. Menkens, University of Bremen, Germany, J.A. Rodriguez, J. Hrbek, Brookhaven National Laboratory

The use of CeO<sub>2</sub>-based materials in catalysis has attracted considerable attention in recent years. Ceria has shown great potential as a novel reducible oxide support with unique oxygen storage capacity (OSC) [1]. Ceria can accommodate a large number of oxygen vacancies and the oxidation states of the Ce cation can be switched readily between Ce<sup>3+</sup> and Ce<sup>4+</sup> depending on the ambient conditions. Hence ceria can actively participate in redox chemical reactions.

The formation of well-ordered, flat CeO<sub>2</sub> films is required in order to minimize substrate effects in surface chemistry of ceria. An earlier successful approach to this problem involved growth of ceria films on Ru(0001) [2]. More recently, CeO<sub>2</sub>(111) was grown on a Cu(111) substrate [3]. High activity of ceria-based model catalysts was demonstrated on the inverse catalyst [4, 5] with ceria nanoparticles supported on noble metal substrates. Overall, there is still little known about the mechanism for the growth of ceria film on metal surfaces, its structure and stoichiometry.

In the present work the growth of thin ceria films on Cu(111) has been investigated *in-situ* by means of low-energy electron microscopy (LEEM). Ce was deposited from an e-beam evaporator onto Cu(111) under O<sub>2</sub> atmosphere (5x10<sup>-7</sup> Torr). Real-time observation of the film growth revealed that at relatively high substrate temperature (above 800K) flat, highly crystalline, epitaxial CeOx(111) film has been formed. In this presentation we will discuss in detail the mechanism of the nucleation and growth, and the atomistic structure of the CeOx film on Cu(111) under varying growth conditions and Cu(111) oxidation state.

[1] A. Trovarelli, *Catalysis by Ceria and Related Metals*, Imperial College Press, London, 2002.

[2] D. R. Mullins, P. V. Radulovic, S. H. Overbury, *Surf. Sci.* **429**, 186 (1999).

[3] V. Matolin, J. Libra, I. Matolinova, V. Nehasil, L. Sedlacek, F. Sutara, *Appl. Surf. Sci.* **254**, 153 (2007).

[4] J. A. Rodriguez, S. Ma, P. Liu, J. Hrbek, J. Evans, and M. Pérez, *Science*, **318**, 1757 (2007).

[5] J. A. Rodriguez, J. Hrbek, *Surf. Sci.*, **604**, 241 (2010).

The authors are thankful to the US Department of Energy (Chemical Sciences Division, contract no. DE-AC02-98CH10886) for financial support. Research carried out in part at the Center for Functional Nanomaterials, Brookhaven National Laboratory, which is supported by the U.S. Department of Energy, Office of Basic Energy Sciences, under contract no. DE-AC02-98CH10886.

2:20pm **IS+SS-TuA2 Quantitative Speciation of Zn(II) During the Solution Synthesis of ZnO Nanowires Using In-Situ XANES Spectroscopy**, K.M. McPeak, Drexel University, M. Becker, B.A. Bunker, University of Notre Dame, J.B. Baxter, Drexel University

Low temperature, aqueous solution synthesis is widely used to deposit ZnO nanowire arrays for applications such as dye sensitized solar cells. Zinc nitrate and hexamethylenetetramine (HMTA) are the most common precursors for the solution synthesis of ZnO nanowires; but after ten years of using this chemistry, the underlying mechanisms of the reaction remain unclear. We report on the in-situ x-ray absorption spectroscopy of ZnO

nanowire growth from HMTA and zinc nitrate precursors. Time-resolved, in-situ x-ray absorption near-edge structure (XANES) spectra, at the Zn K-edge, give detailed information about the local structure of both Zn(II) in solution and the solid phases formed throughout the reaction. A principal component analysis (PCA) algorithm was employed to determine the number and type of probable species present during the growth of ZnO nanowires under real reaction conditions, with temperatures up to 90 °C and concentrations ranging from 4 – 25 mM. Only two species were present for ZnO nanowire growth at all concentrations and temperatures studied: [Zn(6H<sub>2</sub>O)]<sup>2+</sup> and ZnO<sub>(s)</sub>. The proportions of these Zn species as a function of reaction time were determined quantitatively by least-squares fitting (LSF) the experimental time-dependent XANES spectra with linear combinations of the principal component spectra. PCA and target testing conclusively refute previous theories that ZnO nanowire growth from HMTA and zinc nitrate precursors occurs due to the thermal decomposition of an intermediate zinc-amine or zinc-HMTA complex. Additionally, XANES analysis shows that no zinc hydroxide intermediates exist above the detection limit of 0.05 mM. Beyond the focused investigation of ZnO, this study also establishes in-situ XANES spectroscopy, in combination with PCA and LSF, as an excellent quantitative tool to understand the solution synthesis of semiconductor nanostructures and thin films.

2:40pm **IS+SS-TuA3 X-ray Spectromicroscopy of Organic and Inorganic Nanostructures**, S.G. Urquhart, University of Saskatchewan, Canada

INVITED

Understanding the composition and structure of complex surfaces is essential for many scientific questions, from understanding processes in surface corrosion to the development of organic electronic devices. X-ray Spectromicroscopy provides surface sensitive chemical speciation with high lateral spatial resolution, by combining the chemical sensitivity of X-ray absorption and photoemission spectroscopy with the high spatial resolution of X-ray microscopy. This presentation will discuss x-ray spectromicroscopy studies to study phase segregation in mixed Langmuir Blodgett thin films as well as efforts to develop a new zone-plate based surface sensitive spectromicroscopy.

1.) We have used surface sensitive X-ray Photoelectron Emission Microscopy (X-PEEM) to study the mechanisms of phase separation and growth in mixed Langmuir Blodgett thin films.[1,2] Here, the chemical sensitivity of x-ray absorption spectroscopy provides spatially resolved composition information to complement the morphology information provided by AFM.

2.) We are developing of a new form of new surface sensitive x-ray microscopy, based on electron-yield detection in a scanning zone plate microscope. Preliminary results from the development of this new method will be presented.

### References:

1.) Christensen et al., *J. Electron Spectrosc. and Rel. Phenom.* (2008) **162**, 107-114.

2.) S.E. Qaqish, *Langmuir* (2009) **25**, 7401-7409.

Research supported by NSERC (Canada) and performed at the Canadian Light Source (CLS) and the Advanced Light Source (ALS). The CLS is supported by NSERC, NRC, CIHR, U. Saskatchewan, and the ALS is supported by the Director, Office of Science, Office of Basic Energy Sciences, of the U.S. Department of Energy under Contract No. DE-AC02-05CH11231.

4:00pm **IS+SS-TuA7 The Use of *in-situ* Spectro-Electrochemical Tools on the Way to R&D of Rechargeable Li and Mg Batteries**, D.A. Aurbach, Bar-Ilan University, Israel

INVITED

The performance of high energy density rechargeable Li and Li ion batteries depends on passivation phenomena. On thermodynamic basis, both the negative electrodes: Li metal or lithiated carbonaceous materials and the positive electrodes: lithiated transition metal oxides are reactive with the electrolyte solutions that are relevant to these systems (polar-aprotic solvents and Li salts).

Thereby, it is highly important to understand the complicated surface chemistry that characterizes all kinds of rechargeable Li batteries. Based on understanding the correlation between surface phenomena, performance and safety features, it is possible to optimize electrolyte solutions in which irreversible phenomena and electrodes capacity fading will be minimized. Consequently, it was highly important to develop specific spectroscopic and microscopic tools that can be used in conjunction with electrochemical techniques and can be specifically suitable for such highly reactive systems. In this talk we demonstrate the development and use of *in-situ* FTIR spectroscopy for mapping the complicated surface reaction of Li metal electrodes in most relevant electrolyte solutions. Especially important was an approach based on internal reflection modes. The use of *in-situ* Raman spectroscopy for understanding lithiation processes of graphite in ionic liquids will be demonstrated. Application of spectroscopy enables to follow detrimental processes such as co-intercalation of the solvents' cations together with Li insertion, what interferes badly with the passivation phenomena, on which the reversibility and stability of Li-graphite anodes depend. The same techniques were applied to non-aqueous electrochemistry of magnesium, in the framework of R&D of rechargeable Mg batteries. The use of EQCM was helpful in characterizing passivation free Mg electrodes, in ethereal solutions with contain magnesium organo-chloro-aluminate complex electrolytes. Highly useful for the study of surface phenomena related to Li batteries were *in-situ* AFM measurements, with which it was possible to follow delicate phenomena related to surface films formation, exfoliation of Li-graphite electrodes and break down and repair of passivation phenomena on both Li metal and Li graphite electrodes. The study of Mg anodes was nicely promoted by the use of *in-situ* STM measurements. This technique was very suitable for characterization of Mg anodes in passivation free electrolyte solutions. New directions for development of *in-situ* techniques suitable for highly reactive electrochemical systems, will be discussed.

**4:40pm IS+SS-TuA9 Electrochemistry Platforms for In Situ Transmission Electron Microscopy of Li-ion Batteries.** *A. Subramanian, J.P. Sullivan, J. Huang, M.J. Shaw, N. Hudak, Sandia National Laboratories, Y. Zhan, J. Lou, Rice University*

Nanoscale materials offer a number of potential advantages for Li-ion batteries: examples include low-cost LiFePO<sub>4</sub> nanoparticle cathodes that exhibit good rate performance despite having low electrical conductivity and high-capacity conversion anodes that have high cycle life despite large volume changes per cycle, e.g. Si nanowires. However, one of the challenges with the use of nanoscale materials is their electrochemical characterization, particularly assessing structural changes in nanoscale particles, or reaction product layer interfaces, such as the solid-electrolyte-interphase (SEI). This requires tools with atomic to nanoscale spatial resolution. To meet this need, we have developed a micro-electromechanical systems (MEMS)-based platform for performing electrochemical measurements using volatile electrolytes inside a transmission electron microscope (TEM). This platform uses flip-chip assembly with special alignment features and multiple buried electrode configurations. The nanoscale materials of interest are assembled into the viewing area using dielectrophoresis (DEP). This permits the incorporation of a diverse array of nanoscale particles, including the co-assembly of anode materials in proximity to cathode materials. As an initial realization of the MEMS-based platform, we have developed an unsealed platform that permits *in situ* TEM electrochemistry using ionic liquid electrolytes or *ex situ* electrochemistry and TEM imaging using conventional battery electrolytes. We have demonstrated these approaches using  $\beta$ -MnO<sub>2</sub> nanowire cathodes that were individually assembled using DEP. These wires were lithiated over a range of potentials, in ethylene carbonate-based electrolytes with lithium metal as a counter electrode, in order to produce a range of lithium content. Using TEM and solid-state electrical characterization, we observed that lithiation introduces increasing lattice disorder particularly at the nanowire surfaces; yet, the wires remain  $\beta$ -phase. The electrical measurements revealed a monotonic decrease in electrical conductivity with increasing lithium content, consistent with electronic localization at defects or an increased band gap. From these results, we conclude that *in situ* TEM characterization tools will enable important mechanistic understanding of Li-ion battery materials. This work was supported by LDRD and EFRC projects and was performed, in part, at CINT, a U.S. DOE, Office of Basic Energy Sciences user facility. Sandia is a multiprogram laboratory operated by Sandia Corp., a wholly owned subsidiary of Lockheed Martin Company, for the U.S. DOE's NNSA under contract DE-AC04-94AL85000.

**5:00pm IS+SS-TuA10 In-Situ Heating, Imaging, and Analysis of Nanoparticles Using SEM, STEM, and XPS.** *J.L. Sturgeon, RJ Lee Group, Inc., Z. Liu, University of Pittsburgh, K.L. Bunker, T.L. Lersch, J. Mastovich, B.R. Strohmaier, RJ Lee Group, Inc., J.C. Yang, University of Pittsburgh*

Use of an *in-situ*, semiconductor-based heating stage in high-resolution scanning electron microscope (SEM) and scanning transmission electron microscope (STEM) instruments permits rapid, but controlled, temperature changes and the ability to collect images and videos in real time with minimal drift. A Protochips Aduro™ system utilized on a Hitachi S-5500 SEM/STEM allows analysis at elevated temperatures coupled with low voltage SEM/STEM imaging. Catalyst nanoparticles consisting of an iron core surrounded by a carbon shell have been studied using this technology. Elevated temperatures result in a variety of changes to the core-shell structure as well as migration and agglomeration of the iron nanoparticles. X-ray photoelectron spectroscopy (XPS) was also used to study the surface chemistry of these materials before and after heating. These experiments give critical insights into the kinetics of reaction of the iron nanoparticles. Additional analysis at higher accelerating voltages is possible using a dedicated STEM instrument. Other applications using elevated heating of nanoparticles will be discussed.

**5:20pm IS+SS-TuA11 Understanding the Role of Fe Catalyst in Carbon Nanotube Growth Using Atomic-Scale (S)TEM.** *A. Mkhoyan, M.J. Behr, E.S. Aydil, University of Minnesota*

The combination of unique mechanical, thermal, optical, and electronic properties of carbon nanotubes (CNTs) make them a desirable material for use in a wide range of applications. Many of these unique properties are highly sensitive to how carbon atoms are arranged within the graphene nanotube wall. Plasma-enhanced chemical vapor deposition (PECVD) from methane-hydrogen gas mixtures using Fe catalytic nanoparticles enables large-scale growth of CNT films, however, much is still unknown about what happens to the catalyst particle during growth and how it dictates the final nanotube structure. To investigate the fundamental processes of CNT growth by PECVD (S)TEM based characterization techniques were used including convergent-beam electron diffraction (CBED), high-resolution (S)TEM imaging, energy dispersive x-ray spectroscopy and electron energy-loss spectroscopy (EELS).

It is found that hydrogen plays a critical role in determining the final CNT structure through controlling catalyst crystal phase and morphology. A variety of tube structures grow, via a base-growth mode, from single crystalline BCC iron and cementite catalyst particles. At low hydrogen concentrations in the plasma, well-graphitized nanotubes grow from elongated Fe<sub>3</sub>C crystals, while at high hydrogen concentrations, poorly-graphitized nanofibers grow from BCC iron crystals. Although catalyst particles are single crystals, they exhibit combinations of small-angle rotations, twists, and bends along their axial length between adjacent locations. Distortions are most severe away from the base up into the nanotube where the number of walls is large. This suggests that the stresses generated by the surrounding nanotube distort the catalyst particle during growth. The much larger thermal expansion coefficient of Fe<sub>3</sub>C compared to that of the nanotube may also play a role in shaping the crystal into the observed tear-drop morphology. No preferential catalyst orientation relative to the nanotube axis was observed, suggesting that what is required for nanotube growth is not an epitaxial relationship with the catalyst, but rather, only formation of an initial graphitic carbon seed. Z-contrast STEM images combined with atomic-scale EELS measurements also revealed an iron-oxide shell at the very base of each BCC and Fe<sub>3</sub>C catalyst crystal.

## Surface Science

**Room: Picuris - Session SS-TuA**

### Chemical Dynamics at Surfaces

**Moderator: I. Harrison, University of Virginia**

**2:00pm SS-TuA1 Gently Lifting Gold's Herringbone Reconstruction by Tuning Adsorbate Chemistry.** *A.D. Jewell, E.C.H. Sykes, Tufts University*

Recently it was discovered that the structure of the molecule-metal interface in alkane thiol-based self-assembled monolayers (SAMs) is more complex than first believed. Thiols have been shown not only to lift the herringbone reconstruction of Au(111) but remove a significant fraction of the Au surface atoms. The etch pits formed by these vacancies are thought to be one of the weakest areas of the SAM films in terms of susceptibility to and degradation by oxidizing species.

In an effort to slightly weaken the molecule-metal interaction and prevent the formation of etch pits, we have chosen the study the interaction and assembly of trimethylphosphine (PMe<sub>3</sub>) on Au(111) using a scanning tunnelling microscope (STM). This is to our knowledge the first atomic-scale characterization of a phosphine species adsorbed on a metal surface.

At full monolayer coverage PMe<sub>3</sub>, the molecules formed a hexagonally packed layer which exhibited a ( $\sqrt{7} \times \sqrt{7}$ )R19° unit cell. The interaction between PMe<sub>3</sub> and Au caused Au atoms to be ejected from the herringbone reconstruction, but not the substrate surface itself (as in the thiol case) and led to the formation of small Au islands. This effect manifested in the herringbone spacing increasing from that of native gold (6.33 nm) to 11.2 ± 0.9 nm. As this system was exposed to various annealing treatments, a fraction of the molecules desorbed, the Au islands coalesced, and the herringbones disappeared entirely, indicating that the underlying Au surface adopted a 1 × 1 reconstruction. The data indicate that the PMe<sub>3</sub>/Au island formation is a kinetically limited process.

Finally, we have developed a mathematical equation that gives the theoretical island coverage ( $\theta$ ) as a function of the maximum island coverage ( $\theta_{\text{max}}$ ), the native herringbone spacing ( $x_0$ ) and the experimental herringbone spacing ( $x$ ):  $\theta = \theta_{\text{max}}(1 - x_0/x)$ . This should be useful in future studies of many types of SAMs on Au(111), or any similarly reconstructed surface.

2:20pm **SS-TuA2 Tunneling and Guidance in the Diffusion of Polyatomic Molecules at a Metal Surface**, *Z.H. Cheng, E. Chu, D.Z. Sun, D.H. Kim, Y.M. Zhu, M. Luo, G. Pawin, K.L. Wong, K.-Y. Kwon, R. Carp, M. Marsella, L. Bartels*, University of California at Riverside

Pentacene derivatives that have two and four carbonyl groups attached to them diffuse on a Cu(111) surface in a uniaxial fashion, i.e. exclusively along a substrate atomic row, despite the threefold symmetry of the substrate. In this, they resemble the behavior of dithioanthracene and anthraquinone, previously dubbed “molecular walkers”, which move across Cu(111) sequentially stepping the thiol/carbonyl linkers on each side of the molecule. This poses the question of how a fourfold substituted, i.e. quadrupedal, molecule can accomplish uniaxial motion: will it move its substrate linkers on opposite ends of the molecule at the same time resembling the gait of trotting, or will it instead move both linkers on one side at the same time, resembling the gait of pacing? Density functional theory (DFT) suggests the latter. Variable temperature scanning tunneling microscopy (STM) monitoring of the molecular motion reveals a striking difference between the diffusion prefactors of the quadrupedal and bipedal species, with the latter being very low. Wentzel Kramers Brillouin-based modeling of the motion of the substrate linkers in the calculated diffusion barriers suggest that the origin of this discrepancy lies in the relevance of the tunneling of the substrate linkers, allowing bipedal species, which only need to move one substrate linker at a time, to accomplish motion through tunneling of the linker, whereas quadrupedal species, whose diffusion requires concerted motion of two substrate linkers, cannot move in this way, resulting in significantly higher diffusion temperatures.

2:40pm **SS-TuA3 Scanning Tunneling/Atomic Force Microscopy of Individual Atoms/Molecules on Insulating Films**, *G. Meyer, L. Gross, F. Mohn, N. Moll, IBM Zurich Research Laboratory, Switzerland, P. Liljeroth, Utrecht University, Netherlands, J. Repp, University Regensburg, Germany*

#### INVITED

Ultrathin insulating films on metal substrates are unique systems to use the scanning tunneling / atomic force microscope to study the electronic and structural properties of single atoms and molecules, which are electronically decoupled from the metallic substrate. Individual gold atoms on an ultrathin insulating sodium chloride film supported by a copper surface exhibit two different charge states, which are stabilized by the large ionic polarizability of the film [1]. The charge state and associated physical and chemical properties such as diffusion can be controlled by adding or removing a single electron to or from the adatom with a scanning tunneling microscope tip. The simple physical mechanism behind the charge bistability in this case suggests that this is a common phenomenon for adsorbates on polar insulating films. Employing a low temperature tuning fork AFM the different charge states can be observed directly in the force signal [2]. In the case of STM of molecules on ultrathin insulating films the electronic decoupling allows the direct imaging and manipulation of molecular orbitals [3]. As we have recently demonstrated detailed structural information can be attained by Atomic Force Microscopy which leads to the direct imaging of the molecular geometry. I.e. the complete chemical structure of single molecules can be accessed in scanning probe microscopy [4].

1. J. Repp, G. Meyer, F.E. Olsson, M. Persson, ‘Controlling the Charge State of Individual Gold Adatoms’, *Science* 305, 493 (2004)

2. L. Gross, F. Mohn, P. Liljeroth, J. Repp, F. J. Giessibl, G. Meyer, ‘Measuring the Charge State of an Adatom with Noncontact Atomic Force Microscopy’ *Science*, 324, 1428-1431 (2009)

3. P. Liljeroth, J. Repp, G. Meyer, ‘Current-Induced Hydrogen Tautomerization and Conductance Switching of Naphthalocyanine Molecules’ *Science*, 317, 1203-1206 (2007)

4. L. Gross, F. Mohn, N. Moll, P. Liljeroth, G. Meyer ‘The Chemical Structure of a Molecule Resolved by Atomic Force Microscopy’, *Science*, 325, 1110-1114 (2009)

4:00pm **SS-TuA7**, *D.V. Potapenko, R.M. Osgood*, Columbia University

Surface chemistry in photocatalysis is driven by the charge carriers that are created in the bulk of the catalyst and then are transferred to the adsorbed molecules. Both electrons and holes can be injected into molecules from the scanning tunneling microscope tip thus allowing mechanistic studies of photocatalytic processes on a single-molecule basis. We have studied adsorption and tip-induced surface chemistry of anthracene, as well as a number of anthracene derivatives on the TiO<sub>2</sub>(110) surface. These molecules form ordered monolayers on the surface at room temperature with their structure dictated by the surface-charge distribution on TiO<sub>2</sub>(110). Passing the electric current pulses from the STM tip into molecules causes dissociation and in some cases desorption of the molecules as indicated by the changes in the STM images. Halogenated organic molecules were especially susceptible to electron-induced dissociation with an energy threshold of ~ 2.5V. We report on the conditions of the tip-induced chemistry and propose a mechanism for the observed phenomena.

4:20pm **SS-TuA8 A New Mechanism of Atomic Manipulation: Bond-Selective Molecular Dissociation via Thermally Activated Electron Attachment**, *S. Sakulsermsuk, P.A. Sloan, R.E. Palmer*, University of Birmingham, UK

We report a new mechanism of (bond-selective) atomic manipulation in the scanning tunneling microscope (STM). We demonstrate a channel for one-electron induced C-Cl bond dissociation in chlorobenzene molecules chemisorbed on the Si(111)-7x7 surface, at room temperature and above, which is thermally activated. We find an Arrhenius thermal energy barrier to one-electron dissociation of 0.8 ± 0.2 eV, which we correlate explicitly with the barrier between chemisorbed and physisorbed precursor states of the molecule. Thermal excitation promotes the target molecule from a state where one-electron dissociation is suppressed to a transient state where efficient one-electron dissociation, analogous to the gas phase negative ion resonance process, occurs. We expect the mechanism will obtain in many surface systems, and not just in STM manipulation, but in photon and electron beam stimulated (selective) chemistry.

4:40pm **SS-TuA9 State-Resolved Molecular Beam Reflectivity Measurements of Methane Activation on Ni(111)**, *N. Chen, Y. Huang, V. Campbell, A. Utz*, Tufts University

State-resolved measurements of CH<sub>4</sub> reactivity on Ni(111) and Ni(100) have yielded detailed insights into how methane’s vibrational energy promotes reactivity. To date, such measurements have relied on post-dose quantification of reaction products to measure reactivity as a function of methane’s translational energy, internal vibrational and rotational state, and surface temperature. Here, we describe a new detection scheme for measuring state-resolved reaction probabilities. This method uses a variation of the “King and Wells” molecular beam reflectivity method to improve reproducibility and significantly decrease the data acquisition time for state-resolved measurements. Rather than modulate the flux of molecules incident on the surface, we modulate laser excitation. In this way, the partial pressure change due to modulation reveals the difference in reactivity with and without laser excitation, which is the key quantity needed to obtain state resolved reaction probabilities. We demonstrate the method for methane incident on Ni(111) and show that it provides real-time coverage dependent reaction probabilities while decreasing data acquisition time and permitting a more expansive exploration of how energy and chemical identity influences reactivity at the gas-surface interface. We use this experimental method to extend our study of CH<sub>4</sub> activation to additional vibrational states, including the 2ν<sub>4</sub> bend overtone, and different surfaces. Comparing the reactivity of these states provides insight into key features of energy flow during the reaction, and data to assess the generality of non-statistical behavior in gas-surface reactivity.

5:00pm **SS-TuA10 Dynamical Heterogeneity in Surface Reactions**, *A. Utz, D.R. Killelea, V. Campbell, N. Chen*, Tufts University

5:20pm **SS-TuA11 Adsorbate Distribution and Dynamics inside Nanometer-Scale Metal Facets**, *J. Wyrick, Z.H. Cheng, M. Luo, D.Z. Sun, D.H. Kim, Y.M. Zhu, W.H. Lu*, University of California at Riverside, *K. Kim, T.L. Einstein*, University of Maryland, *L. Bartels*, University of California at Riverside

We use low temperature scanning tunneling microscopy to investigate the diffusion and arrangement of CO molecules adsorbed on Cu(111) facets of  $\sim 4$  nm diameter formed by self-assembly of a honeycomb network of anthraquinone molecules. CO molecules and adlayers exhibit properties under such nanoscale confinement that markedly depart from those of extended adlayers: a) the confinement stabilizes dislocation lines (anti-phase domain boundaries) in the adlayer that affect roughly  $\frac{1}{4}$  of the adsorbed molecules; b) confinement prevents the formation of dense islands of adsorbed molecules, depending on coverage either causing dispersion of vacancies in the adlayer or preventing the growth of molecular islands; c) at a coverage of just a few molecules on the facet, we observe that a molecular shell structure is formed, resembling in its underlying mathematics the atomic model. Confined structures are an ideal test bed for measurement of the coverage dependence of molecular diffusion and in this study we find a reduction of the diffusion barrier at a slope of 57%/ML.

5:40pm **SS-TuA12 Ab Initio Calculations of the Preexponential Factor for the Diffusion of CO on Ag(001): The Importance of Inclusion of the Full Phonon Dispersion**, *M. Alcántara Ortigoza, T.S. Rahman*, University of Central Florida, *K.P. Bohnen, R. Heid*, Karlsruhe Institute of Technology, Germany

Knowledge of factors that determine the diffusivity of CO on catalytic surfaces is of utmost importance for understanding why some surfaces render higher reaction rates (e.g. CO oxidation) than others. A rigorous calculation of the diffusion prefactor is not only the first approximation one should target to analyze diffusivity but also a prerequisite to adequately take into account dissipative anharmonic processes since calculation of both the prefactor and anharmonic processes rates require the full dispersion of all phonons in the system as input information. In this work, we obtain from first principles calculations the diffusion path of CO on Ag(001), the corresponding energy barrier, diffusion prefactors, and diffusion rate. The latter have been calculated via the total phonon density of states in the surface Brillouin zone from density functional perturbation theory calculations. Comparison of the results for the prefactors obtained using the full phonon dispersion curve with those confined only to the adsorbate modes on a frozen substrate point to significant differences and to the importance of having a knowledge of the full vibrational dynamics of the system, particularly at (low) temperatures which are relevant to experimental measurements.

---

# Tuesday Afternoon Poster Sessions

## Surface Science

Room: Southwest Exhibit Hall - Session SS-TuP

### Surface Science Poster Session

**SS-TuP1 MORTON S. TRAUM AWARD FINALIST: Uptake of Copper Acetamidinate ALD Precursor on Metal Surfaces and the Effect of Coadsorption of Hydrogen, Q. Ma\*, F. Zaera, University of California, Riverside**

Acetamidinate precursors have shown great promise for atomic layer deposition (ALD) applications, but potentially deposit impurities that may degrade the quality of the films and hinder their practical applications. To help solve this problem, the uptake and thermal activation of bis([N,N'-di-sec-butylacetamidinate)Cu] and N,N'-di-sec-butylacetamidine on metals were characterized under ultrahigh vacuum (UHV) conditions by using a combination of X-ray photoelectron spectroscopy (XPS), low-energy ion scattering (LEIS), and temperature programmed desorption (TPD).

In initial studies on a Ni(110) single crystal, a temperature window between approximately 350 and 450 K was identified for the ALD of the Cu acetamidinate on Ni surface: lower temperatures are insufficient for activation of the dissociative adsorption, and higher temperatures lead to continuous decomposition beyond Cu monolayer saturation. Approximately three dosing cycles are required to reach full Cu monolayer saturation, the equivalent of a film growth rate of  $\sim 0.75 \text{ \AA/cycle}$  in ALD. Preadsorption of hydrogen on the surface does not modify any of this behavior because of its rapid desorption at temperatures below 350 K once the gas-phase  $\text{H}_2$  is removed.

The surface chemistry of the Cu precursor is complex, leading to the desorption of not only hydrogen but also butene and N-sec-butylacetamidine ( $\text{H}_2\text{N}-\text{C}(\text{CH}_3)=\text{N}-\text{CH}(\text{CH}_3)(\text{CH}_2\text{CH}_3)$ ), it seems that the amidine ligands decompose via beta-hydride elimination from one of their terminal sec-butyl moieties. Copper precursors leading to relatively stable organic surface intermediates are required in ALD because their clean removal can only happen in the second half-cycle of processes that rely on hydrogenation reactions. The ligand of the copper acetamidinate precursors further decomposed on Ni (110) surfaces. The free hydrogenated amidine ligand is less reactive and no N-sec-butylacetamidine is produced by its thermal activation, but the remaining chemistry is seen with similar temperature transitions.

**SS-TuP2 MORTON S. TRAUM AWARD FINALIST: Understanding and Controlling Rotation at the Single-Molecule Level: Turning Rotors into Motors, H.L. Tierney\*, A.D. Jewell, A.E. Baber, E.V. Iski, E.C.H. Sykes, Tufts University**

While molecular machines driven by chemical, light or thermal energies can be found throughout nature, little progress has been made toward creating synthetic counterparts. The gap between nature and nanotechnology remains due to the limited fundamental understanding of the transfer of energy to mechanical motion at the nanoscale. Understanding and actuating the rotation of individual molecules on surfaces is a crucial step towards the development of nanoscale devices such as fluid pumps, sensors, delay lines, and microwave signaling applications. Towards this end we have used a group of small molecules in order to understand the fundamental aspects of molecular rotation. Thioethers constitute a simple, robust system with which molecular rotation can be actuated thermally, mechanically and electrically, and can be studied using scanning tunneling microscopy (STM) as a function of molecular chemistry and proximity of neighboring molecules. Interestingly, the thermal onset to rotation was found to be nearly identical for studied thioether molecules with alkyl tails of two carbons or more. It is proposed that this plateau in thermal onset was due to an interplay between degrees of freedom in the alkyl tail vs. the S-metal bond length. While small amounts of thermal energy are capable of inducing rotation, thermodynamics dictates that thermal energy alone cannot be used to perform useful work in the absence of a temperature gradient. Therefore, for molecules to meet their full potential as components in molecular machines, methods for coupling them to external sources of energy that selectively excite the desired motions must be devised. To this end, we have studied using an electrical current to rotate individual dibutyl sulfide molecules on command. For these studies the source of energy is supplied via high energy electrons from the STM tip. By monitoring the rate of rotation as a function of tunneling electron energy (action spectroscopy) we have demonstrated that the rotors can be driven electrically via a

mechanism that involves excitation of a C-H stretch. Finally, using theoretical methods the minimum energy adsorption site was determined and the mechanism of rotation was elucidated for the simplest thioether, dimethyl sulfide. These theoretical results indicate that the rotation of a small, simple molecule is actually rather complex; as the  $\text{CH}_3$  groups of dimethyl sulfide rotate around the Au-S bond, the central S atom precesses around a surface Au atom.

**SS-TuP3 MORTON S. TRAUM AWARD FINALIST: Growth of Ag on Ge(110) and Ge(111) Studied by LEEM, C. Mullet\*, University of California, Davis, S. Chiang, University of California at Davis**

We studied Ag island growth on reconstructed Ge(110) and Ge(111) surfaces with low energy electron microscopy (LEEM). At 480 C, one-dimensional (1D) island growth was observed on Ge(110). Island nucleation proceeds from defects in the Ge substrate, with island thickness corresponding to the size of the substrate defect where the island nucleation occurred. As Ag is deposited, islands lengthen but do not thicken. At 9 ML, Ag coverage islands were up to 10  $\mu\text{m}$  long, and thicknesses varied from 100 nm to 250 nm. One-dimensional islands were also produced by Ag deposition at room temperature followed by sample heating. Round Ag islands resolvable in LEEM were observed and coalesced into many long 1D islands as temperature was increased. Islands formed by deposition at room temperature followed by heating to a particular temperature were shorter and thicker than islands grown by deposition on a substrate held at that same temperature. Ag growth on Ge(111) is Stranski-Krastanov. Multilayer Ag island formation begins after the Ag ( $\sqrt{3}\times\sqrt{3}$ )R30° phase completes at one monolayer. Ag islands exhibit hexagonal faceting. For both the Ge(111) and Ge(110) surfaces, Ag islands induce changes in the Ge substrate that leave a "footprint" observable in LEEM after all Ag has been desorbed from the surface.

\*Funding from NSF CHE-0719504; NSF PHY-0649297 (REU)

**SS-TuP4 Kinetics and Mechanism of NO Reduction with CO on Ir Surfaces, T. Fujitani, A. Takahashi, I. Nakamura, National Institute of Advanced Industrial Science and Technology (AIST), Japan**

The reaction of NO and CO has been studied over various transition- and noble-metal catalysts because of its importance for three-way catalytic converters. Recently, Ir-based catalysts were found to be effective for the selective reduction of NO with CO in the presence of  $\text{O}_2$ . However, the reaction mechanism, kinetics, and adsorption behavior for the NO + CO reaction on Ir-based catalyst surfaces are not fully understood.

In this study, we investigated the adsorption and thermal reactivity of NO and CO over Ir single crystals to clarify the influence of the Ir surface structure. Furthermore, we examined the kinetics and mechanism of the NO + CO reaction over Ir single crystals at high-pressure and compared the results with results for a conventional Ir/SiO<sub>2</sub> powder catalyst.

The kinetics of the NO reduction with CO over the Ir single crystal and the powder Ir/SiO<sub>2</sub> catalyst were investigated under real reaction conditions. N<sub>2</sub> and CO<sub>2</sub> were formed by the reaction of NO + CO. The Ir(111) plane showed low activity for N<sub>2</sub> and CO<sub>2</sub> production compared with the Ir(100) and Ir(211) planes. The TOFs for N<sub>2</sub> and CO<sub>2</sub> formation for the Ir planes decreased in the order (100) > (211) >> (111). The apparent activation energies for N<sub>2</sub> and CO<sub>2</sub> formation were estimated to be 107–115 kJ/mol and 110–120 kJ/mol, respectively; and these values were almost the same, regardless of the changes of the Ir surface structure. Furthermore, the order of the pre-exponential factors for the various surface structures was in good agreement with the order of the planes with respect to NO dissociation activity, indicating that the catalytic activity for NO reduction over Ir surfaces was strongly dependent on the NO dissociation activity.

The activation energies for N<sub>2</sub> and CO<sub>2</sub> formation over an Ir/SiO<sub>2</sub> catalyst were estimated to be 117.2 kJ/mol and 123.1 kJ/mol, respectively, and these values were similar to those of the Ir single crystal. The TOFs for N<sub>2</sub> and CO<sub>2</sub> formation over Ir/SiO<sub>2</sub> were almost same for those for Ir(211), which indicates that the Ir surface structure of Ir/SiO<sub>2</sub> was close to that of Ir(211). That is, the Ir(211) surface can be regarded as an appropriate model catalyst for the NO + CO reaction over an Ir/SiO<sub>2</sub> catalyst because the apparent activation energies and the TOFs for N<sub>2</sub> and CO<sub>2</sub> formation over Ir(211) were in good agreement with those over the Ir/SiO<sub>2</sub> catalyst.

**SS-TuP5 Development of Boundary Layer in the Flowing Water on the Solid Surface with Various Wettability, M. Sakai, Kanagawa Academy of Science and Technology, Japan, M. Nishimura, T. Furuta, A. Nakajima, Tokyo Institute of Technology, Japan, A. Fujishima, Tokyo University of Science, Japan**

Recently, the importance of controlling wettability on the solid surface is recognized in various industries. Superhydrophobic surfaces with water

\* Morton S. Traum Award Finalist

contact angles exceeding 150° are currently the subject of great interest and intensive study. Superhydrophobic coatings that produce rough surfaces at the micro- and nanoscale level with low surface energies have been prepared by several methods. On the other hands, highly hydrophilic surface is obtainable, when the photocatalyst TiO<sub>2</sub> is irradiated by ultraviolet light. In the current paper, we evaluated friction drag of water on various surfaces including these surfaces. The amount of friction drag was evaluated by the static pressure during flowing in the tubes coated by various materials. Compared to Darcy-Weisbach's equation, a superhydrophobic coating and highly hydrophilic coating decreased the friction drag of the flowing under the condition of small Reynolds number. However, a highly hydrophilic coating contributed significantly to the reduction of friction drag, when Reynolds number is large. Moreover, the velocity gradient of the flowing water in the tube was measured by particle image velocimetry (PIV). The development of boundary layer depended on the wettability in the tubes, when the flowing was the same in the flow rate. The mechanism was discussed from the viewpoints of fluid mechanics and surface materials science.

**SS-TuP6 Hydrogen Termination of Si(110) Surface in UHV Conditions, M. Yoshimura, A. Visikovskiy, Toyota Technological Institute, Japan**

Hydrogen termination on silicon surfaces is very important in science and technology. Hydrogen (H) is used for surface passivation, and may play role of surfactant for epitaxial growth and also present in many technological processes including chemical vapor deposition. The behavior of H on Si(100) and Si(111) surfaces is extensively studied. However, the information on interaction of H with Si(110) is very limited. The (1x1) bulk-terminated structure was reported for chemically hydrogenated Si(110) in solution [1,2]. The surface structure and processes occur on Si(110) hydrogenated in ultra-high vacuum (UHV) may be very different from chemically treated samples. There are very few reports on *in situ* hydrogenation of Si(110) surface. Here, we report scanning tunneling microscopy (STM) study of atomic H adsorption on Si(110) in UHV.

The high efficiency hot capillary source was used to produce atomic H flux. The large concentration of highly reactive H atoms in the flux allows us to reach surface saturation for hydrogenation at ~2 L exposure. Chemically etched tungsten tips have been used for STM (Omiron VT-system).

The initial adsorption process of hydrogen reveals itself as suppression of individual protrusions of pentagon pairs on STM image. The number of these "missing" protrusions increases with H coverage, although the overall "16x2" structure of clean Si(110) preserves. More drastic changes were observed on unreconstructed areas exposed to small amount of H at elevated temperatures. Si pentagon pairs, usually randomly distributed on these areas, were arranged in patches with local "5x4" periodicity. Further exposure at room temperature (RT) led to loosing of atomic resolution on STM images. At higher temperatures (400–500°C) the surface have reconstructed to the zigzag row structures. Depending on relative shift of neighboring zigzag rows the local periodicity was either (2x3) or (2,1)x(0,3). The up-and-down terrace structure of "16x2" reconstruction could still be observed, probably, due to insufficient temperature to initiate massive Si transport to smooth out the surface. At temperatures more than ~550°C the H atoms start to desorb from Si(110). These kinds of structure have not been observed before for H/Si(110) surface. No (1x1) reconstruction reported for chemically hydrogenated Si(110) was confirmed. Only small patches of (1x1) were observed in very narrow temperature window at ~350°C.

References

- [1] K. Arima, J. Ktoh, and K. Endo, Appl. Phys. Lett. 85 (2004) 6254.
- [2] S. Horie, K. Arima, K. Hirose, J. Katoh, T. Ono, and K. Endo, Phys. Rev. B 72 (2005) 113306.

**SS-TuP7 Spectroscopic Investigation on Water Behavior in Mesoporous Silica, Y. Aoki, J. Hieda, O. Takai, N. Saito, Nagoya University, Japan**

Mesoporous materials are widely used in industrial fields such as biotechnology and chemical engineering; catching and filtering a specific molecule, supplying novel reaction field for nanocatalysis. In particular, mesoporous silica is defined as a material with size-regulated mesopores (2–50 nm). Generally, highly-ordered arrangement of pores is attractive for chemists because the most of properties are controlled by the arrangement.

Recently some researchers reported that the internal water trapped by mesopores extraordinary behaved compared with bulk water. For examples, the water showed the lower melting point and increasing effect of non-freezing water. These phenomena were originated from the increasing ratio of interactions to water molecules from surface.

In this research, we aimed to reveal water behaviors in mesoporous silica from IR spectroscopy, Raman spectroscopy, and DSC. Mesoporous silica

was synthesized conventional thermal calcinations with several organic templates because it control the pore diameters. The synthesized mesoporous silica was characterized by XRD, TEM and N<sub>2</sub> adsorption-desorption isotherm curve.

The complete removal of organic template and the OH-termination in inside wall resulted in the presence of water in the mesopores. As the water features, we observed the both types of non-freezing and freezing water. Finally, the types of water were separated in the properties by both spectroscopy and DSC.

**SS-TuP8 Mechanism of Laser Assisted Field Evaporation from Oxides, M. Tsukada, H. Tamura, Tohoku University, Japan, K. Mckenna, University College London, UK**

**SS-TuP9 Surface Roughness of Anodized Titanium Coatings, D.A. Chinn, M.T. Dugger, Sandia National Laboratories**

Samples of grade five 6Al4V titanium alloy were coated with two commercial fluoropolymer anodizations (Tiodize and Canadize) and compared. Neither coating demonstrates significant outgassing. The coatings show very similar elemental analysis, except for the presence of lead in the Canadize coating, which may account for its lower surface friction in humid environments. Surface roughness has been compared by SEM, contact profilometry, optical profilometry, power spectral density and bidirectional scattering distribution function (BSDF). The Tiodize film is slightly smoother by all measurement methods, but the Canadize film shows slightly less scatter at all angles of incidence. Both films exhibited initial friction coefficients of 0.2 to 0.4, increasing to 0.4 to 0.8 after 1000 cycles of sliding due to wear of the coating and ball. The coatings are very similar and should behave identically in most applications.

**SS-TuP10 Measurement of the Dielectric Properties of SiO<sub>2</sub> Wafers using Optical Spectroscopy, D. Popovic, A. Zekic, University of Belgrade, Serbia, V. Milosavljevic, Dublin City University, Ireland & University of Belgrade, Serbia**

Low dielectric constant materials (low-k) are used as interlevel dielectrics in integrated circuits. As components have scaled and transistors have gotten closer and closer together, the insulating dielectrics have thinned to the point where charge builds up and crosstalk adversely affects the performance of the device. It is this reduction in scale which drives the need for insulating materials with lower dielectric constant. A 'low-k' material is one with a small value for dielectric constant relative to silicon dioxide (SiO<sub>2</sub>) a former dielectric of choice. There are many materials with lower dielectric constants, but few of them can be suitably integrated into a semiconductor manufacturing process.

The SiO<sub>2</sub> is frequently used in a plasma chamber as a wafer for etching. The interaction of the plasma and the SiO<sub>2</sub> surface leads to incorporations/removing material for structure of SiO<sub>2</sub> and also to increasing of the dielectric constant. So the optimization problem in materials development for semiconductors is to lower the permittivity of the dielectric material as far as possible without compromising mechanical integrity.

The dielectric function spectra of low dielectric constant (low-k) materials have been determined using spectroscopic ellipsometry, near-normal incidence spectroscopic reflectometry, and Fourier transform infrared transmission spectrometry over a wide spectral range from 0.03 to 5.4 eV (230nm to 40.5µm wavelength region). The electronic and ionic contributions to the overall static dielectric constant were determined for representative materials used in the semiconductor industry for interlayer dielectrics. The main contributions to the static dielectric constant of the low-k materials studied were found to be the electronic and ionic absorptions.

To perform the study, square shape wafers (15x15mm) are placed in the discharge tube. The angle between wafers plane and a constructed channel is 45°. The DC discharge is produced in a Pyrex tube of 5mm inner diameter and an effective plasma length of 72mm. The discharge tube is evacuated using a vacuum pump that gives a base pressure of 2Pa. The working pressures from 50 to 266 Pa are achieved using a gate valve positioned above the rotary pump. Gas flow into the chamber is controlled via mass flow controllers that precisely determine gas content in the discharge tube. The working gas is a sulphur-hexafluoride (SF<sub>6</sub>) with flow rate up to 40 sccm. The power supply used was a Keithley Model 248 high voltage supply with a maximum voltage of 5kV and discharge current of 5 mA. In this experimental campaign the maximum voltage is 2.2kV. The wafer processing time is 30 min.

**SS-TuP11 Stereoselective Adsorption Configurations of S-Proline Molecules via N Dative Bonding on Ge(100),** *Y.-S. Youn*, Korea Advanced Institute of Science and Technology (KAIST), Korea, *K.-J. Kim, B. Kim*, Pohang Accelerator Laboratory, Korea, *D.H. Kim*, Daegu University, Korea, *H. Lee*, Sookmyung Women's University, Korea, *S. Kim*, Korea Advanced Institute of Science and Technology (KAIST), Korea  
The adsorption configurations of S-proline on Ge(100) were studied using scanning tunneling microscopy (STM), density functional theory (DFT) calculations, and high-resolution core-level photoemission spectroscopy (HRCLPES). We identified three adsorption structures of S-proline on Ge(100) through analysis of the STM images, DFT calculations, and HRCLPES results: (i) an 'intrarow O-H dissociated and N dative bonded structure', (ii) an 'O-H dissociation structure', and (iii) an 'N dative bonded structure'. Moreover, because adsorption through the N atom of S-proline produces a new chiral center due to symmetry reduction by N dative bonding, we found that the adsorption configurations have either (R,S) and (S,S) chirality with a preference for reaction at the Re face.

**SS-TuP12 Islands and Holes as Measures of Mass Balance in Growth of the ( $\sqrt{3}\times\sqrt{3}$ )R30° Phase of Ag on Si(111),** *A. Belianinov*, Iowa State University & Ames Laboratory U.S. D.O.E.

It is well-known that conversion of Si(111)-(7x7) into the ( $\sqrt{3}\times\sqrt{3}$ )R30° phase of adsorbed Ag requires a change in the Si density, and causes formation of islands and holes at the surface. By mass balance, the ratio of areas of islands and holes ( $R_{IH}$ ) should be approximately 1. However, we find that the ratio is significantly higher, depending on preparation conditions. A possible explanation would be that there are different types of ( $\sqrt{3}\times\sqrt{3}$ )R30° structures. However, neither scanning tunneling microscopy nor density functional theory (implemented as a genetic algorithm search) supports this explanation. The reason for the unexpectedly high values of  $R_{IH}$  is unknown.

P.A.C.S. Numbers 68.37.Ef, 68.55.-a, 81.15.Aa, 68.47

**SS-TuP13 Secondary Electron Yield for As-Received, Electrodeposited, and Crystalline Silver Surfaces,** *T.P. Graves, P.D. Fuqua, P.M. Adams, R. Spektor, J.R. Lince, D.B. Witkin*, The Aerospace Corporation

Silver electroplating is commonly used to provide low electrical loss characteristics for RF and microwave devices. These RF devices can also be susceptible to multipactor discharge, a resonant electron phenomenon that relies on electron density growth by secondary electron emission. The secondary electron yield (SEY) can determine whether a multipactor discharge can form; therefore, understanding SEY variations in silver surfaces is necessary for accurate multipactor breakdown prediction. In this work, SEY is measured for a variety of silver surfaces using a retarding potential method. Starting with as-received silver with no specific surface preparation, SEY values are shown to be considerably increased due to adsorbed gases on both bulk and electrodeposited silver substrates. Auger analysis was performed to determine the contaminant layers, as it is these technical silver surfaces that are realistic for space hardware where in-situ surface conditioning is not possible. Additional SEY measurements were performed on both polycrystalline and single crystal silver surfaces to determine the effect of the crystalline orientation on the SEY. Different crystallographic orientations at the surface of the electrodeposit may arise due to differences in plating variables such as bath chemistry, electrode geometry and localized current density. These measurements serve to better understand possible improvements in plating processes to minimize secondary electron emission and multipactor risk. Lastly, the effect of baking and multipactor conditioning on silver SEY is presented. Formation of thin carbon films are observed as a result of multipactor exposure, and x-ray photoelectron and Raman spectroscopy film analysis results are presented.

**SS-TuP14 Characterization and Chemical Activity of Supported Ni-Au and Pt-Au Bimetallic Clusters: Reactions of Methanol,** *S.A. Tenney, B.A. Cagg, W. He, D.A. Chen*, University of South Carolina

The activity of methanol on Ni-Au and Pt-Au clusters deposited at 300 K on TiO<sub>2</sub> (110) was investigated using temperature programmed desorption (TPD), scanning tunneling microscopy (STM), and low energy ion scattering (LEIS). Bimetallic clusters were grown by first depositing the metal with stronger metal-support interactions (Ni or Pt) onto the surface in order to seed the more mobile Au at existing Ni or Pt clusters. The preexisting Ni or Pt clusters also inhibited the sintering of Au at higher temperatures. The composition at the surface of the clusters was established by the major products observed in TPD experiments. Methyl (~717 K) was produced on the TiO<sub>2</sub> support, CO (~429 and ~775 K) and H<sub>2</sub> (~357 K) were produced at Ni sites, and formaldehyde (~580 K) production was attributed to the Au-titania interface. CO (~503 K) and H<sub>2</sub> (~503 K) were also characteristic of Pt at the surface. LEIS data for 0.25 ML of total

coverage shows that for clusters with > 50% bulk Au composition, the surface of the cluster is almost entirely pure Au. TPD of methanol on clusters with > 50% bulk Au composition still show activity characteristic of Ni or Pt at the surface, suggesting that methanol is able to induce the migration of Ni and Pt to the surface of the clusters. Increasing the amount of Au on the surface for pure Au clusters beyond 1 ML resulted in a decrease of the formaldehyde signal, which is attributed to a subsequent decrease in the Au-TiO<sub>2</sub> interface as more Au is deposited onto the surface. Formaldehyde production on 0.25 ML of pure Au and 25% Ni / 75% Au clusters showed no decrease in activity even after 6 consecutive TPD cycles to 800 K.

**SS-TuP15 Growth of Nanoparticles and Reactivity of a Copper Metal-Organic Precursor on Functionalized Silicon Surfaces,** *K.A. Perrine, J. Lin, A.V. Tepyakov*, University of Delaware

As the sizes of the devices are quickly approaching the nanometer scale in the microelectronics industry, the need to control reactions at the molecular level and at the interface becomes very important for developing cleaner deposition techniques. For example, metal contacts grown using atomic layer deposition (ALD) have already made an impact on modern devices.

A common precursor used to grown copper metal contact, Cu<sup>I</sup> (hexafluoroacetylacetonato) vinyltrimethylsilane or Cu(hfac)VTMS, has been previously studied at the molecular level on Si(100)-2x1 and other surfaces using surface sensitive techniques. Here we use this precursor as a reactant on several functionalized silicon surfaces to produce and control the size distribution of metallic nanoparticles.

We compare the reaction of Cu(hfac)VTMS with H-Si, NH<sub>2</sub>-Si, NH-Si, and OH-Si surface reactive sites and follow it by *in situ* infrared spectroscopy (FTIR), temperature-programmed desorption (TPD), X-ray photoelectron spectroscopy (XPS), atomic force microscopy (AFM), and complement with Density Functional Theory calculations. The growth of the hfac vibrational signatures indicates reaction on these functionalized surfaces and losses in the Si-H stretch spectral region can be used to follow the deposition kinetics. The surface is used here as a reducing agent providing the hydrogen to remove the ligands of the copper deposition precursor and to produce metallic nanostructures.

**SS-TuP16 Preparative Mass Spectrometry: A Novel Approach for the Creation of Catalyst Materials,** *G. Johnson*, Pacific Northwest National Laboratory, *W.-P. Peng*, National Dong Hwa University, Taiwan, Republic of China, *R.G. Cooks*, Purdue University, *J. Laskin*, Pacific Northwest National Laboratory

Soft- and reactive landing of mass-selected ions onto surfaces is a unique approach for the highly controlled preparation of catalyst materials that are often inaccessible using conventional synthesis techniques. Mass selection allows polyatomic ions with known charge and chemical identity to be deposited onto surfaces under carefully controlled conditions, thereby avoiding purification steps which are typically necessary with traditional catalyst preparation methods. A new apparatus has been designed and assembled at PNNL that allows *in situ* reactivity and time of flight secondary ion mass spectrometry analysis of surfaces prepared or modified through soft- and reactive landing. The capabilities of this instrument for the preparation and analysis of catalyst materials are demonstrated for two different systems consisting of monolayer catalysts produced by the deposition of organometallic metal-salen and ruthenium bipyridine cations onto self assembled monolayer surfaces. It is shown that through soft landing of vanadium-salen cations and a proton donor it is possible to achieve proton mediated reactivity in an inert fluorinated monolayer that is normally only observed in highly acidic solutions. In addition, it is demonstrated that gas-phase ligand stripping may be used to generate highly reactive undercoordinated metal complexes which exhibit enhanced activity towards reactive landing in comparison to fully ligated species. The immobilized complexes, which are covalently bound to the surface, are shown to exhibit catalytic activity when exposed to gaseous reagents.

**SS-TuP17 Charge Transfer and Shake Satellites in XPS: A Unified View,** *C.J. Nellin*, Maury's Trail, *P.S. Bagus*, University of North Texas, *H.-J. Freund*, Fritz-Haber-Institut der Max-Planck-Gesellschaft, Germany

The satellites in X-Ray photoemission spectroscopy, XPS, can provide information about the electronic structure, especially for ionic materials. [1,2] We present a new analysis of the XPS satellites that, when applied to CeO<sub>2</sub> which is an important substrate for model studies of catalysis, enables a new understanding of this material. While the origin of intra-atomic effects in terms of atomic near-degeneracies is well understood, [1] there are two different ways of describing the inter-atomic effects that lead to satellites. The first is to ascribe the satellites to charge transfer, CT, from ligands, or other neighboring atoms, into unoccupied or partly occupied shells of the ionized atom. This interpretation is commonly applied to oxides and other ionic crystals. [2] In the CT model, the satellites gain



intensity through the mixing of XPS allowed configurations with XPS forbidden configurations. However, changes in the orbitals between the initial and final states are normally neglected in the CT model. On the other hand, the second way of understanding satellites as shake satellites, [3,4] ascribes the driving force for the loss of intensity from the main peak into the satellites to the orbital relaxation, which screens the core-hole. This orbital relaxation allows valence excited, or shake, states to obtain intensity. [3] However, both mechanisms must be taken into account to correctly describe the inter-atomic contributions to XPS satellites and, in the present work, we reconcile these two different points of view. We show that the covalent mixing of metal and ligand orbitals in the wavefunctions, for both initial and final states, is a powerful way to understand the intensities of satellites due to inter-atomic effects. For the XPS of NiO, where both intra and inter-atomic effects must be taken into account, our analysis of the CI wavefunctions shows the underlying covalent character of the main and satellite peaks. We also stress the importance of covalent mixing in the initial state in order for there to be substantial satellite intensity. We show that different degrees of covalent character in the initial states of CeO<sub>2</sub> and LaAlO<sub>3</sub> lead to very different satellite energies and intensities for the isoelectronic metal cations. Our analysis provides direct and unambiguous evidence that the inter-atomic satellite features are closely related to the covalent binding in the material.

- (1) PS Bagus, ES Ilton: Phys. Rev. B **73**, 155110 (2006).
- (2) FMF de Groot: J. Electron Spectrosc. Relat. Phenom. **67**, 529 (1994).
- (3) T Aberg: Phys. Rev. **156**, 35 (1967).
- (4) L Sangaletti, F Parmigiani, PS Bagus: Phys. Rev. B **66**, 115106 (2002).

**SS-TuP18 XPS Investigation of Volcanic Ash and Other Basalt Materials**, P. Mack, T. Nunney, R.G. White, A. Wright, ThermoFisher Scientific, UK

XPS has been used to analyse the ash released from a number of volcanoes, including that from Mount St Helens, USA and Eyjafjallajökull, Iceland. The results indicate that the differences in the composition of the basalt from different regions reflect the geological structure of the region. Some of the compositional differences depend upon whether the geological plates are moving together, causing more crust material to be mixed with the lava or whether the plates are moving apart and so the lava is predominantly from sub-surface sources. Further complications arise from the fact that the ash from some eruptions (e.g. Eyjafjallajökull) also contains material from an overlying glacier. It has been found that the material from Eyjafjallajökull is richer in calcium than that from Mt St Helens.

The use of XPS to fingerprint this type of material has been investigated. The effect of ion sputtering of the material has also been investigated as a means to generate more representative data.

**SS-TuP19**, S. Axnanda, W.-P. Zhou, M.G. White, J. Hrbek, Brookhaven National Laboratory

Recently, the ethanol electro-oxidation reaction has attracted considerable attention because of the advantages of using ethanol as fuel in liquid fuel cells.<sup>1</sup> Ethanol can be produced from renewable biomass sources, and has high energy density and less toxic than methanol. However, the ethanol oxidation kinetics is slow, impeding its use in the direct ethanol fuel cells (DEFCs). Tremendous efforts have been made to develop new ethanol oxidation catalysts to improve its efficiency. Binary Pt-Sn alloy catalysts are some of the more extensively investigated anode materials for DEFCs. It was found that the increased activity of binary electrocatalysts with respect to Pt alone was attributed to the bifunctional effect and electronic interaction between Pt and alloyed metals.<sup>2,3,4</sup> However, studies from supported nanocatalyst show disagreements in mechanism of what degree of alloying between Pt and Sn and what amount of Sn alloyed with Pt will improve the activity of the electrocatalysts towards EOR.<sup>5, 6, 7, 8</sup> It is still unclear whether the alloyed Sn, or the SnO<sub>2</sub> phase is the reason in the increase in Pt-Sn electrocatalysts activity towards EOR.<sup>1,5-8</sup>

In the work presented here, we are investigating surface alloy of Pt-Sn/Pt(111) and SnO<sub>2</sub>/Pt(111) as model catalysts for ethanol electro-oxidation. Characterization is performed by a combination of surface science techniques (X-Ray photoelectron spectroscopy (XPS), low energy electron diffraction (LEED), temperature programmed desorption (TPD), and low energy ion scattering spectroscopy (LEISS)) and classical electrochemical measurements. This integrated approach can be used to identify the fundamental properties of SnO<sub>2</sub>/Pt(111) and Sn-Pt/Pt(111) electrodes and to correlate them with the activity of each electrode towards EOR.

1. E. Antolini, J. Power Sources 170 (2007) 1-12
2. Rigsby, M. A., Zhou, W. -P., Lewera, A., Duong, H. T., Bagus, P. S., Jaegermann, W., Hunger, R., and Wieckowski, A., Experiment and Theory of Fuel Cell Catalysis: Methanol and Formic Acid Decomposition on Nanoparticle Pt/Ru. J. Phys. Chem. C, 2008 112 (39) 15595-15601

3. N. M. Markovic, H. A. Gasteiger, P. N. Ross, X. Jiang, I. Villegas, M. J. Weaver, Electrochim. Acta 40 (1995) 91
4. S. L. Goikovic, T. R. Vidakovic, D. R. Durovic, Electrochim. Acta 48 (2003) 3607
5. C. Lamy, S. Rousseau, E. M. belgsir, C. Countanceau, J.-M Leger, Electrochim. Acta 49 (2004) 3901
6. W. Zhou, Z. Zhou, S. Song, W. Li, G. Sun, P. Tsiakaras, Q. Xin, Appl. Catal. B 46 (2003) 273
7. L. Jiang, G. Sun, S. Sun, J. Liu, S. Tang, H. Li, B. Zhou, Q. Xin, Electrochim. Acta 50 (2005) 5384
8. F. Colmati, E. Antolini, E. R. Gonzalez, J. Electrochem. Soc. 154 (2007) B39

**SS-TuP20 One-dimensional Coordination Chains of 4,4'-azopyridine on Cu(100) by Self-assembly**, H.A. Lim, S.L. Tai, Indiana University

We have observed highly-ordered 1D chains of 4,4'-azopyridine (AZPY) formed by self-assembly on the pristine Cu(100) surface at room temperature. AZPY is of particular interest as a building block due to its  $\pi$ -conjugated system, photoactive azo site and coordinative bonding with transition metals in metal organic framework materials. Scanning tunneling microscopy shows that the APY molecules grow in one-dimensional chains, mostly starting from copper step edges, with an end-to-end pyridine-Cu-pyridine interaction. The APY chain structure, oriented along the [110] direction, is a significant departure from the side-to-side molecular arrangement in self-assembled azobenzene chains at surfaces. As the coverage increased mobile molecules are observed to be confined inside 2D APY corrals composed of a framework of intersecting chains. X-ray photoelectron spectroscopy is also used for characterization. Further studies are underway to investigate these assemblies on other surfaces as well as functionality of these systems for applications such as nano-electronics, molecular magnetism and single-site heterogeneous catalysis.

**SS-TuP21 Surface Adhesion Properties of Block Copolymer Films**, M. Palacio, S. Schrickler, B. Bhushan, The Ohio State University

Block copolymers are of interest as scaffold materials for cell growth and regeneration because novel, structurally diverse polymers can be synthesized from biocompatible blocks. The nanostructure and surface morphology of block copolymers can be modulated using synthetic techniques and the nanostructures can be used to affect surface mechanical behavior. We present atomic force microscopy (AFM) studies on the morphology and corresponding protein adhesion interactions of a novel class of methyl methacrylate and acrylic acid diblock and triblock copolymers. Distinct nanomorphologies were found on diblock and triblock copolymers even though their chemical compositions are identical. This has implications on the role of nanomorphology in cell-polymer interactions. Protein adhesion on a biomaterial surface is critical to understanding its biocompatibility. Bovine serum albumin (BSA) was attached to the AFM tip in order to model protein-block copolymer interactions.

**SS-TuP22 XPS Organic Depth Profiling Analysis of Poly-glycidyl Methacrylate Brushes**, S. Anabulsi, J.F. Moulder, Physical Electronics, R. Barbey, H.A. Klok, Ecole Polytechnique Fédérale de Lausanne, Switzerland

The application of XPS C<sub>60</sub> sputter depth profiling to characterize synthesized poly-glycidyl methacrylate (PGMA) brush-like thin film structures will be presented. In contrast to low voltage (250 V) Ar sputtering, C<sub>60</sub> sputtering with XPS analysis was able to obtain quantitative chemical state information as a function of depth with minimal ion beam induced chemical damage. To minimize sputtering artifacts and improve interface definition, Zalar (azimuthal) rotation and appropriate instrument geometry for C<sub>60</sub> sputter depth profiling was used for this work. The XPS depth profiles show the chemical changes associated with various solutions applied to these organic films.

**SS-TuP23 Particles from the Ozonolysis of Unsaturated Silane Self-Assembled Monolayers**, T.M. McIntire, O. Ryder, University of California, Irvine, P. Gassman, Z.H. Zhu, Pacific Northwest National Laboratory, S. Ghosal, Lawrence Livermore National Laboratory, B. Finlayson-Pitts, University of California, Irvine

Airborne particles have well-documented effects on human health, visibility, and the chemistry of the atmosphere. Particles play a major role in climate change and are a large source of uncertainty in model predictions of global warming. A significant part of this uncertainty is the lack of understanding of the nature of the organic component. This deficiency includes the chemical speciation and the distribution of the organics between the surface and the bulk of liquid particles, as well as changes due to oxidation during transport in the atmosphere.

Self-assembled monolayers (SAMs) represent a well-defined system for elucidating mechanisms of mixed gas-condensed phase reactions and serve as proxies for organic-coated airborne dust particles. Previous studies have shown that ozone reactions of terminal alkene-silane SAMs generates surface-bound acids, aldehydes, and secondary ozonide (SOZ), as well as gaseous products such as CO, CO<sub>2</sub>, HCHO, and HCOOH. In addition, the surprising formation of large, hydrophobic organic particles was observed by AFM and Auger electron spectroscopy. A particularly noteworthy result of atmospheric interest is that the uptake of water was not increased upon oxidation of these films, despite the formation of polar carbonyl-containing groups, and SOZ. This has important implications for particles in the atmosphere, since it is generally assumed that oxidation converts hydrophobic surfaces to hydrophilic which take up water more readily, thereby affecting visibility and cloud formation.

The goal of this work was to determine the product functional groups and the 3-D structure of particles produced from the ozonolysis of SAMs formed by attachment of 7-octenyltrichlorosilane (C8= SAM) to silica substrates. A combination of analytical techniques such as single particle FTIR, NanoSIMS, and TOF-SIMS were utilized to study the surface composition and morphology after oxidation. Atmospheric implications for the 3-D structure of SOA, SAM reactions and stability in air, ozonolysis of alkenes on surfaces, and the oxidation of alkenes on airborne dust particles will be discussed.

**SS-TuP24 Temperature Programmed Desorption Study of CO on Cr(110) and Cr<sub>2</sub>O<sub>3</sub>(0001)/Cr(110)**, J.L. Walters, G. Arellano, W.A. Harrison, C.A. Ventrice Jr., H. Geisler, Texas State University - San Marcos

The adsorption kinetics of CO on Cr(110) and on Cr<sub>2</sub>O<sub>3</sub>(0001)/Cr(110) was investigated using temperature programmed desorption (TPD). The adsorption of CO was performed with the substrate maintained at 120 K, and a feedback control system was used to generate linear heating rates. For the Cr<sub>2</sub>O<sub>3</sub>(0001)/Cr(110) surface a saturation coverage of CO was measured to occur at 0.5 L. The desorption kinetics is estimated to be 1<sup>st</sup> order with an attractive lateral interaction between CO molecules. The Redhead method was used to measure the activation energy for desorption of the CO. This analysis resulted in a value of 49.2 kJ/mol ± 2.6 kJ/mol for the activation energy. For the adsorption of CO on Cr(110) no CO desorption is detected for coverage below 0.5 L. This indicates that at this coverage all of the CO is dissociating and reacting with the Cr(110) surface. Deposition of 1L CO on clean Cr(110) shows only one broad signal at 300 K. By deposition of 2 L of CO or larger, a shift of the signal to 280 K and the appearance of a second signal at 210 K can be observed. The broadening and shifting of the desorption signals can be attributed to the lateral interaction between the CO molecules and their adsorption on different binding sites on the Cr(110) surface.

**SS-TuP25**, I. Nakamura, T. Fujitani, National Institute of Advanced Industrial Science and Technology (AIST), Japan

The reduction of Rh in three-way catalysts is currently required. Pd catalysts, which have shown a high initial activity for NO reduction compared with that of Rh catalysts, have received much attention as possible substitutes for Rh. To develop high performance Pd catalysts, the nature of active sites must be clarified, as well as the effect of oxide supports on the supported Pd. In this study, we investigated the influence of an Al<sub>2</sub>O<sub>3</sub> support on the electronic state and NO dissociation activity of supported Pd using a Pd-deposited Al<sub>2</sub>O<sub>3</sub>/NiAl(110) surface. NO was exposed at 300 K to the 2 ML Pd/Al<sub>2</sub>O<sub>3</sub> surfaces annealed at different temperatures. Only molecularly adsorbed NO was observed on the Pd/Al<sub>2</sub>O<sub>3</sub> surface after deposition of Pd at 300 K. In contrast, the formation of atomic nitrogen was seen on the Pd/Al<sub>2</sub>O<sub>3</sub> surface annealed above 350 K, suggesting that NO dissociation sites were created after annealing. The adsorbed NO was completely dissociated over the Pd/Al<sub>2</sub>O<sub>3</sub> surface annealed above 500 K. We compared the NO dissociation activity over the 500-K-annealed Pd/Al<sub>2</sub>O<sub>3</sub> surface with that observed over a stepped Pd(311) single crystal surface, since the step sites on Pd surfaces are known to be active sites for NO dissociation. It was clearly shown that the NO dissociation reaction over the Pd/Al<sub>2</sub>O<sub>3</sub> surface proceeded at a much lower temperature compared with that required for NO dissociation over the Pd(311) surface. We found that the active sites created on the annealed Pd/Al<sub>2</sub>O<sub>3</sub> surface had a high NO dissociation ability. To clarify the nature of the Pd active sites for NO dissociation, we examined the electronic state of the Pd particles deposited on the Al<sub>2</sub>O<sub>3</sub> surface. It was shown that the Pd was oxidized to Pd<sup>n+</sup> ( $n < 2$ ) by lattice oxygen atoms in Al<sub>2</sub>O<sub>3</sub> after annealing above 500 K. Therefore, we concluded that the positively charged Pd<sup>n+</sup> species created by annealing the Pd-deposited Al<sub>2</sub>O<sub>3</sub> surface at temperatures higher than 500 K were effective for NO dissociation at low temperatures.

**SS-TuP26 Analysis of the Characteristics of Nickel-Plating Baths**, A.O. Gezerman, B.D. Corbacioglu, Yildiz Technical University, Turkey

Nickel plating processes, popularly used in Europe in the 1950s, have been increasingly employed in Turkey in recent years; as a result, industrial usage has developed rapidly. Nickel plating is the preferred process for this study because of the uniformity of the plating thickness on the plated surface and the ease with which complex components can be plated. It is also resistant to corrosion and has good hardness levels.

In this experiment, the following parameters were investigated: the effect of varying the amount of nickel, the thickness of the plating, and sheen (whether shiny or dull).

In this study, brightener and carrier agents have been used to determine the best operational parameters for the Kale Kilit Factory. The compositions of the brightener and carrier agents used in the experiment is included in this text.

# Wednesday Morning, October 20, 2010

## Surface Science

Room: Picuris - Session SS1-WeM

## Oxide Surface Structure

**Moderator:** C.H.F. Peden, Pacific Northwest National Laboratory

8:00am **SS1-WeM1 How Valuable Is Information from *Ab Initio* Phase Diagrams Beyond the Thermodynamically Allowed Region - the Puzzling (1 × 1)-H Structure on Polar ZnO(0001)-Zn**, *M. Valtiner, M. Todorova, J. Neugebauer*, Max-Planck-Institut fuer Eisenforschung, Germany

The (1 × 1) hydrogen reconstruction observed on Zn-terminated polar ZnO(0001) surfaces [1] is a prominent surface structure, which has so far defied any explanation attempts: none of the surface reconstructions observed in ab initio based equilibrium surface phase diagrams is consistent with the experimental observations [2]. Extending these equilibrium phase diagrams into the region of non-equilibrium conditions for the hydrogen chemical potential we show the occurrence of a new and so far not reported surface structure. The new structure consists of a (1 × 1) H covered triangular shaped reconstructions. It is stabilised and obeys electron counting, due to a simultaneous protonation of step-edge oxygen and surface terminating Zn atoms. It will be shown that the experimental conditions justify the consideration of hydrogen chemical potential outside the stability range of the H<sub>2</sub> molecule [3].

[1] T. Becker et al., Surf. Sci. 486, L502 (2001).

[2] M. Valtiner et al., Phys. Rev. Lett. 103, 065502 (2009).

[3] M. Valtiner et al., submitted (2010).

8:20am **SS1-WeM2 Hydroxylation of the MgO(001) Surface and its Effect on Metal Nucleation**, *M. Brown, E. Carrasco, M. Sterrer, H.-J. Freund*, Fritz-Haber-Institut der Max-Planck-Gesellschaft, Germany

8:40am **SS1-WeM3 First, Find the Atoms: Mapping Epitaxial Nanostructures with Direct X-ray Methods**, *R. Clarke*, University of Michigan, Ann Arbor **INVITED**

Epitaxial heterostructures constitute a large fraction of the materials systems used in current optoelectronics technology. As device dimensions continue to shrink to the nanoscale, atomic interfaces play an increasingly dominant role in their characteristics and performance. Moreover, new classes of devices are envisioned based on novel phenomena emerging from the complex ionic and electronic rearrangements occurring at interfaces. Energy harvesting, catalysis, quantum information processing and smart sensors are but a few of the possible applications. An essential requirement for harnessing these transformative developments is to provide accurate and detailed maps of the structure, chemical composition and strain at epitaxial interfaces prepared by various deposition methods, including molecular beam epitaxy, metallorganic chemical vapor deposition, focused ion beam and pulsed laser deposition. This presentation will describe some of the exciting science that can be done with current and envisioned capabilities in x-ray surface scattering. Examples include the use of direct methods for achieving sub-Ångstrom resolution maps of complex oxide interfaces, quantum-dot tailoring and focused ion beam directed assembly. Such experiments provide a basis for understanding how local structure can give rise to novel properties.

\*Supported by DOE Basic Energy Sciences Contract DE-FG02-06ER46273 and the University of Michigan Energy Frontiers Research Center. </P>

9:20am **SS1-WeM5 W-oxide Clusters on Cu(110) Surfaces: Electronic Structure and Selforganisation**, *M. Wagner, A. Gumbsch, S. Surnev*, Karl-Franzens University Graz, Austria, *Z. Dohnalek*, Pacific Northwest National Laboratory, *A. Fortunelli*, CNR Pisa, Italy, *F.P. Netzer*, Karl-Franzens University Graz, Austria

Oxide clusters with well-defined size and stoichiometry supported on metal surfaces are interesting nanoscale objects with attractive features for both fundamental research and technological applications. It has been shown recently that (WO<sub>3</sub>)<sub>3</sub> cluster molecules, formed by vacuum sublimation of WO<sub>3</sub> powder, can be deposited as monodisperse clusters on TiO<sub>2</sub> (110) surfaces [1]. In the present work, we investigate the interaction and electronic properties of (WO<sub>3</sub>)<sub>3</sub> species at the single molecule level with Cu(110) and reconstructed Cu(110)-O surfaces using low-temperature (5K) scanning tunneling microscopy (STM) and spectroscopy (STS). In order to decouple the (WO<sub>3</sub>)<sub>3</sub> cluster states from the metal substrate states, the

clusters have been deposited also on a NaCl buffer layer (grown on Cu(110)). The comparison of the STM (STS) fingerprints of the (WO<sub>3</sub>)<sub>3</sub> clusters on the NaCl and the Cu surfaces, together with respective DFT calculations, allows us to gauge the cluster-Cu interaction and to determine the hybridisation of the cluster orbitals with metal states. At low temperature (<20K) the (WO<sub>3</sub>)<sub>3</sub> clusters are stable as individual units on the Cu(-O) surfaces, but at elevated temperature (room temperature and above) the clusters react with Cu substrate atoms. They selforganise via condensation and, depending on the coverage, form 1-D W-oxide line structures (nanowires) or arrange into ordered 2-D W-oxide nanolayer phases with well-defined atomic structures. These 2-D structures are investigated experimentally with STM and LEED and theoretically by DFT calculations.

Supported by the ERC Advanced Grant SEPON

[1] O. Bondarchuk, X. Huang, J. Kim, B.D. Kay, L.-S. Wang, J.M. White, Z. Dohnalek, Angew. Chem. Int. Ed. 45 (2006) 4786

9:40am **SS1-WeM6 Growth and Properties of Iron Oxides on YSZ(001)**, *I. Ermanoski, G.L. Kellogg*, Sandia National Laboratories

10:40am **SS1-WeM9 Growth and Characterization of Ordered Tungsten Trioxide Films on Pt(111)**, *Z. Li, Z. Zhang, Y.K. Kim, S. Smith*, Pacific Northwest National Laboratory, *F.P. Netzer*, Karl-Franzens University Graz, Austria, *R.J. Rousseau, B.D. Kay, Z. Dohnalek*, Pacific Northwest National Laboratory

Catalysts based on WO<sub>3</sub> have been found to be active in a number of reactions including isomerization of alkanes and alkenes, partial oxidation of alcohols, selective reduction of nitric oxide, and metathesis of alkenes. In the present study we explore the growth of novel ordered WO<sub>3</sub> thin films on Pt(111) via direct sublimation of monodispersed (WO<sub>3</sub>)<sub>3</sub> clusters. The prepared films are characterized using x-ray photoelectron spectroscopy (XPS), temperature-programmed desorption (TPD), low energy electron diffraction (LEED), reflection-adsorption infrared spectroscopy (RAIRS), and scanning tunneling microscopy (STM). The factors that affect the WO<sub>x</sub> structure such as WO<sub>3</sub> exposure and substrate temperature were explored. At submonolayer coverages, the as-deposited (WO<sub>3</sub>)<sub>3</sub> clusters are partially reduced leading to chainlike tungsten oxide structures with W in (6+) and (5+) oxidation states. Higher substrate temperatures (< 800 K) lead to further reduction of deposited (WO<sub>3</sub>)<sub>3</sub>. At higher coverages, an ordered (3 × 3) structure composed of (WO<sub>3</sub>)<sub>3</sub> trimers is observed upon 700 K deposition. The experimental findings are complemented by DFT calculations that provide further insight into the observed WO<sub>3</sub> structures.

This research was performed in the Environmental Molecular Sciences Laboratory, a national scientific user facility sponsored by the Department of Energy's Office of Biological and Environmental Research and located at Pacific Northwest National Laboratory.

11:00am **SS1-WeM10 Towards a Reliable Characterisation of Oxide Layers on Pure Aluminium using High Energy Resolution FE-AES**, *I. Vandendael, T. Hauffman, Y. Van Ingelgem, A. Hubin, H. Terryn*, Vrije Universiteit Brussel, Belgium

Al<sub>2</sub>O<sub>3</sub> on metallic aluminium is a widely used material of high technological importance. For the local chemical characterisation of these substrates FE-AES bears potential thanks to its high lateral resolution. In this study, the O KLL and Al KLL Auger electron spectral lines are recorded with a high energy resolution from pure aluminium, thin Al<sub>2</sub>O<sub>3</sub> and thick Al<sub>2</sub>O<sub>3</sub> layers on metallic aluminium. The behaviour of these aluminium oxide layers under electron beam irradiation is investigated.

It is demonstrated that, thanks to the high energy resolution used, it is possible to discriminate between the metallic and oxidised aluminium on the basis of the Al<sub>0</sub> KL<sub>2,3</sub>L<sub>2,3</sub> and Al<sup>3+</sup> KL<sub>2,3</sub>L<sub>2,3</sub> Auger electron peaks recorded within one and the same spectrum. Oxygen electron-stimulated desorption is observed for both aluminium oxides. Effective cross-sections for this oxygen desorption are estimated for the thin and thick oxide layers. It is shown that when an Al<sub>2</sub>O<sub>3</sub> layer is irradiated with an electron beam surface charging occurs. These phenomena remain limited thanks to the presence of the underlying metallic aluminium substrate. The electron beam-induced effects are compensated by setting the angle of incidence of the primary electron beam to 15°. Finally, it is shown that inhomogeneities at the surface of the analysed oxides result in significant chemical shifts of the O KLL and Al KLL Auger electron transitions. It is investigated whether these inhomogeneities can be linked with lateral differences in hydroxyl fraction at the surface.

## Surface Science

Room: Santa Ana - Session SS2-WeM

### Electron, Photon and Ion Beam Induced Surface Modification

**Moderator:** J.A. Yarmoff, University of California, Riverside

8:00am **SS2-WeM1 Focused Electron Beam Induced Processing: Experiments, Simulations, and Applications**, *P.D. Rack*, University of Tennessee **INVITED**

The rapid and precise direct-write growth of nanoscale features by electron-beam-induced deposition (EBID) and etching (EBIE) requires the optimization of the growth parameters to maintain nanoscale feature dimensions. The tremendous and complex EBID/EBIE parameter space includes the precursor gas pressure, primary electron beam energy, electron beam current, surface diffusion rates of adsorbed precursor species, thermal effects on desorption, and the cascade of electron species produced by elastic and inelastic scattering processes. These variables affect the probability of precursor dissociation and hence determine the feature growth velocity and the size of the structure through a series of complex, coupled nonlinear interactions. In this presentation, a variety of experimental studies will be presented to demonstrate the various electron-gas, gas-solid, and electron-solid interactions that are germane to the electron beam induced processing technique. A dynamic computer simulation based on Monte-Carlo calculation sequences will then be described and compared to various experimental observations. Finally, several nanoscale device applications will be demonstrated.

8:40am **SS2-WeM3 Electron Beam Deposition for Nanofabrication: Insights from Surface Science**, *H. Fairbrother*, Johns Hopkins University, *J. Wuuk*, Princeton University, *J. Gorham*, National Institute of Standards and Technology, *S. Rosenberg*, Johns Hopkins University, *C.W. Hagen*, TU Delft, the Netherlands, *W. van Dorp*, University of Groningen, the Netherlands

Electron beam induced deposition (EBID) is attracting increased interest as a single-step, direct-write process capable of depositing free standing, nanometer-sized structures with high spatial resolution ( $\approx 1$  nm). However, the largest single limitation of EBID is that the deposited metallic nanostructures typically contain unacceptable levels of organic contamination which adversely affects the material's properties, thereby limiting potential applications. A more detailed understanding of the electron stimulated, decomposition of EBID precursors is needed to rationalize the relationships between organometallic ligand architecture and the composition of the deposits. Such mechanistic detail will allow greater control over the composition and function of nanostructures deposited by EBID while providing the necessary rational design criteria to fashion new organometallic precursors. Other scientific issues associated with EBID include a lack of quantitative information on the fundamental surface dynamics and deposition processes as well as overcoming the challenges of implementing successful purification strategies. The application of surface analytical techniques enables changes in the metal oxidation state, surface and gas phase composition as well as structure and chemical composition that accompany electron interactions with organometallic precursors to be studied *in situ* and in real time. In addition, I will describe how these various electron stimulated processes can be studied to extract data on reaction cross-sections and kinetics, information that would facilitate the development and testing of predictive models that can accurately describe EBID. Mechanistic insights into purification strategies that can be obtained through surface analytical techniques are also detailed. Throughout, I will discuss unresolved challenges and opportunities associated with EBID.

9:00am **SS2-WeM4**, *X. He*, *J.A. Yarmoff*, University of California, Riverside

A system of many electrons can display emergent phenomena that cannot be extrapolated from the behavior of independent electrons. Non-adiabatic resonant charge transfer is used to reveal this multi-electron behavior by employing singly charged alkaline earth ions in a low energy ion scattering experiment. The spin of the single valence electron of such an ion behaves as a magnetic impurity that interacts with the continuum of many-body excitations in the metal, resulting in Kondo and mixed valence resonances near the Fermi energy.<sup>1,2</sup> The occupation of these resonances is acutely sensitive to changes of surface temperature, which leads to an anomalous temperature dependence of the ion neutralization probability. We report a maximum in the neutralization probability near 600 K for 2-4 keV Sr<sup>+</sup> ions scattered from polycrystalline gold. Correlated electron effects, which have traditionally been manifest at low temperature, are observable well above

room temperature because the projectile's ionization level shifts and crosses the target's Fermi energy as it approaches the surface where the interaction between the localized and extended electrons is very strong. This interaction becomes more pronounced as the work function of the surface is lowered by Sr implantation into the near-surface region. Further study will involve well-characterized single crystal surfaces that will enable detailed investigation of the relationships between the formation of correlated electron states and the atomic structure of the solid.

<sup>1</sup>H. X. Shao, P. Nordlander, and D. C. Langreth, *Phys. Rev. Lett.* **77**, 948 (1996).

<sup>2</sup>J. Merino and J. B. Marston, *Phys. Rev. B* **58**, 6982 (1998).

9:20am **SS2-WeM5 Parallel Scanning Near-Field Photolithography: The Snomipede**, *E. ul Haq*, University of Sheffield, UK, *Z. Liu*, University of Nottingham, UK, *S. Alang Ahmad*, University of Sheffield, UK, *Y. Zhang*, University of Glasgow, Ireland, *L.S. Wong*, University of Manchester, UK, *J.K. Hobbs*, *G.J. Leggett*, University of Sheffield, UK, *J. Micklefield*, University of Manchester, UK, *C.J. Roberts*, University of Nottingham, UK, *J.M.R. Weaver*, University of Glasgow, UK

There has been enormous interest in the organisation of molecules at interfaces with nanometre spatial resolution, but important challenges still remain to be addressed. Of the established techniques, electron beam lithography is expensive, and requires exposure under vacuum, while scanning probe methods are slow and (with few exceptions) do not permit fabrication over large areas. Here, a new approach is described that yields arbitrary pattern fabrication over macroscopic areas. Scanning near-field photolithography enables the arbitrary fabrication of molecular structures as small as 9 nm ( $\lambda/30$ ). We have developed a parallel near-field lithography device that fuses scanning near-field optical techniques with the 'Millipede' concept of massively parallel serial fabrication: a 'Snomipede'. Two Snomipede designs will be described, one based around the use of a liquid crystal spatial light modulator to direct diffraction-limited spots into an array of sixteen cantilevers with hollow, pyramidal tips, and the other based around the use of a Brewster angle zone plate, coupled to a digital mirror array, to direct the light spots. Their use for nanopatterning will be demonstrated by patterning siloxanes self-assembled monolayers formed from amino siloxanes molecules with a photocleavable protecting group. Structures with line widths of 100 nm have been formed in parallel over regions over 1 mm wide. Resulting structures have been derivatised with initiators for atom transfer radical polymerisation, from which biocompatible brushes have been grown. The potential of the Snomipede for reactive processing at the nanoscale will be demonstrated by fabricating 70 nm structures in photoresist using a probe array submerged under water.

9:40am **SS2-WeM6 Understanding the Effects of Radiation on the Cerium Oxide Thin Films by Experiment and Simulation**, *A. Kumar*, University of Central Florida, *V. Shutthanandan*, *R. Devanathan*, *S. Kuchibhatla*, *S. Thevuthasan*, Pacific Northwest National Laboratory, *S. Seal*, University of Central Florida

The damaging effect of radiation in applications such as immobilization of toxic radionuclides, fission and fusion reactors, and radiation therapy has attracted considerable scientific interest. The search for radiation tolerant materials has revealed that fluorite structural derivatives, such as zirconia and cerium oxide, have the ability to accommodate high energy radiation induced defects. Particularly for biomedical applications, cerium oxide is of more interest because not only it can prevent the damage from radiation but also it has the ability to quench free radicals and reactive oxygen species produced as the result of high energy radiation by regenerative switching between the +3 and +4 valence states of cerium. However the underlying mechanisms of radiation interaction and the resulting physicochemical and structural changes of cerium oxide are not well understood. In order to gain a fundamental understanding of radiation tolerance of cerium oxide nanostructures, we explored the behavior of single and polycrystalline ceria under radiation. High quality single and poly crystalline nanocerium thin films were grown on YSZ and sapphire respectively by using oxygen plasma assisted molecular beam epitaxy and exposed to 2 MeV He<sup>+</sup> radiation at fluences extending over three order of magnitude ( $10^{14}$  to  $10^{17}$  ions/cm<sup>2</sup>) using the ion beam accelerator at EMSL, in Pacific Northwest National Laboratory. The chemical changes occurring in the thin films due to radiation exposure were characterized *in situ* by x-ray photoelectron spectroscopy (XPS). The experimentally observed changes in valence state were correlated by simulating the nanocerium thin film by molecular dynamics and studying the displacement cascades produced by cerium and oxygen as primary knock on atom. The structural evolution of nanocerium thin films due to radiation exposure will be discussed in detail with implications for the use of cerium oxide as a radiation tolerant material.

10:40am **SS2-WeM9 Methyl Radical Velocity Distributions from Ketone Photooxidation on TiO<sub>2</sub>(110)**, *D. Wilson, M. White*, Stony Brook University

11:00am **SS2-WeM10 Laser Nitriding for Niobium Superconducting Radio-Frequency Accelerator Cavities**, *S. Singaravelu*, Old Dominion University, *J.M. Klopff, G. Krafft*, Jefferson Lab, *M.J. Kelley*, College of William & Mary

Particle accelerators are a key tool for scientific research ranging from fundamental studies of matter to analytical studies at light sources. Cost-for-performance is critical, both in terms of initial capital outlay and ongoing operating expense, especially for electricity. It depends on the niobium superconducting radiofrequency (SRF) accelerator cavities at the heart of most of these machines.

Presently Nb SRF cavities operate near 1.9 K, well (*and expensively*) below the 4.2 K atmospheric boiling point of liquid He. Transforming the 40 nm thick active interior surface layer from Nb to delta NbN (T<sub>c</sub> = 17 K instead of 9.2 K) appears to be a promising approach. Traditional furnace nitriding appears to have not been successful for this. Further, exposing a complete SRF cavity to the time-temperature history required for nitriding risks mechanical distortion.

Gas laser nitriding instead has been applied successfully to other metals [P.Schaaf, Prog. Mat. Sci. 47 (2002) 1]. The beam dimensions and thermal diffusion length permit modeling in one dimension to predict the time course of the surface temperature for a range of per-pulse energy densities. As with the earlier work, we chose conditions just sufficient for boiling as a reference point.

We used a Spectra Physics HIPPO nanosecond laser (l = 1064 nm, E<sub>max</sub> = 0.392 mJ, beam spot @ 34 microns, PRF = 15 – 30 kHz) to obtain an incident fluence of 1.73 – 2.15 J/cm<sup>2</sup> for each laser pulse at the target. The target was a 50 mm diameter SRF-grade Nb disk maintained in a nitrogen atmosphere at a pressure of 550 – 625 torr and rotated at a constant speed of 9 rpm.

The materials were examined by scanning electron microscopy (SEM), electron probe microanalysis (EPMA) and x-ray diffraction (XRD). The SEM images show a sharp transition with fluence from a smooth, undulating topography to significant roughening, interpreted here as the onset of ablation. EPMA measurements of N/Nb atom ratio as a function of depth found a constant value to depths greater than the SRF active layer thickness. Certain irradiation conditions resulted in values consistent with formation of delta NbN. Under certain irradiation conditions, XRD data were consistent only with delta NbN on top of Nb metal.

Funding: authored by Jefferson Science Associates LLC under US DOE Contract De-AC05-06OR23177. We are indebted to Prof. P. Schaaf (Goettingen) for the simulation code and helpful discussions.

11:20am **SS2-WeM11 A Model for the Hydroaffinity OH(1x1)-Si(100) and SiO<sub>2</sub> via Ion Beam Analysis (IBA), Tapping Mode Atomic Force Microscopy (TMAFM) and Surface Energy Analysis from Contact Angle Analysis**, *Q.B. Xing, N. Herbots, M.A. Hart, R.J. Culbertson, J.D. Bradley*, Arizona State University

11:40am **SS2-WeM12 UV Induced Work Function Changes of Metal Oxide Surfaces**, *M. Conrad, S. Gutmann, M.M. Beerbom, R. Schlaf*, University of South Florida

The work function of a number of metal oxide thin films was measured using low intensity x-ray and ultraviolet photoemission spectroscopy (LIXPS, UPS).

Our experiments revealed that UPS based work function measurements of a variety of metal oxide surfaces previously exposed to the ambient or in contact with water vapor caused an immediate work function reduction of the order of 0.5 eV. This artifact was demonstrated using LIXPS work function measurements, which expose the sample surface to only a small fraction of the radiation flux encountered during UPS measurements. This enabled the measurement of the work function prior to the UPS characterization, revealing the UPS-related work function reduction. LIXPS measurement performed after the UPS measurements showed that sample charging effects can be ruled out as causes of the work function reduction, and that the work function change is permanent. These results suggest that a photochemical hydroxylation of the surface through photodissociation of water molecules occurs during the UPS measurement, which results in a surface dipole reducing the work function. Additional experiments investigated the influence of standard XPS measurements as well as LIXPS measurements on the work function. These experiments demonstrated that XPS measurements also cause a work function reduction similar to UPS measurements, albeit during a longer exposure time frame. In contrast, LIXPS measurements do not result in a significant work function reduction,

i.e. can be used as a reliable work function characterization tool for oxide surfaces.

## Tribology Focus Topic

**Room: Tesuque - Session TR+MN+NS+SS-WeM**

## Influence of Atmosphere, Temperature, and Materials on Friction

**Moderator: J.D. Schall**, Oakland University

8:00am **TR+MN+NS+SS-WeM1 ‘Demystifying’ Gas Phase Lubrication: Tribochemistry, Third Bodies and Competition**, *I.L. Singer*, Naval Research Laboratory **INVITED**

Gas phase lubrication, also called vapor phase lubrication, refers to processes in which the gas surrounding a sliding (or rolling) contact contributes to lubrication [1]. It has wide ranging applications from internal combustion engines to MEMS. Some gases simply condense on surfaces, others decompose and deposit lubricating films on the surface, e.g. hydrocarbon films decompose and deposit graphite. Some can be made to react on the surface, as do various monomers that tribopolymerize and form lubricious third bodies at the contact. Alternatively, gases can react with the surface to form films; the most ubiquitous example is the oxide film formed on metals, which prevents (on earth, but not in outer space) surfaces from weld upon contact. Reaction films have been studied extensively by surface scientists; less well understood are tribofilms, films formed by rubbing action. Another important component to the lubrication process is film removal, which can occur during sliding or rolling; the competition between film formation and film removal always needs to be considered. In some cases, gas lubrication provides low friction and low wear; in other cases, it can increase friction and wear. In this talk, I will review gas phase lubrication processes and present several gas phase lubrication studies that still mystify me.

[1] For overview, see [http://nsfaffresh.org/wiki/index.php?title=Gas\\_Phase\\_Lubrication](http://nsfaffresh.org/wiki/index.php?title=Gas_Phase_Lubrication)

8:40am **TR+MN+NS+SS-WeM3 Understanding Vapor Phase Lubrication Mechanism of Alcohol for MEMS and Other Materials**, *S.H. Kim*, Pennsylvania State University

Microelectromechanical systems (MEMS) are usually fabricated from silicon-based materials which have poor tribological properties such as high friction, high adhesion, and low wear-resistance. We have recently demonstrated unprecedented success of MEML lubrication using alcohol vapor. The main difference of alcohol vapor phase lubrication (VPL) from other coating-based approaches is that it allows continuous replenishment of lubricant molecules from the vapor phase, rather than relying on one-time loaded coating layers. In our precious studies, we have observed tribochemically-formed polymeric species. Then, an interesting question is if the polymeric species is responsible for effective lubrication or not. This talk addresses the origin of tribochemical reaction products and the lubrication mechanism for alcohol VPL for silicon oxide surfaces. In summary, the tribochemical polymerization appears to be associated with the substrate wear process occurring due to insufficient adsorbate supply or high mechanical load. The tribochemical reactions do not seem to be the primary lubrication mechanism for vapor phase lubrication of SiO<sub>2</sub> surfaces with alcohol, although they may lubricate the substrate momentarily upon failure of the alcohol vapor delivery to the sliding contact.

9:00am **TR+MN+NS+SS-WeM4 Mechanistic Aspects of Vapor Phase Lubrication of Silicon**, *M.T. Dugger, J.A. Ohlhausen, S.M. Dirk*, Sandia National Laboratories

The lubrication of silicon surfaces with alcohol vapors has recently been demonstrated [D.B. Asay, et. al, Langmuir 24 (2007) p.155]. With a sufficient concentration of pentanol vapor present, sliding of a silica ball on an oxidized silicon wafer can proceed with no measurable wear. The initial results of time-of-flight secondary ion mass spectrometry (ToF-SIMS) analysis of wear surfaces revealed a reaction product having thickness on the order of a monolayer, and with an ion spectrum that included fragments having molecular weights of 200 or more that occurred only inside the wear tracks. The parent alcohol molecule (pentanol) has molecular weight of 88 amu, suggesting that reactions of adsorbed alcohols on the wearing surfaces allowed polymerization of the alcohols to form higher molecular weight species. In addition to pin-on-disk studies, lubrication of silicon surfaces with pentanol vapors has also been demonstrated using MicroElectroMechanical Systems (MEMS) devices. Extraordinary increases in the operating life of MEMS devices have been observed with vapor phase lubrication. Devices with thermal actuators as well as

electrostatic actuators have been successfully operated, demonstrating that the heated surfaces of the thermal actuators do not form prohibitively large amounts of reaction product from the alcohol vapor. The same reaction product between pentanol and the silicon surface observed in pin-on-disk tests has also been found on MEMS contacting surfaces using ToF-SIMS analysis.

Recent investigations of the reaction mechanisms of the alcohol molecules with the oxidized silicon surfaces have shown that wearless sliding requires a concentration of the alcohol vapor that is dependent upon the contact stress during sliding, with higher stress requiring a greater concentration of alcohol. Different vapor precursors including those with acid functionality, olefins, and methyl termination also produce polymeric reaction products, and can lubricate the silica surfaces. Doping the operating environment with oxygen was found to quench the formation of the polymeric reaction product, and demonstrates that polymer formation is not necessary for wearless sliding.

9:20am **TR+MN+NS+SS-WeM5 Tribological Study of Octadecylphosphonic Acid Self-Assembled Monolayers Across Velocity Regimes**, *O. Matthews, S. Barkley*, Luther College, *C. Bouxsein, M. Deram, N. Eigenfeld*, St. Olaf College, *A. Poda, W.R. Ashurst*, Auburn University, *B. Borovsky*, St. Olaf College, *E. Flater*, Luther College

Bioelectromechanical systems (MEMS) are critically-limited by interfacial phenomena such as friction and adhesion. The most common method of reducing friction between MEMS surfaces is the use of molecularly-thin self-assembled monolayer (SAM) coatings. Typically silicon MEMS have been coated with silane-based SAMs, such as octadecyltrichlorosilane (OTS), and have resulted in some modest improvement in device performance and lifetime. Continued progress in the development of MEMS may require new materials systems to be implemented. Through a collaborative effort, we investigate the frictional properties of octadecylphosphonic acid monolayers deposited on aluminum oxide surfaces across speed regimes. Measurements using an atomic force microscope (AFM) and a nanoindenter-quartz crystal microbalance are performed each with a microsphere-terminated probe. This allows for a comparative study with similar contact sizes, pressures, surface roughness, and interfacial chemistry. Speeds between the different instruments range from microns per second to meters per second. Preliminary AFM friction vs. load and friction vs. velocity measurements are presented, with the goal of investigating phosphonate SAM/ metal oxide systems as alternative MEMS materials.

9:40am **TR+MN+NS+SS-WeM6 Triboelectrification and Triboplasma Generation and its Application for Surface Modification**, *S.V. Singh, P.K. Michelsen, Y. Kusano*, Technical University of Denmark

Triboplasma gas discharges are often induced by triboelectrification around a sliding contact. Only an empirical classification is available for triboelectrification, whereas a detailed physical mechanism behind it is still unknown. Laboratory triboplasmas are mostly characterized by using optical diagnostics, and the optical emissions are reported to be observed mostly in ultraviolet region, corresponding to nitrogen emission lines. These measurements do not directly address triboelectrification. Here we present the evidence of electrostatic charging at the sliding contact and gas break down between the contacts through electrical measurements. Furthermore, the applicability of triboplasma for surface modification on polymeric materials was studied. Two capacitive probes were used for the investigation of a triboelectrification and triboplasma generated in a pin-on-rotating disk apparatus. These probes were mounted above the disk and on the pin, respectively. Measurements show a clear evidence of tribocharging, charge decay and triboplasma generation. Several combination of sliding contact materials with tendency to gain opposite charging and different sliding speeds, as high as 1000 rotation per minute, were carefully chosen. In addition, influence of different gas environment and pressure were investigated. Triboplasma induced surface modifications were characterized by water contact angle and X-ray photoelectron spectroscopy measurements.

10:40am **TR+MN+NS+SS-WeM9 Friction at Cryogenic Temperatures**, *S.S. Perry*, University of Florida **INVITED**

There are a number of applications where operation over a wide temperature range is required for device success. These extreme conditions are often the motivation for variable temperature studies in tribology; however, a paucity of relevant tribology data exists for temperatures below 273 K.

In the range from 300 K to 100 K the friction coefficient of various solid lubricants has recently been shown to increase with decreasing temperature. Molecular scale measurements employing an atomic force microscope over a temperature range from 140 K to 750 K at a vacuum level of  $2 \times 10^{-10}$  torr have identified a temperature activated behavior of the friction and friction

coefficient for the solid lubricants graphite and molybdenum disulfide. These molecular scale experiments were performed under conditions for which interfacial sliding was confirmed, interfacial wear was absent, and the role of adsorbed contaminants could be dismissed.

The potential influence of interfacial wear as well as the mechanism underlying the measured temperature dependence will be discussed.

11:20am **TR+MN+NS+SS-WeM11 In-Situ Scanning Auger Analysis of a Tribological Wear Scar in UHV Conditions**, *B.P. Miller, O.J. Furlong, W.T. Tysoe*, University of Wisconsin-Milwaukee

Lubrication of sliding copper-copper interfaces for use in brushes in electrical motors provides a particular challenge. Not only is a reduction in friction and wear required, but also allowing for high conductivity through the contact. Therefore, a self-limiting tribofilm is essential. The following explores the surface chemistry and tribology of dimethyl disulfide (DMDS) on copper surfaces to establish whether it is sufficiently reactive to potentially form a tribofilm near room temperature as required for lubrication of the sliding copper-copper contact in an electric motor. The surface chemistry and decomposition pathways of DMDS on copper surfaces are analyzed using temperature-programmed desorption (TPD), reflection-absorption infrared spectroscopy (RAIRS) and X-ray photoelectron spectroscopy (XPS). It is shown that DMDS reacts to form methyl thiolate species on the copper surface at room temperature. After heating to about 430K, methane and C<sub>2</sub> hydrocarbons desorb leaving molecular sulfur adsorbed onto the surface. A UHV tribometer chamber was equipped with a scanning electron gun having a ~100 micron diameter spot size. DMDS was dosed in the gas phase while performing friction measurements so that *in-situ* elemental analysis of the wear scar could be made. An increase in the sulfur signal is witnessed inside compared to outside of the tribological wear scar. A depth profile Auger analysis of the sample showed selective diffusion of sulfur into the bulk only inside the wear scar attributed to tribologically induced effects. This novel method of analysis can give important insights into the fundamentals of tribological systems.

11:40am **TR+MN+NS+SS-WeM12 First Principles Calculations and Atomistic Simulations of Tribology at Sliding Molybdenum Disulfide Surfaces**, *T. Liang, S.R. Phillpot, S.B. Sinnott*, University of Florida

Molybdenum disulfide is the most commonly used solid lubricant coating in aerospace applications. In this work, we carry out first principles density functional theory (DFT) calculations of the potential energy surface between two MoS<sub>2</sub> surfaces and examine the influence of oxidation on the results. In addition, we present the results of a recently developed empirical many-body potential for Mo and S systems and examine nano-scale friction between sliding MoS<sub>2</sub> surfaces using classical molecular dynamics (MD) simulations. In particular, MD simulations of interfacial sliding at various loads, temperatures and sliding directions are carried out. The loads and friction forces are extracted to calculate the friction coefficient of the MoS<sub>2</sub> as a function of temperature, and the results are compared to experimental pin-on-disk measurements of MoS<sub>2</sub> coatings and atomic force microscopy measurements on single crystal MoS<sub>2</sub> surfaces. The results from both the DFT calculations and the MD simulations help us to better understand the origins of lubricity on MoS<sub>2</sub>.

# Wednesday Afternoon, October 20, 2010

## Electronic Materials and Processing

Room: Dona Ana - Session EM+SS-WeA

### High-k Dielectrics for III-V Electronics

Moderator: A.C. Kummel, University of California at San

Diego

2:00pm EM+SS-WeA1 **High-k III-V MOSFETs Enabled by Atomic Layer Deposition.** *P. Ye*, Purdue University **INVITED**

The principal obstacle to III-V compound semiconductors rivaling or exceeding the properties of Si electronics has been the lack of high-quality, thermodynamically stable insulators on III-V materials. For more than four decades, the research community has searched for suitable III-V compound semiconductor gate dielectrics or passivation layers. The literature testifies to the extent of this effort. The research on ALD approach is of particular interest, since the Si industry is getting familiar with ALD Hf-based dielectrics and this approach has the potential to become a manufacturable technology.

Using In-rich InGaAs as surface channel, high-performance inversion-mode high-k/III-V NMOSFETs have been demonstrated. By further improving on-state performance, such as maximum drain current  $I_{dss}$  and peak transconductance  $G_m$ , the off-state performance or subthreshold characteristics need to be seriously evaluated for digital applications. In this talk, we review some new progresses on deep-submicron inversion-mode  $\text{In}_{0.7}\text{Ga}_{0.3}\text{As}$  NMOSFETs using 2.5 nm-5.0 nm ALD  $\text{Al}_2\text{O}_3$  as high-k gate dielectrics. The  $G_m$  exceeds 1.1-1.3 mS/ $\mu\text{m}$  and starts to approach the values from InGaAs HEMTs. The scaling metrics, such as threshold voltage ( $V_T$ ),  $I_{on}/I_{off}$  ratio, sub-threshold swing ( $S.S.$ ), the drain induced barrier lowering ( $DIBL$ ), as a function of the gate length from 150 nm to 250 nm are systematically studied. Retro-grade structure and halo-implantation are also applied to III-V MOSFET field to improve the off-state performance of InGaAs MOSFETs. In order to achieve better gate control capability, new structure design like FinFET demonstrated successfully in Si devices, is strongly needed for short-channel III-V MOSFETs. However, unlike Si, the dry etching of III-V semiconductor surface has been believed to be difficult and uncontrollable, especially related with surface damage and integration with high-k dielectrics. We also review some results on the first experimental demonstration of inversion-mode  $\text{In}_{0.53}\text{Ga}_{0.37}\text{As}$  tri-gate FinFET using damage-free etching and ALD  $\text{Al}_2\text{O}_3$  as gate dielectric. The SCE is greatly suppressed.

The work is in close collaborations with Y.Q. Wu, Y. Xuan, J.J. Gu and M. Xu. We also would like to thank valuable discussions with D. Antoniadis, M.S. Lundstrom, R.M. Wallace, K.K. Ng, M. Hong, and J. Woodall.

2:40pm EM+SS-WeA3 **Passivation of  $\text{Al}_2\text{O}_3/\text{InGaAs}(100)$  Interfaces by Atomic Layer Deposition and Annealing.** *F.L. Lie, B. Imangholi*, University of Arizona, *W. Rachmady*, Intel Corp., *A.J. Muscat*, University of Arizona

Identification of the source of interfacial defects between high-k films and III-V substrates is crucial for developing passivation methods. Efforts have been made to isolate defects based on a specific chemical moiety at an interface. A study reported that doubly-O coordinated Ga and displaced As formed when GaAs is exposed to oxygen, induces mid-gap states<sup>1</sup>. Another study suggested that high activity interface defects originate from structural disorder instead of specific chemical moieties<sup>2</sup>. This project aims to understand the nature of  $\text{Al}_2\text{O}_3/\text{InGaAs}$  interface defects by relating composition to electrical performance. The modification of InGaAs(100) surfaces due to surface cleaning,  $\text{Al}_2\text{O}_3$  deposition, and post deposition annealing (PDA) was investigated using capacitance-voltage (CV) curves, large AC signal conductance (LSC), and x-ray photoelectron spectroscopy (XPS).  $\text{Al}_2\text{O}_3$  films were deposited by atomic layer deposition (ALD) using trimethylaluminum (TMA) and water precursors on native oxide covered and aqueous HF etched InGaAs(100) surfaces. XPS analysis on a native oxide sample revealed ~8Å oxide (52% As, 29% Ga, and 21% In) and a monolayer excess of As on an As-terminated substrate. TMA reacted on this surface during ALD, thinning the oxide to ~4.2 Å (45% As, 29% Ga, and 27% In). Aqueous HF treatment removed the native oxide and produced an As-rich surface, which re-oxidized in air. Surfaces consisted of ~4.2 Å oxide (91% As) and 1.5 monolayer excess As on an As-terminated surface. ALD  $\text{Al}_2\text{O}_3$  on the liquid-cleaned surface produced a chemically sharp  $\text{Al}_2\text{O}_3/\text{InGaAs}$  interface with less than a monolayer of As oxide. CV and LSC measurements were performed on Au/Ni/10 nm  $\text{Al}_2\text{O}_3/\text{InGaAs}$  stacks. The deep-level surface recombination velocity (SRV) values extracted represent the net effect of interface defects, which includes the defect density and capture cross section. The similar SRV values obtained

for native oxide (34±6 cm/s) and aqueous HF (29±13 cm/s) prepared surfaces suggest that the presence or absence of oxides was not the only determining factor. PDA in forming gas and  $\text{NH}_3$  ambients significantly improved the electrical quality, as reflected in SRV values of 1 to 5 cm/s for both surfaces. XPS analysis showed increased excess As and  $\text{Ga}_2\text{O}_3$  at the interface of both surfaces, likely due to thermally or H-induced reactions between interfacial As oxide and Ga atoms in the substrate. These results suggest that high activity defects in III-V's could be associated with interfacial dangling bonds and are amenable to standard passivation methods used in Si technology.

<sup>1</sup>Hale M. J. et al, J. Chem. Phys. 119(13), 2003

<sup>2</sup>Caymax M. et al, Microelectron. Eng. 86, 2009

3:00pm EM+SS-WeA4 **An In Situ Examination of Atomic Layer Deposited  $\text{Al}_2\text{O}_3/\text{InAs}(100)$  Interfaces.** *A.P. Kirk, M. Milojevic, D.M. Zhernokletov, J. Kim, R.M. Wallace*, University of Texas, Dallas

An in situ half-cycle atomic layer deposition/X-ray photoelectron spectroscopy (ALD/XPS) procedure was conducted in order to learn more about the evolution of the  $\text{Al}_2\text{O}_3$  dielectric interface with undoped InAs(100). Without breaking vacuum, monochromatic XPS was used to examine the InAs(100) surface following ammonium sulfide passivation or ammonium hydroxide etching and then after each individual ALD pulse of trimethyl aluminum (TMA) and deionized water (DIW) precursors (e.g. single TMA pulse/XPS scan; single DIW/XPS scan; etc.). Ammonium sulfide was more effective at minimizing native oxides than ammonium hydroxide. Regardless of chemical cleaning technique, after depositing up to 1 nm of  $\text{Al}_2\text{O}_3$ , elemental arsenic ( $\text{As}^0$  or As-As bonds) remained at the interface which may have adverse implications for devices such as metal oxide semiconductor field effect transistors (MOSFET). After heating to 300 °C (typical ALD reactor temperature), As-S bonding was reduced below the XPS detection limit. The  $\text{In}^{3+}$  chemical state (e.g.  $\text{In}_2\text{O}_3$ ) was preserved while trivalent In and As oxidation states were minimized following exposure to TMA. The chemical reaction pathways appear to be similar to that observed for GaAs and InGaAs. We will also present electrical characterization studies and examine the correlation to the in situ interface analysis.

4:00pm EM+SS-WeA7 **Fermi-level Unpinning of  $\text{HfO}_2/\text{In}_{0.53}\text{Ga}_{0.47}\text{As}$  Gate Stacks using Hydrogen Anneals.** *R. Engel-Herbert, Y. Hwang, N.G. Rudawski, S. Stemmer*, University of California, Santa Barbara

Compound (III-V) semiconductors are currently being investigated to replace Si as channel material in metal oxide semiconductor field effect transistors. A significant challenge is the high trap density ( $D_{it}$ ) at the dielectric/III-V semiconductor interface, causing Fermi level pinning. Recently, it has been reported that the  $D_{it}$  can be reduced by sulfur passivation and hydrogen annealing for  $\text{Al}_2\text{O}_3/\text{In}_{0.53}\text{Ga}_{0.47}\text{As}$  interfaces.

In this presentation, we will present our studies of the effect of forming gas anneals on the electrical properties of  $\text{HfO}_2/\text{In}_{0.53}\text{Ga}_{0.47}\text{As}$  metal oxide semiconductor capacitors.  $\text{HfO}_2$  films with thicknesses between 9 and 18 nm were deposited in-situ on As-decapped n-type  $\text{In}_{0.53}\text{Ga}_{0.47}\text{As}$  channels by chemical beam deposition using hafnium *tert*-butoxide (HTB) as the source. Samples were post-deposition annealed in forming gas. For comparison samples annealed in nitrogen were also studied. Capacitance-voltage (CV) and conductance-voltage (GV) curves were measured at room temperature. The interface trap density  $D_{it}$  was quantified using both the Terman and the conductance methods. The conductance method showed that the  $D_{it}$  was reduced from  $1.3 \times 10^{13} \text{cm}^{-2} \text{eV}^{-1}$  to  $8 \times 10^{12} \text{cm}^{-2} \text{eV}^{-1}$  near midgap. The conductance peak shifted in frequency with a change in negative gate voltage, consistent with an unpinned Fermi level. The 1 MHz CV curve reached the calculated minimum capacitance value, indicating Fermi level unpinning. The nitrogen annealed control sample did not reach the minimum capacitance and the conductance peak shift at negative bias was moderate, indicating Fermi level pinning at midgap. We will also present comparisons of the extracted band bending for both nitrogen and forming gas annealed stacks and discuss the mechanisms by which forming gas anneals can reduce the midgap  $D_{it}$ .

4:20pm EM+SS-WeA8 **Valence Band Alignment in low-k Dielectric/Cu Interconnects as Determined by X-ray Photoelectron Spectroscopy.** *S. King, M. French, M. Jaehnic, M. Kuhn*, Intel Corp.

Electrical leakage in low-k/Cu interconnect structures is becoming a growing vital concern as the nano-electronics industry moves to increasingly tighter metal spacing's for sub 22 nm technology nodes and continues to replace dense  $\text{SiO}_2$  dielectrics with low density / porous  $\text{SiOC:H}$  "low-k" dielectric materials. In order to understand the various possible leakage mechanisms in low-k/Cu interconnects, a knowledge of the



basic band alignment between Cu and low-k dielectric materials is needed but has gone largely unreported. In this regard, we have utilized X-ray Photoelectron Spectroscopy (XPS) to measure the Valence Band Alignment and Schottky Barrier at interfaces of importance to Cu/low-k interconnects. XPS has been used extensively for determining the band alignment of numerous semiconductors to other semiconductors, metals, and dielectrics. In this paper, we demonstrate that XPS can also be utilized to determine the band alignment at interfaces between amorphous dielectrics and metals of interest to the low-k/Cu interconnects industry. Specifically, we have utilized XPS to determine the Schottky Barrier between Cu and low-k dielectric SiC and SiCN capping layers deposited on Cu via Plasma Enhanced Chemical Vapor Deposition (PECVD). We have also utilized XPS to determine the valence band alignment at SiCN:H/SiOC:H interfaces. Lastly, the impact of various plasma surface treatments on the band alignment at these interfaces was also investigated.

4:40pm **EM+SS-WeA9 III-V CMOS: A sub-10 nm Electronics Technology?**, *J.A. del Alamo*, Massachusetts Institute of Technology  
**INVITED**

CMOS scaling is at the heart of the microelectronics revolution. The ability of Si CMOS to continue to scale down transistor size while delivering enhanced performance is becoming increasingly difficult with every generation of technology. For Moore's law to reach beyond the limits of Si, a new channel material with a high carrier velocity is required. A promising family of materials for this is III-V compound semiconductors.

III-Vs are well known for their unique suitability for high frequency electronics. III-V-based integrated circuits are currently in use in a variety of communications and defense applications. The prospect of III-Vs entering the logic roadmap is tantalizing. This work reviews some of the critical issues.

The barrier for insertion of a new channel material into the CMOS roadmap is huge. Any new technology has to beat Si designs in performance at device footprints that allow the integration of billions of transistors on the same chip. In addition, cost-effective manufacturing must be realized.

To make this work, a III-V CMOS technology has to solve a number of challenging technical problems. The development of a gate stack that includes a high-K dielectric and yields a high-quality semiconductor interface with a III-V compound semiconductor is up there as one of the greatest and most fascinating problems in modern semiconductor technology. Recent research suggests that this is an eminently attainable goal. Transistor size scalability is also a major worry. Will it be possible to scale future III-V transistors to the required dimensions while preventing excessive short-channel effects and attaining the demanding parasitic resistance objective? This is a topic that will call for extensive experimental and simulation research. Fortunately, calibrated simulators today reproduce quite well the characteristics of 30 nm gate length III-V FETs and should be valuable in projecting to devices in the 10 nm range. If planar device designs are unsuitable, 3D designs might offer a viable path. Recent 3D device demonstrations with impressive characteristics give hope that this is a promising strategy. A future III-V CMOS technology will also have to "look and feel" as much as Si as possible. This calls for the formation of thin high-quality III-V layers on top of large Si wafers. In fact, depending on what emerges as the best option for the p-channel device, a major challenge in itself, two dissimilar materials might need to be integrated side by side in very close proximity on top of a Si wafer. These are all great problems that will require the coordinated attention of scientists and technologists with expertise in many different domains.

5:20pm **EM+SS-WeA11 Potential Profiles of III-V MOSCAPs with Kelvin Probe Force Microscopy In Situ**, *W. Melitz, J. Shen, S. Lee, J.S. Lee, A.C. Kummel*, University of California at San Diego, *S. Bentley, D. Macintyre, M. Holland, I. Thayne*, University of Glasgow, UK

Cross-sectional scanning probe microscopy (SPM) is an imaging technique which can map the potentials inside an operational MOSCAP or MOSFET device. Kelvin probe force microscopy (KPFM) measures the contact potential difference (CPD) of a conductive cantilever and a sample surface with a precision of better than 10 meV. In cross-sectional KPFM, (X-KPFM) a fully functional MOSFET or MOSCAP is cleaved in UHV, and the potential inside the working device is measured in two-dimensions; UHV cleaving is critical to preserve an oxide-free surface so the unperturbed potentials can be measured. Cross-sectional KPFM can determine the effect of surface passivation of the gate oxide in operational devices, influence of the fixed charge in the gate oxide with semiconductor channel material, structural features and their effects on the potential distribution, and even work function offsets of the gate and semiconductor. The biggest challenges in imaging cleaved devices is obtaining good cleaves and finding the structure of interest while maintaining good tip conditions for high resolution. Using a comb structure for the electrodes increases the density of the devices on the cleave face to increase the

number of working devices. The cleave edge of the sample drastically affects the stability of the cantilever. In order to increase the stability, the devices were embedded in a >300nm insulator; therefore, the device of interest is not located directly on the edge face. Using this capping technique, high spatial resolution in a UHV cleaved MOSCAP with KPFM shows the amount of band bending in the semiconductor channel caused by the fixed charge in the oxide. High resolution KPFM has also been demonstrated for a range of external gate biases, illustrating the flexibility of KPFM for investigating MOS devices. Current efforts focus on implementing KPFM into patterned scaled MOSCAP and MOSFET devices.

## Surface Science

**Room: Santa Ana - Session SS-WeA**

## Chemisorption and Surface Reactions

**Moderator: A. Utz, Tufts University**

2:00pm **SS-WeA1 Characterization of the Chemical Signal Created by CO Oxidation on Pt/GaN Nanodiodes**, *J.R. Creighton, M.E. Coltrin, R.P. Pawlowski, K.C. Baucom*, Sandia National Laboratories

Previous results from Gabor Somorjai's group demonstrated the production of chemicurrent during catalytic reactions on Pt and Pd surfaces using a Schottky diode structure described as a "catalytic nanodiode" [1-2]. During the exothermic oxidation of CO, some fraction of the chemical energy may be dissipated by formation of hot electrons in the catalytic metal via electronic excitation. If the catalytic metal film is thin enough (nanometer scale) some of these hot electrons may be collected on the semiconductor side of the Schottky barrier in the form of a "chemicurrent". We have fabricated several versions of catalytic nanodiodes, and during CO oxidation we also detect a current that is unambiguously a result of the chemical reaction. We typically measure current densities up to 100 nA/mm<sup>2</sup> and reaction conversion efficiencies in the range of 10<sup>-5</sup>-10<sup>-3</sup> electrons per CO<sub>2</sub> produced; results which are quantitatively similar to reports in more recent publications [3-4].

However, details of the electronic nature this chemical signal indicates that it is derived from a **voltage source**; not from a current source. In fact, the chemical signal is primarily, if not entirely, due to the thermoelectric voltage generated by changes in the **lateral** temperature gradient between the two electrical contacts in the nanodiode. We have used a 3D heat transfer model to simulate the time dependent temperature profile in the nanodiode during CO oxidation on Pt/GaN devices. This information, along with independent experimental measurements of the Seebeck coefficient allows us to quantitatively simulate the thermoelectric voltage signal generated during a typical experiment involving time-dependent CO oxidation. Our results indicate that the nanodiode is simply operating as a **thermal detector** via a thermoelectric voltage. Unfortunately we have not yet found evidence supporting true "chemicurrent" formation during CO oxidation on Pt/GaN nanodiodes.

References:

- [1] Z.J. Xiao and G.A. Somorjai, *J. Phys. Chem. B* 109 (2005) 22530.
- [2] J. Xiaozhong, A. Zupero, J.M. Gidwani, and G.A. Somorjai, *J. Amer. Chem. Soc.* 127 (2005) 5792.
- [3] J.Y. Park, J. R. Renzas, B.B. Hsu, and G.A. Somorjai, *J. Phys. Chem. C*, 111 (2007) 15331
- [4] J.Y. Park, J. R. Renzas, A.M. Contreras, and G.A. Somorjai, *Topics in Catalysis*, 46 (2007) 217

2:20pm **SS-WeA2 Structural Investigation of Methylthiolate/Au (111) Interface: A Photoemission Core Level Shift Study**, *A. Chaudhuri*, University of California, Irvine

Self assembled monolayers have been the subject of considerable interest for the last two decades. The high order, dense and stable structures, and bio compatible nature of these systems make them interesting for a wide range of technological application in industry. The thiolate /Au(111) interface is regarded as one of the classical examples of self assembled monolayer systems and is ideal for study in laboratories, due to the robust nature of the surface.

Despite of a number of studies, the adsorption sites of the thiolate and, hence, the structure of this interface is a long standing controversial issue. The conflict between theoretical calculations and the experimental observations for thiol-Au system has been fuelled by contradictory models to determine the adsorption site based on different experimental techniques. These models are different from each other and fail to depict a mechanism for a complete structure formation. In this present work, we have

investigated the local structure of methylthiolate in the ordered Au(111) - ( $\sqrt{3} \times \sqrt{3}$ )R30° phase using core-level- shifts measurements of the surface and bulk components of Au 4f<sub>7/2</sub> photoelectron binding energy.

**2:40pm SS-WeA3 Mechanistic Study of Photochemical Grafting of Alkenes to Group IV Semiconductors, X. Wang, R.J. Hamers, R. Ruther, University of Wisconsin-Madison**

The grafting of organic molecules on semiconductor surfaces initiated by UV light has become an efficient means to tailor the chemical and physical properties of surfaces of materials, enabling their integration with various applications of the devices. The mechanism of photochemical grafting of alkenes to group IV semiconductors (diamond, silicon, germanium, etc) has remained poorly understood. We have demonstrated that a previously unrecognized process—photoelectron emission from semiconductors to reactant liquid—is a nearly universal mechanism for initiating grafting of alkenes to surfaces and is broadly applicable to a wide range of semiconductors.

The charge transfer processes that occur during the photochemical grafting to diamond surfaces were investigated by spectrally resolved photoelectron yield experiments. X-ray and ultraviolet photoelectron spectroscopy measurements (XPS, UPS) establish a clear correlation between the photoelectron yield, the grafting efficiency at different wavelengths, and the valence electronic structure of the substrate and of the reactant molecule.

While our initial work focused on detailed studies on diamond, more recently we have shown that this mechanism is also responsible for initiating UV-induced grafting onto other semiconductors, most notably both silicon and germanium. By intentionally reducing the bulk carrier lifetime in Si (by doping with Au) and comparing the grafting efficiency, we showed that the rate of UV-induced grafting is independent of the bulk carrier lifetime. This observation is important as it allows us to immediately rule out the bulk exciton mechanism as the primary pathway. Our results also showed that the rate of grafting was directly connected to the electron affinity of the reactant molecules. These results are important because they show that photoemission can also dominate as an initiation process with smaller bandgap semiconductors, such as silicon and germanium, where photoemission and exciton processes can both take place. We have hypothesized that the reason why the photoemission can be dominant even on silicon is that photoemission is an irreversible process, while in an exciton process the concentration of holes is reduced by recombination processes. Our studies provide new insights into the nature of photochemical functionalization on the surfaces of semiconductors and a fundamental understanding of the mechanism will facilitate the design and synthesis of well defined functional interfaces.

**3:00pm SS-WeA4 Reaction of Diisocyanates at the Ge(100)-2 × 1 Surface, K.T. Wong, S.N. Chopra, S.F. Bent, Stanford University**

Interest in organic functionalization of semiconductors has increased in recent years, as it offers the ability to mate existing knowledge of microelectronics fabrication with the tailorability of organic molecules to precisely control interfacial properties. Such control is necessary for today's microelectronics with continually decreasing feature sizes. In particular, this study focuses on organic functionalization of the germanium surface; germanium is a group IV semiconductor, like silicon, which may be used in devices for its favorable electronic properties. Here, we study the adsorption of two diisocyanate molecules on the Ge surface: 1,3-phenylene diisocyanate, in which the isocyanate functional groups are connected by a relatively stiff phenylene ring, and 1,4-diisocyanatobutane, in which they are connected by a more flexible alkyl chain. Using multiple internal reflection Fourier transform infrared spectroscopy in ultra high vacuum, we show that both molecules bind to the Ge(100)-2×1 surface primarily by a [2+2] cycloaddition reaction across the C=N bond of one isocyanate functional group. This result is similar to previous results for other isocyanate-containing molecules reacted with the Ge(100)-2×1 surface. X-ray photoelectron spectroscopy results agree with the [2+2] cycloaddition assignment and provide evidence that some isocyanate functional groups interact with the surface via a dative bond through an oxygen lone pair. We propose that this is likely the result of some adsorbates forming an additional interaction with the surface through the second isocyanate functional group. Density functional theory calculations demonstrate the feasibility of such products. The relatively weak binding of a second functional group by dative bonding may make these molecules ideal candidates for studying displacement by subsequent exposure to a second precursor. It may be possible to displace the dative-bonded isocyanate functional group, thereby creating additional free isocyanate groups on the surface.

**4:00pm SS-WeA7 Multiple Time and Length Scales in Nanocatalysts Probed in a Single Synchrotron Experiment: The Combined use of XAFS, XRD, DAFS and IR, A.I. Frenkel, Yeshiva University INVITED** X-ray absorption fine structure (XAFS) and x-ray diffraction (XRD) techniques give complementary information about the structure of catalytic materials. XRD is effective in crystalline materials that possess medium to long range order (bulk catalysts, substrates and templates) while XAFS provides short range structural details in disordered, amorphous and/or low-dimensional materials. In addition, XAFS gives information about the electronic properties of the catalysts. These two methods have been developed and advanced *independently* from each other at synchrotron sources in the US and abroad. To analyze catalysts *in situ*, in particular *in operando* (under their operating conditions), a new approach is needed, namely, the simultaneous collection of the XRD and XAFS data in real time as the reaction progresses, together with the online product analysis. Diffraction Anomalous Fine Structure (DAFS) is a structure-sensitive technique that allows to deconvolute multiple phases of the same element (e.g., metal nanoparticles and metal oxide) that can coexist in the sample. Application of quick scanning monochromator mode to XAFS measurement (called QEXAFS) allows to study kinetics of structural transformations within the reactants, catalysts and the reaction products. Such combinations allow to measure the time-dependent changes in the *actual* structure (in the short, medium and long range order), electronic properties and chemical activity of catalysts synchronously.

The first in US dedicated instrument for such combined measurements was built at the beamlines X18A and X18B of the National Synchrotron Light Source at Brookhaven National Laboratory. The current setup includes transmission and fluorescence XAFS detectors, QEXAFS monochromator enabling 10ms time EXAFS scan time, 2D area detector for XRD, residual gas analyzer and the automated gas mixing system. The upgrades currently under way include the addition of Diffuse Reflectance Infrared Fourier Transform Spectroscopy (DRIFTS) instruments developed jointly by members of Synchrotron Catalysis Consortium at BNL and Harrick Scientific.

I will present several applications of the combined use of these instruments for catalysis research, including the studies of kinetics of reduction and oxidation of Cu-ceria catalysts, the investigation of the mechanism of reduction of CuFe<sub>2</sub>O<sub>4</sub> with CO, and others.

**4:40pm SS-WeA9 The Interaction of Oxygen with Single Crystal Stepped Copper Surfaces: a XPS and STM Study, E. Broitman, Carnegie Mellon University, V.V. Pushkarev, Lawrence Berkeley National Laboratory, B.S. Holsclaw, Carnegie Mellon University, T.J. Lawton, A.E. Baber, E.C.H. Sykes, Tufts University, A.J. Gellman, Carnegie Mellon University**

Fundamental knowledge of metal oxidation processes is an important problem for the understanding of corrosion. In particular, the oxygen reaction with copper surfaces is considered to be a model system and has consequently been extensively studied. However, to our knowledge, most of the studies have been carried out in individual samples of single orientations. In this work, the influence of steps on the oxidation of copper surfaces is studied by the use of a spherically-shaped sample with a (111) plane in its center. This sample allows the possibility to study the orientation dependence continuously up to a deviation of 10° from the (111) plane.

The copper crystal was cleaned in a UHV preparation chamber with a base pressure < 1X 10<sup>-10</sup> Torr using several cycles of sputter cleaning with Ar<sup>+</sup> ions of 1 KeV energy and annealing up to 600°C. The sample, kept at room temperature, was subsequently exposed to oxygen using a leak valve with dosing values in the range 100 to 1000 Langmuir. Two-dimensional surface imaging chemical analysis was carried out at room temperature using a Theta Probe monochromated Al K<sub>α</sub> x-ray photoelectron spectroscopy (XPS) system (Thermo Scientific) in snapshot mode with a 100 μm spot size. Data processing was performed using the software Avantage provided with the instrument. Scanning Tunneling Microscopy (STM) was also done at room temperature using a commercially available STM Variable Temperature system (Omicron).

XPS images have shown that the oxygen content in the surface increases in the areas with higher step density. STM images revealed a complex oxidation mechanism. Adsorption of oxygen leads to the formation of a surface oxide by preferential incorporation of Cu atoms from step edges. It was observed at higher dosing that the descending step edge to a large terrace results to be more faceted and jagged than a descending step edge of a smaller terrace. It can be assumed that oxygen landing on the terrace diffuses to the descending step edge and oxidizes it. In this way, larger terraces above a step edge would have more oxygen diffusing to the descending step edge, producing more faceting than in the descending steps of the smaller terraces.

5:00pm **SS-WeA10 Cu(100) Oxidation: Potential Copper-Releasing Pathways for  $c(2 \times 2)$  to Missing-Row Reconstruction Transition**, *M. Lee, A.J.H. McGaughey*, Carnegie Mellon University, *J.C. Yang*, University of Pittsburgh

Previous experimental and theoretical results show that the  $(2\sqrt{2} \times \sqrt{2})R45^\circ$  missing-row reconstruction is a stable intermediate state during the early stages of Cu(100) oxidation. When the oxygen coverage on a Cu(100) surface reaches 0.5 monolayers [the  $c(2 \times 2)$  phase], the surface structure transforms into the missing-row reconstruction by the release of every fourth row of copper atoms from the top copper layer. The released copper atoms are assumed to then diffuse away. The specific mechanisms and energetics of this transition are not yet fully understood. To investigate this transition, we use density functional theory calculations to predict potential copper-releasing pathways and their energy barriers using the climbing image nudged elastic band method. In the  $p(2\sqrt{2} \times \sqrt{2})$  unit-cell, there are two potential copper releasing pathways. For each pathway, two energy barriers are predicted because there is an intermediate state between the  $c(2 \times 2)$  phase and the missing-row reconstruction. The energy barriers are 1.61 eV and 1.04 eV for the first pathway and 2.19 eV and 0.38 eV for the second pathway. To assess system size effects and alternative pathways, we also investigate the  $p(2\sqrt{2} \times 2\sqrt{2})$  and  $p(4 \times 4)$  unit-cells. In applying the copper releasing pathways analyzed for the  $p(2\sqrt{2} \times \sqrt{2})$  unit-cell to the larger unit-cells, there will be multiple ways to arrive at the final state. For example, in the  $p(2\sqrt{2} \times \sqrt{2})$  unit-cell, two copper atoms should be released to form a complete missing-row. There are two ways for the missing-row formation: moving the copper atoms one by one or moving two copper atoms together. We expect that the copper releasing pathways and energy barriers will vary with the nature of the releasing copper movements.

5:20pm **SS-WeA11 Formation, Characterization and Reactivity of Adsorbed Oxygen on BaO/Pt(111)**, *K. Mudiyansele*, Pacific Northwest National Laboratory, *C.-W. Yi*, Sungshin Women's University, Republic of Korea, *J. Szanyi*, Pacific Northwest National Laboratory

The formation of  $O_{ad}$  species and their reactivities in CO oxidation on BaO/Pt(111) were studied with temperature programmed desorption (TPD), infrared reflection absorption (IRA) and X-ray photoelectron (XP) spectroscopies. Two BaO/Pt(111) model systems with different BaO coverages were prepared and studied. The Pt(111) surface in both of these systems was not completely covered with BaO. On the system with lower BaO coverage (~50 % of the Pt(111) surface was free of BaO), two different  $O_{ad}$  species form following the adsorption of  $O_2$  at 300 K;  $O$  adsorbed on clean Pt(111) sites and at the Pt-BaO interface. On the system with higher BaO coverage (~70 % of the Pt(111) surface is covered by BaO) two types of  $O_{ad}$  are seen at the Pt/BaO interface. The desorption of oxygen from the BaO-free portion of the Pt(111) surface gives an  $O_2$  desorption peak with a maximum desorption rate at ~ 690 K. Recombinative desorption of interfacial  $O_{ad}$  gives two explosive-desorption features at ~ 760 and ~ 790 K in the TPD spectrum. The reactivities of these adsorbed  $O$  species with CO to form  $CO_2$  follow their order of desorption; i.e., the  $O_{ad}$  associated with the clean Pt(111) surface and desorbs at 690 K reacts first with CO, followed by the  $O_{ad}$  species at the BaO/Pt(111) interface (first the one that desorbs at ~ 760 K and finally the one that is bound the most strongly to the interface, and desorbs at ~ 790 K).

5:40pm **SS-WeA12 Molecular Vibrations at Surfaces by First-Principles Molecular Dynamics: Hydrogen-Bonded Networks of Amino Acids on Copper**, *A. Ievins, S.J. Jenkins*, University of Cambridge, UK

## Tribology Focus Topic

Room: Tesuque - Session TR+NS+SS-WeA

## Mechanical & Chemical Effects on Friction and Wear

Moderator: S.S. Perry, University of Florida

2:00pm **TR+NS+SS-WeA1 Quantitative Assessment of Sample Stiffness and Sliding Friction from Force Curves in Atomic Force Microscopy**, *J.R. Pratt, G.A. Shaw*, NIST, *L. Kumanchik*, University of Florida, *N.A. Burnham*, Worcester Polytechnic Institute

It has long been recognized that the angular deflection of an atomic force microscope (AFM) cantilever under "normal" loading conditions can be profoundly influenced by the friction between the tip and the surface. It is shown here that a remarkably quantifiable hysteresis occurs in the slope of loading curves whenever the normal flexural stiffness of the AFM cantilever is *greater* than that of the sample. This situation arises naturally in cantilever-on-cantilever calibration, but also when trying to measure the stiffness of nanomechanical devices or test structures, or when probing any type of surface or structure that is much more compliant along the surface

normal than in transverse directions. Expressions and techniques for evaluating the coefficient of sliding friction between the cantilever tip and sample from normal force curves, as well as relations for determining the stiffness of a mechanically compliant specimen are presented. The model is experimentally supported by the results of cantilever-on-cantilever spring constant calibrations. The cantilever spring constants determined here agree with the values determined using the NIST electrostatic force balance within the limits of the largest uncertainty component, which had a relative value of less than 2.5%. This points the way for quantitative testing of micromechanical and nanomechanical components, more accurate calibration of AFM force, and provides nanotribologists access to information about contact friction from normal force curves [1].

1. J. Appl. Physics **107**, 044305 (2010), doi:10.1063/1.3284957

2:20pm **TR+NS+SS-WeA2 Nanotribological Properties of Polyzwitterionic Brushes**, *Z. Zhang, A.J. Morse, S.P. Armes*, University of Sheffield, UK, *A.L. Lewis*, Biocompatibles UK Ltd., UK, *G.J. Leggett*, University of Sheffield, UK

The frictional properties of surface grown zwitterionic polymer brushes: poly(2-(methacryloyloxy)ethyl phosphorylcholine) (PMPC) have been characterized using friction force microscopy (FFM) in different liquid media.

### 1. Effect of molecular weight and solvent on the frictional properties

For brushes thicker than 192 nm, the coefficient of friction decreased with increasing brush thickness, while for brush layers with smaller thicknesses, the coefficient of friction varied little with molecular weight. It is suggested that water molecules bound to PMPC chains act as an interfacial lubricant; as brush thickness increases, the amount of bound water increases and the coefficient of friction decreases. This hypothesis is supported by comparative studies of the approaching parts of force-displacement plots acquired for PMPC brush samples with different molecular weights under water. In particular, it was found that thicker brushes exerted a greater repulsive force to the AFM probe. Gold-coated probes were used throughout this part to avoid any complication might be caused by tip surface chemistry. FFM has also been used to investigate the cononsolvency behaviour of PMPC. Friction force was measured for PMPC brushes with a dry thickness of 307 nm while immersed in alcohol/water binary mixtures with different compositions. A distinct increase was observed in the coefficient of friction at an ethanol-water ratio of 90:10, and a 2-propanol-water ratio of 70:30, but not for methanol/water mixtures. This result is attributed to the conformational change of the polymer brush, which induced the loss of hydration layer.

### 2. Influence of solvent and tip chemistry on the contact mechanics

To study the contact mechanics of tip-sample interactions in FFM, AFM probes were chemically functionalized by deposition of three different types of self-assembled monolayer of dodecanethiol ( $C_{11}H_{23}$ ) or mercaptoundecanoic acid ( $C_{10}COOH$ ), or cysteamine ( $C_2NH_2$ ). In alcohol solvents, friction force acquired using acid- or  $CH_3$ - functionalized tip has a linear relationship with the applied load, but nonlinear for amine-terminated tip. It is also noted that the coefficient of friction is highest in 2-propanol for all three types of probe, which again suggests that conformation of PMPC brush is one of the key factors. In aqueous medium, the friction-load relationships were nonlinear and characterized by the Derjaguin-Muller-Toporov model of contact mechanics. Coefficient of friction measured by amine-functionalized probes were greater than that of acid-functionalized probes, and than  $CH_3$ - ones, which was attributed to the interaction between polymeric chains and probes.

2:40pm **TR+NS+SS-WeA3 Atomic-scale Processes in Friction and Wear: From Diamond to Graphene**, *R.W. Carpick*, University of Pennsylvania **INVITED**

Nanoscale friction and wear are primary limitations for small-scale devices such as atomic force microscopy (AFM) probes and micro- or nano-electronic mechanical systems with contacting surfaces, and is also relevant to understanding friction and wear in larger-scale contacts. We first present studies that quantify the nanoscale volume loss in sliding wear using AFM and periodic *ex-situ* transmission electron microscopy (TEM) imaging. Novel carbon-based AFM tip materials, including ultrananocrystalline diamond and diamondlike carbon, exhibit superior wear resistance compared to conventional materials (silicon and silicon nitride)<sup>1-3</sup>. We then present results from wear tests performed inside of the TEM using modified *in-situ* indentation techniques. This permits real-time visualization of the contact geometry and shape evolution of a single asperity with sliding over a countersurface. This allows us to measure wear with a higher degree of precision than previously possible. Insights comparing the wear resistance of carbon-based and Si-based materials, particularly in the context of atom-by-atom wear processes, will be discussed<sup>4</sup>. Finally, we will discuss how nanoscale friction in graphene and other atomically-thin sheets is governed by the high flexibility intrinsic to the atomic scale<sup>5</sup>.

1. *Prevention of nanoscale wear in atomic force microscopy through the use of monolithic ultrananocrystalline diamond probes.* J. Liu, D.S. Grierson, J. Notbohm, S. Li, S.D. O'Connor, K.T. Turner, R.W. Carpick, P. Jaroenapibal, A.V. Sumant, J.A. Carlisle, N. Neelakantan & N. Moldovan, **Small**, in press (2010).

2. *Ultra-low nanoscale wear through atom-by-atom attrition in silicon-containing diamond-like-carbon.* H. Bhaskaran, B. Gotsmann, A. Sebastian, U. Drechsler, M. Lantz, M. Despont, P. Jaroenapibal, R.W. Carpick, Y. Chen & K. Sridharan, **Nature Nanotechnology** 5, 181-185 (2010).

3. *Wear resistant diamond nanoprobe tips with integrated silicon heater for tip-based nanomanufacturing.* P.C. Fletcher, J.R. Felts, Z. Dai, T.D. Jacobs, H. Zeng, W. Lee, P.E. Sheehan, J.A. Carlisle, R.W. Carpick & W.P. King, **ACS Nano**, accepted (2010).

4. *On the application of transition state theory to atomic-scale wear.* T.D. Jacobs, B. Gotsmann, M.A. Lantz & R.W. Carpick, **Tribol. Lett.**, accepted (2010).

5. *Frictional characteristics of atomically-thin sheets.* C. Lee, Q. Li, W. Kalb, X.-Z. Liu, H. Berger, R.W. Carpick & J. Hone, **Science** 328, 76-80 (2010).

4:00pm **TR+NS+SS-WeA7 Lubricin Reduces Microscale Cartilage Wear.** *J.M. Coles, D.P. Chang, Duke University, L. Zhang, G.D. Jay, Brown University / Rhode Island Hospital, F. Guilak, S. Zauscher, Duke University*

Articular cartilage is the load bearing surface of mammalian joints. Relatively little wear occurs in cartilage and the tissue is able to sustain millions of loading cycles despite limited regenerative capacity. Though many studies of cartilage friction and lubrication have been performed, often with a stated goal of understanding cartilage wear prevention, very few have measured wear directly and none have directly assessed the effects of synovial fluid constituents in mediating wear. Here we show that the synovial fluid glycoprotein lubricin reduces microscale cartilage wear in vitro. We used colloidal probe microscopy to induce wear and use the change in the average height of the surface as a measure of worn volume. The height change in locations worn in the presence of lubricin was significantly less than in those worn in the control solution. These data indicate that lubricin is important for cartilage preservation physiologically and may have implications for treating or preventing joint disease.

4:20pm **TR+NS+SS-WeA8 Friction of Metallic Nanoparticles: The Influence of Particle Morphology, Orientation and Air Exposure.** *D. Dietzel, T. Moeninghoff, C. Herding, M. Feldmann, H. Fuchs, Westfaelische Wilhelms-Universitaet Muenster, Germany, C. Ritter, U.D. Schwarz, Yale University, A. Schirmeisen, Westfaelische Wilhelms-Universitaet Muenster, Germany*

The contact area dependence of the interfacial friction experienced during the translation of the antimony is studied under different conditions using the tip of an atomic force microscope as a manipulation tool [1]. In vacuum a dual behavior in the friction-area curves is found had been found earlier, characterized by the observation that some particles exhibit friction below the detection limit while other similarly sized particles showed constant shear stress values [2]. New investigations with improved sensitivity confirm the reproducibility of this effect and that neither the particle's morphology nor their relative orientation towards the substrate lattice change this behavior. In contrast, we find that a temporary exposure to ambient air can lead to a drastic increase in the particle's friction.

[1] A. Schirmeisen and U. D. Schwarz, *ChemPhysChem* 10 (2009) 2358

[2] D. Dietzel et al., *Physical Review Letters* 101 (2008) 125505

4:40pm **TR+NS+SS-WeA9 Modeling Materials in Contact using Molecular Simulation.** *J.D. Schall, R.V. Petrach, Oakland University*

**INVITED**

Molecular dynamics (MD) simulation has become an extremely powerful tool for materials science research due to the wealth of atomic level information it provides. In this talk an overview of the MD simulation method will be given. Then a number of applications where MD simulations have been applied to study materials in contact will be discussed. Topics will include the tribology of amorphous carbon films in the presence of hydrogen, and recent work involving the indentation of free-standing graphene sheets. In simulation of the tribology of amorphous carbon, chemical reactions between opposing films were monitored and used to elucidate the mechanisms for enhanced friction and wear properties and to discover the mechanisms of transfer layer formation. These simulations illustrate the need for surface passivation of amorphous carbon films in applications where low friction is desired. We have also investigated the role of silicon on the properties of these films using a

parametrization of Brenner's second generation reactive empirical bond order potential for Si-C-H interactions. Recent results of the simulation of indentation of free-standing graphene films will be shared.

5:20pm **TR+NS+SS-WeA11 Modeling Tribochemistry of DLC vs DLC in the Presence of Water.** *J.A. Harrison, P.T. Mikulski, M.T. Knippenberg, United States Naval Academy*

Because the structure and properties of diamond-like carbon (DLC) can vary depending upon deposition conditions, the tribological response of DLC (and diamond) is very sensitive to environmental conditions. For instance, the presence of water vapor has been shown to negatively impact the friction performance of hydrogenated DLCs but to improve the performance of nanocrystalline and ultrananocrystalline DLCs. Tribochemical reactions of the water with the DLC are thought to be at the heart of this long-standing puzzle.

With that in mind, we have been working to develop a potential energy function that is capable of modeling DLC in the presence of water. To be realistic, such a potential energy function should be able to model tribochemical reactions that may occur as a result of the sliding. In addition, because H, C, and O have very different electronegativities, the potential energy function must be capable of modeling charges and fluctuating charges that arise from electronegativity differences in a realistic way. This talk will outline our efforts at potential development and present some preliminary results of DLC friction in the presence of water.

\*\*Supported by The Air Force Office of Scientific Research.

5:40pm **TR+NS+SS-WeA12 Effects of Impact and Sliding Forces on Failure Behavior of a DLC Coating.** *J.F. Su, L. Wang, X. Nie, University of Windsor, Canada*

The wear and tribological properties of diamond-like carbon (DLC) coatings have been investigated and well documented under various laboratorial and industrial conditions. However, investigations into failure behavior of the coatings when subjected to cyclic impact-sliding loads are scarce. In this study, an inclined ball-on-plate impact-sliding tests were used to evaluate the fatigue cracking and peeling failure behavior of a DLC (a-C:H) coating and a TiN coating as comparison. By adjusting the impact velocity of a steel impacting ball that is connected to and driven by air cylinder, various dynamic impact loads can be obtained. The impact load vs. time curves were recorded and showed three stages, i.e., impact loading stage, vibration stage and quasi-static sliding stage for each impact-sliding cycle. Four loading combinations of impact/static forces (50N/100N, 100N/100N, 50N/200N and 100N/200N) were used in the tests. The test results showed that the DLC coating performed better than the TiN coating under the impact forces but worse under the sliding stages where the quasi-static force was applied by the air cylinder.

# Thursday Morning, October 21, 2010

**Energy Frontiers Topical Conference**  
**Room: Mesilla - Session EN+NS-ThM**

**Nanostructures for Energy Conversion & Storage II**  
**Moderator: K.S. Leschkes, Applied Materials**

8:00am **EN+NS-ThM1 Rare Earth Oxide Nanocavity Upconversion**,  
*V.D. Jankovic, J. Hoang, J.P. Chang, UCLA*

Rare-earth (RE) oxides represent an important class of photonic materials owing to their nonlinear optical and upconversion (UC) properties which find applications in high power lasers, remote sensing, optical communications and photovoltaics. In the context of solar cells, these materials could increase cell efficiencies by upconverting photons with energies below and near the silicon bandgap (1.1eV) which are poorly absorbed by the indirect band-gap semiconductor to higher energy photons that can be absorbed more efficiently. Unfortunately, up-conversion efficiencies in rare-earth ions are usually low due to non-radiative processes such as concentration quenching. One strategy to address this problem is to couple RE ions with metal nanoparticles. Noble metal nanoparticles exhibit localized surface plasmon resonances which can readily be tuned to a particular spectral range of interest by means of size, shape and local dielectric environment. By coupling metal nanoparticles' plasmon resonances to rare earth ion energy transitions, the absorption cross sections of rare earth ions can be significantly improved.

In this work, we designed and synthesized Au|Yb:Er:Y<sub>2</sub>O<sub>3</sub> core|shell nanorods as a potential route to improve solar cell efficiencies in the near infrared regime. A modified Mie scattering algorithm determined the optimum theoretical Au nanorod aspect ratio to be 9, for a resonance close to the Yb 980-nm energy transition. The Au nanorods were synthesized using a surfactant mediated growth technique, in which cetyltrimethylammoniumbromide micelles were used to direct the growth of Au nanoparticles in the [111] direction while suppressing the growth in [100] and [110] directions. Au nanorods with aspect ratios from 6 to 12 have been synthesized by varying the concentration of the reducing agent, ascorbic acid. Spatially and compositional controlled Yb:Er Y<sub>2</sub>O<sub>3</sub> shells were deposited using sequential radical enhanced atomic layer deposition process. The plasmon-Er color center and plasmon-Yb sensitizer distance was systematically varied by controlling the thickness of the Y<sub>2</sub>O<sub>3</sub> spacer layer from 1nm to 10nm. The length, aspect ratio, nanorod monodispersity and shell thickness were verified using transmission electron microscopy, while the shell composition was verified by energy dispersive X-Ray spectroscopy. Photoluminescence and radiative lifetime measurements with 980 nm excitation were used to investigate the distance dependence effects of the noble metal-emitter coupling on the optical properties of the core|shell nanorods. Quantitative measurements of the absorption cross section are underway and will also be presented

8:20am **EN+NS-ThM2 Thermal Transport Property of SiGe Nanowire**, *E.K. Lee*, Samsung Advanced Institute of Technology, Republic of Korea, *J.W. Lee*, Sungkyunkwan University, Republic of Korea, *L. Yin*, Texas A&M University, *B.L. Choi, S.J. Lee*, Samsung Advanced Institute of Technology, Republic of Korea, *D.M. Whang*, Sungkyunkwan University, Republic of Korea, *C.H. Yu*, Texas A&M University, *J.M. Kim*, Samsung Advanced Institute of Technology, Republic of Korea

8:40am **EN+NS-ThM3 Hydrogen Storage in Metal Organic Frameworks (MOFs)**, *N. Nijem, J.-F. Veyan*, University of Texas at Dallas, *L. Kong, K. Li, J. Li, D.C. Langreth*, Rutgers University, *Y.J. Chabal*, University of Texas at Dallas

Hydrogen storage is one of the most challenging problems in hydrogen-based energy technologies. One of the goals of hydrogen storage is the ability to store a high volumetric density of hydrogen at room temperature. As a result, studies exploring molecular hydrogen interaction in storage materials are important to facilitate further development of materials. Metal-organic Frameworks are promising candidates for hydrogen storage because their high surface area and porosity facilitate high hydrogen physisorption on specific sites of the structures and because many options are possible to enhance the interaction of molecular hydrogen with the host.

This work explores the incorporation of hydrogen into various MOFs using infrared (IR) absorption spectroscopy to characterize its interaction. IR spectroscopy can distinguish possible H<sub>2</sub> binding sites based on the perturbation of the internal H<sub>2</sub> stretch mode. IR measurements are performed on saturated metal center MOFs varying the ligand and/or the

metal center and on unsaturated metal center MOF-74-M (M=Zn, Mg and Ni). We combine room temperature, high pressure with low temperature (20-100K) measurements and theoretical van der Waals density functional (vdW-DF) calculations to derive quantitative information from IR shifts and dipole moment strengths.

Our results show that, in contrast to the current understanding, IR shifts are independent of binding energies and depend instead on the chemical environment of the molecule, including effects such as H<sub>2</sub>-H<sub>2</sub> interactions. For example, we see little difference in IR shifts between saturated MOFs with low binding energy (~4kJ/mol), and unsaturated MOFs with higher binding energy (~10kJ/mol) sites at room temperature. Furthermore, we show that dipole moments of adsorbed H<sub>2</sub> depends greatly on parameters such as geometry of adsorption site and H<sub>2</sub>-H<sub>2</sub> interactions. Measurements performed at low temperatures on MOF-74 show that IR shifts of H<sub>2</sub> is greatly red shifted (an additional ~30 cm<sup>-1</sup>) due to H<sub>2</sub>-H<sub>2</sub> interactions on close proximity adsorption sites, and that dipole moments of adsorbed H<sub>2</sub> can appreciably vary with loading.

Our analysis indicate that the intensity of H<sub>2</sub> IR band cannot always be a measure of the amount of H<sub>2</sub> adsorbed, therefore methods such as variable temperature IR (VTIR) used to deduce binding energies cannot always be implemented.

9:00am **EN+NS-ThM4 The Influence of Acid Treatment of TiO<sub>2</sub> Film Prepared by FFCVD on the Performance of Dye-Sensitized Solar Cell**, *B.R. Chen, Y.J. Chen*, National Dong Hwa University, Taiwan, Republic of China

9:20am **EN+NS-ThM5 Development of Novel Nanomaterials as the Building Blocks for Next-Generation Solar Cells**, *J.M. Pietryga, D.C. Lee, I. Robel, V.I. Klimov*, Los Alamos National Laboratory **INVITED**

The use of colloiddally synthesized nanomaterials in devices is attractive not only because of the low-cost and scalability of solution-based fabrication methods, but because of the facile control over electronic and optical properties of these materials made possible by structural fine-tuning. As the range of applications-of-interest has become more sophisticated, such tuning has progressed beyond simple control over effective band gap using quantum size effects to include much more fundamental modification of electronic structure and dynamics. Design and synthesis of novel nanomaterials that exploit such effects to create unique materials for use in next-generation solar cells are an important part of the ongoing effort within the Center for Advanced Solar Photophysics, a DOE Energy Frontier Research Center. I will examine a number of specific examples from this work, including germanium nanocrystals with partial direct-gap behavior and unique infrared-active heterostructures with extremely long-lived charge-separated excited states, and how such materials may be incorporated into devices.

10:40am **EN+NS-ThM9 CdSe-Coated ZnO Nanowires for Extremely Thin Absorber Solar Cells**, *H. Majidi, J.B. Baxter*, Drexel University

Solar cells can provide an abundant, clean, and sustainable source of electricity, but high costs have limited their implementation. Extremely thin absorber (ETA) cells are robust solid state cells that utilize low cost processing while promising potential efficiencies above 15%. However, the highest reported efficiency of ETA cells is only 2.5%. Improving this efficiency will require fundamental understanding and control of the charge transfer in materials and interfaces within the cell.

We report on materials synthesis and photovoltaic response of ETA cells consisting of a vertical array of *n*-type ZnO nanowires coated with CdSe absorber and with the pores between nanowires filled with *p*-type CuSCN. CdSe absorbs visible light and injects photoexcited electrons into the ZnO nanowires. The architecture of the ETA cell enables use of absorbers with smaller carrier lifetimes than those used in thicker planar films, and elimination of liquid electrolytes renders them more robust than conventional dye sensitized solar cells. However, CdSe deposition must be carefully controlled to obtain highly crystalline, uniform, and conformal coatings with an optimal thickness to achieve maximum light harvesting and charge injection efficiency.

We have deposited CdSe coatings at room temperature using electrodeposition with precise control over morphology and material properties. Detailed information about nucleation, crystal growth, and morphology of the coating on both planar ZnO films and ZnO nanowire arrays was obtained by electrochemical probes and electron microscopy at the early stages of deposition. Under potentiostatic deposition, applied potential of ~-1.25 V resulted in instantaneous nucleation and high areal density of nuclei and, hence, conformal coatings. Smaller applied potentials ~-1.05 V resulted in sparse and progressive nucleation and non-uniform

coatings. However, deposition at potentials larger than -1.6 V resulted in precipitation in electrolyte solution. After annealing, x-ray diffraction and transmission electron microscopy show nanocrystalline CdSe in both hexagonal and cubic phases. Using the optimal potential range determined from the potentiostatic studies, we investigated galvanostatic deposition of CdSe coatings on ZnO nanowire arrays. The thickness of CdSe coating is precisely controlled by electrodeposition charge density, and the deposition is conformal and uniform, which is ideal for ETA cells. UV-Vis transmission spectroscopy and photoelectrochemical solar cell measurements demonstrate that CdSe coatings effectively sensitize ZnO nanowires to visible light.

11:00am **EN+NS-ThM10 Titanium Dioxide Nanowires for Dye-Sensitized Solar Cells, Lithium Ion Batteries and Photocatalysis, E.S. Aydil, B. Liu, A. Khare, University of Minnesota**

One-dimensional titanium dioxide nanowires find applications ranging from photocatalysis to lithium ion batteries and dye sensitized solar cells. A simple and environmentally benign method was developed for growing oriented single-crystalline TiO<sub>2</sub>-B and/or anatase TiO<sub>2</sub> nanowire arrays on titanium foil over large areas. These nanowire arrays are suitable for use as the anode in lithium-ion-batteries; they exhibit specific capacities ranging from 200-250 mAh/g and retention of these capacities at high charge-discharge rates and over as many as 200 charging-discharging cycles. These promising properties are attributed to both the nanometer size of the nanowires and their oriented alignment. The comparable electrochemical performance to existing technology, improved safety, and the ability to roll titanium foils into compact three-dimensional structures without additional substrates, binders or additives suggest that these TiO<sub>2</sub> nanowires on titanium foil are promising anode materials for large scale energy storage. Another application of these nanowires is in photocatalysis. Ideally, after photogeneration, electrons and holes must be segregated to different parts of the photocatalyst to take part in separate oxidation and reduction reactions. One way to achieve spatial control of electron-hole separation is by building junctions into the catalyst with built-in electric fields that tend to separate the electron and the hole into two different regions of the catalyst. We sought to accomplish this by controllably forming junctions between different phases of TiO<sub>2</sub>. A solution method followed by a subsequent heating process has been developed to prepare core-shell TiO<sub>2</sub> nanowires made of TiO<sub>2</sub>-B core and anatase shell. We control the anatase phase surface coverage on the TiO<sub>2</sub>-B phase and show that the maximum photocatalytic activity is obtained when the solution containing the reactants can contact both the anatase and TiO<sub>2</sub>-B phases. The photocatalytic activity drops both with bare TiO<sub>2</sub>-B nanowires and with completely anatase covered TiO<sub>2</sub>-B nanowires. In contrast, nanowires partially covered with anatase phase gives the highest photocatalytic activity. The improved photocatalytic activity is attributed to the effective electron-hole separation at the junction between the anatase and TiO<sub>2</sub>-B phases, which reduces charge recombination and increases the electron and hole lifetimes. Finally, we have developed a method to grow rutile TiO<sub>2</sub> nanowires on transparent conducting oxide substrates for use in dye-sensitized solar cells (DSSC). A light-to-electricity conversion efficiency of 3% could be achieved by using 4 mm-long TiO<sub>2</sub> nanorod films as the photoanode in a DSSC.

11:20am **EN+NS-ThM11, S.M. Pursel, S.H.A. Lee, T.E. Mallouk, M.W. Horn, The Pennsylvania State University**

Dye sensitized solar cells (DSSCs) continue to be the subject of intensive research because of their potential low cost with efficiencies near 11%. In this talk, we report on engineered one-dimensional TiO<sub>2</sub> nanowire photoanodes as an alternative to the standard colloidal based photoanodes currently used in most DSSC's. By using one dimensional nanowire photoanodes, there is potential to speed up electron collection thereby permitting the use of faster acting redox couples in future electrolytes. The nanowire photoanodes are made by evaporation of TiO<sub>2</sub> at an oblique deposition angle. Dense arrays of nanowires, of any thickness, can be deposited with an orientation normal to the front contact. Deposition methods that enable growth of nanowires with a consistent diameter (~30 nm) and interwire spacing (~5-10 nm) have been developed for use with DSSCs, unlike most sputtered wires. Optically uniform films have been deposited over 7 cm diameter substrates. These arrays are improvements over past lithographically or hydrothermally deposited nanowires in terms of dye loading, which in our case match or improve upon the dye loading of standard colloidal based photoanodes. Dye loading data, obtained through spectroscopic measurements of desorbed dye, is presented along with SEM images of the various architectures of nanowire arrays. Devices are constructed using ruthenium based N719 dye, I<sup>-</sup>/I<sub>3</sub><sup>-</sup> based electrolyte, and Pt coated FTO counter electrodes and temporary sealing. Performance data is obtained under AM 1.5G or D simulated solar illumination. Electron transport data is obtained through electrochemical impedance spectroscopy

(EIS) and open circuit voltage decay (OCVD). Data is analyzed using published theoretical models to quantify transport properties.

11:40am **EN+NS-ThM12 Dye Sensitized Solar Cells with Aerogel-Templated Nanostructured Photoanodes Fabricated using Atomic Layer Deposition, A. Yanguas-Gil, J.W. Elam, Argonne National Laboratory, V.O. Williams, Northwestern University, M. Mushfiq, D.M. Hess, R. Winter, U. Sampathkumaran, Innosense LLC, M.J. Pellin, Argonne National Laboratory, J.T. Hupp, Northwestern University**

The combination of sol/gel processing techniques with Atomic Layer Deposition is a versatile and scalable route to fabricate nanostructured electrodes with different functional materials. By controlling the sol/gel process it is possible to create scaffolds with very different microstructures and pore-size distributions, while ALD allows a layer-by-layer control of the electrode composition. One of the main advantages of this approach is the possibility of creating nanostructured electrodes with multiple functional coatings that lead to a faster transport of the injected electrons to the transparent conducting oxide, [1, 2] thus paving the way for the use of alternative redox shuttles that would allow higher photovoltages and higher efficiencies.

In this work we present results on the influence that the sol/gel process and the ALD steps have on the microstructure and transport properties of the photoanodes, and the optical properties and efficiency of the cells. In particular, we have studied the influence of the aging and drying steps in the aerogel/xerogel growth, and we have compared the performance of TiCl<sub>4</sub> and Ti(OiPr)<sub>4</sub> as precursors during the ALD step. Our results show that aerogel-templated nanostructured electrodes are a promising alternative to nanoparticle-based photoanodes for dye sensitized solar cells. Our work is funded by the US Department of Energy, Office of Energy Efficiency and Renewable Energy, Industrial Technologies Program.

[1] A. B. F. Martinson, J. W. Elam, M. J. Pellin and J. T. Hupp, *Nano Lett.* **7**, 2183 (2007).

[2] T. W. Hamann, A. B. F. Martinson, J. W. Elam, M. J. Pellin and J. T. Hupp, *J Phys. Chem. C* **112**, 10303 (2008).

## Surface Science

### Room: Picuris - Session SS-ThM

## Adsorption and Reactivity on Oxide Surfaces

Moderator: G. Williams, Jefferson Laboratory

8:00am **SS-ThM1 Adsorption and Reaction on Poorly Crystalline  $\gamma$ -Al<sub>2</sub>O<sub>3</sub> Surfaces, J.H. Kwak, D. Mei, R.J. Rousseau, J. Szanyi, Y. Wang, C.H.F. Peden, Pacific Northwest National Laboratory** **INVITED**

$\gamma$ -alumina ( $\gamma$ -Al<sub>2</sub>O<sub>3</sub>), one of the metastable 'transition' alumina structural polymorphs, is an important catalytic material both as an active phase and as a support for other catalytically active phases, with widespread applications ranging from petroleum refining to automotive emission control. As such, the bulk and surface structure of  $\gamma$ -Al<sub>2</sub>O<sub>3</sub>, and its formation and thermal stability have been and continue to be the subject of a considerable research. However, due to the low crystallinity and very fine particle size of  $\gamma$ -Al<sub>2</sub>O<sub>3</sub>, it is very difficult to apply well-established analytical techniques for determining its surface structures. Of particular importance for understanding the catalytic properties of  $\gamma$ -alumina, relating its surface structure to the origin of Lewis and Brønsted acidity has been of considerable interest and has been studied by solid state NMR and FTIR spectroscopies, and most recently by theoretical calculations. In this presentation, we describe recent studies using ultra-high resolution NMR spectroscopy as an especially useful probe of the  $\gamma$ -Al<sub>2</sub>O<sub>3</sub> surface structure, and its relevance to catalytic behavior. In particular, we correlate the NMR spectra with measurements of the adsorption and reaction of light alcohols. In this way, we demonstrate a strong dependence of this chemistry on the presence of specific 5-coordinate Al<sup>3+</sup> ions. These sites, in turn are a function of the dehydration temperature of the alumina material before use. From these correlations, we are able to explain a considerable number of prior observed phenomena.

8:40am **SS-ThM3 Evolution and Growth of Polar ZnO Nanostructures and their Correlation with Native Point Defects, D.R. Doutt, T.A. Merz, Y.F. Dong, L.J. Brillson, Ohio State University**

We have used a complement of depth-resolved cathodoluminescence spectroscopy (DRCLS), Kelvin probe force microscopy (KPFM), atomic force microscopy (AFM), and surface photovoltage spectroscopy (SPS) to measure how polarity, morphology, and nanoscale growth on ZnO surfaces correlate with electrically-active native point defects. Previous DRCLS showed that ZnO nanostructures can grow spontaneously on bare, air-

exposed ZnO surfaces and produce electronically-active defects. SPS measures the filling and emptying of these states and thereby their energy level position in the band gap. CLS associates these optical transitions with  $V_{Zn}$  and  $V_{O-R}$  related ( $V_{O-R}$ ) defects, respectively. Positron annihilation spectroscopy shows that 2.1eV DRCLS emission correlates with  $V_{Zn}$  vs. depth, anticorrelating with 2.5 eV  $V_{O-R}$  emission. SPS correlates these emissions with optical unfilling and filling transitions, respectively, within the same near-surface region on a nanometer scale. The SPS  $V_{Zn}$  trap state features vary laterally, increasing in nanostructured regions common to ZnO surfaces versus atomically-flat regions. Near both hexagonal pits on (0001) and individual ZnO nano-mounds on both polar faces, 2.1 eV trap densities increase with radial proximity. KPFM maps before and after 2.25 eV illumination show increased potential that reveals large concentrations of  $V_{Zn}$  distributed non-uniformly around and extending away from the hexagonal surface pits. These observations all suggest that ZnO nanostructures grow by oxidation of Zn at the free ZnO surface due to mobile Zn atoms extracted from the underlying lattice.

We measured the morphology, potential, and defect distributions of these structures vs. annealing temperature in flowing oxygen over a 400°C range. AFM/KPFM maps of room temperature and annealed (0001) surfaces reveal deep (~150 nm) hexagonal pits with spoke-like *trenches* extending from both the corners and faces of the hexagonal formation and >50 meV positive potentials that increase with temperature. Conversely, (000-1) surfaces initially show few pits with random geometry and *raised* spoke-like ridges extending from pits. After 1 hr at 200 °C, pitting increases with strong (~150 mV) negative potentials and newly formed spoke-like *trenches*. At 300°C, nanoscale mounds grow 5 – 50 nm high and potentials vary further. From AFM increases in nanorod mass vs. temperature, Arrhenius plots yield  $130 \pm 10$  meV (0001) and  $150 \pm 10$  meV(000-1) activation energies, consistent with the low (0.57 eV) activation energy for Zn interstitial diffusion. Overall, this complement of techniques reveals the interplay between ZnO surface nanostructure, polarity, and electronic defects.

9:00am **SS-ThM4 Atomic Structure and Site Specific Reactivity at Ferroelectric Oxide Surfaces.** *L. Kraya, D.A. Bonnell*, The University of Pennsylvania

The functionality of ferroelectric compounds are inspiring new approaches for catalysis, water splitting, information storage, and nanofabrication. The atomic details of interactions at ferroelectric surfaces are as important as those on other oxides but have been less amenable to examination. Recently we have determined the thermodynamic stability of a wide range of reconstructions on BaTiO<sub>3</sub> (100) and also demonstrated that surface reactions depend on the orientation of the ferroelectric polarization. Here we examine the 3x1 and R5xR5 reconstruction in atomic detail. Reaction of the R5xR5 structure with CO<sub>2</sub> is imaged by scanning tunneling microscopy as a function of exposure and the site occupation quantified. In addition, the effect of locally reorienting the ferroelectric polarization with an STM tip is determined by scanning tunneling spectroscopy. Offsets in local I/V curves are related to energy level shifts due to the local field induced by the polarization.

These results will be contrasted with those on non ferroelectric oxides.

9:20am **SS-ThM5 Selective Oxidation of Ammonia on RuO<sub>2</sub>(110): a Combined DFT and KMC Study.** *T.S. Rahman, S. Hong*, University of Central Florida, *A. Karim*, Brookhaven National Laboratory

We have used a combination of density functional theory (DFT) and kinetic Monte Carlo (KMC) simulations to calculate the reaction rates for the selective oxidation of ammonia on the RuO<sub>2</sub>(110) surface. We find that the overall energy barrier for  $NH_3 + O \rightarrow NH + H_2O$  is 0.56 eV, while that for  $N + N \rightarrow N_2$ , and  $N + O \rightarrow NO$  to be 0.27 and 0.14 eV, respectively. In accompanying KMC simulations, in which we include in addition to the above key processes, several intermediates and their reactions ( 18 processes), we find selectivity towards NO and N<sub>2</sub> formation, as a function of O<sub>2</sub> pressure range, in excellent qualitative and quantitative agreement with experiment [1]. As for the high reactivity of RuO<sub>2</sub>(110) we concur that hydrogen bonding between ammonia, and its intermediates, with adsorbed and substrate oxygen play a critical role by making H abstraction facile such that NH decomposition is a spontaneous, non-activated process. As for the high selectivity of RuO<sub>2</sub>(110) for ammonia oxidation, the significantly-restricted N diffusion caused by reaction intermediates present on the RuO<sub>2</sub>(110) surface severely affects the recombination rate for  $N+N \rightarrow N_2$  while  $N+O \rightarrow NO$  is much less affected by such reduced N diffusion due to dissociatively-adsorbing O<sub>2</sub> species on RuO<sub>2</sub>(110). As a result, NO production is remarkably favored than N<sub>2</sub> production even at low O<sub>2</sub> pressure. These results highlight the important role of the chains of undercoordinated Ru atoms on this surface.

[1] Y. Wang, K. Jacobi, W.-D. Schoene, and G. Ertl, J. Phys. Chem. B 109, 7883 (2005).

Work supported in part by DOE Grant DE-FG02-07ER15842

9:40am **SS-ThM6 Electron Paramagnetic Resonance Evidence for the Formation of O<sub>2</sub> on the Surface of Ultra Thin MgO/Mo Films.** *A. Gonchar, T. Risse, H.-J. Freund*, Fritz-Haber-Institut der Max-Planck-Gesellschaft, Germany

10:40am **SS-ThM9 Franck-Condon Broadening of the XPS of Ionic Materials.** *P.S. Bagus*, University of North Texas, *C.J. Nelin*, Maury's Trail, *E.S. Ilton*, Pacific Northwest National Laboratory

We present an analysis of the width of X-Ray photoelectron spectroscopy, XPS, features that relates the broadening of these features to the chemical activity and reactivity of oxide surfaces. The use of synchrotron radiation allows high resolution measurements of core-level XPS with instrumental resolutions of ~250 meV, or even higher. However, the XPS spectra of many materials, especially oxides and other ionic systems, have features that are much broader than would be expected from instrumental and lifetime broadenings. For example, there are four levels that contribute to the main Mn 2p<sub>3/2</sub> XPS peak of MnO that are not fully resolved with high resolution synchrotron measurements [1] even though the levels are separated from each other by ~1.5 eV. [2] In another example for the XPS of CeO<sub>2</sub>, [3] broadenings of the theoretical results of ~2.5 eV FWHM are required to have the theory match experiment. While surface effects or other inhomogeneities might, in principle, account for large broadenings, we investigate here the contribution to XPS broadening due to vibrational excitations in the final ionic states. Large Franck-Condon broadenings are known for photoemission from molecules [4] but have not been studied in connection with the broad features in the XPS of ionic crystals. We investigate changes in the metal-oxygen bond length for ionic states of MnO and CeO<sub>2</sub>, where a metal core-level has been ionized, using wavefunctions and energies for embedded cluster models of these materials. Initial and final state potential energy surfaces are determined for breathing motions of the nearest oxygen neighbors of the ionized metal cation. These surfaces allow us to determine the Franck-Condon envelope for transition from the  $v=0$  initial, unionized state to vibrationally excited levels of the final, ionized state and show the broadenings that arise from these excitations. Furthermore, we make correlations between the changes in the metal-oxygen bond distances in the ionic states with changes, increases, in the final state covalent metal-oxygen bonding over the initial state covalent character. This correlation may provide a new and novel way to use high resolution photoemission to obtain information about the nature and strength of the bonding in ionic materials.

(1) V Bayer, R Podloucky, C Franchini, F Allegretti, X Bo, G Parteder, MG Ramsey, S Surnev, FP Netzer: Phys. Rev. B **76**, 165428 (2007).

(2) PS Bagus, ES Ilton: Phys. Rev. B **73**, 155110 (2006).

(3) PS Bagus, CJ Nelin, ES Ilton, M Baron, H Abbott, E Primorac, H Kuhlbeck, S Shaikhutdinov, HJ Freund: Chem. Phys. Lett. **487**, 237 (2010).

(4) PS Bagus, EK Viinikka: Phys. Rev. A **15**, 1486 (1977).

11:00am **SS-ThM10 Ethylene Glycol Adsorption and Decomposition over CeO<sub>2</sub> (111) Surfaces.** *T.-L. Chen, F.C. Calaza, S.H. Overbury, D.R. Mullins*, Oak Ridge National Laboratory

Hydrogen production from the reforming of oxygenated hydrocarbons is highly dependent on the heterogeneous reactions provided by its catalysts. Cerium oxide supported metal catalysts can offer a means of reducing precious metal loading and achieving higher selectivity. Thus studying the direct contribution from the metal oxide surface to the decomposition of the molecules can give insight into the catalytic reforming process.

In light of our previous characterization on C<sub>1</sub>-C<sub>3</sub> oxygenate reactions on well-defined cerium oxide thin films, we further examine ethylene glycol as a model system for bio-mass derived hydrocarbons. As the simplest diol, ethylene glycol has two symmetric hydroxyl groups which are available to interact with the surface. The adsorbates can bond to the surface through either one or both of these oxygens, which may lead to a different decomposition pathways.

On the surface of the fully oxidized ceria ethylene glycol appears to initially bond to the surface through only one of the C-O groups. As the temperature is increased both ends interact with the surface and one C-O group is converted into a carboxylate group (COO). The primary reaction products are acetaldehyde, ethylene, acetylene, water and H<sub>2</sub>. CO desorption was also observed indicating some of the oxygenates experienced C-C bond breaking. On a reduced surface one end of the molecules undergoes C-O cleavage resulting in a C-Ce bond rather than an additional C-O bond. The surface intermediate is a carbanion, similar to what was observed for acetaldehyde. More acetylene is observed from a reduced surface.

The dependence of the reaction pathways on the coverage of ethylene glycol was also examined on the oxidized and reduced surfaces. At larger



coverage, the formation of carboxylates or carbanions is hindered which suggests that the formation of these species may be sterically limited.

Research sponsored by the Division of Chemical Sciences, Geosciences, and Biosciences, Office of Basic Energy Sciences, US Department of Energy, under contract DE-AC05-00OR22725 with Oak Ridge National Laboratory, managed and operated by UT-Battelle, LLC. Use of the National Synchrotron Light Source, Brookhaven National Laboratory, was supported by the US Department of Energy, Office of Science, Office of Basic Energy Sciences, under Contract No. DE-AC02-98CH10886.

11:20am **SS-ThM11 Synthesis and Characterization of Cerium Oxide Nanoparticles with Well-defined Crystallographic Terminations, S.H. Overbury, M. Li, Z. Wu, D.R. Mullins, J. Howe**, Oak Ridge National Laboratory

Through hydrothermal synthesis techniques it is possible to create oxide nanoparticles with highly uniform dimensions and shapes and therefore with crystallographically well-defined terminations. These mono-faceted nanocrystals provide an opportunity to examine structure dependence in surface chemistry with the advantage of using methods appropriate to high surface area materials. We have synthesized cubic, octahedral and rod-shaped nanoparticles of CeO<sub>2</sub> that are terminated exclusively in (100), (111) or a mixture of (100) + (110) crystallographic terminations, respectively. These have been used to compare reducibility, stability and adsorption of water, oxygen and alcohol with the goal of characterizing and understanding the effect of surface structure upon the reaction of these molecules with the surface or with other adsorbates. Multi-wavelength Raman and FTIR in the DRIFTS mode are performed in controlled ambient pressure gas streams, and are combined with pulsed / switched chemisorption and temperature programmed techniques. UV Raman reveals that the CeO<sub>2</sub> nanocrystals contain stable bulk-like Frenkel defects, identified by a characteristic Raman feature, and these are more prevalent in the rod-like particles with (110) + (100) termination. Reduction of the nanoparticles in hydrogen at 673 K leads to oxygen vacancies that are identified by a Raman feature near 560 cm<sup>-1</sup> and the rods are more easily reduced while the octahedral are the least. Oxygen vacancies are immediately removed by O<sub>2</sub> at room temperature on all ceria polymorphs. Upon adsorption of isotopically labeled O<sub>2</sub> at 80 K on reduced surfaces, peroxide and superoxide species are observed and these dissociate or desorb as the temperature is increased. Clustered and isolated peroxides are distinguished by their Raman frequency and their relative ratio depends upon degree of reduction and surface structure. Adsorption of D<sub>2</sub>O and H<sub>2</sub>O on each of the surfaces was probed by DRIFTS at room temperature following dehydroxylation at 673 K. Following a pulse of water, OD (OH) features are observed with characteristic IR frequencies. These results are compared to "single crystal" RAIRS studies on CeO<sub>2</sub>(111) oriented films and with previously published IR studies of highly dispersed, polycrystalline CeO<sub>2</sub> crystals of undefined structure terminations. The features observed agree with previous work but their prevalence differ between the faceted nanocrystals and the differences allow structural assignments of the IR features. The results lead to a re-assignment of the IR features.

11:40am **SS-ThM12 Surface Analysis of Selected Metal-Doped Adsorbent Materials for Logistics Fuels Desulfurization, R.A. Quinlan, NSWC, Carderock Division, J.M. Heinzl, NSWC, A.N. Mansour, NSWC, Carderock Division**

Transportation fuels, i.e., gasoline, diesel and jet fuels have been identified as a potential hydrogen source for fuel cell applications due to their high energy densities, ease of storage and availability. However, these liquids, especially the diesel and jet fuels, can contain extremely high concentrations of sulfur. If hydrogen or reformat syngas is to be produced from these high sulfur content fuels, catalyst degradation of the reformer system can occur. Additionally, sulfur compounds such as H<sub>2</sub>S and COS are capable of poisoning follow-on processing operations and the electrode catalyst of the fuel cell. Therefore, desulfurization is paramount for the development of logistics fuels as a hydrogen production source. Recently titania and silica supported silver have shown high performance as regenerable desulfurization sorbents. A variety of techniques have been employed to specifically investigate the active form of the material, and the nature of the adsorptive sites and their interactions with the support, as well as the adsorbed species. Specifically, x-ray photoelectron spectroscopy (XPS) to study the surface chemistry and x-ray absorption spectroscopy (XAS) to study the bulk structure of composite materials were utilized. This provides insight into how the Ag/support system enables such high adsorptive capacities.

# Thursday Afternoon, October 21, 2010

## Energy Frontiers Topical Conference

Room: Mesilla - Session EN+SS+TF-ThA

### Transparent Conductors

Moderator: S. Gupta, University of Alabama

2:00pm EN+SS+TF-ThA1 **Synthesis of ZnO:F by DC Reactive Magnetron Sputtering**, *X. Noirfalise*, University of Mons, Belgium, *T. Godfroid*, Materia Nova, Belgium, *G. Guisbiers*, IEMN Lille, France, *R. Snyders*, University of Mons, Belgium

2:20pm EN+SS+TF-ThA2 **Relationship Between Resistivity Stability and Structure of Transparent Conducting Impurity-doped ZnO Thin Films**, *J.-I. Nomoto*, *T. Hirano*, *T. Miyata*, *O. Ueda*, *T. Minami*, Kanazawa Institute of Technology, Japan

2:40pm EN+SS+TF-ThA3 **Bulk and Surface Physics of Indium Oxide Thin Films Grown on Cubic Zirconia by O-plasma Assisted Molecular Beam Epitaxy**, *R.G. Egdell*, University of Oxford, UK **INVITED**

Tin doped indium oxide (In<sub>2</sub>O<sub>3</sub>) aka ITO is one of the most important transparent conducting oxides, yet it is only recently that many fundamental aspects the bulk and surface physics of indium oxide itself and of ITO have been addressed [1-3]. We have an ongoing programme concerned with growth of In<sub>2</sub>O<sub>3</sub> on Y-stabilised ZrO<sub>2</sub> by oxygen plasma assisted molecular beam epitaxy and will review our most recent work in this area. Issues that will be addressed include the following:

The influence of surface energies and strain on the growth of In<sub>2</sub>O<sub>3</sub> on low index zirconia surfaces. Mechanisms for relief of strain, including crystallographic tilting and development of nanostructures during high temperature MBE growth.

The influence of strain on the optical properties of ultrathin In<sub>2</sub>O<sub>3</sub> films.

Surface structure and surface physics of In<sub>2</sub>O<sub>3</sub> and ITO surfaces, including development of electron accumulation layers for material with low bulk doping levels.

#### References

- 1 P D C King *et al.*, Physical Review Letters 2008 **101** 116808
- 2 A Walsh *et al.*, Physical Review Letters 2008 **100** 167402/1-4
- 3 K H L Zhang *et al.*, Chemistry of Materials 2009 **21** 4353-4355

3:40pm EN+SS+TF-ThA6 **Recent Developments in Transparent Conducting Oxides for Thin-Film Solar Cells**, *J. Burst*, *M. Scott*, *T. Gessert*, National Renewable Energy Laboratory, *S. Weiss*, *B. Rogers*, Vanderbilt University, *T. Coutts*, Timothy J. Coutts Consulting, Inc

Transparent conducting oxides (TCOs) are utilized in all thin-film solar cells. Their function is to reduce electrical losses associated with collection of photogenerated current. However, they exhibit optical and electrical losses of their own and many researchers have tried to reduce these losses either by adjusting deposition conditions, post-deposition annealing, or by using completely novel materials. In our own work, we have shown that it is important to develop TCOs with high free-carrier mobility rather than high concentrations, which causes increased optical losses. Our latest results suggest significant gains in the performance of thin-film solar cells may be made via relatively minimal changes to the TCOs.

We have shown that the properties of transparent conducting oxides (TCOs) can be improved by doping them with approximately 1 atomic % cations whose oxides exhibit high dielectric permittivity. Our experiments have shown that TCOs doped with "high permittivity" cations have increased permittivity compared to the undoped TCO. Also, for similar carrier concentrations and mobilities, the doped TCOs have free-carrier absorption bands shifted to longer wavelengths (1500 nm doped v. 1300 nm undoped), thereby reducing optical losses compared to the undoped TCO. These observations are consistent with predictions based on the Drude free-electron model. In addition, there is evidence that the increased permittivity helps screen scattering centers, thereby leading to enhanced mobility. We will demonstrate that increasing film permittivity reduces optical losses in several standard TCO materials (ZnO, SnO<sub>2</sub>, and In<sub>2</sub>O<sub>3</sub>). Film resistivity as low as  $6 \times 10^{-5} \Omega\text{-cm}$  (corresponding to a sheet resistance of about  $1 \Omega/\text{sq}$  for a film 500 nm thick) has been achieved without compromising the high optical transmittance. The study has also indicated that TCO films with additions that alter permittivity appear to be less sensitive to variation in deposition ambient and temperature. Although this insight will clearly assist development of future TCO materials, we believe the results are even more

relevant to present TCOs that may embody industrial advantages but remain limited by low mobility. *This abstract is subject to government rights.*

4:00pm EN+SS+TF-ThA7 **The Study of AZO/Au/AZO as a Transparent Electrode for Organic Light Emitting Diodes**, *J.H. Park*, Hanyang University, Republic of Korea

Transparent conducting oxide (TCO) thin films and coatings are an important and integral part of a number of electro optical devices because TCOs play an important role as transparent electrodes for flexible optoelectronic devices such as liquid crystal displays, solar cell panels, and organic light emitting devices (OLEDs). Typical TCOs are impurity-doped indium oxides, tin oxides and zinc oxides that offer commercially acceptable performance in terms of conductivity transmittance, environmental stability, reproducibility and surface morphology. The Al-doped ZnO (AZO) films show low resistance and high transmittance in the visible range of the spectrum. However, their resistivity is rather high in some cases to adapt as a transparent electrode for advanced applications. Recently, in order to improve properties of TCO, thin metal or metal alloy film was embedded between TCO layers. In this study, we will discuss the effect of Au middle layer thickness on the electrical and optical properties of the multilayer TCOs and OLED applications. The AZO films were deposited on Corning eagle 2000 glass substrates by atomic layer deposition (ALD). The optimization conditions of AZO films were 1/19 ratio of TMA/DEZ and 180°C. And Au middle layer was deposited by e-beam evaporator. The AZO/Au/AZO films exhibit better electrical properties compared to the AZO films. The carrier concentration was increased from  $1.9 \times 10^{20}$  to  $5.8 \times 10^{20} \text{ cm}^{-3}$ . The mobility was decreased from 12.6 to 12.4  $\text{cm}^2/\text{Vs}$ . The resistivity was decreased from  $2.6 \times 10^{-3}$  to  $8.5 \times 10^{-4} \Omega \text{ cm}$ . However transmittance was decreased from 91 to 76 %, on average. The AZO/Au/AZO films were used as anode electrodes for red emission OLED application. The device showed that a maximum luminance of  $2.4 \times 10^3 \text{ cd/m}^2$  at 11 voltage. More detailed electrical and physical results will be discussed and presented.

4:20pm EN+SS+TF-ThA8 **Origin of the Distribution of Electrical Properties of ITO Sputtered Films on Substrate**, *Y. Hoshi*, *Y. Yasuda*, Tokyo Polytechnic University, Japan, *H. Shimizu*, Niigata University, Japan  
The ITO films deposited by magnetron sputtering and facing target sputtering at low substrate temperature have quite different distributions of film properties. However, their origin was still not clear. In this paper, we clarify the origin of the different distributions between the sputtering methods, and will propose a sputtering method to deposit the ITO films with good uniformity.

In the deposition of ITO films by a conventional planar magnetron sputtering, the films deposited at the center of the substrate have higher oxygen content than the films deposited at the end of the substrate. It should be noted that the film deposited by a facing target sputtering has much lower oxygen content than the films deposited by conventional planar magnetron sputtering. As a result, the ITO films with poor transparency were always obtained by the sputtering in pure Ar gas, when a Facing Target Sputtering system was used.

These phenomena can be explained by the following model; When sputter-deposition of ITO films was performed at a low temperature, only oxygen atoms produced by the sputter-emission from the target surface promote the oxidation of indium atoms on the film surface. In other words, oxygen molecules cannot oxidize the indium atoms at a low temperature.

In addition, oxygen atoms sputter-emitted from the target have different angular distributions than indium atoms have. That is, the emission ratio of oxygen atoms to indium atoms sputter-emitted from the target surface changes depending on the emission angle and gradually decreases with an increase of the emission angle. This phenomenon mainly causes the distribution of the properties of ITO films on the substrate, although bombardment of high energy negative oxygen ions also affects the distribution of film properties in planar magnetron sputtering.

In order to deposit uniform film on the substrate, compensation of the angular distribution in the emission ratio of oxygen atoms to indium atoms is necessary. Use of two sputtering sources arranged like a facing target sputtering system is one of the solutions to compensate the distribution and obtain the films with more excellent uniformity.

4:40pm EN+SS+TF-ThA9 **Deposition of Al-doped ZnO by Atomic Layer Deposition Using Ozone as the Oxygen Source**, *W.L. Gladfelter*, *H. Yuan*, *B. Luo*, *S.A. Campbell*, University of Minnesota

Transparent conducting oxide (TCO) films are used in many photovoltaic and optoelectronic devices. The need to deposit conformal films at relatively low temperature has raised interest in atomic layer deposition

(ALD). Literature reports establish that n-doped zinc oxide has been deposited by ALD using water as the source of oxygen and aluminum or gallium as the dopant. The interest in replacing water with ozone has led to many new ALD routes to metal oxide films, including ZnO. In this presentation we will describe an effective ALD route to Al-doped ZnO. Aluminum-doped ZnO (AZO) films were grown on Si and SiO<sub>2</sub>/Si substrates in the temperature range from 150 - 300°C using diethylzinc as the zinc precursor and ozone as the oxygen source. Trimethylaluminum was used as the aluminum precursor. Two approaches to doping were studied. In one a nanolaminate was formed by interspersing a trimethylaluminum/ozone cycle in between the diethylzinc/ozone cycles. The overall aluminum concentration depended on the number of diethylzinc/ozone cycles. The second approach involved co-injection of both metal precursors in which their relative concentrations were controlled by adjusting the precursor vessel temperature. The influence of the deposition method on the composition, structural, electrical, and optical properties of the AZO films as a function of doping metal concentration will be reported. X-ray diffraction patterns showed all the samples were polycrystalline and exhibited preferential (0001) orientation. The (0002) reflection for AZO films shifted in opposite directions depending on the deposition method. The carbon content of the films was below the detection limit of Auger electron spectrometry. The lowest resistivity ( $6 \times 10^{-4} \Omega \cdot \text{cm}$ ) of the AZO films was obtained using the co-injection process. The average optical transmission was over 85 % in the range of 400-800 nm and the optical band gap increased with increasing doping in accordance with Burstein-Moss effect. The resistivity of AZO films grown by the co-injection method decreased to  $3 \times 10^{-4} \Omega \cdot \text{cm}$  after rapid thermal annealing (RTA) in an Ar atmosphere.

5:00pm **EN+SS+TF-ThA10 Atomic Layer Deposited (ALD) Al-doped ZnO Films for Transparent Conductor Applications**, *P. Banerjee*, University of Maryland, *W.-J. Lee, G.-Y. Bae*, Dong-Eui University, Republic of Korea, *S.-B. Lee, G.W. Rubloff*, University of Maryland

Among various materials for thin film transparent conductor applications, Al-doped ZnO (AZO) is a particularly attractive material because of its excellent properties, such as higher thermal stability, good resistance against damage by hydrogen plasma and potentially, low cost compared to indium tin oxide (ITO). Of the various available deposition techniques, Atomic layer deposition (ALD) provides superb control at the nanoscale for thickness, uniformity, conformality and Al doping of AZO films. This is particularly attractive for use in nanostructures, as well as in more conventional applications such as liquid crystal displays.

We report here results for structural, optical and electrical properties of ultrathin ALD AZO films as a function of at% Al. AZO films of ~ 100nm thickness were deposited on quartz substrates at 150C using a commercial BENEQ TFS 500 reactor using diethyl zinc (DEZ) and H<sub>2</sub>O as precursors for ZnO, and trimethyl aluminum (TMA) and H<sub>2</sub>O as precursors for Al<sub>2</sub>O<sub>3</sub>. Al-doping was incorporated in a film by introducing a single cycle of TMA-H<sub>2</sub>O after fixed cycles of DEZ-H<sub>2</sub>O pulses. This 'super' cycle was repeated until the desired thickness was achieved. Al-doping was varied from 0.0at% to 24.5at%, on various samples, as determined by EDX. In addition, XRD, AFM, UV-Vis spectroscopy and temperature-dependent (80K-340K) Hall measurements were carried out to understand the structural, optical and electrical properties in these films.

Strong texture effects were observed in the AZO films on the quartz substrates as the films preferentially crystallized along the [100] direction. This texturing effect is different from the [002] normally reported for AZO films deposited using established methods other than ALD. Crystallinity and electrical conductivity peaked at 3at% Al, consistent with previous published work. AFM results show a dramatic drop in surface roughness with Al doping. Optical transmittances of over 80% were obtained for all films in the visible region.

Calculation of lattice parameter constants from XRD data and analysis within the framework of the Burstein-Moss effect, reveal that AZO films act as substitutionally doped films for Al doping less than ~7.3at%. Beyond this value of doping, phase segregation and possible formation of a low conductivity phase cause a reduction in the concentration and mobility of free carriers and hence a degradation of the electrical properties.

5:20pm **EN+SS+TF-ThA11 Silicon-Titanium Oxides as Transparent Conductors for Photovoltaic Applications**, *J. Chivers, T. Vandervelde*, Tufts University

We report on the use of Earth-abundant silicon-dioxide and titanium-dioxide as a transparent conducting oxide (TCO) and antireflective (AR) coating. TCOs are a critical component in modern photovoltaic devices, used as a front-side contact that won't block incident light. At present, many TCOs require rare-Earth materials (e.g. Indium), which is problematic for large-scale manufacturing. The abundant, well characterized materials used here can be integrated into an existing product line quickly and

cheaply. The varied band gap and index of refraction conditions inherent in the SiTiO<sub>2</sub> system allow controlled variation of material properties during monolithic growth. Some TCOs may also act as an AR coating, further increasing light absorption. The ideal AR coating would gradually change from the index of refraction of air to that of the underlying semiconductor. Most AR coatings used today make this transition in a small number of steps, which limits their efficacy. In this work, we investigate deposition processes that slowly grade the index of refraction while maintaining conductivity and transparency.

## Surface Science

**Room: Picuris - Session SS-ThA**

## Environmental Interfaces

**Moderator: H. Fairbrother, Johns Hopkins University**

2:00pm **SS-ThA1 Environmental Interfaces: Where the Vacuum, Cleanliness, and Size Gaps Must Be Minimized**, *G. Brown, Jr.*, Stanford University, *S. Yamamoto*, University of Tokyo, Japan, *T. Kendelewicz*, Stanford University, *J. Newberg, H. Bluhm, M. Salmeron*, Lawrence Berkeley National Laboratory, *A. Nilsson*, Stanford Synchrotron Radiation Lightsource, *Y. Wang, M. Michel*, Stanford University, *Y. Choi, P. Eng*, University of Chicago, *J. Ha*, University of California at Berkeley, *A. Spormann*, Stanford University

**INVITED**

Environmental interfaces come in many varieties, including solid-water, solid-gas, solid-microbial biofilm-water, solid-organic film-water, etc., and they exist under a variety of conditions, none of which involve UHV. In addition, the solids involved in environmental interfaces are often in the nanoparticle size range, which may result in properties, such as surface structures and reactivities, that differ from their bulk counterparts. Another common complication is that the surfaces of environmental solids are often coated by natural organic matter and/or microbial biofilms, which could have dramatic effects on their surface charge properties, extent of aggregation, and reactivity. In contrast, most surface science studies involve clean single crystal surfaces on which metals, molecules, or organic molecules are attached under carefully controlled conditions, typically involving UHV. In order to increase our understanding of the chemical and biological processes at environmental interfaces, the pressure, cleanliness, and size gaps must be overcome to the extent possible in surface science studies. We will discuss recent near-ambient pressure XPS studies of the interfaces between alpha-Fe<sub>2</sub>O<sub>3</sub> (0001) and water and Fe<sub>3</sub>O<sub>4</sub> and water, which have revealed the extent of dissociation of water and hydroxylation of these surfaces. We will also present the results of new x-ray standing wave fluorescence yield spectroscopy studies of the interaction of aqueous metal ions with alpha-Fe<sub>2</sub>O<sub>3</sub> nanoparticles coated by polyacrylic acid and natural organic matter thin films as well as with microbial biofilm-coated single crystal metal oxides. The results of these studies have revealed that the intrinsic order of reactivities of different metal oxide surfaces coated by organic matter or microbial biofilms is not affected by the coatings. However, time-dependent studies have shown that the rates of partitioning of metal ions between aqueous solutions and metal oxide surfaces are diffusion controlled. Finally, we will discuss differences in surface structures of nanoparticulate (avg. diameter = 10 nm) vs. microparticulate (avg. diameter = 550 nm) of alpha-Fe<sub>2</sub>O<sub>3</sub> derived from XAFS spectroscopy studies of Zn(II) ions sorbed on the particle surfaces.

2:40pm **SS-ThA3 Ion Segregation and Deliquescence of Alkali Halide Nanocrystals on SiO<sub>2</sub> Revealed by Scanning Polarization Force Microscopy**, *K. Arima*, Osaka University, Japan, *P. Jiang*, Lawrence Berkeley National Laboratory, *D.-S. Lin*, National Tsing Hua University, Taiwan, Republic of China, *A. Verdager*, CSIC-ICN, Spain, *H. Bluhm, M. Salmeron*, Lawrence Berkeley National Laboratory

The adsorption of water on alkali halide (KBr, KCl, KF, NaCl) nanocrystals on SiO<sub>2</sub> and their deliquescence was investigated as a function of relative humidity (RH) from 8% to near saturation by scanning polarization force microscopy (SPFM). SPFM is a noncontact AFM operation mode based on electrostatic forces, which gives two images (topographic image modulated by a local dielectric constant and surface potential image) simultaneously. At low humidity water adsorption solvates ions at the surface of the crystals and increases their mobility. This results in a large increase in the dielectric constant, which is manifested in an increase in the electrostatic force and in an increase in the apparent height of the nanocrystals. Above a critical RH (58% RH in the case of KBr nanocrystals) the diffusion of ions leads to Ostwald ripening, where larger nanocrystals grow at the expense of the smaller ones. At the deliquescence point droplets were formed. For KBr, KCl and NaCl, the droplets exhibit a negative surface potential relative to the surrounding region, indicative of the preferential segregation of anions

to the air-solution interface. We will also show spectra obtained by ambient pressure X-ray photoelectron spectroscopy to complement the SPFM results.

### 3:00pm SS-ThA4 Investigation of H/D Exchange in Water Layers on Hydrophilic/Hydrophobic Organic Surfaces, N.M. Barrentine, R.L. Grimm, J.C. Hemminger, University of California, Irvine

Water interactions with organic surfaces are of great importance to chemistry in the environment as well as a variety of device manufacturing and performance issues. We have carried out studies of the interaction of D<sub>2</sub>O with organic surfaces as a function of the hydrophilic/hydrophobic nature of the surface. Temperature programmed desorption (TPD) experiments are used to follow the strength of the interaction of adsorbed D<sub>2</sub>O with the surface and to follow the extent of H/D exchange that occurs on the surface. Self-assembled monolayers (SAM) of alkanethiols on Au(111) surfaces are used as a highly characterized organic surface. Hydrophilic SAMs are generated using 6-mercapto-1-hexanoic acid (HSC<sub>5</sub>H<sub>10</sub>COOH) on Au(111). Similarly, hydrophobic SAMs are generated using 1-octanethiol (HSC<sub>7</sub>H<sub>14</sub>CH<sub>3</sub>). TPD experiments were carried out following adsorption of D<sub>2</sub>O on the SAM surface at a temperature of 120 K. H/D exchange was observed by simultaneously monitoring  $m/z = 20$  (D<sub>2</sub>O<sup>+</sup>), 19 (HDO<sup>+</sup>), and 18 (OD<sup>+</sup> and H<sub>2</sub>O<sup>+</sup>) in the TPD experiments. Our experiments showed an increase in the  $m/z$  19/20 ratio for experiments with the hydrophilic SAM in comparison to the hydrophobic SAM, indicative of H/D exchange with the acidic proton of the 6-mercapto-1-hexanoic acid SAM. Results will also be presented for mixed hydrophilic/hydrophobic monolayers as a function of the hydrophilic/hydrophobic ratio.

### 3:40pm SS-ThA6 Photochemistry of O<sub>2</sub> on Reduced Rutile TiO<sub>2</sub>(110), G.A. Kimmel, N. Petrik, Pacific Northwest National Laboratory

We investigate the adsorption and photon-stimulated reactions of O<sub>2</sub> on reduced, rutile TiO<sub>2</sub>(110). After adsorption at 28 K and annealing to 100 K, at least 85% of the O<sub>2</sub> has not dissociated. Typically, less than 50% of this molecularly adsorbed O<sub>2</sub> desorbs via hole-mediated reactions during irradiation with ultraviolet (UV) photons. However, UV irradiation dissociates ~20 – 45 % of the chemisorbed O<sub>2</sub>, which we propose to occur through electron attachment reactions. In addition, weakly bound (physisorbed) O<sub>2</sub> readily reacts with chemisorbed O<sub>2</sub> during UV irradiation. A simple model based on the oxygen coverage and the charge of the chemisorbed oxygen, which accounts for the observations, is presented. These results show that the photochemistry of oxygen on TiO<sub>2</sub>(110) is both diverse and more complicated than previously appreciated.

### 4:00pm SS-ThA7 Pentagons and Heptagons in the First Water Layer on Pt(111), S. Nie, P.J. Feibelman, N.C. Bartelt, K. Thürmer, Sandia National Laboratories

We present STM observations of the first layer of water on Pt(111). Because scanning parameters typically used for high-resolution imaging can easily disturb the fragile water layer, acquiring images is particularly challenging. Nonetheless, employing an extremely small tunneling current, we were able to extract enough structural detail to decipher how individual water molecules arrange themselves.

At a growth temperature of 140K, we found large regions consisting of the  $\sqrt{37}$  and  $\sqrt{39}$  phases previously observed in diffraction experiments [1]. The main characteristic of both are triangularly-shaped regions, which appear as depressions in STM. The triangles are embedded in a hexagonal lattice of water molecules, which, remarkably, is rotated by approximately 30° relative to the  $\sqrt{3}\times\sqrt{3}$ -R30° structure that is the usual starting point for discussions of ice films. We propose that the triangular regions consist of a central hexagon of water molecules surrounded by alternating pentagons and heptagons. Twelve water molecules in the center of this (“575757” di-interstitial) defect lie approximately flat, with O atoms directly atop Pt atoms. Elsewhere, the water molecules lie “H-down,” i.e., with an H atom beneath the O. Image simulations based on DFT calculations are consistent with this non-conventional model.

The dramatic structural differences between the  $\sqrt{39}$  phase and 3-D ice consisting of stacked unrotated classic bilayers suggests that 3-D islands do not grow on top of the wetting layer, rather the wetting-layer molecules substantially rearrange when 3-D ice nucleates.

This work was supported by the DOE Office of Basic Energy Sciences, Division of Materials Sciences and Engineering under contract DE-AC04-94AL85000.

[1] For example, A. Glebov, A. P. Graham, A. Menzel and J. P. Toennies, *J. Chem. Phys.* **106**, 9382 (1997).

### 4:20pm SS-ThA8 Wetting Monolayer Structure on Metals, P.J. Feibelman, N.C. Bartelt, Sandia National Laboratories

The  $\sqrt{37}$  and  $\sqrt{39}$  rotated H<sub>2</sub>O-molecule adlayers that form at low T on Pt(111) have been a mystery since 1997. [1] Their structures must optimize among: 1) forming as many H-bonds as possible, 2) allowing the maximum number of H<sub>2</sub>O's to lie flat, with O-atoms in atop sites, and 3) minimizing strain in bond lengths and angles. But, 1) rules out vacancy structures, 2) begs why rotation, leaving few O atoms in atop sites, would be preferred, and 3) is troublesome in the models proposed in Ref. 1, given their areal compression relative to ordinary ice.

Haq, et al. spun off a clue in an effort to interpret a spectroscopically observed metastable water monolayer on Ru(0001). Flat-lying molecules that have each other as neighbors can lie closer to the metal than in the conventionally imagined “ice-like” adlayer, where adjacent molecules’ dangling H-bonds force the flat molecules up. [2] Thus, they proposed a water layer on Ru(0001) comprising chains of flat H<sub>2</sub>O molecules separated by molecules whose dangling H-bonds point toward the metal. Elaborating, we find that a checkerboard of compact flat-lying and H-down phases is even somewhat better bound, and this, together with new, telling STM images, has led us to plausible, low-energy structures for water on Pt(111).

STM images of these structures show  $\sqrt{37}$  and  $\sqrt{39}$  arrays of dark triangles separated by ribbons of H<sub>2</sub>O-molecule hexagons. [3] We assign the triangles to di-interstitial molecular “defects,” wherein six flat-lying H<sub>2</sub>O's, with O atoms ~2.2Å directly atop Pt's, anchor the water layer to the metal. In DFT calculations, these “defect” structures, containing three 5-member and three 7-member rings of H<sub>2</sub>O molecules, have lower energy than any purely hexagonal mesh. A competing explanation of the dark triangles as vacancy islands [4] is significantly less bound, because of its many dangling bonds. Remarkably, analogous 555777 structures on Ru(0001), never observed, are better bound than any purely hexagonal structure tried to date.

[1] A. Glebov, et al., *J. Chem. Phys.* **106**, 9382(1997).

[2] S. Haq, et al., *Phys. Rev. B* **73**, 115414 (2006).

[3] S. Nie, et al, unpublished.

[4] S. Standop, et al., unpublished.

\*Work supported by the DOE Office of Basic Energy Sciences, Div. of Mat. Sci. and Eng., under contract DE-AC04-94AL85000.

### 4:40pm SS-ThA9 Experimental Evidence for Mixed Dissociative and Molecular Adsorption of Water on a Rutile TiO<sub>2</sub>(110) Surface without Oxygen Vacancies, L.E. Walle, A. Borg, Norwegian University of Science and Technology, P. Uvdal, Lund University, Sweden, A. Sandell, Uppsala University, Sweden

Rutile TiO<sub>2</sub>(110) has for many years been regarded as the benchmark surface for fundamental studies of metal oxide surface chemistry. Since water is an integral part of the environment, the H<sub>2</sub>O/TiO<sub>2</sub>(110) system has received more attention than any other comparable system [1,2]. While the dissociation of water on the oxygen deficient TiO<sub>2</sub>(110) surface has been characterized in detail, there is as of yet no consensus reached between experimentalists and theorists regarding a very fundamental question: Does water dissociate upon adsorption on the defect-free TiO<sub>2</sub>(110) surface?

We have studied the interaction of water with the rutile TiO<sub>2</sub>(110) surface using synchrotron radiation photoemission at beamline D1011 at the MAX-lab synchrotron radiation source, and in this contribution we demonstrate that O 1s spectra recorded at grazing emission angle at optimized photon energy in conjunction with valence spectra allow for the observation of OH on the surface even when substrate oxygen is present. The surface was prepared free from oxygen vacancies following the recipe in ref. [3].

Here we find evidence for mixed molecular and dissociative water adsorption at monolayer coverage on the rutile TiO<sub>2</sub>(110) surface free from oxygen vacancies. At monolayer coverage the OH:H<sub>2</sub>O ratio is close to 0.5 and reducing the coverage by heating yields an increased OH:H<sub>2</sub>O ratio. At room temperature neither species originating from the monolayer on the defect free surface can be detected. The OH species of the monolayer hence recombines and leaves the surface at much lower temperatures than OH formed by water dissociation on oxygen vacancies.

#### References

U. Diebold, *Surf. Sci. Rep.* **48**, 53 (2003).

C. L. Pang, R. Lindsay, and G. Thornton, *Chem. Soc. Rev.* **37**, 2328 (2008).

S. Wendt, P. T. Sprunger, E. Lira, G. K. H. Madsen, Z. Li, J. Ø. Hansen, J. Matthiesen, A. Blekinge-Rasmussen, E. Laegsgaard, B. Hammer, and F. Besenbacher, *Science* **320**, 1755 (2008).

5:00pm **SS-ThA10 Atomic Scale Study of Surface Corrosion and Wet Oxidation of Cu(110) Surface by Water**, *B.-Y. Choi*, Lawrence Berkeley National Laboratory, *Y. Shi*, University of California, Berkeley, *M. Salmeron*, Lawrence Berkeley National Laboratory

Dissociated water molecules are at the origin of corrosion and wet oxidation of metals. An atomic scale research is necessary to understand the processes involved in many material industries and the environment science. We investigate the steps leading to corrosion and wet oxidation of Cu(110) surface due to adsorption and dissociation of water molecules using scanning tunneling microscopy. Water is dissociated at 150K and seems to form H<sub>2</sub>O-OH mixed chain structures along the [110] direction. Growth of a single atomic Cu wire is observed nucleating at the step edges, along with the mixed water chain at high temperature around 180K. The strong bond between hydroxyl molecules and Cu produces the nonvolatile molecule-metal combined structure which is the alternating stripe of them. Further annealing the substrate over 300K dissociates water molecules to leave oxygen atoms on a surface, which form single atomic rows of Cu-O along the [001] direction. This allows us to analyze the initial steps of wet oxidation of Cu at the atomic scale. The results provide fundamental views of the water related surface chemistry of Cu, with applications to surface engineering of copper-based electrode and catalyst.

# Friday Morning, October 22, 2010

**Energy Frontiers Topical Conference**  
**Room: Mesilla - Session EN+SS-FrM**

## Photocatalysis and Solar Fuels

**Moderator:** S.-H. Lee, University of Colorado

8:20am **EN+SS-FrM1 Hybrid Metal-Semiconductor Nanomaterials for Electrochemical Hydrogen Generation**, *M.R. Dirmyer, E.P. Luther, A.K. Burrell, B.C. Tappan, A.H. Mueller*, Los Alamos National Laboratory

For the full utilization of intermittent alternative energy sources such as wind and solar energy, issues regarding energy storage must be addressed. An attractive solution is the production of a chemical fuel, allowing for both storage and transportation from so called "stranded" production sites. The electrochemical splitting of water to generate hydrogen allows for the production of such fuel, be it in a denser chemical form or H<sub>2</sub>. Electrode materials for such an electrocatalytic process must have a high surface area, and be catalytically efficient and robust in order to be viable for such a process.

The research presented addresses the aforementioned challenges using two elegant, Los Alamos National Lab exclusive nanotechnologies: 1) combustion synthesis of conducting noble metal nanofoam scaffolding to serve as the cathode and 2) Polymer Assisted Deposition (PAD) of catalytically active films onto a conductive metal scaffold to functionalize the anode. The resulting foams have ultralow densities, controlled nanopore diameters, and rank with the highest surface area metals ever produced, making them ideal candidates for various catalytic applications. The deposition mechanism of PAD, as well as the high conductivity of the metal foam, enables the utilization of the entire interior surface of the foam for electrochemical reactions, exploiting the advantages of the thin film form of the coating while retaining the electrical advantages of a bulk metal electrode. Metallic copper foams have been coated with CIS-based thin-film absorber layers. These materials show photocurrent under illumination with 1.5 AM solar simulated light. Electrochemical water-splitting data will also be presented.

8:40am **EN+SS-FrM2 Surface Electronic Properties of Tantalum Oxynitride Perovskites**, *S. Balaz, S. Porter, P.M. Woodward, L.J. Brillson*, The Ohio State University

We used a complement of X-ray photoemission spectroscopy (XPS), depth-resolved cathodoluminescence spectroscopy (DRCLS), Kelvin Probe Force Microscopy (KPFM), and Atomic Force Microscopy (AFM) to measure the surface electronic properties of the tantalum oxynitride series ATaO<sub>2</sub>N (A = Ca, Sr, Ba) and RTaON<sub>2</sub> (R = La, Pr), promising candidates for photocatalytic splitting of water under illumination by visible light. Besides creating perovskites with band gaps that straddle the redox potentials of water closely, a major challenge to conversion efficiency is the recombination of free carriers by trap states formed by lattice defects. We used DRCLS to measure the energies and densities of these recombination centers with respect to the bulk oxynitride energy bands and Fermi levels. Previously reported UV-VIS diffuse reflectance measurements indicate band gap absorption onsets at 2.4, 2.1, 1.8 [1], 2.0, and 2.0 eV [2] for CaTaO<sub>2</sub>N, SrTaO<sub>2</sub>N, BaTaO<sub>2</sub>N, LaTaON<sub>2</sub> and PrTaON<sub>2</sub>, respectively. DRCL spectra reveal both broad band-to-band transitions in the 2-5 eV range as well as intense and narrow sub-band gap peak features at 1.95, 1.70, 1.70 and 1.79 ± 0.01 eV for the same oxynitride sequence. The relatively constant DRCLS gap state energies indicate similar defects derived from the oxygen and nitrogen 2p orbitals comprising the valence band for all five compounds. By varying the incident beam energy, we probed the surface to the bulk with DRCLS, showing these peak energies nearly unchanged as a function of depth. However 0.1-0.2 eV shifts within the outer 10 nm suggest surface interactions that modify these localized states. The higher energy CL features reflect the slowly rising conduction band densities of states plus more pronounced O 2p-Ta 5d transitions calculated by density functional theory [1]. XPS valence band spectra show Fermi levels 0.5-2 eV above the valence bands, while KPFM work functions vary in the range 4.7 – 4.9 eV, indicating valence band maxima comparable to the 5.67 eV oxidation potential of water. Charging and potentials that vary laterally with nanoscale thickness can affect the XPS and KPFM values significantly but not DRCLS. The appearance of strong defect emissions at energies well within the band gap is indicative of strong recombination that can limit optical conversion efficiencies. Hence, these studies reveal the importance of O- and N-derived native point defects in limiting the efficiency of oxynitride photocatalysts.

[1] Y.-I. Kim, P. M. Woodward, K.Z. Baba-Kishi, and C.W. Tai *Chem. Mater.* 2004, **16**, 1267.

[2] S. Porter, Y.-I. Kim, P. Woodward, Am. Phys. Soc. March Meeting, March 15-19, 2010, abstract X27.00003.

9:00am **EN+SS-FrM3 Zinc-Gallium Oxynitrides as Visible-Light Photocatalysts: Band Gaps and Formation Energies**, *H. Schmidt, D.J. Doren, V.B.R. Boppa, R.F. Lobo*, University of Delaware

Solid solutions of GaN and ZnO have been shown to be a promising class of photocatalysts, capable of splitting water under visible-light irradiation. The structural and electronic properties of Ga<sub>1-x</sub>Zn<sub>x</sub>N<sub>1-x</sub>O<sub>x</sub> have been studied using density-functional theory with the Linear Augmented Plane Wave (LAPW) method at varying values of x. A GGA+U approach is used to better describe the semicore 3d states of Ga and Zn. These calculations show that there exists a p-d coupling between the N 2p and Zn 3d states, leading to a decreased band gap. The band gaps in the mixed metal oxynitrides are lower than either ZnO or GaN, thus allowing excitation by visible light. The trend in band gaps over the range of Zn concentrations (x) is consistent with experimental results. The expected band gap minimum is at a composition that is difficult to synthesize. Formation energies have been calculated to understand the limitations on synthesis of these materials. Several starting materials and synthesis environments have been studied in the formation energy calculations to determine how the thermodynamically preferred products depend on experimental conditions and whether high concentrations of zinc can be obtained in these materials.

9:20am **EN+SS-FrM4 Electronic Structure Analysis and Photocatalytic Properties of Novel Spinel Zinc Gallium Oxy-Nitride Semiconductors**, *B. Boppa, H. Schmidt, D.J. Doren, R.F. Lobo*, University of Delaware

A sol-gel precursor was used to synthesize zinc gallium oxy-nitrides with visible light band gaps. At low temperatures, novel spinel oxynitrides were produced with band gaps of 2.5 to 2.7eV, surface areas of 16 to 36 m<sup>2</sup>/g, and nitrogen content less than 1.5%. As the temperature was raised, these spinels get consumed to form wurzitic oxy-nitrides also with band gaps less than 3 eV but with surface areas of 4 to 6 m<sup>2</sup>/g. The reduction in the band gap for the spinel oxy-nitrides is associated with the incorporation of N2p orbitals in the valence band with corresponding changes in the anion position parameter. We established that the presence of a small fraction of gallium tetrahedral centers and anion vacancies might affect its unique electronic properties. The changes associated with the gallium coordination environment as the spinel zinc gallate precursor transforms to a spinel oxynitride at 550°C and further changes into a wurzite oxynitride at 850°C are studied through x-ray diffraction, ultraviolet-visible diffuse reflectance spectroscopy, neutron powder diffraction, x-ray absorption spectroscopy and other techniques. Electronic structure and formation energies of the spinel and wurzite oxy-nitrides were studied using density-functional theory (DFT) with the Linear Augmented Plane Wave (LAPW) method at varying dopant concentrations. Furthermore, these novel spinel photocatalysts were found to be active in degrading methylene blue in visible light and oxygen production from silver nitrate. The protocol developed opens a different avenue for the synthesis of semiconductors possessing the spinel crystal structure and with band gaps engineered to the visible region with potential applications for both opto-electronics and photocatalytic applications.

9:40am **EN+SS-FrM5 Synthesis and Surface Characterization of Nano-Scaled Structures for Energy Conversion Devices**, *W. Patterson, M. Robson, K. Artyushkova, P. Atanassov*, University of New Mexico

Using a microemulsion-based synthesis approach to create silica particles with internal porosity characterized by a nano-scale, bi-modal pore size distribution, we have developed functional templates for non-Platinum catalysts for fuel cell technologies. This material is derived from novel silica particles synthesized through oil/water/surfactant microemulsion templating under controlled conditions to have two distinct pore size regimes (~5 nm and ~40 nm). The larger pores, determined by the volume of microemulsion droplets, allow for more facile infiltration of precursors as compared to fumed silica previously used as the templating material. The smaller pores are determined by micellar dimensions and allow sites for creation of active site centers.

After formation of the silica, a subsequent carbon/active-site precursor co-impregnation process is followed by pyrolysis and etching. This leads to formation of open-frame structures of synthetic carbon supports decorated with the nano-phase metallic catalyst of choice. The resulting high surface area material is a bi-porous, carbonaceous matrix decorated with a low loading of non-precious metal. Last year, this effort resulted in demonstrating Pt/C catalysts for oxygen reduction. We have since focused efforts towards non-Pt precursors for pyrolytic formation of a nitrogen-

containing carbon backbone structure in combination with transition metals, Co and Fe.

Synthesis conditions, such as the amount of precursor, pyrolysis temperature, and etching conditions play an important role in formation of the porous structure of the resulting electrocatalyst. Well designed nanoporous structures can effectively minimize transport limitations, thus increasing the accessibility of the active sites by gas and electrolyte phases in the fuel cell active layer.

Thorough characterization including SEM, TEM, XRD, and XPS was performed. Detailed physisorption was performed to characterize the pore structure and surface area of the materials. A thorough analysis of the surface composition and structure as a function of pyrolysis temperature for the pyrolyzed Co-N precursor with sucrose was performed and high-resolution XPS spectra were acquired.

Using methodology previously developed for correlation of material structure to properties, we provide an enhanced characterization of composition and structure, identification of active sites, and some insight into the mechanism of reduction/oxidation reactions.

**10:00am EN+SS-FrM6 Enhancement of Visible-Light Photocatalytic Efficiency of TiO<sub>2</sub> Nanopowder by Anatase/Rutile Interface Formation.** *Y.J. Chen, C.S. Lin*, National Dong Hwa University, Taiwan, Republic of China

In this article we report that the presence of anatase/rutile interface is essential on realization of visible-light photocatalytic ability of TiO<sub>2</sub> produced by the novel flat-flame chemical vapor condensation (FFCVC) method. Previous study shows that when nitrogen is replaced by argon as precursor carrier gas as well as quench gas in the FFCVC process, the synthesized TiO<sub>2</sub> nanopowder changes from anatase/rutile dual phases to anatase single phase. The UV-vis absorption spectra suggest that the synthesized TiO<sub>2</sub> with single anatase phase may still possess visible light absorption capability when the process parameters are carefully chosen. However, the photocatalytic efficiency drops to minimal value for the single-phase TiO<sub>2</sub> compared with that for dual-phase TiO<sub>2</sub>. To confirm that the photocatalytic efficiency difference is caused by the formation of anatase/rutile interface, we synthesize the TiO<sub>2</sub> nanopowder using argon as carrier gas while using either nitrogen or argon as quench gas for comparison. Results show that when using nitrogen as quench gas, the TiO<sub>2</sub> powder is mostly anatase phase with minor rutile content, while when using argon as quench gas, the TiO<sub>2</sub> powder is almost anatase phase with hardly any rutile content. From the x-ray diffraction analysis, the grain size of anatase from both processes is similar, indicating that the choice of quench gas does not influence significantly on the nucleation process of the TiO<sub>2</sub> nanopowder. On the other hand, the use of nitrogen as quench gas does promote the formation of rutile phase, even though the rutile content is still minimal. This observation indicates that the nitrogen as quench gas does have some effect, although weak, on TiO<sub>2</sub> nanopowder during its final coalescence and growth stage. The visible-light photocatalytic experiment shows that even two powder samples are similar, the photocatalytic efficiency of TiO<sub>2</sub> with minor rutile content is significant while that of TiO<sub>2</sub> with single anatase phase is insignificant. Since the anatase from both processes is considered the same, the photocatalytic efficiency difference must be due to that minor rutile formation. Since the photocatalytic reaction occurs mostly on the anatase surface, the enhancement of photocatalytic efficiency by the formation of rutile phase leads to the conclusion that the anatase/rutile interface is the major cause for the efficiency enhancement. We will show the XPS, EPR, and XRD characterization of powders and discuss the materials science behind the phenomenon.

## Surface Science

Room: Santa Ana - Session SS-FrM

### Reactivity of Oxides, Mainly TiO<sub>2</sub>

Moderator: G.A. Kimmel, Pacific Northwest National Laboratory

**8:20am SS-FrM1 Electronic, Chemical, and Morphological Structure of Ag Nanoclusters Grown on FeO<sub>x</sub>/Cu(100).** *F.N. Womack, R. Singh, Y. Losovyi, O. Kizilkaya, R.L. Kurtz, P.T. Sprunger*, Louisiana State University  
Iron oxides are used as catalysts in a number of processes crucial to our standard of living, most notably the water-gas shift reaction and the Haber process for producing ammonia. Recent work[1-3] on ultra-thin iron oxide films suggests that their catalytic efficiency can be improved by the addition of metal nanoparticles. We have performed ARPES and LEED experiments on ultra-thin film FeO<sub>x</sub> grown on Cu(100). In agreement with our STM results, FeO structure (electronic) is observed at monolayer coverage, but Fe<sub>3</sub>O<sub>4</sub> is observed above 2.5 ML. Moreover, Ag growth, at submonolayer coverages on both oxide phases, there is an increase in binding energy of the Ag 4d band indicating charge transfer from the iron oxide. This partial reduction of Ag may provide sites on the film surface for both oxidation and reduction of adsorbed species. In addition to electronic structure, STM atomic/morphological structure will be presented, as well as induced chemisorption changes, probed by both HREELS and TPD.

[1] L. Giordano et al., Physical Review Letters 101, 1 (2008).

[2] C. Lemire et al., Surface Science 552, 27 (2004).

[3] Y. N. Sun et al., Surface Science 603, 3099 (2009).

**8:40am SS-FrM2 Effect of Ti Dopant in Ceria on the Structure of Metal Nanoparticles.** *Y. Zhou, J. Zhou*, University of Wyoming

Ceria plays a major role in the chemistry of supported metal nanoparticles. The nanostructure, redox properties and oxygen storage capacity of ceria can affect the morphology, structure, as well as catalytic reactivity of supported metal nanoparticles. The addition of other metal elements such as Ti can result in structural and electronic modifications of ceria, which not only can enhance the thermal stability of ceria, but also improve its redox properties and oxygen storage capacity. In this paper, we discuss the effect of Ti dopant in the ceria support on the structure of metal particles at the fundamental level. Ti-doped CeO<sub>x</sub>(111) thin films were prepared on Ru(0001) as model supports under ultrahigh vacuum conditions. Their structures were examined in detail by LEED, XPS and STM. The nucleation and growth of metal particles including Au and Ni on the doped-ceria surfaces were investigated upon deposition at 300 K as well as after heating to higher temperatures, which is compared to that on the pure ceria supports. The research is sponsored by University of Wyoming start-up fund and Wyoming NASA Space grant.

**9:00am SS-FrM3 Nucleation Behavior of Supported Nanoparticles Fabricated from an Organometallic Precursor under Ultra High Vacuum: A DFT and STM Study.** *H. Khosravian, Z. Liang, A. Uhl, R. Meyer, M. Trenary*, University of Illinois at Chicago

In this combined STM and DFT study, we examine the adsorption of Rh(CO)<sub>2</sub>(acac) (acac is acetylacetonate) on a TiO<sub>2</sub>(110) single crystal surface, which is aimed at developing an understanding of the relationship between the preferred adsorption sites of the supported organometallic species, and the nucleation behavior of this precursor compound on different surface terminations. The STM images of clean TiO<sub>2</sub>(110) show large terraces with the characteristic row pattern that arises from alternating lines of bridging oxygen and uncapped titanium ions. After exposing Rh(CO)<sub>2</sub>(acac) to the surface at room temperature the formation of small particles is observed, with diameters of 1 nm or less, and a height of 2.5 Å (i.e., monolayer height). After annealing the sample to 630°C the density and number of the particles is significantly reduced. The particles appear to be monodispersed, with their sizes increased to several nm in lateral directions, and about 5 Å in height (i.e., bilayer height). The findings can be rationalized in terms of deligation of the parent species and agglomeration of the denuded rhodium. The details of the adsorption and deligation Process have been characterized with DFT calculations.

**9:20am SS-FrM4 Oxygen Adatom Formation and Charge Transfer upon O<sub>2</sub> Dissociation on Reduced TiO<sub>2</sub>(110).** *I. Lyubinetsky, Y. Du*, Pacific Northwest National Laboratory, *N.A. Deskins*, Worcester Polytechnic Institute, *Z. Zhang*, Baylor University, *Z. Dohnalek, M. Dupuis*, Pacific Northwest National Laboratory

Combination of the statistical analysis by scanning tunneling microscopy and density functional theory calculations has been used to investigate the

initial stages of molecular oxygen dissociation on the reduced TiO<sub>2</sub>(110) surface at 300 K. Major O<sub>2</sub> dissociation channel results in the bridging O vacancy (V<sub>O</sub>) healing and deposition of a single O adatom (O<sub>a</sub>), while minor channel results in formation of O<sub>a</sub> pair on regular Ti sites. For latter channel, an intermediate, metastable nearest-neighbor O<sub>a</sub>-O<sub>a</sub> configuration is observed after O<sub>2</sub> dissociation. This initial configuration is destabilized by Coulomb repulsion of charged O<sub>a</sub>'s that separate further along the Ti row into energetically more favorable second-nearest neighbor configuration. The potential energy profile calculated for O<sub>2</sub> dissociation on Ti rows and following O<sub>a</sub>'s separation strongly supports the experimental observations. Our results also suggest that the itinerant electrons associated with the V<sub>O</sub>'s are being utilized in the O<sub>2</sub> dissociation process at the Ti rows, whereas at least two oxygen vacancies per O<sub>2</sub> molecule are required in order for this process to become viable. Overall, the electrons originating from V<sub>O</sub>'s provide a larger fraction of charge required for O<sub>2</sub> dissociation, while a smaller fraction can be attributed to Ti interstitials.

[1] Du, Y.; Dohnalek, Z.; Lyubinsky, I. *J. Phys. Chem. C* 2008, *112*, 2649.

[2] Du, Y.; Deskins, N. A.; Zhang, Z.; Dohnalek, Z.; Dupuis, M.; Lyubinsky, I. *Phys. Chem. Chem. Phys.*

2010, DOI: 10.1039/C000250J.

9:40am **SS-FrM5 Chemistry and Physics of Oxide Surfaces: New Insights from Spectroscopic Studies on ZnO and TiO<sub>2</sub> Single Crystals.** C. Wöll, Karlsruhe Institute of Technology, Germany **INVITED**

10:20am **SS-FrM7 Imaging Hindered Rotations of Alkoxy Species on TiO<sub>2</sub>(110).** Z. Zhang, R.J. Rousseau, Pacific Northwest National Laboratory, J. Gong, University of Texas at Austin, B.D. Kay, Z. Dohnalek, Pacific Northwest National Laboratory

The first scanning tunneling microscopy (STM) study of the rotational dynamics of organic species on oxides is presented. Variable-temperature STM and dispersion-corrected density functional theory (DFT-D) are used to study the alkyl chain conformational disorder and dynamics of 1-, 2-, 3- and 4-octoxy species on rutile TiO<sub>2</sub>(110). Initially, the geminate pairs of the octoxy and bridging hydroxyl species are created via octanol dissociation on bridging-oxygen (O<sub>b</sub>) vacancy defects. The STM images provide time averaged snapshots of octoxy species rotating among multiple energetically nearly-degenerate configurations accessible at a given temperature. The calculations show that the underlying corrugated potential energy surface is a result of the interplay between attractive van der Waals dispersion forces leading to weak attractive C···Ti and repulsive C···O<sub>b</sub> interactions which lead to large barriers of 50-70kJmol<sup>-1</sup> for the rotation of the octoxy alkyl chains across the O<sub>b</sub> rows. The relative populations of various conformations as well as the rotational barriers are found to be perturbed as a result of additional C···hydroxyl repulsions when the geminate hydroxyl groups are present.

This research was performed in the Environmental Molecular Sciences Laboratory, a national scientific user facility sponsored by the Department of Energy's Office of Biological and Environmental Research and located at Pacific Northwest National Laboratory.

10:40am **SS-FrM8 Hydrogen Bonding Controls the Dynamics of Catechol Adsorbed on a TiO<sub>2</sub>(110) Surface.** S.-C. Li, Tulane University, L.-N. Chu, X.-Q. Gong, East China University of Science and Technology, China, U. Diebold, Tulane University and Vienna University of Technology, Austria

Direct studies of how organic molecules diffuse on metal oxide surfaces can provide insights into catalysis and molecular assembly processes. We studied individual catechol molecules, C<sub>6</sub>H<sub>4</sub>(OH)<sub>2</sub>, on a rutile TiO<sub>2</sub>(110) surface with scanning tunneling microscopy (STM). Surface hydroxyls enhanced the diffusivity of adsorbed catechol molecules. The capture and release of a proton caused individual molecules to switch between 'mobile' and 'immobile' states within a measurement period of minutes. Density functional theory (DFT) calculations show that the transfer of H from surface hydroxyls to the molecule and its interaction with surface hydroxyls substantially lowered the activation barrier for rotational motion across the surface. Hydrogen bonding can play an essential role in the initial stages of the dynamics of molecular assembly.

11:00am **SS-FrM9 Design of Highly Stable Molecular Interfaces to TiO<sub>2</sub> Surfaces.** R.A. Franking, University of Wisconsin-Madison, S.A. Chambers, Pacific Northwest National Laboratory, R.J. Hamers, University of Wisconsin-Madison

11:20am **SS-FrM10 CO Photooxidation on Reduced TiO<sub>2</sub>(110) Surface.** N. Petrik, G.A. Kimmel, Pacific Northwest National Laboratory

Photo-induced reactions between O<sub>2</sub> and CO on reduced rutile TiO<sub>2</sub>(110) surface are studied at low temperature (~30K). Photon stimulated desorption (PSD) of O<sub>2</sub>, CO<sub>2</sub> and CO (not reported earlier) are observed with comparable yields. Results indicate that CO<sub>2</sub> is produced from the chemisorbed O<sub>2</sub> molecule residing in the oxygen vacancy and CO molecule physisorbed on the Ti site next to it. The PSD angular distribution for CO<sub>2</sub> is non-cosine, narrow and off-normal: it peaks at ~ 40 degrees to the surface normal in the (001) plane (across the Ti and O rows on the surface). The results are consistent with CO<sub>2</sub> produced from the (Ti)-O-C-O-O-(V<sub>O</sub>) transition state complex predicted theoretically. CO PSD from the TiO<sub>2</sub>(110) surface is enhanced dramatically by the presence of chemisorbed O<sub>2</sub> molecules, where photo-desorbing CO may be a by-product of the CO photooxidation process.



# Authors Index

**Bold page numbers indicate the presenter**

## — A —

Abrahams, R.D.: SS2-TuM10, 15  
Adams, P.M.: SS-TuP13, 22  
Aksoy, F.: IS+SS-TuM5, 11; SS1-MoM11, 5  
Alang Ahmad, S.: SS2-WeM5, 26  
Alcántara Ortigoza, M.: SS-TuA12, **19**  
Alexander, J.: SS2-MoA1, 8  
Alnabulsi, S.: SS-TuP22, **23**  
Altman, E.L.: SS1-TuM12, **13**  
Ambrosch-Draxl, C.E.: SS2-TuM5, 14  
Andersen, J.N.: IS+SS-TuM1, **11**; IS+SS-TuM5, 11

Anthony, J.E.: SS2-TuM1, **13**  
Antony, A.: SS1-MoM2, 4  
Aoki, Y.: SS-TuP7, **21**  
Ardalan, P.: SS2+EM-MoM10, 6  
Arellano, G.: SS-TuP24, 24  
Arima, K.: SS-ThA3, **39**  
Armes, S.P.: TR+NS+SS-WeA2, 32  
Artyushka, K.: SS1-TuM11, 13  
Artyushkova, K.: EN+SS-FrM5, 42  
Ashurst, W.R.: TR+MN+NS+SS-WeM5, 28  
Asscher, M.: SS2+EM-MoM2, 5  
Asthagiri, A.: SS1-MoM2, 4  
Atanassov, P.: EN+SS-FrM5, 42; SS1-TuM11, 13  
Aurbach, D.A.: IS+SS-TuA7, **16**  
Axnanda, S.: SS-TuP19, **23**  
Aydil, E.S.: EN+NS-ThM10, **35**; IS+SS-TuA11, 17

## — B —

Baber, A.E.: SS-TuP2, 20; SS-WeA9, 31  
Bae, G.-Y.: EN+SS+TF-ThA10, 39  
Bagge-Hansen, M.: AC+SS-MoM9, **2**  
Bagus, P.S.: SS-ThM9, **36**; SS-TuP17, 22  
Bailly, A.: SS1-MoA1, 7  
Baker: SS1-TuM3, 12  
Balaz, S.: EN+SS-FrM2, **42**  
Ballard, J.B.: SS2-MoA1, **8**  
Ballav, N.: SS2-TuM11, 15  
Balmes, O.: IS+SS-TuM1, 11  
Banerjee, P.: EN+SS+TF-ThA10, **39**  
Barbey, R.: SS-TuP22, 23  
Barkley, S.: TR+MN+NS+SS-WeM5, 28  
Barrentine, N.M.: SS-ThA4, **40**  
Bartels, L.: SS2-TuM4, 14; SS-TuA11, 19; SS-TuA2, **18**  
Bartel, N.C.: GR+SS+TF+EM-MoM2, 2; SS-ThA7, 40; SS-ThA8, 40  
Baucom, K.C.: SS-WeA1, 30  
Bauer, E.: AC+SS-MoM5, 1  
Bauer, E.D.: AC+SS-MoM5, 1; AC+SS-MoM8, 1  
Baxter, J.B.: EN+NS-ThM9, 34; IS+SS-TuA2, 16  
Becker, J.S.: SS2+EM-MoM4, **6**  
Becker, M.: IS+SS-TuA2, 16  
Beerbom, M.M.: SS2-WeM12, 27  
Behr, M.J.: IS+SS-TuA11, 17  
Belianinov, A.: SS-TuP12, **22**  
Bent, S.F.: SS2+EM-MoM10, 6; SS-WeA4, 31  
Bentley, S.: EM+SS-WeA11, 30  
Bhushan, B.: SS-TuP21, 23  
Bishop, S.: SS2+EM-MoM9, 6  
Blomberg, S.: IS+SS-TuM1, 11  
Bluhm, H.: IS+SS-TuM1, 11; IS+SS-TuM3, **11**;  
IS+SS-TuM5, 11; IS+SS-TuM6, 11; SS-ThA1, 39; SS-ThA3, 39  
Bohnen, K.P.: SS-TuA12, 19  
Bonnell, D.A.: SS-ThM4, 36  
Boppana, B.: EN+SS-FrM4, **42**  
Boppana, V.B.R.: EN+SS-FrM3, 42  
Borg, A.: SS-ThA9, 40  
Borovsky, B.: TR+MN+NS+SS-WeM5, 28  
Borysiuk, J.: GR+SS+TF+EM-MoM5, 2  
Bouxein, C.: TR+MN+NS+SS-WeM5, 28  
Bradley, J.D.: SS2-WeM11, 27  
Brillson, L.J.: EN+SS-FrM2, 42; SS-ThM3, 35

Broach, A.L.: AC+SS-MoM3, 1; AC+SS-MoM4, 1  
Broitman, E.: SS-WeA9, **31**  
Brown, Jr., G.: SS-ThA1, **39**  
Brown, M.: SS1-WeM2, **25**  
Brown, R.D.: SS2+EM-MoM4, 6  
Brumbach, M.T.: AC+SS-MoM11, **2**  
Bumm, L.A.: SS2-TuM10, **15**  
Bunker, B.A.: IS+SS-TuA2, 16  
Bunker, K.L.: IS+SS-TuA10, 17  
Burnham, N.A.: TR+NS+SS-WeA1, **32**  
Burrell, A.K.: AC+SS-MoM5, 1; EN+SS-FrM1, 42  
Burst, J.: EN+SS+TF-ThA6, **38**

## — C —

Cabailh, G.: SS1-MoA1, 7  
Cagg, B.A.: SS-TuP14, 22  
Calaza, F.C.: SS1-MoM1, **3**; SS-ThM10, 36  
Camara, N.: GR+SS+TF+EM-MoM10, 3  
Camassel, J.: GR+SS+TF+EM-MoM10, 3  
Camillone III, N.: SS1-MoA10, 8  
Campbell, C.T.: SS1-MoM8, 4; SS2-MoA8, **9**  
Campbell, P.M.: GR+SS+TF+EM-MoM1, 2;  
GR+SS+TF+EM-MoM8, 3  
Campbell, S.A.: EN+SS+TF-ThA9, 38  
Campbell, V.: SS-TuA10, 19; SS-TuA9, 18  
Carp, R.: SS-TuA2, 18  
Carpick, R.W.: TR+NS+SS-WeA3, **32**  
Carrasco, E.: SS1-WeM2, 25  
Chabal, Y.J.: EN+NS-ThM3, 34; SS2-MoA1, 8;  
SS2-MoA7, 9  
Chambers, S.A.: SS-FrM9, 44  
Chang, D.P.: TR+NS+SS-WeA7, 33  
Chang, J.P.: EN+NS-ThM1, 34  
Chaudhuri, A.: IS+SS-TuM2, 11; SS-WeA2, **30**  
Chen, B.R.: EN+NS-ThM4, **34**  
Chen, D.A.: SS-TuP14, 22  
Chen, F.: SS2-MoA6, 9  
Chen, N.: SS-TuA10, 19; SS-TuA9, **18**  
Chen, T.-L.: SS1-MoM1, 3; SS-ThM10, **36**  
Chen, Y.J.: EN+NS-ThM4, 34; EN+SS-FrM6, **43**  
Chen, Z.W.: SS1-MoA11, **8**  
Cheng, C.-M.: SS2-TuM3, 14  
Cheng, Z.H.: SS2-TuM4, 14; SS-TuA11, 19; SS-TuA2, 18  
Chesneau, F.: SS2-TuM11, **15**  
Chiang, S.: GR+SS+TF+EM-MoM10, 3; SS2-MoA10, 9; SS-TuP3, 20  
Chinn, D.A.: SS-TuP9, **21**  
Chivers, J.: EN+SS+TF-ThA11, **39**  
Cho, J.: SS2-MoA7, 9  
Cho, K.J.: SS2-MoA1, 8  
Choi, B.L.: EN+NS-ThM2, 34  
Choi, B.-Y.: SS-ThA10, **41**  
Choi, H.-S.: SS2-MoA1, 8  
Choi, Y.: SS-ThA1, 39  
Choi, Y.M.: IS+SS-TuA1, 16  
Chopra, S.N.: SS-WeA4, 31  
Chorkendorff, I.: SS1-MoA3, **7**  
Chu, E.: SS-TuA2, 18  
Chu, L.-N.: SS-FrM8, 44  
Chun, W.-J.: SS1-MoA11, 8  
Ciftlikli, E.Z.: SS2-MoA3, 8  
Clarke, R.: SS1-WeM3, **25**  
Coles, J.M.: TR+NS+SS-WeA7, **33**  
Coltrin, M.E.: SS-WeA1, 30  
Conrad, M.: SS2-WeM12, **27**  
Cooks, R.G.: SS-TuP16, 22  
Corbacioglu, B.D.: SS-TuP26, 24  
Cornish, A.: IS+SS-TuM5, 11  
Coutts, T.: EN+SS+TF-ThA6, 38  
Creighton, J.R.: SS-WeA1, **30**  
Crowe, M.: SS1-MoM8, 4  
Croy, J.R.: SS1-MoA2, 7  
Cruguel, H.: SS1-MoA1, 7  
Culbertson, J.C.: GR+SS+TF+EM-MoM8, 3  
Culbertson, R.J.: SS2-WeM11, 27

Cushing, G.: SS1-MoM6, 4  
Cyganik, P.: SS2-TuM11, 15

## — D —

Dahanayaka, D.H.: SS2-TuM10, 15  
Datye, A.: SS1-TuM11, 13  
de Heer, W.A.: GR+SS+TF+EM-MoM9, 3  
del Alamo, J.A.: EM+SS-WeA9, **30**  
Denecke, R.: SS1-TuM2, **12**  
Deng, X.: SS1-MoM11, 5  
Deppert, K.: IS+SS-TuM1, 11  
Deram, M.: TR+MN+NS+SS-WeM5, 28  
Desai, T.V.: SS2-TuM9, 14  
Deskins, N.A.: SS-FrM4, 43  
Devanathan, R.: SS2-WeM6, 26  
Diebold, U.: SS2-FrM8, 45  
Dietzel, D.: TR+NS+SS-WeA8, 33  
Dirk, S.M.: TR+MN+NS+SS-WeM4, 27  
Dirmyer, M.R.: EN+SS-FrM1, **42**  
Dohnalek, Z.: SS1-WeM5, 25; SS-FrM4, 43; SS-FrM7, **44**  
Dohnálek, Z.: SS1-WeM9, 25  
Dolle, P.: SS1-MoA1, 7  
Donald, S.: SS1-MoM6, 4  
Dong, H.: SS2-MoA7, 9  
Dong, Y.F.: SS-ThM3, 35  
Doren, D.J.: EN+SS-FrM3, 42; EN+SS-FrM4, 42  
Dougherty, D.B.: SS2-TuM6, 14  
Doutt, D.R.: SS-ThM3, **35**  
Drube, W.: IS+SS-TuM9, **11**  
Du, Y.: SS-FrM4, 43  
Dugger, M.T.: SS-TuP9, 21; TR+MN+NS+SS-WeM4, **27**  
Duguet, T.: SS2-MoA11, 10  
Dupuis, M.: SS-FrM4, 43  
Durakiewicz, T.: AC+SS-MoM5, 1; AC+SS-MoM8, 1

## — E —

Eddy, Jr., C.R.: GR+SS+TF+EM-MoM8, 3  
Egdell, R.G.: EN+SS+TF-ThA3, **38**  
Eigenfeld, N.: TR+MN+NS+SS-WeM5, 28  
Einstein, T.L.: SS-TuA11, 19  
El Gabaly, F.: IS+SS-TuM6, 11  
Elam, J.W.: EN+NS-ThM12, 35  
Eng, P.: SS-ThA1, 39  
Engel-Herbert, R.: EM+SS-WeA7, **29**  
Engstrom, J.R.: SS2-TuM9, **14**  
Enriquez, H.: GR+SS+TF+EM-MoM10, 3  
Eralp, T.: IS+SS-TuM5, 11  
Ermanoski, I.: SS1-WeM6, **25**  
Evans, J.: SS2-MoA11, 10

## — F —

Faggini, M.F.: SS2+EM-MoM1, 5  
Fairbrother, H.: SS2-WeM3, **26**  
Falta, J.: IS+SS-TuA1, 16  
Faubel, M.: IS+SS-TuM2, 11  
Feibelman, P.J.: SS-ThA7, 40; SS-ThA8, **40**  
Feldmann, M.: TR+NS+SS-WeA8, 33  
Finlayson-Pitts, B.: SS-TuP23, 23  
First, P.N.: GR+SS+TF+EM-MoM6, 3;  
GR+SS+TF+EM-MoM9, 3  
Fischer, K.: SS1-TuM2, 12  
Flack, F.S.: SS2-MoA6, 9  
Flake, J.: SS1-MoA9, 8  
Flater, E.: TR+MN+NS+SS-WeM5, **28**  
Flege, J.I.: IS+SS-TuA1, 16  
Fortunelli, A.: SS1-WeM5, 25  
Frank, P.F.: SS2-TuM5, 14  
Franking, R.A.: SS-FrM9, **44**  
French, M.: EM+SS-WeA8, 29  
Frenkel, A.I.: SS-WeA7, **31**  
Freund, H.-J.: SS1-MoA7, 7; SS1-MoA8, 8; SS1-WeM2, 25; SS-ThM6, 36; SS-TuP17, 22  
Friedman, A.L.: GR+SS+TF+EM-MoM8, 3  
Friend, C.: SS1-TuM3, **12**

Fuchs, H.: TR+NS+SS-WeA8, 33  
 Fujishima, A.: SS-TuP5, 20  
 Fujitani, T.: SS-TuP25, 24; SS-TuP4, 20  
 Fukui, K.: SS1-MoA11, 8  
 Fuqua, P.D.: SS-TuP13, 22  
 Furlong, O.J.: TR+MN+NS+SS-WeM11, 28  
 Furuta, T.: SS-TuP5, 20

— **G** —  
 Garaudée, S.: SS1-MoA1, 7  
 Garcia Flores, H.G.: AC+SS-MoM3, 1; AC+SS-MoM4, 1  
 Gaskill, D.K.: GR+SS+TF+EM-MoM1, 2; GR+SS+TF+EM-MoM8, 3  
 Gassman, P.: SS-TuP23, 23  
 Geisler, H.: SS-TuP24, 24  
 Gellman, A.J.: SS1-MoM5, 4; SS-WeA9, 31  
 Gessert, T.: EN+SS+TF-ThA6, 38  
 Gezerman, A.O.: SS-TuP26, 24  
 Ghosal, S.: SS-TuP23, 23  
 Gladfelter, W.L.: EN+SS+TF-ThA9, 38  
 Godfroid, T.: EN+SS+TF-ThA1, 38  
 Godignon, Ph.: GR+SS+TF+EM-MoM10, 3  
 Götzhäuser, A.: SS2-TuM12, 15  
 Gonchar, A.: SS-ThM6, 36  
 Gong, J.: SS-FrM7, 44  
 Gong, X.-Q.: SS-FrM8, 44  
 Gorai, P.: SS2+EM-MoM11, 6  
 Gorham, J.: SS2-WeM3, 26  
 Graham, K.S.: AC+SS-MoM5, 1  
 Grass, M.: IS+SS-TuM6, 11  
 Graves, T.P.: SS-TuP13, 22  
 Green, E.: GR+SS+TF+EM-MoM6, 3  
 Grimm, R.L.: SS-ThA4, 40  
 Griveau, J.-C.: AC+SS-MoM8, 1  
 Gross, L.: SS-TuA3, 18  
 Guilak, F.: TR+NS+SS-WeA7, 33  
 Guisbiers, G.: EN+SS+TF-ThA1, 38  
 Gumbsch, A.: SS1-WeM5, 25  
 Gupta, A.: SS2+EM-MoM1, 5  
 Gustafson, J.: IS+SS-TuM1, 11  
 Gutmann, S.: SS2-WeM12, 27  
 Guziewicz, E.: AC+SS-MoM8, 1

— **H** —  
 Ha, J.: SS-ThA1, 39  
 Hagen, C.W.: SS2-WeM3, 26  
 Hakanoglu, C.: SS1-MoM2, 4  
 Halevi, B.: SS1-TuM11, 13  
 Halterman, R.L.: SS2-TuM10, 15  
 Ham, H.C.: SS1-TuM10, 13; SS1-TuM6, 13  
 Hamers, R.J.: SS-FrM9, 44; SS-WeA3, 31  
 Han, Y.: SS2-MoA11, 10  
 Harrison, I.: SS1-MoM6, 4  
 Harrison, J.A.: TR+NS+SS-WeA11, 33  
 Harrison, W.A.: SS-TuP24, 24  
 Hart, M.A.: SS2-WeM11, 27  
 Haubrich: SS1-TuM3, 12  
 Hauffman, T.: SS1-WeM10, 25  
 Hawkins, J.M.: SS1-MoM2, 4  
 He, W.: SS-TuP14, 22  
 He, X.: SS2-WeM4, 26  
 Heid, R.: SS-TuA12, 19  
 Heinrich, H.: SS1-MoA2, 7  
 Heinzl, J.M.: SS-ThM12, 37  
 Held, G.: IS+SS-TuM5, 11  
 Hellberg, C.S.: GR+SS+TF+EM-MoM1, 2  
 Hemminger, J.C.: IS+SS-TuM2, 11; SS-ThA4, 40  
 Herbots, N.: SS2-WeM11, 27  
 Herding, C.: TR+NS+SS-WeA8, 33  
 Hess, D.M.: EN+NS-ThM12, 35  
 Hieda, J.: SS-TuP7, 21  
 Hill, M.A.: AC+SS-MoM10, 2  
 Hinch, B.J.: SS2-MoA3, 8  
 Hines, M.A.: SS2+EM-MoM1, 5  
 Hinojosa, Jr., J.A.: SS1-MoM2, 4  
 Hirano, T.: EN+SS+TF-ThA2, 38  
 Hite, J.K.: GR+SS+TF+EM-MoM8, 3  
 Hlawacek, A.: SS2-TuM5, 14  
 Hoang, J.: EN+NS-ThM1, 34

Hobbs, J.K.: SS2-WeM5, 26  
 Holland, M.: EM+SS-WeA11, 30  
 Holsclaw, B.S.: SS-WeA9, 31  
 Hong, S.: SS2-MoA3, 8; SS2-TuM4, 14; SS-ThM5, 36  
 Horn, M.W.: EN+NS-ThM11, 35  
 Hoshi, Y.: EN+SS+TF-ThA8, 38  
 Howe, J.: SS-ThM11, 37  
 Hrbek, J.: IS+SS-TuA1, 16; SS1-MoM10, 5; SS-TuP19, 23  
 Hsue, C.-S.: SS2-TuM3, 14  
 Hu, Y.: GR+SS+TF+EM-MoM9, 3  
 Huang, J.: IS+SS-TuA9, 17  
 Huang, M.: SS2-MoA1, 8; SS2-MoA6, 9; SS2-MoA7, 9  
 Huang, Y.: SS1-MoM5, 4; SS-TuA9, 18  
 Hubin, A.: SS1-WeM10, 25  
 Hudak, N.: IS+SS-TuA9, 17  
 Hupp, J.T.: EN+NS-ThM12, 35  
 Hwang, G.S.: SS1-TuM10, 13; SS1-TuM6, 13  
 Hwang, Y.: EM+SS-WeA7, 29

— **I** —  
 Ievins, A.: SS-WeA12, 32  
 Ilton, E.S.: SS-ThM9, 36  
 Imangholi, B.: EM+SS-WeA3, 29  
 Iski, E.V.: SS-TuP2, 20

— **J** —  
 Jackson, L.P.: SS2-TuM10, 15  
 Jaehnic, M.: EM+SS-WeA8, 29  
 Jankovic, V.D.: EN+NS-ThM1, 34  
 Jay, G.D.: TR+NS+SS-WeA7, 33  
 Jeng, H.T.: SS2-TuM3, 14  
 Jenkins, S.J.: SS-WeA12, 32  
 Jenks, C.J.: SS1-TuM1, 12  
 Jernigan, G.G.: GR+SS+TF+EM-MoM1, 2  
 Jewell, A.D.: SS-TuA1, 17; SS-TuP2, 20  
 Jia, Q.: AC+SS-MoM5, 1  
 Jiang, P.: SS-ThA3, 39  
 Jin, W.: SS2-TuM6, 14  
 Johansson, E.: SS2+EM-MoM4, 6  
 Johnson, D.P.: AC+SS-MoM10, 2  
 Johnson, G.: SS-TuP16, 22  
 Joyce, J.: AC+SS-MoM5, 1; AC+SS-MoM8, 1  
 Jupille, J.: SS1-MoA1, 7

— **K** —  
 Kankate, L.: SS2-TuM12, 15  
 Karim, A.: SS-ThM5, 36  
 Karp, E.: SS1-MoM8, 4  
 Kasemo, B.H.: SS1-MoA6, 7  
 Kaufman-Osborn, T.: SS2+EM-MoM9, 6  
 Kay, B.D.: SS1-WeM9, 25; SS-FrM7, 44  
 Kelley, M.J.: SS2-WeM10, 27  
 Kellogg, G.L.: GR+SS+TF+EM-MoM2, 2; SS1-WeM6, 25  
 Kendelewicz, T.: SS-ThA1, 39  
 Kennison, J.A.: AC+SS-MoM5, 1  
 Khare, A.: EN+NS-ThM10, 35  
 Khosravian, H.: SS-FrM3, 43  
 Kiefer, B.: SS1-TuM11, 13  
 Killelea, D.R.: SS-TuA10, 19  
 Kim, B.: SS-TuP11, 22  
 Kim, D.H.: SS2-TuM4, 14; SS-TuA11, 19; SS-TuA2, 18; SS-TuP11, 22  
 Kim, J.: EM+SS-WeA4, 29  
 Kim, J.M.: EN+NS-ThM2, 34  
 Kim, K.: SS-TuA11, 19  
 Kim, K.H.: SS1-MoA7, 7  
 Kim, K.-J.: SS-TuP11, 22  
 Kim, S.: SS-TuP11, 22  
 Kim, S.H.: TR+MN+NS+SS-WeM3, 27  
 Kim, Y.K.: SS1-WeM9, 25  
 Kimmel, G.A.: SS-FrM10, 44; SS-ThA6, 40  
 King, S.: EM+SS-WeA8, 29  
 Kirk, A.P.: EM+SS-WeA4, 29  
 Kirk, W.P.: SS2-MoA7, 9  
 Kizilkaya, O.: SS-FrM1, 43  
 Klimov, V.I.: EN+NS-ThM5, 34  
 Klok, H.A.: SS-TuP22, 23

Klopf, J.M.: SS2-WeM10, 27  
 Knippenberg, M.T.: TR+NS+SS-WeA11, 33  
 Koel, B.: SS1-TuM9, 13  
 Kolodziej, J.J.: SS2+EM-MoM8, 6  
 Kondratenko, Y.: SS2+EM-MoM11, 6  
 Kong, L.: EN+NS-ThM3, 34  
 Krafft, G.: SS2-WeM10, 27  
 Kraya, L.: SS-ThM4, 36  
 Krukowski, S.K.: GR+SS+TF+EM-MoM5, 2  
 Kuchibhatla, S.: SS2-WeM6, 26  
 Kuhn, M.: EM+SS-WeA8, 29  
 Kumanchik, L.: TR+NS+SS-WeA1, 32  
 Kumar, A.: SS2-WeM6, 26  
 Kummel, A.C.: EM+SS-WeA11, 30; SS2+EM-MoM9, 6  
 Kurtz, R.L.: SS1-MoA9, 8; SS-FrM1, 43  
 Kusano, Y.: TR+MN+NS+SS-WeM6, 28  
 Kwak, J.H.: SS-ThM1, 35  
 Kwon, K.-Y.: SS-TuA2, 18

— **L** —  
 Lagally, M.G.: SS2-MoA6, 9  
 Langhammer, C.: SS1-MoA6, 7  
 Langreth, D.C.: EN+NS-ThM3, 34  
 Laoufi, I.: SS1-MoA1, 7  
 Larsson, M.K.: SS1-MoA6, 7  
 Laskin, J.: SS-TuP16, 22  
 Lawton, T.J.: SS-WeA9, 31  
 Lazzari, R.: SS1-MoA1, 7  
 Lee, D.C.: EN+NS-ThM5, 34  
 Lee, E.K.: EN+NS-ThM2, 34  
 Lee, H.: SS-TuP11, 22  
 Lee, J.: SS1-MoM11, 5  
 Lee, J.S.: EM+SS-WeA11, 30; SS2+EM-MoM9, 6  
 Lee, J.W.: EN+NS-ThM2, 34  
 Lee, M.: SS-WeA10, 32  
 Lee, S.: EM+SS-WeA11, 30  
 Lee, S.-B.: EN+SS+TF-ThA10, 39  
 Lee, S.H.A.: EN+NS-ThM11, 35  
 Lee, S.J.: EN+NS-ThM2, 34  
 Lee, W.-J.: EN+SS+TF-ThA10, 39  
 Leggett, G.J.: SS2-WeM5, 26; TR+NS+SS-WeA2, 32  
 Lersch, T.L.: IS+SS-TuA10, 17  
 Lewis, A.L.: TR+NS+SS-WeA2, 32  
 Lewis, N.S.: SS2+EM-MoM4, 6  
 Lewis, T.: IS+SS-TuM2, 11  
 Li, J.: EN+NS-ThM3, 34  
 Li, K.: EN+NS-ThM3, 34  
 Li, M.: SS1-TuM12, 13; SS-ThM11, 37  
 Li, S.-C.: SS-FrM8, 44  
 Li, Z.: SS1-WeM9, 25  
 Liang, T.: TR+MN+NS+SS-WeM12, 28  
 Liang, Z.: SS-FrM3, 43  
 Lie, F.L.: EM+SS-WeA3, 29  
 Liljeroth, P.: SS-TuA3, 18  
 Lim, H.A.: SS-TuP20, 23  
 Lin, C.-H.: SS2-TuM3, 14  
 Lin, C.S.: EN+SS-FrM6, 43  
 Lin, D.-S.: SS-ThA3, 39  
 Lin, J.: SS-TuP15, 22  
 Lince, J.R.: SS-TuP13, 22  
 Liu: SS1-TuM3, 12  
 Liu, B.: EN+NS-ThM10, 35  
 Liu, D.-J.: SS1-TuM1, 12  
 Liu, F.: SS2-MoA6, 9  
 Liu, Q.: SS2-TuM6, 14  
 Liu, Z.: IS+SS-TuA10, 17; IS+SS-TuM5, 11; IS+SS-TuM6, 11; SS1-MoM11, 5; SS2-WeM5, 26  
 Lobo, R.F.: EN+SS-FrM3, 42; EN+SS-FrM4, 42  
 Lorbek, S.B.: SS2-TuM5, 14  
 Losovyi, Y.: SS1-MoA9, 8; SS-FrM1, 43  
 Lou, J.: IS+SS-TuA9, 17  
 Lu, W.H.: SS2-TuM4, 14; SS-TuA11, 19  
 Ludwig, W.: SS1-MoA8, 8  
 Lundgren, E.: IS+SS-TuM1, 11  
 Luo, B.: EN+SS+TF-ThA9, 38  
 Luo, M.: SS2-TuM4, 14; SS-TuA11, 19; SS-TuA2, 18

Luther, E.P.: EN+SS-FrM1, 42  
 Lyding, J.W.: SS2-MoA1, 8  
 Lyubinskiy, I.: SS-FrM4, 43

— **M** —

Ma, Q.: SS-TuP1, 20  
 Macintyre, D.: EM+SS-WeA11, 30  
 Mack, P.: SS-TuP18, 23  
 Madix, R.J.: SS1-MoA8, 8; SS1-TuM3, 12  
 Majidi, H.: EN+NS-ThM9, 34  
 Mallouk, T.E.: EN+NS-ThM11, 35  
 Manos, D.M.: AC+SS-MoM9, 2  
 Mansour, A.N.: SS-ThM12, 37  
 Marsella, M.: SS-TuA2, 18  
 Martin, N.: IS+SS-TuM1, 11  
 Martinotti, D.: GR+SS+TF+EM-MoM10, 3  
 Mastovich, J.: IS+SS-TuA10, 17  
 Matranga, C.: SS1-MoM11, 5  
 Matthews, O.: TR+MN+NS+SS-WeM5, 28  
 McCarty, K.F.: IS+SS-TuM6, 11  
 McCleskey, T.M.: AC+SS-MoM5, 1  
 McDaniel, A.H.: IS+SS-TuM6, 11  
 McGaughey, A.J.H.: SS-WeA10, 32  
 McIntire, T.M.: SS-TuP23, 23  
 McKenna, K.: SS-TuP8, 21  
 McPeak, K.M.: IS+SS-TuA2, 16  
 Mei, D.: SS-ThM1, 35  
 Melitz, W.: EM+SS-WeA11, 30  
 Menkens, B.: IS+SS-TuA1, 16  
 Menzel, D.: SS1-MoA7, 7  
 Merz, T.A.: SS-ThM3, 35  
 Messing, M.E.: IS+SS-TuM1, 11  
 Methaapanon, R.M.: SS2+EM-MoM10, 6  
 Meyer, G.: SS-TuA3, 18  
 Meyer, R.: SS1-MoM9, 4; SS-FrM3, 43  
 Michel, M.: SS-ThA1, 39  
 Michelsen, P.K.: TR+MN+NS+SS-WeM6, 28  
 Micklefield, J.: SS2-WeM5, 26  
 Mikulski, P.T.: TR+NS+SS-WeA11, 33  
 Miller, B.P.: TR+MN+NS+SS-WeM11, 28  
 Miller, D.L.: GR+SS+TF+EM-MoM6, 3  
 Milojevic, M.: EM+SS-WeA4, 29  
 Milosavljevic, V.: SS-TuP10, 21  
 Minami, T.: EN+SS+TF-ThA2, 38  
 Mirecki Millunchick, J.: SS2+EM-MoM5, 6  
 Mitchell, J.N.: AC+SS-MoM5, 1  
 Miyata, T.: EN+SS+TF-ThA2, 38  
 Mkhoyan, A.: IS+SS-TuA11, 17  
 Modine, N.A.: SS2+EM-MoM5, 6  
 Moenninghoff, T.: TR+NS+SS-WeA8, 33  
 Mohn, F.: SS-TuA3, 18  
 Moll, N.: SS-TuA3, 18  
 Moore, D.P.: AC+SS-MoM3, 1; AC+SS-MoM4, 1;  
 AC+SS-MoM5, 1  
 Morse, A.J.: TR+NS+SS-WeA2, 32  
 Moulder, J.F.: SS-TuP22, 23  
 Mudiyanselage, K.: SS-WeA11, 32  
 Mueller, A.H.: EN+SS-FrM1, 42  
 Mullet, C.: SS2-MoA10, 9; SS-TuP3, 20  
 Mullins, D.R.: SS1-MoM1, 3; SS-ThM10, 36; SS-  
 ThM11, 37  
 Mulugeta, D.: SS1-MoA7, 7  
 Muscat, A.J.: EM+SS-WeA3, 29  
 Mushfiq, M.: EN+NS-ThM12, 35  
 Muzik, H.: SS2-TuM12, 15  
 Myers-Ward, R.L.: GR+SS+TF+EM-MoM8, 3

— **N** —

Nabok, D.: SS2-TuM5, 14  
 Nadesalingam, M.P.: SS2-MoA7, 9  
 Nakajima, A.: SS-TuP5, 20  
 Nakamura, I.: SS-TuP25, 24; SS-TuP4, 20  
 Navin, J.: SS1-MoM6, 4  
 Nelin, C.J.: SS-ThM9, 36; SS-TuP17, 22  
 Netzer, F.P.: SS1-WeM5, 25; SS1-WeM9, 25  
 Neugebauer, J.: SS1-WeM1, 25  
 Newberg, J.: SS-ThA1, 39  
 Nie, S.: GR+SS+TF+EM-MoM2, 2; SS-ThA7, 40  
 Nie, X.: TR+NS+SS-WeA12, 33  
 Nijem, N.: EN+NS-ThM3, 34

Nilsson, A.: SS-ThA1, 39  
 Nishimura, M.: SS-TuP5, 20  
 Noirfalise, X.: EN+SS+TF-ThA1, 38  
 Nomoto, J.-I.: EN+SS+TF-ThA2, 38  
 Nunnery, T.: SS-TuP18, 23  
 Nyakiti, L.O.: GR+SS+TF+EM-MoM1, 2

— **O** —

Ohlhausen, J.A.: AC+SS-MoM11, 2;  
 TR+MN+NS+SS-WeM4, 27  
 Ohta, T.: GR+SS+TF+EM-MoM2, 2  
 Ono, L.K.: SS1-MoA2, 7  
 Oppeneer, P.M.: AC+SS-MoM8, 1  
 Osgood, R.M.: SS-TuA7, 18  
 Otte, A.F.: GR+SS+TF+EM-MoM9, 3  
 Oughaddou, H.: GR+SS+TF+EM-MoM10, 3  
 Outlaw, R.A.: AC+SS-MoM9, 2  
 Overbury, S.H.: SS1-MoM1, 3; SS-ThM10, 36;  
 SS-ThM11, 37

— **P** —

Pai, W.W.: SS2-TuM3, 14  
 Palacio, M.: SS-TuP21, 23  
 Palmer, R.E.: SS-TuA8, 18  
 Park, J.H.: EN+SS+TF-ThA7, 38  
 Paskiewicz, D.M.: SS2-MoA6, 9  
 Patterson, M.: SS1-MoA9, 8  
 Patterson, W.: EN+SS-FrM5, 42  
 Pawin, G.: SS-TuA2, 18  
 Pawlowski, R.P.: SS-WeA1, 30  
 Peden, C.H.F.: SS-ThM1, 35  
 Pellin, M.J.: EN+NS-ThM12, 35  
 Peng, W.-P.: SS-TuP16, 22  
 Perrine, K.A.: SS-TuP15, 22  
 Perry, S.S.: TR+MN+NS+SS-WeM9, 28  
 Petrach, R.V.: TR+NS+SS-WeA9, 33  
 Petrik, N.: SS-FrM10, 44; SS-ThA6, 40  
 Phillips, M.: GR+SS+TF+EM-MoM6, 3  
 Phillipot, S.R.: TR+MN+NS+SS-WeM12, 28  
 Pietryga, J.M.: EN+NS-ThM5, 34  
 Poda, A.: TR+MN+NS+SS-WeM5, 28  
 Popovic, D.: SS-TuP10, 21  
 Porter, S.: EN+SS-FrM2, 42  
 Potapenko, D.V.: SS-TuA7, 18  
 Potocar, T.G.: SS2-TuM5, 14  
 Pratt, J.R.: TR+NS+SS-WeA1, 32  
 Pugmire, D.L.: AC+SS-MoM3, 1; AC+SS-MoM4,  
 1  
 Pursel, S.M.: EN+NS-ThM11, 35  
 Puschig, P.C.: SS2-TuM5, 14  
 Pushkarev, V.V.: SS1-MoM5, 4; SS-WeA9, 31

— **Q** —

Quinlan, R.A.: SS-ThM12, 37

— **R** —

Rachmady, W.: EM+SS-WeA3, 29  
 Rack, P.D.: SS2-WeM1, 26  
 Rahman, T.S.: SS2-MoA3, 8; SS2-MoA4, 9; SS2-  
 TuM4, 14; SS-ThM5, 36; SS-TuA12, 19  
 Randall, J.N.: SS2-MoA1, 8; SS2-MoA7, 9  
 Ren, M.: SS1-MoA9, 8  
 Repp, J.: SS-TuA3, 18  
 Reutt-Robey, J.E.: SS2-TuM6, 14  
 Riseborough, P.S.: AC+SS-MoM8, 1  
 Risse, T.: SS-ThM6, 36  
 Ritter, C.: TR+NS+SS-WeA8, 33  
 Robach, O.: SS1-MoA1, 7  
 Robel, I.: EN+NS-ThM5, 34  
 Roberts, C.J.: SS2-WeM5, 26  
 Robey, S.W.: SS2-TuM6, 14  
 Robson, M.: EN+SS-FrM5, 42  
 Rodriguez, J.A.: IS+SS-TuA1, 16; SS1-MoM10, 5  
 Rogers, B.: EN+SS+TF-ThA6, 38  
 Roldan Cuenya, B.: SS1-MoA2, 7  
 Rosenberg, S.: SS2-WeM3, 26  
 Rousseau, R.J.: SS1-WeM9, 25; SS-FrM7, 44; SS-  
 ThM1, 35  
 Rousset, P.: AC+SS-MoM3, 1; AC+SS-MoM4, 1  
 Rubloff, G.W.: EN+SS+TF-ThA10, 39  
 Rudawski, N.G.: EM+SS-WeA7, 29

Russell, S.M.: SS1-TuM1, 12  
 Rutherford, R.: SS-WeA3, 31  
 Ryder, O.: SS-TuP23, 23

— **S** —

Sadowski, J.T.: IS+SS-TuA1, 16  
 Saini, R.: SS2-MoA1, 8  
 Saint-Lager, M.-C.: SS1-MoA1, 7  
 Saito, N.: SS-TuP7, 21  
 Sakai, M.: SS-TuP5, 20  
 Sakulsermsuk, S.: SS-TuA8, 18  
 Salmeron, M.: SS-ThA1, 39; SS-ThA10, 41; SS-  
 ThA3, 39  
 Sampathkumaran, U.: EN+NS-ThM12, 35  
 Sandell, A.: SS-ThA9, 40  
 Savage, D.E.: SS2-MoA6, 9  
 Savara, A.: SS1-MoA8, 8  
 Schall, J.D.: TR+NS+SS-WeA9, 33  
 Schauerermann, S.: SS1-MoA8, 8  
 Schirmeisen, A.: TR+NS+SS-WeA8, 33  
 Schlaf, R.: SS2-WeM12, 27  
 Schmidt, H.: EN+SS-FrM3, 42; EN+SS-FrM4, 42  
 Schricker, S.: SS-TuP21, 23  
 Schulte, K.: IS+SS-TuM5, 11  
 Schulze, R.K.: AC+SS-MoM10, 2  
 Schüpbach, B.: SS2-TuM11, 15  
 Schwarz, U.D.: TR+NS+SS-WeA8, 33  
 Scott, M.: EN+SS+TF-ThA6, 38  
 Seal, S.: SS2-WeM6, 26  
 Seebauer, E.G.: SS2+EM-MoM11, 6  
 Senanayake, S.D.: IS+SS-TuA1, 16; SS1-MoM10,  
 5  
 Seyller, T.: GR+SS+TF+EM-MoM3, 2  
 Shavorskiy, A.: IS+SS-TuM5, 11  
 Shaw, G.A.: TR+NS+SS-WeA1, 32  
 Shaw, M.J.: IS+SS-TuA9, 17  
 Shen, J.: EM+SS-WeA11, 30  
 Shen, M.: SS1-TuM1, 12  
 Shi, X.Q.: SS2-TuM3, 14  
 Shi, Y.: SS-ThA10, 41  
 Shimizu, H.: EN+SS+TF-ThA8, 38  
 Shuttthanandan, V.: SS2-WeM6, 26  
 Sibener, S.J.: SS2+EM-MoM4, 6  
 Singaravelu, S.: SS2-WeM10, 27  
 Singer, I.L.: TR+MN+NS+SS-WeM1, 27  
 Singh, A.: SS2-TuM10, 15  
 Singh, R.: SS-FrM1, 43  
 Singh, S.V.: TR+MN+NS+SS-WeM6, 28  
 Sinnott, S.B.: TR+MN+NS+SS-WeM12, 28  
 Sloan, P.A.: SS-TuA8, 18  
 Smith, S.: SS1-WeM9, 25  
 Snow, C.S.: AC+SS-MoM11, 2  
 Snyders, R.: EN+SS+TF-ThA1, 38  
 Song, Y.J.: GR+SS+TF+EM-MoM9, 3  
 Soukiasian, P.: GR+SS+TF+EM-MoM10, 3  
 Spektor, R.: SS-TuP13, 22  
 Spormann, A.: SS-ThA1, 39  
 Sprunger, P.T.: SS1-MoA9, 8; SS-FrM1, 43  
 Stacchiola, D.J.: SS1-MoM10, 5  
 Stein, O.: SS2+EM-MoM2, 5  
 Stemmer, S.: EM+SS-WeA7, 29  
 Stephens, J.A.: SS1-TuM10, 13; SS1-TuM6, 13  
 Sterrer, M.: SS1-WeM2, 25  
 Streber, R.: SS1-TuM2, 12  
 Strohmeier, B.R.: IS+SS-TuA10, 17  
 Stroschio, J.A.: GR+SS+TF+EM-MoM9, 3  
 Sturgeon, J.L.: IS+SS-TuA10, 17  
 Su, J.F.: TR+NS+SS-WeA12, 33  
 Subramanian, A.: IS+SS-TuA9, 17  
 Sullivan, J.P.: IS+SS-TuA9, 17  
 Sun, D.Z.: SS2-TuM4, 14; SS-TuA11, 19; SS-  
 TuA2, 18  
 Surnev, S.: SS1-WeM5, 25  
 Sykes, E.C.H.: SS1-TuM5, 12; SS-TuA1, 17; SS-  
 TuP2, 20; SS-WeA9, 31  
 Szanyi, J.: SS-ThM1, 35; SS-WeA11, 32  
 Szelągowska-Kunstman, K.: SS2-TuM11, 15

— **T** —

Tait, S.L.: SS-TuP20, 23

Takahashi, A.: SS-TuP4, 20  
 Takai, O.: SS-TuP7, 21  
 Tamura, H.: SS-TuP8, 21  
 Tappan, B.C.: EN+SS-FrM1, 42  
 Tedesco, J.L.: GR+SS+TF+EM-MoM1, 2;  
 GR+SS+TF+EM-MoM8, 3  
 Teichert, C.K.: SS2-TuM5, 14  
 Tenney, S.A.: SS-TuP14, 22  
 Teplyakov, A.V.: SS2+EM-MoM3, 5; SS-TuP15,  
 22  
 Terfort, A.: SS2-TuM11, 15  
 Terryn, H.: SS1-WeM10, 25  
 Thayne, I.: EM+SS-WeA11, 30  
 Thevuthasan, S.: SS2-WeM6, 26  
 Thiel, P.A.: SS1-TuM1, 12; SS2-MoA11, 10  
 Thissen, A.: IS+SS-TuM11, 12  
 Thomas, J.C.: SS2+EM-MoM5, 6  
 Thompson, P.E.: GR+SS+TF+EM-MoM1, 2  
 Thürmer, K.: GR+SS+TF+EM-MoM2, 2; SS-  
 ThA7, 40  
 Tierney, H.L.: SS-TuP2, 20  
 Tinkey, H.: GR+SS+TF+EM-MoM6, 3  
 Todorova, M.: SS1-WeM1, 25  
 Torrance, D.B.: GR+SS+TF+EM-MoM6, 3;  
 GR+SS+TF+EM-MoM9, 3  
 Trenary, M.: SS1-MoM9, 4; SS-FrM3, 43  
 Tskipuri, L.: SS2-TuM6, 14  
 Tsuei, K.-D.: SS2-TuM3, 14  
 Tsukada, M.: SS-TuP8, 21  
 Turchanin, A.: SS2-TuM12, 15  
 Twigg, M.E.: GR+SS+TF+EM-MoM8, 3  
 Tysoe, W.T.: TR+MN+NS+SS-WeM11, 28  
**— U —**  
 Ueda, O.: EN+SS+TF-ThA2, 38  
 Uhl, A.: SS-FrM3, 43  
 ul Haq, E.: SS2-WeM5, 26  
 Urquhart, S.G.: IS+SS-TuA3, 16  
 Utz, A.: SS-TuA10, 19; SS-TuA9, 18  
 Uvdal, P.: SS-ThA9, 40  
**— V —**  
 Valtiner, M.: SS1-WeM1, 25  
 Van der Ven, A.: SS2+EM-MoM5, 6  
 van Dorp, W.: SS2-WeM3, 26  
 Van Hove, M.A.: SS2-TuM3, 14  
 Van Ingelgem, Y.: SS1-WeM10, 25  
 van Rijn, R.: IS+SS-TuM1, 11  
 Vandendael, I.: SS1-WeM10, 25  
 Vandervelde, T.: EN+SS+TF-ThA11, 39

Ventrice Jr., C.A.: SS-TuP24, 24  
 Verdaguer, A.: SS-ThA3, 39  
 Veyan, J.-F.: EN+NS-ThM3, 34; SS2-MoA1, 8;  
 SS2-MoA7, 9  
 Visikovskiy, A.: SS-TuP6, 21  
 Vizzini, S.: GR+SS+TF+EM-MoM10, 3  
 Von Ehr, J.R.: SS2-MoA1, 8  
**— W —**  
 Wagner, M.: SS1-WeM5, 25  
 Wallace, R.M.: EM+SS-WeA4, 29; SS2-MoA7, 9  
 Walle, L.E.: SS-ThA9, 40  
 Walters, J.L.: SS-TuP24, 24  
 Wang, C.: SS1-MoM11, 5  
 Wang, L.: TR+NS+SS-WeA12, 33  
 Wang, X.: SS-WeA3, 31  
 Wang, Y.: SS-ThA1, 39; SS-ThM1, 35  
 Watanabe, K.: SS1-MoA7, 7  
 Watson, D.: IS+SS-TuM5, 11  
 Weaver, J.F.: SS1-MoM2, 4  
 Weaver, J.M.R.: SS2-WeM5, 26  
 Weeks, J.: SS2-TuM6, 14  
 Weiss, S.: EN+SS+TF-ThA6, 38  
 Westerstrom, R.: IS+SS-TuM1, 11  
 Whang, D.M.: EN+NS-ThM2, 34  
 Wheeler, V.D.: GR+SS+TF+EM-MoM1, 2  
 White, M.: SS2-WeM9, 27  
 White, M.G.: SS1-MoA10, 8; SS-TuP19, 23  
 White, R.G.: SS-TuP18, 23  
 Wickert, S.: SS1-TuM2, 12  
 Williams, V.O.: EN+NS-ThM12, 35  
 Wilson, D.: SS2-WeM9, 27  
 Winkler, A.H.: SS2-TuM5, 14  
 Winter, B.: IS+SS-TuM2, 11  
 Winter, R.: EN+NS-ThM12, 35  
 Witkin, D.B.: SS-TuP13, 22  
 Wnuk, J.: SS2-WeM3, 26  
 Wöckel, C.: SS1-TuM2, 12  
 Woll, A.R.: SS2-TuM9, 14  
 Wöll, C.: SS-FrM5, 44  
 Womack, F.N.: SS-FrM1, 43  
 Wong, K.L.: SS-TuA2, 18  
 Wong, K.T.: SS-WeA4, 31  
 Wong, L.S.: SS2-WeM5, 26  
 Woodward, P.M.: EN+SS-FrM2, 42  
 Wright, A.: SS-TuP18, 23  
 Wu, Z.: SS-ThM11, 37  
 Wyrick, J.: SS-TuA11, 19

**— X —**  
 Xiao, X.D.: SS2-TuM3, 14  
 Xing, Q.B.: SS2-WeM11, 27  
 Xu, S.S.: SS1-TuM3, 12  
 Xu, F.: SS1-MoM5, 4  
 Xu, G.: SS2-TuM3, 14  
**— Y —**  
 Yamamoto, S.: SS-ThA1, 39  
 Yang, F.: IS+SS-TuA1, 16  
 Yang, J.C.: IS+SS-TuA10, 17; SS-WeA10, 32  
 Yang, X.: SS1-TuM9, 13  
 Yanguas-Gil, A.: EN+NS-ThM12, 35  
 Yarmoff, J.A.: SS2-WeM4, 26  
 Yasuda, Y.: EN+SS+TF-ThA8, 38  
 Ye, P.: EM+SS-WeA1, 29  
 Yi, C.-W.: SS-WeA11, 32  
 Yildirim, H.: SS2-MoA4, 9  
 Yin, J.: SS1-MoM9, 4  
 Yin, L.: EN+NS-ThM2, 34  
 Yoshimura, M.: SS-TuP6, 21  
 Youn, Y.-S.: SS-TuP11, 22  
 Yu, C.H.: EN+NS-ThM2, 34  
 Yuan, H.: EN+SS+TF-ThA9, 38  
 Yuen, C.: SS2-MoA11, 10  
**— Z —**  
 Zaera, F.: SS1-MoM3, 4; SS-TuP1, 20  
 Zauscher, S.: TR+NS+SS-WeA7, 33  
 Zavadil, K.R.: AC+SS-MoM11, 2  
 Zekic, A.: SS-TuP10, 21  
 Zhan, Y.: IS+SS-TuA9, 17  
 Zhang, L.: TR+NS+SS-WeA7, 33  
 Zhang, X.Q.: SS2-TuM3, 14  
 Zhang, Y.: SS2-MoA6, 9; SS2-WeM5, 26  
 Zhang, Z.: SS1-MoA9, 8; SS1-WeM9, 25; SS-  
 FrM4, 43; SS-FrM7, 44; TR+NS+SS-WeA2,  
 32  
 Zhao, A.D.: SS2-TuM3, 14  
 Zharnikov, M.: SS2-TuM11, 15  
 Zhernokletov, D.M.: EM+SS-WeA4, 29  
 Zhou, J.: SS1-MoA10, 8; SS-FrM2, 43  
 Zhou, W.-P.: SS-TuP19, 23  
 Zhou, Y.: SS-FrM2, 43  
 Zhu, Y.M.: SS2-TuM4, 14; SS-TuA11, 19; SS-  
 TuA2, 18  
 Zhu, Z.H.: SS-TuP23, 23  
 Zorić, I.L.: SS1-MoA6, 7